Characterization of chemical and biological clogging and their interactions within a micro-irrigation system in the context of the reuse of treated effluents in irrigation

N. Rizk

UNIVERSITE D'AIX MARSEILLE

Ecole Doctorale des Sciences pour l'Environnement

Discipline : *Génie des Procédés*

THÈSE

Présentée en vue d'obtenir le grade de

DOCTEUR DE L'UNIVERSITÉ D'AIX-MARSEILLE
Faculté des Sciences et Techniques

par

Nancy Rizk

Caractérisation du colmatage chimique et biologique et leurs interactions au sein d'un dispositif de micro-irrigation dans le contexte de la réutilisation des eaux usées épurées en irrigation

Characterization of chemical and biological clogging and their interactions within a micro-irrigation system in the context of the reuse of treated effluents in irrigation

Soutenue publiquement le 21 juillet 2017 devant le jury composé de :

Dr. Nassim AIT MOUHEB	Chargé de recherche	G-EAU, IRSTEA, Montpellier	Examinateur
Pr. Christophe DAGOT	Professeur	Université de Limoges	Rapporteur
Dr. Renauld ESCUDIE	Directeur de recherche	LBE, INRA, Narbonne	Rapporteur
Pr. Marc HERAN	Professeur	Université de Montpellier	Président du jury
Dr. Bruno MOLLE	Ingénieur de Recherche	G-EAU, IRSTEA, Montpellier	Examinateur
Pr. Nicolas ROCHE	Professeur	Université d'Aix-Marseille	Directeur de thèse
Pr. Guilhem Bourrié	Directeur de recherche	EMMAH, INRA, Avignon	Invité

ACKNOWLEDGEMENTS

“I am thankful to all those who said ”NO”. It’s because of them, I did it myself” Wayne W. Dyer

This thesis was carried out in collaboration between IRSTEA (Institut national de Recherche en Sciences et Technologies pour l'Environnement et l'Agriculture, UMR G-eau) and M2P2 (Mécanique, Modélisation et Procédés Propres, AMU-CNRS) laboratory. I would like to thank all the members of these two structures for having welcomed me during these three years and the NGO T.E.R.R.E Liban that funded this research.

I would also like to thank the people who supervised this work: Prof. Nicolas ROCHE at Aix-Marseille University who agreed to direct my thesis, as well as Dr. Nassim AIT MOUHEB and Dr. Bruno MOLLE at IRSTEA institute for their investment in this thesis. I would like to thank them for their availability, advice and support.

I also thank my dissertation committee members Prof. Christophe DAGOT and Dr. Renauld ESCUDIE, who agreed to make reports on this thesis, and Prof. Marc HERAN for agreeing to evaluate this work and for its participation in the jury. I also thank Prof. Guilhem Bourrié for the valuable advice he gave me for the setting of numerical experimentations.

This research paper would not have been possible without the help and assistance of David TANG, Jean-Francois BONICEL, David BASTIDON, Jean-Philippe TRANI, François LIRON and Geoffrey FROMENT the technicians and engineers from IRSTEA team and Jean-Paul NISTERON the technician from Aix-Marseille University. I would thank Dr. Joel COUVE and Dr. Bernard FRAISSE from Montpellier University for their permission and help to use the analytical laboratory materials.

I would like to express my gratitude to the many people who supported and encouraged me through this research. To all the team of IRSTEA Montpellier especially Jaafar AL MUHAMMAD, Souha GAMRI, David NORTES MARTINEZ, Sandrine DHENAIN, Pierre-Olivier MALATERRE, David DORCHIES, Daniel MOURA, Augustin LUXIN, Rami AL BACHA, Cyril CHEVARIN, and many more.

I also do not forget to thank all PhD students and trainees with whom I shared good times. To my friends from outside the laboratory and to Dr. Roger MOUSSA my guarantor who without him I could not have visited some superb places in the south of France and shared many experiences.

My deepest thanks goes to my family and especially my father, mother and sister for their support, prayers, encouragement and because they believed in me throughout the school, university and thesis. Without them I would not be in France and this work would not be done.

And finally a big thanks for my darling who concentrated all his effort and his energy so that I can be in good condition for the finalization of this work even if thousands of kilometers separated us he was waiting for any occasion to help me in France and thanks to his love and successive encouragement I felt his presence always beside me.

Thank you God for all your blessings and because you were by my side.

“A river cuts through rock, not because of its power, but because of its persistence” James N. Watkins

Contents

Nomenclature

Latin alphabet

$\dot{a}_i$	Empirical ion-size parameter	-
t	Time	s
A_i, A_t	Cell and total surface respectively	m^2
ae	Field application efficiency	$\%$
c_{K_s}	Concentration solubility	-
ce	Conveyance efficiency	$\%$
D_h	Hydraulic Diameter	m
e	Gap width between the inner cylinder and the outer cylinder	m
H	Working pressure head at the dripper	bar
h	Height of the reactor cylinders	m
I	Ionic strength	-
ie	Scheme irrigation efficiency	$\%$
K_d	Constant of proportionality that characterizes each dripper	-
m_b	Mass of biofilm that develops on all the plates at a period t	mg
m_{COD}	Consumed COD corresponding to the same period t	mg
n	Cells number	-

q	Dripper discharge	m^3/s
R_1, R_2	Radii of the two cylinders	m
Re	Reynolds number	-
Re_c	Critical Reynolds number	
S	Saturation	-
S_i, S_m	Cell and average strain rate respectively	s^{-1}
SI	Saturation Index	-
T	Temperature	°C
Ta	Taylor number	-
Ta_c	Critical Taylor number	-
V	Flow velocity	m/s
X	Average flow rate at the same time (t)	$m^3.s^{-1}$
x	Dripper discharge exponent	
Y	Yield rate	

Greek alphabet

α	Constant	0,1556
Γ	Aspect ratio (h/e)	-
γ_i	The activity coefficient	-
λ	Radiation wavelengt	$\mathring{A}$
μ	The dynamic viscosity of the fluid	for water 1.00×10^{-3} Pa.s
ν	The kinematic viscosity of fluid	for water $1.00 \times 10^{-06}\ m^2/s$
Ω	Angular velocity	rad/s
Ω_c	Critical angular velocity	rad/s

Φ	Pipe diameter	m
ρ	Fluid density	for water $1000\ kg/m^3$
σ	Standard deviation of dripper flow rate at a specific time	
τ	Wall shear stress	N/m^2
2θ	Incidence angle of the x-ray beam deflected by an angle of 2θ	

Abbreviations

ACC	Amorphous Calcium Carbonate
COD	Carbon Oxygen Demand
CU	Coefficient of Uniformity
CV	Coefficient of Variation
DOC	Dissolved Organic Carbon
Dra	Discharge ratio variation
DTG	TGA derivative
EPS	Extracellular Polymeric Substances
IE	Inhabitant Equivalents
IM	Inorganic Matter
LDPE	Low Density Polyethylene
LSSR	Low Shear Stress Reactor
NPC	Non-Pressure Compensating
NTK	Nitrogen Kjeldahl
OM	Organic Matter
PC	Pressure Compensating
PE	Polyethylene

rpm Rotations per minute

SD Standard Deviation

SEM Standard Error of the Mean

SS Suspended Solids

SU Statistical Uniformity

TCR Taylor-Couette Reactor

TG-MS Thermogravimetric analysis–mass spectrometry

TGA Thermogravimetric Analysis

TOC Total Organic Carbon

TS Total Solids

TSS Total Suspended Solids

TTF Turbulent Taylor Flow

TVF Turbulent Vortex Flow

VS Volatile Solids

WVF Wavy Vortex Flow

XRD X-Ray Diffraction

Acronymes

CAT Complete Alkalimetric Title

CFD Computational Fluid Dynamics

DGV Doppler Global Velocimetry

EPA Environmental Protection Agency

FAO Food and Agriculture Organization

IWMI International Water Management Institute

LDV Laser Doppler Velocimetry

LIF Laser Induced Fluorescence

NPC2 Non-Pressure-compensating drippers ($2\ l/h$)

PIDV Particle Image Displacement Velocimetry

PIV Particle Image Velocimetry

PTV Particle Tracking Velocimetry

UNESCO United Nations Educational, Scientific and Cultural Organization

UNWWAP United Nations World Water Assessment Programme

WRG Water Resources Group

WWTP WasteWater Treatment Plant

Chemical elements

BOD_5 5-day Biochemical Oxygen Demand

$Ca_3(PO_4)_2$ Calcium Phosphate

Ca^{2+} Calcium ions

$CaCl_2$ Calcium chloride

$CaCO_3$ Calcium Carbonate

CaO Calcium Oxide

$CaPO_4$ Calcium orthophosphates

CO_2 Carbon Dioxide

Fe_2O_3 Iron(III) oxide

H_2CO_3 Carbonic Acid

H_2O Water

$H_2PO_4^-$ Dihydrogen phosphate ion

HCO_3^- Bicarbonate ion

Mg^{2+} Magnesium ions

$NaHCO_3$ Sodium bicarbonate

NaOH Sodium Hydroxide

NO_2^- Nitrite

NO_3^- Nitrate

OH^- Hydroxide ions

PO_4^{3-} Mineral phosphorus

SiO_2 Silicon dioxide

General Introduction:

Problems of overexploitation of water resources and their pollution increases every year around the world. In addition, water withdrawals for agriculture are becoming more and more important with the increasing demand for food. Today, irrigation uses 70% of the world's water resources. Faced with the problem of water resource rarefaction, especially in arid and semi-arid countries, reuse of treated wastewater for irrigation appears to be an efficient solution. Problems related to water shortage are limited and the crop yield is improved due to the fertilizer potential of this resource. Indeed, the treated wastewaters are rich in nutrients (nitrogen, phosphorus and potassium). Therefore, their use can reduce fertilizer inputs while increasing crop yield.

Among several irrigation techniques for the reuse of treated wastewater, micro-irrigation is the most efficient and safest. It consists of bringing irrigation water to the bottom of the crops. This technique allows achievement of water savings by reducing the losses by infiltration and evaporation. Micro-irrigation also reduces the health risks associated with the use of treated wastewater by limiting the contact of farmers and crops with irrigation water. However, clogging of drippers is a common problem in drip irrigation. It causes a dysfunction of the irrigation system as the uniformity of the distribution progressively decreases. This results in reduced crop yield and damage to irrigation systems. The clogging of micro-irrigation devices can be traced to (i) accumulation of particulate matter due to the presence of suspended solids (physical clogging), (ii) precipitation of soluble salts present at a concentration above saturation (chemical clogging) and (iii) biofilm development (biological clogging) (Dosoretz et al., 2011[85]). These phenomena are interlinked and are observed in all the components of micro-irrigation systems (pipes, drippers, etc.). The small section of the drippers (on the order of millimeters) makes them more vulnerable to clogging. The clogging of localized irrigation drippers is of concern to farmers and often justifies the use of treatment procedures. Mineral particles more than $80\ \mu m$ are retained by filtration. The chemical elements are removed using acidic solutions. Chlorination treatment is often used to control the development of biofilm in irrigation systems, but its effectiveness remains limited (Levy et al., 2011[168]).

Many researchers have investigated dripper clogging by biofilm development in an experimental context using treated wastewater (Karaca and Uçan, 2013[146], Tarchitzky et al., 2013[271]). Other works have focused more on the influence of hydrodynamic conditions in the pipes and drippers on the development of these associations of microorganisms. However no studies have focused on chemical clogging and the possibility of modeling salt precipitation and the interaction between chemical precipitation and biofilm development inside pipes and drippers.

We suggest in this work that has been done within IRSTEA (Institut national de Recherche en Sciences et Technologies pour l'Environnement et l'Agriculture, UMR G-eau) and M2P2 (Mécanique, Modélisation et Procédés Propres, AMU-CNRS) laboratory to study the mechanisms of chemical and biological clogging, and their interactions in micro-irrigation.

The main objective of this thesis is to introduce new elements on the clogging of drippers and fouling of pipes done at laboratory scale under well-controlled conditions in the context of the reuse of wastewater in irrigation. In order to acheive this objectif, this research is divided into three parts.

In the first part of the study, we will explore an experimental set-up composed of batch reactors which allows us to follow the chemical precipitation while mastering the operating conditions. The experimental results allowed us to validate and calibrate the modeling of the precipitation under PHREEQC's software. This numerical model allows prediction and quantification of chemical precipitation for a given water quality under various operating conditions of pH, temperature and CO_2 partial pressure.

In the second part, an analysis of the effect of the shear stresses on the biofilm development will be carried out using a Taylor-Couette reactor (TCR). The TCR is a good method for developing the biofilm under particular hydrodynamic conditions which in this study will be similar to those encountered in irrigation.

In the third part, we will study the development of biofilm with and without calcium carbonate. To do this, an irrigation set-up was implemented and a follow-up of the clogging of drippers and pipes was done. The results will show the interaction between biofilm development and calcium carbonate precipitation.

The plan of the manuscript is therefore sorted in the following way:

In Chapter I, we will present the state of art of the study context concerning water reuse in irrigation as well as the works done on biofilm development (parameters influencing its development, etc.), chemical precipitation and their interaction. In Chapter II, we will describe the experimental set-ups as well as the protocols used. In Chapter III, we will discuss the experimental and numerical results on chemical precipitation using treated wastewater. And in Chapter IV, we will discuss the biofilm development and the interaction between biofilm and calcium carbonate.

Chapter I

Context and Objectives

Part I.1

Wastewater reuse in irrigation

I.1.1 Context and issues related to the reuse of treated wastewater

Mediterranean countries, developing countries and arid regions are particularly vulnerable to water stress and suffer from most of the current global changes such as erosion of diversity, climate change, population growth, industrialization and especially the increasing degradation of water resources (over-exploitation, pollution, salinization, etc.). A continuation of the development trend will lead to a 55% increase of global water demand by 2050 (WRG, 2009[1]; UNWWAP, 2015 [1]). By 2025, 1.8 billion people will live in countries or regions where water availability is less than $100\ m^3$/ capita / year according to the International Water Management Institute (IWMI). As a result, humanity is facing a multitude of water-related problems and major improvements in water management strategies are indispensable for a sustainable future (Bagatin et al., 2014[24]; Alnouri et al., 2015[13]). Water recycling and especially wastewater reuse is becoming a critical element for managing our water resources for both environmental and economic reasons. Another reason to reuse wastewater is that its volume is constantly increasing with the expansion and intensification of urban planning. The U.S. Environmental Protection Agency (EPA) defines wastewater reuse as, "using wastewater or reclaimed water from one application for another application. The deliberate use of reclaimed water or wastewater must be in compliance with applicable rules for a beneficial purpose (landscape irrigation, agricultural irrigation, aesthetic uses, ground water recharge, industrial uses, and fire protection). A common type of recycled water is water that has been reclaimed from municipal wastewater (sewage)." Agriculture, especially crop production, is the sector that consumes the biggest quantity of water. Water use for crop irrigation accounts for 70% and in some cases 90% of the water needs in the world (Kalavrouziotis et al., 2011[145]; UNESCO 2003[280]). To

[1] http://www.unesco.org/fileadmin/MULTIMEDIA/HQ/SC/images/WWDR2015Facts$_{F}igures_{E}NG_{w}eb.pdf$
Accessed June 2017

.

reduce the pressure on freshwater resources and preserve them for the supply of drinking water, many countries reuse treated wastewater for irrigation.

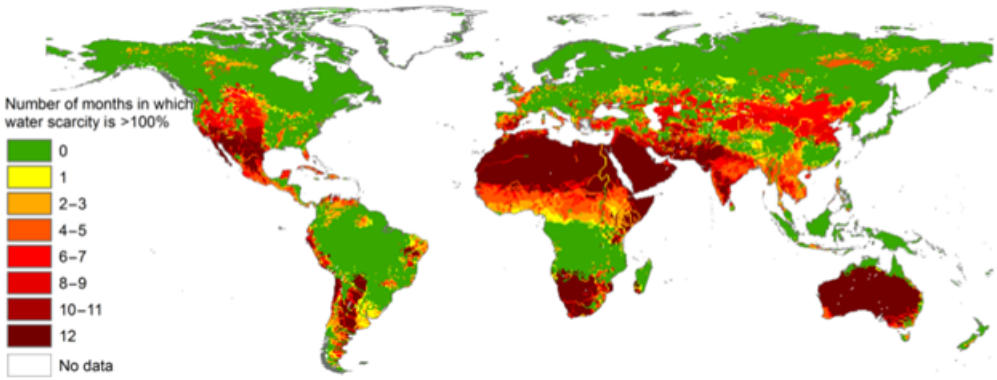

Figure I.1: Map showing areas of the world with water scarcity. Map by Mesfin M. Mekonnen and Arjen Y, 2016[189], courtesy Science Advances. CC-BY-NC-4.0 (National Geographic, 15/02/2016)

I.1.2 Worldwide application of wastewater in irrigation

Irrigation with wastewater even with no treatment or just primary treatment is a common practice in developing countries like China, India, Mexico, etc. due to high treatment costs (Lazarova and Bahri, 2005[165]). In water scare regions of developed countries such as Australia, the Middle East, and coastal or inland areas of France and Italy, treated wastewater is used for irrigation (IWMI, 2007[138]). In Spain, 408 million m^3 of treated wastewater is reused; In Italy, ambitious projects are being created (22,000 ha of vegetable crops are irrigated with treated wastewater from a sewage treatment plant with a capacity of more than one million inhabitants). Cyprus has the most ambitious objective: to reuse 100% of treated wastewater (Lazarova and Brissaud, 2007[166]).

For this reason, the selection of appropriate wastewater treatment at an affordable cost and adapted irrigation practices are the two main necessary measures to protect public health and prevent harmful conditions and damage to crops, soil and groundwater. Various reclamation technologies can be used to treat wastewater prior to irrigation, such as lagoon ponds, constructed wetlands, conventional wastewater treatment plants, membrane bioreactors, membrane filtration and others. However, these methods generally need large land areas and involve high investment costs (Norton-Brandao et al., 2013[214]). More details are found in paragraph I.1.5 for the benefits and the disadvantages of the reuse of treated wastewater for irrigation.

I.1.3 Wastewater

Wastewater is all waters entering sewage pipes whose natural properties are transformed by domestic uses, industrial, agricultural and other enterprises. Rainwater that flows into these pipelines is also included (Bliefert and Perraud, 2001[36]). There are several categories of pollutants:

- Particulate pollution, which refers to biodegradable and non-biodegradable mineral suspensions (MS or SS for suspended solids) or organic (VS for volatile solids).

- Organic pollution which includes biodegradable materials (BOD_5), non-biodegradable materials, toxic substances, inhibitory material, dissolved and particulate matter.

- Nitrogen pollution consists of nitrogen in reduced form (organic nitrogen, ammoniacal nitrogen (NTK = nitrogen Kjeldahl)) or oxidized (nitrite ($NO_2{}^-$), nitrate ($NO_3{}^-$)).

- Phosphorus pollution composed of mineral phosphorus (including $PO_4{}^{3-}$) and organic phosphorus.

- Microbiological pollution consisting of bacteria, viruses, protozoa and fungi.

For wastewater reuse and even for a rejection in nature, treatment series must be made. The concentrations of the input elements of the treatment plant are variable and depend on the size of the agglomerations and the origin of these waters. Table I.1 shows the flow of pollutants released per inhabitant per day according to the decree of 10/12/1991.

Table I.1: Flow of pollutants released per inhabitant per day for a volume of 150 liters of water.

	SS	COD COD	BOD_5	NTK	P
Flow per capita / day for a volume of 150 liters of water	90g	100-130 g O_2	60g O_2	13-15g N	4g P

I.1.4 Water treatment in a Wastewater Treatment Plant (WWTP)

Developed countries have generated techniques and guidelines for safe reuse of wastewater in irrigation for the purposes of health and environment. Water treatment represents a technological and economic challenge with the common goal of preserving biodiversity and protecting water resources. Depending on the degree of elimination of pollution and the processes implemented, several treatment levels are generally defined: pretreatment, primary treatment and secondary treatment. In some cases, tertiary treatment is applied, particularly when treated water must be disposed of in particularly sensitive

areas. There are also extensive treatments known as lagoons, which combine biological, physical and natural. Table I.2 shows the different stages of water treatment in a WWTP from pretreatment to tertiary treatment.

Table I.2: Different stages of water treatment in a WWTP from pretreatment to tertiary treatment.

Treatments	Objectives
Pretreatment: -Screening -Degreasing -Degritting -Shredding	Removal of: -Particles larger than 2 mm -Grease -Sand Reduction in amount of waste
Primary treatment: -Primary decantation -Primary decantation with the addition of reagent	Elimination of particulate pollution Efficiency: SS: 50-60%; COD and BOD_5: 25-35%; NTK and P: < 10% Efficiency: SS: 90%; COD and BOD_5: 60-70%; NTK: < 10% ; P: 80%
Secondary treatment: -Suspended bacteria treatment processes -Fixed bacteria treatment processes	Elimination of biodegradable pollution Dissolved and particulate COD, BOD_5, N and P
Tertiary treatment: -Refining treatment -Disinfection	Improvement of quality of treated water on the parameters SS, COD, BOD_5, N and P. Abatement of pathogenic germs

According to French regulations, the discharge levels of urban effluents into non sensitive zones for WWTPs treating a gross load $<$ $120kg$ BOD_5 / day ($<$ 2000 inhabitant equivalents "IE") and $>$ $120kg$ BOD_5 / day ($>$ 2000 inhabitant equivalents "IE") are presented in Table I.3 (decree of 22 June 2007).

Table I.3: Values to respect for urban effluents discharges into non-sensitive areas.

Parameter	BOD_5	COD	SS	P
Concentration to not exceed or minimum efficiency to be reached (<2000 IE)	35 mg/L 60%	- 60%	- 60%	< 1 or 2 mg P/L
Concentration to not exceed or minimum efficiency to be reached (>2000 IE)	25 mg/L 70% (120 < load < 600 kg/day) 80% (load > 600 kg/day)	125 mg/L 75%	35 mg/L 90%	< 1 or 2 mg P/L

I.1.5 Beneficial and negative impacts of the reuse of treated wastewater for agricultural irrigation

The reuse of wastewater in irrigation results in both positive and negative impacts on soil, crops and health. This practice can benefit soil and farmers, while at the same time posing a risk of contamination to the ecosystem.

I.1.5.1 Benefits of wastewater reuse

The use of treated wastewater in irrigation can positively influence crop production and improve physico-chemical characteristics of soil (Kiziloglu et al., 2007[155]). The presence of nitrogen, phosphorus, organic matter, and other trace elements in the water provides a good source of nutrients for the growth, yield and quality of crops, minimizes soil degradation, improves fertility and restores the nutrient contents of soil (Benitez et al., 2001[33]; Plauborg et al., 2010[232]; Abusam and Al-Anzi, 2011[3]; Khurana and Singh, 2012[154]; Christou et al., 2014[63]; Almuktar et al., 2015[11]; Almuktar and Scholz, 2016[12]). The extra supply of organic carbon or the addition of micro-organisms via wastewater increases the soil microbial activity. This increase in microbial activity of the soil brings benefits to both agriculture and the development of flora and fauna in the soil ecosystem (Friedel et al., 2000[106]). Wastewater reuse can also have an economic benefit since it has limited costs compared to other techniques developed to obtain fresh water. Production of treated wastewater may cost less than the supply of deep groundwater, water import and desalination (Veolia, 2006[283]). A cost-benefit analysis was done in 2014 on treated wastewater reuse by IRSTEA for ONEMA. One focus was the sport of golf in the city of Sainte Maxime, France. Golf consumes 12% of total water volume issued in Sainte Maxime. Using treated wastewater instead of drinking water, golf has an additional cost of 2 million € for the new watering system but it is largely offset by the 5.9 million € of savings in terms of re-grassing, fertilizer and especially water purchase (Loubier and Declercq, 2014[182]).

I.1.5.2 Negative impacts of wastewater reuse in agriculture

The main downside of reusing treated wastewater in agriculture is the pollution of soil, the potential contamination of crops (Khan et al., 2008[153]) and water sources (Batarseh et al., 2011[28]). Municipal wastewater contains a huge quantity and variety of pathogenic agents, such as bacteria, protozoa and viruses. The study of microbial contamination is focused on the pollution of crops rather than the soils receiving wastewater. This is because a greater number of people are exposed to pathogenic

microorganisms through consumption of contaminated crops. It also has a significant risk of helminth, bacterial/viral and protozoan infections for farm workers and their families, causing diarrhea and hookworm disease (Blumenthal and Peasey, 2002[38]). Crops are polluted by direct contact with wastewater during irrigation. Pollution of the edible parts of plants depends not only on the quality of water, but also on the quantity applied to soil, the irrigation method and the type of crop. Other risk factors have only measurable effects over longer periods and increase with the continued use of wastewater, such as the salinity of the soil (Levy et al., 2011[168]; Muyen et al., 2011[203]), the accumulation of toxic chemicals (Kukul et al., 2007[160]) heavy metals and organic compounds (Mapanda et al., 2005[186]; Rattan et al., 2005[239]) . Different levels of risk are perceived for different heavy metals. While some of them are nutrients for plants at trace concentrations (Cu, Fe, Mn, Mo, Zn, Ni) others have been shown to produce harmful effects on exposed organisms or are absorbed by plants and accumulated through the food web (Cr, As, Pb, Hg, Al, Cd). Pollution of soil by organic polluants (pesticides, polyaromatic hydrocarbons, organochlorides, paraffin, organic solvents, etc.) can have different effects in soil organisms depending on the compound. For example some antibiotics (chlortetracycline, etc.) can decrease crop growth and inhibit the microbial activity of the soil. Figure I.2 shows the 20 countries with the highest use of untreated wastewater for agricultural irrigation. China is the country with the highest volume of untreated wastewater in agriculture (Jimenez et al., 2008[139]), followed by Mexico then the United States. We can also see in this figure sites where monitoring studies are aimed at determining the occurrence of organic pollutants in soils after irrigation with wastewater.

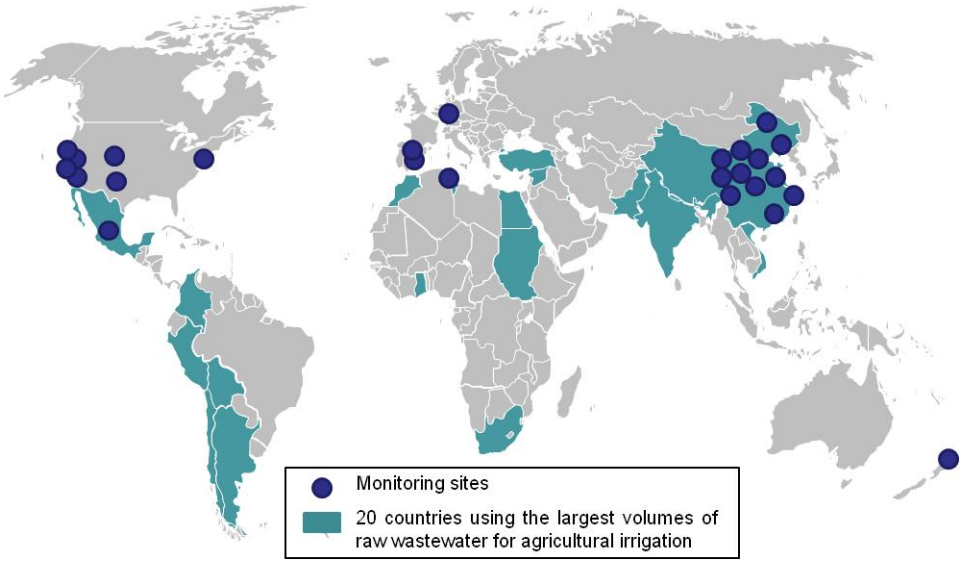

Figure I.2: Monitoring studies for pollutants of emerging concern in wastewater irrigated soils throughout the world and comparison with the 20 countries using the largest volumes of raw wastewater for agricultural irrigation(Duràn–Àlvarez and Jiménez–Cisneros, 2014 [90]).

Part I.2

Irrigation generalities

I.2.1 Irrigation systems

Irrigation systems are generally classified into two categories: gravity irrigation systems and pressurized irrigation systems (sprinkler and drip irrigation).

All irrigation techniques can be used to distribute treated effluent. The choice of irrigation technique for reuse of treated water essentially depends on several parameters such as performance potential, cost, health impact, technical constraints and efficiency of irrigation.

Irrigation efficiency can refer to the uptake of water in the root zone of a plant but can also refer to how much water is lost when it flows (Van der Kooij et al., 2013[281]). A scheme irrigation efficiency of $50-60\%$ is good; 40% is reasonable, while a scheme irrigation efficiency of $20-30\%$ is poor (FAO Annex: Irrigation efficiencies, 1989). It can be calculated using the following formula:

$$\text{ie} = \frac{\text{ce} \times \text{ae}}{100} \tag{I.1}$$

with

ie : scheme irrigation efficiency ($\%$)

ce : conveyance efficiency ($\%$)

ae : field application efficiency ($\%$)

Field application efficiency (ae) mainly depends on the irrigation method and the level of farmer discipline. Conveyance efficiency (ce) mainly depends on the length of the canals, the soil type or permeability of the canal banks and the condition of the canals.

I.2.1.1 Surface irrigation

Surface irrigation, also called gravity irrigation (figure I.3), is the oldest technique and the one most used in the world. It concerns around 80% of the world's irrigated area (Pereira et al., 2006[223]). The water is distributed by gravity through a network of channels in the open air from which it infiltrates the ground. The distribution of water is ensured by the topography and infiltration properties of the soil. This technique has low investment costs, very low energy consumption and good adaptation to the distribution of sewage (limitation of the risks of contact by projection, no clogging of irrigation systems). However, it is characterized by low field application efficiency (50% as a world average) and high water losses which make this technique inappropriate in a context of water stress. To avoid these losses and in order to improve the uniformity of distribution, it is recommended to use sprinkler irrigation or micro-irrigation.

Figure I.3: Surface irrigation (©2010 Cornell University)
https://nrcca.cals.cornell.edu/soil/CA3/CA0324.php

I.2.1.2 Sprinkler irrigation

Sprinkler irrigation (Figure I.4) refers to techniques designed to artificially reproduce natural rainfall. After pumping, water is sprayed into the air by sprinklers in the form of a jet and distributed on agricultural plots. The pressure requirements at the inlet of the system consist specially on the sprinkler operating pressure which varies between 1.5 and 5.5 bar. Various devices are used for this type of irrigation including the reels system, full coverage sprinkler and center pivot or linear irrigation.

This technique is characterized by greater efficiency than surface irrigation, varying between 75 and 95% (Compaoré, 2006[65]). It requires significantly higher energy consumption and technical skills by the irrigators. In addition, the wind influences the uniformity of water distribution in the plot (Stevenin, 2016[261]).

Figure I.4: Sprinkler irrigation (Stevenin 2012[260])

The use of this technique with inadequately treated sewage must be restricted so as to limit drift and aerosols that represent a health risk. Indeed, the aerosols formed by the sprinklers can carry pathogens depending on the speed and wind direction when the water quality is not properly followed. The dispersion of the jets in the atmosphere has been studied by Molle et al., (2012 a)[194]. This study recommended practices adapted to the use of treated wastewater in spray irrigation (restricted access to the land during irrigation, monitoring the wind, selection of sprinklers and operating pressure, etc.) in order to limit the possible drift of aerosols and associated risks of health pollution. Clogging problems at sprinkler emission holes may occur with the use of highly mineralized waters. This risk is lower and easier to observe in sprinkler irrigation than in micro-irrigation.

I.2.1.3 Micro-irrigation

Micro-irrigation, also known as drip irrigation is an irrigation technique characterized by low, frequent and localized water supplies near the crops in the form of drops (Figure I.5). This irrigation method is fundamentally different from those seeking to cover a surface (surface or sprinkler irrigation), and consists of bringing water to plants in small amounts once or several times a day. Water diffuses radially under the effect of capillary forces and vertically under the effect of gravity, in a limited volume of soil in the vicinity of the roots, where the plant draws.

Figure I.5: Micro-irrigation (http://www.sandeepdripirrigation.com/drip-irrigation-system.html)

Transport and distribution of water are provided either by a single element for irrigation conduits where drippers are integrated (Figure I.6.a) or by two separate elements (conduits and drippers) in the case of using drippers (Figure I.6.b). The material generally used for such pipes is polyethylene.

I.6.a: I.6.b: I.6.c:

Figure I.6: (a) Micro-irrigation with integrated dripper, (b) Micro-irrigation with on-line dripper, (c) Labyrinth of a dripper taken with binocular microscope (source: PReSTI).

Drippers have a low flow rate between 0.5 and 8 ℓ/h under a pressure of 0.5 to 4 bar, depending if we have pressure compensating dripper (PC) or non-pressure compensating (NPC) (see section I.2.3). Through the dripper, water follows a complex and more or less long path (0.1 to 1 m), which induces a release of pressure. This pressure drop is generated by the friction of the water along the walls in the case of capillary dripper (uniform circuit), flow regulation is therefore proportional to the length of the capillary and to its inner diameter which is constant. In non-uniform circuit drippers (called baffles or labyrinth) (Figure I.6.c), sudden changes in the direction of water cause turbulence. This effect, added to friction along the walls, can cause pressure drop (Bounoua, 2010[40]).

Compared to other techniques of irrigation, micro-irrigation contributes to realizing water savings by reducing losses which is a real advantage for the development of irrigated agriculture in arid or semi-arid areas. These systems allow delivery with measuring the exact amount of water necessary for the crops, and their efficiency varies between 95% (new, well maintained) and 70% (Compaoré, 2006[65]). Drip-irrigation appears to be the most suitable technique for irrigation with wastewater since it reduces health risks by avoiding pathogen-dispersion problems by aerosols and minimizes contact of farmers and crops with water (Xanthoulis, 2006[299]). Fertilizers can also be associated with water delivery to improve crop yields through fertigation.

However, the high cost of installation and the drippers' sensitivity to clogging are the main disadvantages of using this type of irrigation. Clogging may involve different forms of organic and inorganic suspended materials due to the low section of water passage (on the order of mm^2). Moreover, in arid areas limiting watering can lead to salinity problems difficult to solve without the possibility of leaching by rain. Standards of wastewater used in irrigation are provided in Annex A.1.

Table I.4: Comparison of different irrigation techniques for use with treated wastewater

Irrigation Techniques	Advantages	Disadvantages
Surface irrigation	- Low investment costs - Low energy consumption - No projection risks	- Low efficiency - High water losses - Reduced automation
Sprinkler irrigation	- Better efficiency - Robustness - Average distribution rate (5 to 20 mm/h) - Automation	- Average investment cost - Energy dependence - Aerosols
Micro-irrigation	- Reduced water losses - No germs-dispersion problems due to aerosol - Easy automation	- High investment cost - Distributors sensitivity to clogging inducing low uniformity before clogging

I.2.2 Clogging problems in micro-irrigation systems

The clogging of drippers in drip irrigation systems is the major cause of reduced performance at plot level (reduction in flow rate, poor distribution of water) (Pitts et al., 1990[230]) and thus determines the life duration of the distribution system. Clogging can be physical (accumulation of suspended solids), organic (growth of algae and biofilm) and / or chemical (precipitation of chemical elements) and can be observed simultaneously. The clogging of drippers is often caused by a combination of different factors depending on the physicochemical quality of irrigation water, the hydrodynamic conditions, etc. where interactions between different factors play a major role.

I.2.2.1 Physical clogging

Physical clogging (or mineral clogging) is caused by suspended mineral particles in the water. It consists of sand particles, silts and clays ranging in diameter between 2 and 200 μm. The elements below 80 μm are not retained by the filters used in micro-irrigation.
They can act on the obstruction of the drippers in two different ways:

- Obstruction: when particle or aggregate dimensions are greater than the water section passage of the dripper (case of sand particles).

- Slow clogging or silting: When finer particles gradually settle in places where the water flow rate is low (Xanthoulis, 2006[299]). This attachment point serves as support for the next particles and disturbs the flow within the dripper. Deposits are located either in the labyrinth, or at the level of

the input grid designed to prevent large particles from entering the labyrinth (Figure I.7).

Furthermore, clay particles (less than 2 μm in diameter) can aggregate downstream of the filtering system and cause clogging (Pitts et al., 1990[230]; Bounoua, 2010[40]).

Figure I.7: Physical clogging observed in the labyrinth (Bounoua, 2010[40])

I.2.2.2 Chemical clogging

Clogging of drippers can also be caused by the chemical elements contained in the water (Figure I.8). These chemical elements can be inorganic solutes as well as acids along with hydroxides of calcium, magnesium, sodium and potassium (Ricci, 1952[243]). The main inorganic solutes are carbonates, bicarbonates, sulphates and chlorides of calcium, magnesium, sodium and potassium (Kemp, 1970[149]). For acids, the most important parameter is carbonic acid, but we can also have sulfuric and hydrochloric acids (Ricci, 1952[243]). These solutes are present in dissolved form and can precipitate as a result of reactions that can be generated by a change of temperature or pH (Xanthoulis, 2006[299]). The pH change is due to the behavior of the carbon system which is intimately involved in the control of pH as well as in the control of the precipitation of chemical elements. Temperature is also an important factor (MacAdam and Parsons, 2004[183]; Muryanto et al., 2014[202]). Lamm et al., 2007[162] have indicated that the solubility of calcium carbonate ($CaCO_3$) is related to the temperature and decreases as the temperature increases.

Figure I.8: Chemical clogging observed at the output of a conduct orifice (example of clogging by precipitation of $CaCO_3$) (source: PReSTI)

The most commonly encountered precipitates in irrigation equipment are calcium and magnesium carbonates, phosphates, sulfates, and ion precipitates in the ferric form (Nakayama et Bucks, 1986[206]; Hills and al., 1989[128]; Burt and Styles, 1994[48]; Burt et al., 1995[49]; Levy et al., 2011[168]). Calcium carbonate is well recognized as the major element in the chemical clogging of irrigation systems (Schwankel and Prichard, 1990[252]). In general, the contact of water which is rich in carbon dioxide and calcium with the open air, in case of open channel and storage, causes an increase in pH due to the loss of carbon dioxide which induces the precipitation of calcium carbonate (Gal et al., 2002[110]). Fertigation (distribution via irrigation of nutrients such as phosphorus-containing compounds, liquid ammonia, some trace elements [zinc, copper, manganese]) favor the precipitation of solutes (Pitts et al., 1990[230]) and accelerate the precipitation process, resulting in clogging.

I.2.2.3 Biological clogging

Biological clogging is driven by two types of organic matter:

- Inert or degraded organic material (grass, leaves, other microorganisms, etc.)
- Living organic matter that is formed by algae spores, algae themselves, colonies of bacteria as well as fungi or even microscopic shells that grow in the pipes where they find nutrients needed for growth.

The growth of algae requires light, which means it takes place mainly at the output of the orifices (Figure I.9.a). Biofilms generally grow on the walls of pipes and labyrinth drippers (Figure I.9.b).

I.9.a: I.9.b:

Figure I.9: biological clogging (a) by algae at the output of the orifice of the dripper (b) by biofilm in the labyrinth of drippers (source: PReSTI).

According to Magesan et al., (2000)[184], the increase of C/N ratio in wastewater is the cause of this phenomenon as it promotes increased microbial biomass and nematode population. However, these

same authors state that biological clogging occurs only in the case of $C/N > 50$, whereas the majority of domestic treated wastewater has a C/N ratio of about 2.5.

Biofilm development in irrigation systems is a serious source of clogging. Indeed, its presence enhances the adhesion of physical and chemical deposits such as calcium carbonate or particles that are suspended in the irrigation water (Gilbert et al., 1981[118]; Adin and Sacks, 1991[7]) which accentuates the clogging of irrigation systems. In addition, the precipitation and dissolution of minerals can be used for bacterial growth by significantly modifying the porous media (Perez-Paricio, 2000[224]).

Also, the practice of fertigation (input of nutrient through the drip irrigation system) can contribute to clogging by promoting the development of some microorganisms due to an additional intake of nutrient.

I.2.3 Types of drippers

Drippers are classified according to their incorporation in the lateral (point source and line source drippers), flow rate (PC and NPC drippers), form of pressure dissipation, and construction (long-path, tortuous path, short-path, orifice and vortex drippers) (Keller and Bliesner, 1990[150]; Enciso et al., 2005[95]). A basic component of dripper characteristics is the sensitivity of their flow to pressure changes. Water pressure is measured in bars, and most are designed to work best at 1.5 to 2.0 bars of pressure. There are two basic categories of drippers: Self-regulating or PC for pressure compensating and not self-regulating or NPC for non-pressure compensating.

Pressure compensating drippers or PC are designed to discharge water at a very uniform rate under a wide range of water pressures (same flow at 3.0 bars as at 1.0 bar). The pressure head exponent (Eq.I.3) must be less than 0.2 and close to 0. The flow rate is obtained by a diaphragm which, depending on the pressure, deforms and closes more or less the water passage orifice (Tiercelin, 1998[275]).

Non-pressure compensating drippers or NPC are also designed to discharge water at a uniform rate, but the water pressure needs to remain relatively constant or the discharge will vary (Stryker, 2001[265]). Depending on the flow inside the dripper, the value of x (Eq.I.3) should approach 0.5 (Cuenca, 1989[72]).

The relationship between the discharge and pressure can be described in the following equation (Karmeli, 1977[143]):

$$q = K_d H^x \tag{I.2}$$

where q is the dripper discharge; K_d is the constant of proportionality that characterizes each dripper; H is the working pressure head at the dripper; and x is the dripper discharge exponent that is resulting from the flow regime.

To determine K and x, the discharges (q_1, q_2) at two different operating pressure heads (H_1,H_2) must be known. The exponent x may be determined by measuring the slope of a log-plot of H versus q that is,

$$x = \frac{log\frac{q_1}{q_2}}{log\frac{H_1}{H_2}} \tag{I.3}$$

The value of x characterizes the flow regime and discharge versus pressure relationship of the dripper. The lower the value of x, the less discharge will be affected by pressure variations (Figure I.10). In fully turbulent flow, $x = 0.5$ and in laminar flow, $x = 1.0$. Non-compensating orifice and nozzle drippers are always fully turbulent with $x = 0.5$, and x is effectively zero for fully pressure compensating drippers. However, the exponent of long-path drippers may range anywhere between 0.5 and 1.0.

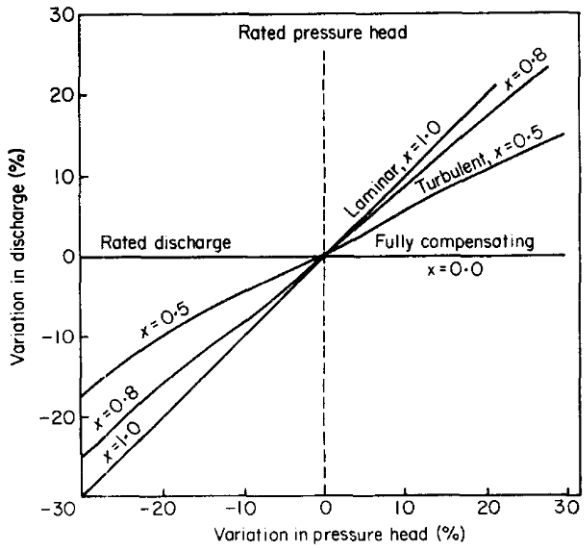

Figure I.10: Discharge variations resulting from pressure changes for dripper having different discharge exponents (Karmeli, 1977[143]).

The calculation of this curve is used to define the sensitivity of variation of the flow to pressure variations. This relationship intervenes in the calculation of maximum ramp length. According to the parameter x, the same pressure change will not result in the same flow change.

In this work, the NPC dripper will be used because it is the most commercialized and widely used in agricultural irrigation.

I.2.4 Hydrodynamics and flow behavior of drippers

In order to understand the fouling phenomena, various studies have focused on analyzing experimentally and numerically the flow along the dripper channel. Modeling works helped to further

characterize the hydrodynamics of these drippers and flow within the labyrinth and to estimate the velocity ranges and shear that may influence the agglomeration mechanisms. This data will be useful later as shear stress is a parameter that influences the growth and fragmentation of aggregates. Wei et al., (2006)[288] used the method of computational fluid dynamics (CFD) to calculate the distribution of pressure and velocity of the flow, and to calculate the relationship between pressure and discharge rate for channels with three different shapes: triangular, rectangular, and trapezoidal (Figure I.11). According to CFD simulations, the changes in pressure gradients occur mainly at the corner of the channels in each of the three labyrinth channels.

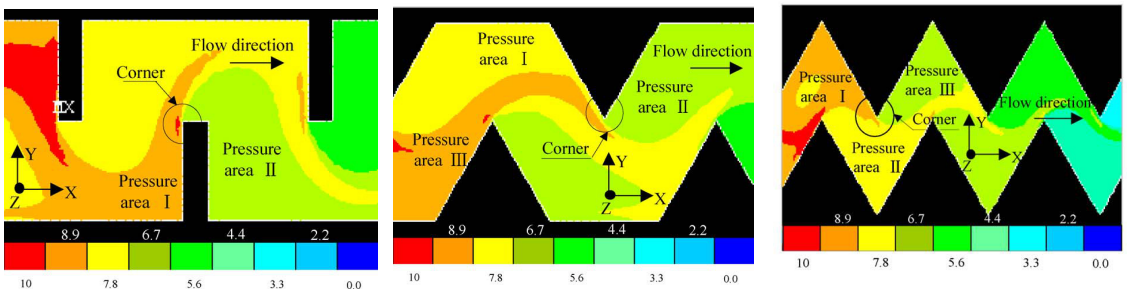

I.11.a: I.11.b: I.11.c:

Figure I.11: Pressure (mH_2O) distributions of the flow in partial channels in rectangular (A), trapezoidal (B) and triangular (C) shaped channels (Wei et al., 2006[288]).

When the flow arrives at the corner, the change in the direction of flow results in a large loss of local pressure, which is the main cause of hydraulic energy dissipation. Therefore, the pressure loss at the corner of the channel will finally determine the degree of hydraulic energy dissipation. The more the pressure varies, the greater the pressure loss will be. The pressure loss in the triangular dripper channels is higher than in trapezoidal drippers which, in turn, is higher than in rectangular drippers (Wei et al., 2006[288]). Consequently, a greater dissipation per unit length occurs in the triangular channel than in the rectangular or trapezoidal channels. In a labyrinth, the flow is divided into two parts: a main flow with a high velocity (red, orange and yellow colors) and a recirculation zone with a low velocity (blue color) (Figure I.12).

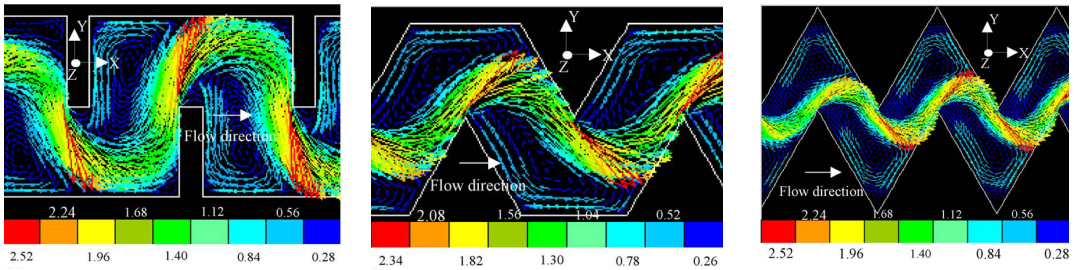

I.12.a: I.12.b: I.12.c:

Figure I.12: Velocity (m/s) distributions of the flow in partial channels in rectangular (A), trapezoidal (B) and triangular (C) shaped channels (Wei et al., 2006[288]).

The distributions of the velocities on the x–y plane shown in Figure I.12 clearly present the flow state of the water in the three channels. The shapes of the flow in the three channels present the same behavior. An obvious turning appears at the corner of the channel, which makes the flow move along an S-shaped path. In addition, some obvious swirl zones appear in the channels. These swirl zones will increase the dissipation of kinetic energy. The kinetic energy of the flow directly affects the efficiency of hydraulic energy dissipation, and the velocity of the flow along the length direction determines the discharge. Consequently, comparing the distributions of velocity along the flow path in the three channels, the rectangular channel has the highest discharge rate per unit of pressure.

I.2.5 Parameters influencing clogging in micro-irrigation

Dripper clogging has become the key obstacle to the development of drip irrigation technology. Several factors can influence the clogging of drippers, like hydraulic behavior which is affected by dripper channel structure (Adin Sacks, 1991[7]; Taylor et al., 1995[273]) and water quality especially when using effluents (Bucks et al., 1979[45]; Adin Sacks, 1987[5]; Ravina et al., 1992[240]; Nakayama et al., 2007[208]). Other parameters found in the literature can affect the clogging of micro-irrigation systems; we can cite the effect of flushing frequency (Lamm Camp, 2007[162]; Puig-Bargues et al., 2010[235]), the location of drippers along the laterals (Capra Scicolone, 1998[52]; Duran-Ros et al., 2009[89]) and the effect of chemical oxidants (Rav-acha et al., 1995[241]). In this work, we are especially interested in studying water quality parameters and dripper hydraulic behavior effects on clogging.

I.2.5.1 Geometry of drippers and hydraulic behavior

Dripper design can help preclude clogging. Pressure compensating drippers, integrated drippers (El-Berry et al., 2003[92]), labyrinth drippers (Capra Scicolone, 2004[53]) and high flow drippers (Ravina et al., 1992[240]) have been found to be the most resistant to clogging. Adin and Sacks, (1991)[7] conducted farmland experiments to study the clogging problem of drippers in wastewater irrigation systems. They found that clogging was closely related to the channel structure and suggested that channel design be improved. Shortening and widening the flow path, and rounding the straight edges on the protruding teeth are possible solutions to reduce dripper clogging . Wu et al., (2004)[297] carried out an investigation on the subsurface drip irrigation system which had been run for 8 years. They attributed dripper clogging to the attached granules and suggested optimizing the channel structure to solve this problem.

I.2.5.2 Water quality

Experiments were conducted with different qualities of treated wastewater to test the sensitivity of the different components of irrigation systems to clogging (Adin and Sacks, 1991[7]; Carpa and Scicolone, 2004[53] and 2005[54]; Liu et al., 2009[177]). It has been demonstrated that biofilm development and its role in dripper clogging is directly related to the quality of irrigation water. These waters are rich in suspended solids, dissolved chemical elements and nutrients.

When such water is used in drip irrigation systems, there is a strong potential for biofilm development. This phenomenon is observed primarily on filters, and then on drippers which will risk their clogging (Gilbert et al., 1979[117]; Bucks and Nakayama, 1984[47]; Adin and Alon, 1986[4]; Adin et al., 1989[6]). Clogging in irrigation systems is often worsened by water temperature changes because the solubility of some components depends on it . Calcium, magnesium and carbonates precipitate in pipes and drippers when temperature is high and pH is above 7.2. The solubility of $CaCO_3$ is inversely proportional to the temperature (Hills et al., 1989[128]). But if increasing temperature promotes precipitation, once the precipitate is formed, decreasing temperature does not dissolve the layer of $CaCO_3$.

These precipitates due to calcium carbonate accumulate in the narrow path of drippers and accelerate clogging. We should know that in surface irrigation systems, where pipes are black and are directly exposed to the sun, water temperature can reach 50°C in summer (Gamri et al., 2016[113]). The formation of phosphate as a precipitate depends on several factors (Boman, 1990[39]) such as pH, temperature and concentration. Ca^{2+} and $PO_4{}^{3-}$ form several combinations; three of them (hypo-, meta- and pyro-phosphate) are insoluble in water. Components that occur naturally as blushite ($CaPO_4$,2 H_2O) and whitlockite ($Ca_3(PO_4)_2$) see their solubility decrease with increasing pH (Bounoua, 2010[40]). For

instance, these parameters can affect the growth of bacteria, which tends to increase the risk of clogging.

Nakayama and Bucks, (1980)[204] established a grid to link water quality and clogging risks:

Table I.5: The different parameters of dripper clogging and their degrees of risk. (Data compilation from the following authors: Nakayama and Bucks, 1980[204]; Ayers and Westcot, 1985[22]; Pitts et al., 1990[230]; Couture, 2004[71])

			Degree of risk		
Parameter	**Symbol**	**Unit**	**Low**	**Average**	**High**
Suspended solids		ppm	< 50	50 - 100	> 100
pH	pH	1 to 14	< 7.0	7.8 – 8.0	> 8.0
Conductivity	ECw	dS/m	< 0.75	0.75 – 3.0	> 3.0
Total dissolved solids	TDS	mg/l	< 500	500 – 2000	> 2000
Sodium Adsorption ratio	SAR	mg/l	< 3	3 - 9	> 9
Residual Sodium Carbonate	RSC	mg/l	< 1.24	1.25 – 2.5	> 2.5
Alkalinity		mg/l	< 120	120 – 200	> 200
Bacterial population		ppm	< 10000	10000 – 50000	> 50000
Bicarbonate	HCO_3^-	mg/l	< 90	90 – 520	> 520
Chlorine	Cl^-	mg/l	< 142	142 – 355	> 355
Boron	B	mg/l	< 0.5	0.5 – 2.0	> 2.0
Nitrate- Nitrogen	NO_3-N	mg/l	< 5	5 – 30	> 30
Iron	Fe	mg/l	< 0.1	0.1 – 1.5	> 1.5
Hydrogen sulfide	H_2S	mg/l	< 0.2	0.2 – 2.0	> 2.0
Manganese	Mn^{2+}	mg/l	< 0.1	0.1 – 1.5	> 1.5

The earlier the clogging of drippers is detected, the easier it is to implement cleaning methods such as acid or chlorine injection. To better understand the mechanisms of dripper clogging, it is required to monitor the evolution of the pressure and flow (in filters and dripper lines) and to study the hydrodynamics of the drippers.

Part I.3

Biofilm

The most common mode of growth for microorganisms is in surface associated communities called biofilms (Costerton, 1978[66]; Metcalf and Eddy, 1991[193]; Sutherland, 2001[268]; Stoodley et al., 2002[264]; Syron and Casy, 2007[269]). Many types of microorganisms can be preset in wastewater, and they have been identified as a major contributor to dripper clogging in drip irrigation systems distributing reclaimed wastewater (Yan et al., 2009[301]).

I.3.1 Definition of Biofilm

Biofilms are an association of microorganisms adhering to each other, which grow on any solid-liquid interface (cellular tissues, marine medium, water pipes, medical and industrial equipment, etc.) (Donlan, 2002[83]; Costerton, 2004[69]). Contrary to what their name suggests, biofilms do not form a continuous film of bacteria; their structure is indeed very complex and heterogeneous, and contains microcolonies embedded in a polymeric extracellular matrix which they secrete (Characklis, 1973[58]). Their composition and nature vary depending on the environment and the conditions under which they are formed (Friese et al., 1997[107]; Eberl et al., 2000[91]). These aggregations of microorganisms are often separated by channels and pores allowing water flow, ions and nutrients (Clutterbuck, 2007[64]). The channels also serve to remove debris and metabolites (Fletcher, 1979[102]; Lewandowski, 2000[169]; Ivleva et al., 2010[137]). Figure I.13 shows some examples of biofilms observed with different microscopic techniques. More details about the composition and structure of the biofilm are found in Annex A.2.

I.3.2 Advantages and disadvantage of biofilms development

Biofilms are commonly used for the treatment of wastewater in fixed cultures processes (Lazarova and Manem, 1995[164]; Gebara, 1999[115]; Nicolella et al., 2000[211]). They play a major role as bio-physico-chemical reactors in the environment. They are involved in controlling the organic matter concentration and metal contaminants in natural and anthropogenic ecosystems (Battin et al., 2003[29]; Horn et al., 2003[131]; El Samrani et al., 2004[94]; Houhou et al., 2009[132]).

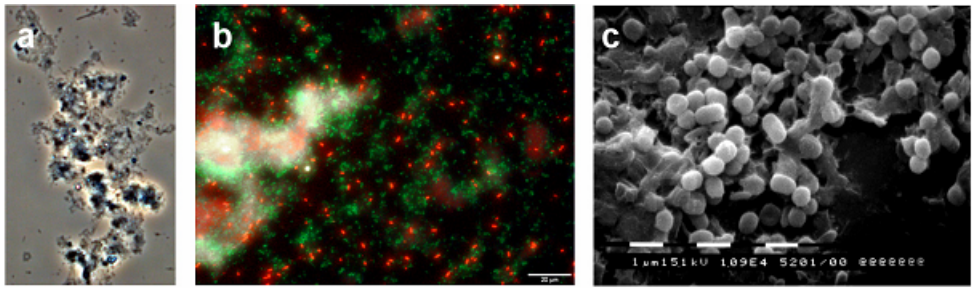

Figure I.13: Images of mixed strain biofilms using three different microscopic techniques. a) Phase contrast micrograph, b) FISH/EPI-fluorescent micrograph, c) SEM image of 3D biofilm. (Andersson, 2009[15]).

The presence of biofilm is undesirable in certain applications where their development can lead to technical, economic and / or health problems. In irrigation systems, biofilm development causes a pressure loss in the pipes by increasing the water friction force (Picologlou et al., 1980[227]). In their research, Li et al., (2012)[171] examined the development of biofilm in micro-irrigation system pipes used with treated water from two different treatment processes. The detachments of biofilm fragments from pipes are deposited in drippers' labyrinths, causing their obstruction. These have low flow section (to the millimeter) and are thus very susceptible to clogging (Gamri et al., 2013[111]). In addition, the biofilm surface is highly adsorbent and the suspended elements in water (particles of clay, sand or other elements) can easily adhere, resulting gradually in the total obstruction of the system (Gilbert et al., 1981[118]).

I.3.3 The different stages of biofilm development

The development can be described by a series of steps influenced by various factors (see paragraph I.3.4). The different steps have been extensively studied and defined (Characklis, 1981[59]; Van Loosdrecht et al., 1989[179]; Costerton, 1999[68]; Gauthier, 2002[114]; Liu and Tay, 2002[176]). The transport of bacteria to the wall, their adherence, their growth and maturation phases and their detachment

phenomena are summarized in Figure I.14.

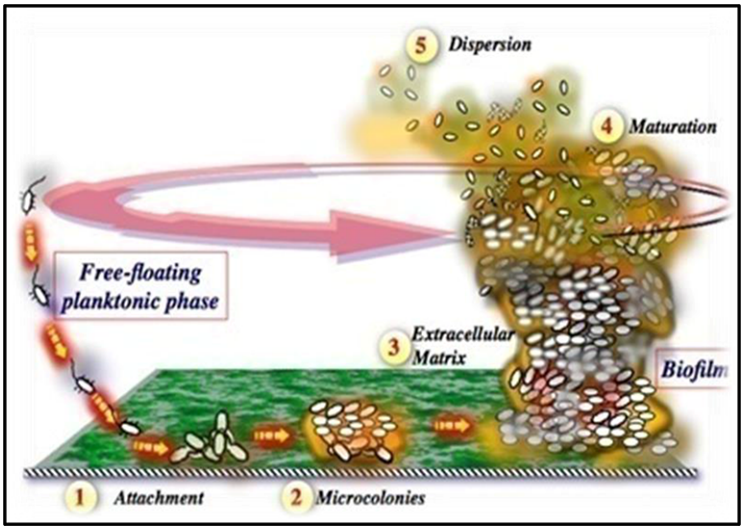

Figure I.14: Stages of biofilm development (1) initial attachment; (2) production of exopolysaccharide (EPS) by bacteria; (3) replication of early colonizers; (4) maturation; (5) dispersion (Sehar and Naz, 2016[253]).

I.3.3.1 The transport of bacteria

The adhesion of bacteria to the surface requires a rapprochement which is provided by transporting them from the fluid to the surface. In a hydrodynamic system, the transfer of bacteria to the surface will be provided by both convection and diffusion (Rijnaarts, 1994[244]; Ginn et al., 2002[119]; Khalizadeh, 2009[152]). This transfer will be faster and influenced by the speed and the flow nature. In this case, the higher is the fluid velocity the higher will be the transport by convection. The nutrient concentration near the surface of the biofilm promotes its growth (Mueller, 1996[200]; Busscher and Van der Mei, 2006[50]).

I.3.3.2 Adhesion

The adsorption of an organic monolayer occurs several minutes after the contacting with the liquid medium. The adhesion of bacteria to the support depends on the properties of the support (see paragraph I.3.4.2) and on the bacteria cell wall properties (hydrophilic / hydrophobic character, charge, physical and electrostatic forces and bonds (Van Loosdercht et al., 1987[178] and 1989[179]; Costerton, 1999[68]; Gauthier, 2002[114]) that vary depending on the bacterial species and environmental factors (see paragraph I.3.4.1) (Characklis, 1981[59]; An and Friedman, 1997[14]; Beloin, 2008[31]). EPS production (Skillman et al., 1999[257]) and the presence of attachment and motility proteins (Goller, 2008[122]) are important factors for bacterial adhesion. More details about EPS are found in Annex A.3.

I.3.3.3 Growth phase and maturation

Once attached to the surface, the microorganisms begin to multiply and produce the necessary exopolymers to form the skeleton of the biofilm (Costerton, 1999[68]; Gauthier, 2002[114]; Khalizadeh, 2009[152]). These EPS will form on the surface, and complexes will ensure the adsorption of other bacteria which allows increasing the thickness of the biofilm. The biofilm begins to grow by division and bacteria multiplication (Lazarova and Manem, 1995[164]; Costerton, 1999[68]; Andersson, 2009[15]). At this stage, bacteria multiplication and biofilm growth are strongly linked to the environmental factors (see paragraph I.3.4.1). The maximum thickness of the biofilm is reached during the maturation phase (Clutterbuck, 2007[64]). This phase is characterized by an equilibrium which is created between the biomass that grows in the presence of substrate (see paragraph I.3.4.1) and the one which is detached from the biofilm through the action of the hydrodynamic forces (see paragraph I.3.4.1). The detached cells are conveyed by the flow and can colonize the system again.

I.3.3.4 The detachment

When the biofilm reaches the stage of maturity, nutrients lack, biofilm age, the amount of biomass fixed, physical, chemical, and biological stresses and hydrodynamic conditions plays a very important role in the structure, density and thickness of the biofilm, and subsequently in its activity and the transfer phenomena (Lazarova and Manem, 1995[164]; Wäsche et al., 2002[287]). These factors are responsible for the biofilms detachment and re-dispersion into the environment (Abrahamson et al., 1996[2]; Andersson, 2009[15]; Mahfoud et al., 2009[185]) favoring the colonization of new ecological niches and therefore the formation of other biofilms (Clutterbuck, 2007[64]). The detachment mechanisms described in the literature are erosion, abrasion and sloughing. Erosion is a mechanism of detaching small parts of the biofilm. It depends essentially on the increase of the shear stress (see paragraph I.3.4.1) and / or the thickness of the biofilm results in an increase in erosion rates (Trulear and Characklis, 1982[278]; Telgmann et al., 2004[274]). Similarly, abrasion causes the detachment of small parts of the biofilm. However, it is generated by the collision of solid particles with the biofilm (Gjaltema et al., 1997[120]; Derlon et al., 2008[78]). Unlike the first two mechanisms, sloughing causes the detachment of large aggregates (Telgmann et al., 2004[274]) which increases the heterogeneity of the biofilm. The limitations of nutrients and oxygen can be at the origin of this process (Applegate et al., 1991[20]; Hunt et al., 2004[134]).

I.3.4 Factors influencing the different stages of biofilm development in micro-irrigation systems

I.3.4.1 Environmental factors

The formation and dispersion of a biofilm depends, according to bacteria, on different environmental factors (temperature, pH, substrate availability, hydrodynamic conditions) (Fletcher, 1988[103]; Donlan, 2002[83]). Some bacteria can adapt to different environments by genetic modifications (Clutterbuck, 2007[64]). Others are influenced by stressful environmental conditions (high concentrations of salts, high temperatures, extreme variations of pH) that decrease the potential of bacterial adhesion to surfaces (Goller, 2008[122]).

a) Temperature Drip-irrigation is widely used in arid and semi-arid regions where the temperature is generally very high especially during the day (Qin et al., 2005[236]; Verheye, 2009[284]). Measures carried out in the irrigation material tests and research laboratory (Irstea Aix en Provence) have shown that the water temperature can exceed $50°C$ in polyethylene pipes during the summer period in the absence of flow (Gamri, 2013[111]). Temperature strongly influences the development of biofilm as it affects the metabolic and enzymatic activity of bacteria as well as their surface properties (Van Loosdrecht et al., 1990[180]; Goller, 2008[122]).

In the work of Qian et al., (2017)[237], the effect of temperature was investigated on biofilm formation in micro-irrigation devices. Two series of experiments were carried out, one at ambient temperature and the second at daily temperature cycle. Daily temperature cycle was varied from 20 to $50°C$. The increase in temperature had a negative impact on the biofilm, consequently greatly reducing its development. Biofilm volumetric coverage for ambient temperature at day 30 of cultivation was 40% versus 10% for the same time but under daily temperature variations. According to Pirt, (1985)[229] the optimum temperature of $45°C$ for the biofilm development should not be exceeded. When this temperature is exceeded, enzymes can be deactivated and surface electrical properties changed (Rogers et al., 1994[247]; Briandet et al., 1999[44]). This will reduce or delay the formation and the growth of biofilm in pipes and drippers.

b) pH Many irrigation water sources are alkaline with pH values between 7.2 and 8.5 due to a high content of calcium, magnesium and bicarbonates (hard waters) (Mengel, 1994[191]). At the same time, phosphate and nitrogen addition by fertigation can lower the water pH to 6 - 6.5 (Imas and Cohen, 2009[136]). For this reason, pH variations can be observed and this may influence the adhesion of bac-

teria to support (Gordon et al., 1981[123]). In response to a change in pH, microorganisms change their metabolism (Yohannes et al., 2004[302]) as well as their surface properties (Briandet et al., 1999[44]) which induces variations in the electrostatic forces which are the origin of support adhesion. Chen et al., (2005)[61] highlights the impact of pH medium changes on *Pseudomonas fluorescens* adhesion. The growth of *P. fluorescens* biofilms is favored at pH = 7 with the establishment of a uniform and thick biofilm. A thin and irregular biofilm is observed at pH = 5.5. Similarly, Stoodley et al., (1997)[262] observed a more compact biofilm at pH 3 (69%) compared to pH = 10. This contraction of the biofilm structure is related to the neutralization of the carboxylate groups of the EPS by protonation. This phenomenon eliminates the electrostatic repulsion of these groups which modifies the structure of biofilms. In addition, the microorganisms produce organic acids that alter the physicochemical conditions of the medium (Chen et al., 2005[61]).

c) Substrate availability As seen in paragraph I.1.3 and in Table I.3, wastewaters and treated wastewaters contain nutrients that can be used as a substrate for biofilm development. The growth of biofilm is influenced by the consumption of nutrients and the excretion of products. The necessary elements for growth of micro-organisms are in the first place carbon, nitrogen and phosphorus. The ratio of C/N/P on a chemicaL oxygen demand (COD) basis for optimal biofilms development is equal to 100/10/1 (Kujundzic, 2007[159]).

The importance of substrate presence in the medium was demonstrated by Melo and Vieira, 1999[190]. They have observed that substrate removal leads to biofilm detachment while removing bacteria does not disturb its stability. Substrate intakes especially in carbon influence the morphology, the formation and the maturation of biofilms. At high concentrations, the specific growth rate (μ in Eq.I.4) is independent of the concentration of nutrients, but at low concentrations the specific growth rate is a strong function of the nutrient concentration. Such a relationship was predicted by Monod, 1940[197]; however, Monod's equation does not predict the relationship over the entire range of nutrient concentration:

$$\mu = \frac{\mu_{max} S}{K_S + S} \tag{I.4}$$

where μ is the specific growth rate (1/time), μ_{max} is the maximum specific growth rate (1/time) for the culture, S is the substrate concentration (mass/volume), and K_S is the half-saturation constant (mass/volume), also known as the affinity constant.

Winjeyekoon et al., (2004)[295] confirmed that a low concentration promotes a porous biofilm with larger transfer phenomena but a high substrate concentration promotes the development of a compact biofilm with low porosity. Chen et al., (2005)[61] demonstrated that *P. fluorescens* adhesion, in-

creases with the concentration of glucose up to a limit of 30 mg/L at which point the adhesion is reduced. Increasing the concentration of various cations (Na^+, Ca^{2+}, Fe^{3+}, etc.) influences the attachment of *Pseudomonas fluorescens* to glass surfaces, reducing the repulsive forces between the negatively charged bacteria and the glass surfaces (Fletcher, 1988[103]).

d) Hydrodynamic conditions The hydrodynamic conditions, and mainly the flow velocity and the forces that result strongly influence the structure and morphology of the biofilm, its activity (production of exopolymer and metabolites) and the distribution of microcolonies (Costerton, 1999[68]; Stoodley et al., 1999[263]; Busscher and Van der Mei, 2006[50]).

The hydrodynamic conditions are not the same in all the positions of a micro-irrigation system which affects biofilm development. They are different, depending on whether it was at the labyrinth level or in the central zone of the dripper or even inside the pipes.

In general, the liquid velocity at the solid-liquid interface is negligible, and a boundary layer is formed. The thickness of this layer depends essentially on the linear velocity of the liquid. Thus, this layer becomes thicker with low flow velocities and the adhesion of bacteria is slowed. However, higher flow velocities amplify the phenomenon of adhesion, but excessively high speeds determine shear forces on the biofilm which induce detachment of bacterial cells (Donlan, 2002[83]; Horn et al., 2003[131]; Busscher and Van der Mei, 2006[50]).

Chen et al., (2005)[61] observed that the adhesion strength of *P. fluorescens* biofilms increases with the flow rates (0.6, 1 and 1.6 m/s) and that biofilms obtained at high speed are denser. The high velocities also favor the production of EPS which promotes maintenance of the structure of biofilms. It was also shown that the flow conditions and in particular the shear stress has an impact on biofilms' bacterial composition. Rochex et al., (2008)[246] observed that increasing shear stress reduces the diversity of bacterial communities that colonize surfaces. The work of Stoodley et al., (1999)[263] was carried out to understand the behavior of a biofilm in response to shear stress. The results show that the thickness of the biofilm can be significantly reduced following the application of a high shear stress. By varying the shear stress from 0 to 10.11 Pa, corresponding to Reynolds numbers of 0 - 5328, the thickness of the biofilm is reduced by 25% (51 ± 19 μm to 37 ± 12 μm), contributing to an increase of its density and a decrease of its porosity. Thus, biofilms can adjust their internal structure to withstand the hydrodynamic stresses.

Furthermore, a sudden increase in the flow rate can cause the detachment of a part or all of the biofilm (Characklis, 1981[59]; Trulear and Characklis, 1982[278], Bakke, 1986[26]; Melo and Vieira, 1999[190]; and Telgmann et al., 2004[274]). The detachment is observed in the seconds following the change in hydrodynamic conditions (Horn et al., 2003[131]). To characterize the detachment of biofilm, Horn et al., (2003)[131] made measurements of the suspended material at the outlet of pipes in which

the biofilm was developed and reached a thickness of 1000 microns. Increasing the flow rate from 0.6 to 1.2 m/s allows measuring a concentration at the outlet of pipes on the order of 900 mg/L within seconds following the variation in the hydrodynamic conditions but no information is provided regarding the size of the detached elements. Derlon et al., 2008[78] characterized the detachment of biofilm developed under different conditions and subjected to shear stresses up to 13 Pa in a Couette reactor and in a low shear stress reactor (LSSR). Biofilms were characterized in terms of attached volatile solids per support surface (mg AVS$/cm^2$). Biofilm was developed with wastewater that has a substrate loading rate of $4g$ COD$/m^2/d$ and under different shear stress. Three zones of detachment related to the range of shear stress were highlighted. The detachment is greater at the first zone (for shear stress lower than 0.3 Pa) than at the second (for shear stress ranging from 0.3 to 2 Pa), the third zone can resist to shear stress magnitude up to 13 Pa. At the first zone, the detached biofilm rate is estimated to be 0.55 mg AVS$/cm^2/Pa$ as opposed to 0.1 mg AVS$/cm^2/Pa$ at the second zone. This work shows that the resistance to the detachment of biofilms increases with depth. The detachment mechanisms involved changes of the biofilm structure. Detachment by erosion promotes a smooth, uniform biofilm, while a heterogeneous and porous biofilm is observed following a detachment by sloughing (Van Loosdrecht et al., 2002[181]).

I.3.4.2 The properties of the support

Any material in contact with a fluid containing bacteria is a potential support for biofilm formation. In irrigation systems, the materials of water transmission pipes consist only of plastic (generally polyvinylchloride (PVC) and polyethylene (PE) Gamri, 2013[111]).

Metallic material (copper, brass, etc.) may be encountered in some parts of the assembly in particular the connections and valves used. The attachment surface properties are involved in the phenomenon of surface adhesion. The choice of materials used as support also seems to be very important. Bacterial adhesion to supports is influenced by its chemical properties (Lehtola et al., 2004[167]), its roughness (Yu et al., 2010[303]) and its hydrophobicity (Hogt et al., 1983[129]).

a) Chemical composition of the surface Some surfaces release substances which can inhibit bacterial attachment to the surface and slow the development of the biofilm. Thus it has been shown that biofilm development is less important on copper surfaces (Lehtola et al., 2004[167]; Van Der Koiij et al., 2005[282];. Morvay et al., 2011[199]) as long as it does not corrode.

b) Surface roughness The roughness is characteristic of the material used and its condition (new or used). This parameter is involved as it promotes the attachment of microorganisms that may be housed in the grooves (Characklis, 1990b[60]) where the attachment surface is increased. On a roughened surface the repulsive forces are less (Donlan, 2002[83]) and in addition the bacteria are protected from shear stress (Van Loosdrecht et al., 1990[180]) and from disinfectants or antiseptics.

c) Physicochemical properties of the surface. The physicochemical properties of the surface can influence the rate of attachment and its magnitude. Polymer surfaces such as PE, PVC or Teflon which can be found in irrigation systems are characterized by their hydrophobic character in contrast to metallic surfaces (An and Friedman, 1997[14]). Adherence to polymers is influenced by the characteristics of the support and the bacterial surface (Verrier et al., 1987[285]). Hydrophobic microorganisms like *C. albicans*, for example, are more strongly adsorbed to hydrophobic and unpolarized surfaces such as Teflon or other plastic materials, as on hydrophilic materials such as glass or metals. The cells are able to bypass the repulsive forces that they can exert on the substrate, via the action of hydrophobic bonds (Bendinger, 1993[32]). Unlike the hydrophilic bacteria attach better to hydrophilic surfaces (Hogt et al., 1983[129]). Metallic surfaces are thus more favorable than plastic supports to biofilm development.

Saur et al., (2017)[251] studied biofilm development on PVC and polypropylene (PP) plates. Based on previous work, the surface roughness is essentially the same but there is a significant difference between PP and PVC surface energy. PP surface energy was considered lower than PVC surface energy, and this affects biofilm development. According to the results, the biofilm surface coverage on PP surface is two times higher than on PVC surface.

Part I.4

Characterization of chemical and biological clogging in micro-irrigation systems using treated wastewater

As mentioned earlier, dripper clogging can result from physical, chemical, and biological deposits. This study only focuses on chemical and biological clogging, and the interaction between them. Part I.3 in Chapter I shows the parameters that influence biofilm development, but some of them also influence chemical precipitation like pH and temperature. The high concentration of water in salts, bicarbonates, manganese, total iron, hydrogen sulfide, calcium, and magnesium increase the possibility of chemical precipitation and dripper clogging, particularly if the irrigation water is highly alkaline. Calcium carbonate or lime is the most common precipitate (Schwankel and Prichard, 1990[252]).

Many researchers have studied chemical and/or biological clogging of micro-irrigation systems. Some of the studies were in the field and used real effluent (Hadfi et al., 2011[125]; Tarchitzky et al., 2013[271], Katz et al., 2014[148]), and others took place in the laboratory and used real or synthetic effluents (Liu and Hung, 2009[177]; Gamri et al., 2013[111]).

Tarchitzky et al., (2013)[271] used different treated wastewater (TWW) to characterize the fouling layers inside pipes and drippers. In parallel, dripper flow rates were measured in situ. The age of analyzed drippers is between 2 and 16 years. The average summer temperature is between 31 and 34°C.

Total and volatile solids, Scanning Electron Microscopy equipped with Energy Dispersive X-ray spectroscopy (SEM-EDAX) and Diffuse Reflectance Infrared Fourier Transform Spectroscopy (DRIFTS) were used to determine the quantity and chemical characteristics of the fouling. Fouling was found in all of the dripper laterals, and it contained a high percentage of organic matter (OM), except for two

instances where the material was mainly inorganic. The organic matter of the fouling in the laterals and dripper were essentially aliphatic (2850 and 2930 cm^{-1}) and amid (1560, 1640-1655 cm^{-1}) (Figure I.15). A high correlation was found between the content of total and organic carbon in the fouling and the total phosphorus concentration, the sum of calcium and magnesium concentrations and the TWW pH.

According to Andritsos and Karabelas, (1999)[16], inorganic precipitation increases when pH increases. As in the work of Tarchitzky et al., (2013)[271], initial inorganic or mineral precipitation seems to favor biofilm development.

The inorganic material obtained after combustion at 400°C is composed of silica i.e., clay (1043 cm^{-1}) (Figure I.15).

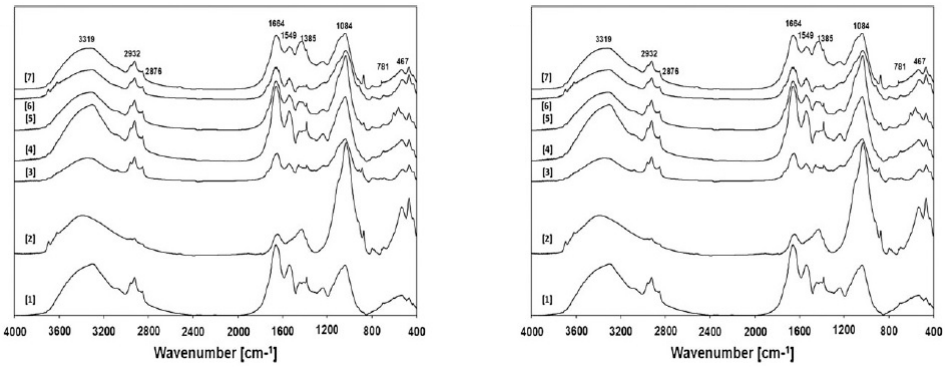

I.15.a: I.15.b:

Figure I.15: DRIFT spectra of the fouling material: (a) before combustion; and (b) after combustion at 400°C (Tarchitzky et al., 2013[271]).

In addition, for systems containing high quantities of fouling the correlation between equipment age and the amount of accumulated total solids (TS) was high: the older the equipment, the higher the TS concentration was. The concentration of volatile solids (VS) was highly correlated with the age of the irrigation system. This is due to a modification of the surface property that favor biofilm attachment and development.

Another study was done to characterize fouling in micro-irrigation systems using treated wastewater. Katz et al., (2014)[148] used TWW to evaluate fouling inside the drippers and pipes. Chlorination and acidification were performed to evaluate the efficency of chemical treatments at preventing fouling accumulation. Dripper flow rate and coefficients of variation (CV) were monitored to investigate fouling inside the drippers. Results show that the organic composition of the fouling is mainly composed of aliphatic and amide groups, and the inorganic groups are composed mainly of silica, reflecting the results of Tarchitzky et al., 2013[271].

A comparison between dripper and pipe deposits shows that biofilm survive better inside the drip-

per than in the pipe even after chlorination treatment. Biofilms were detected inside drippers even if the pipe was clean. This can be attributed to a denser biofilm because of high flow velocity inside the dripper. Denser EPS prevents biocide penetration into the biofilm, thereby protecting the micro-organisms (Li et al., 2011[170]; Katz et al., 2014[148]).

According to Zhang and Bishop, (2003)[306], chlorination of pipes to eliminate organic matter (OM) may favor biofilm development in drippers. Chlorination decreases the size of OM which will thus become more available to the microorganisms in drippers.

Katz et al., (2014)[148] underline that biofilm development inside drippers narrows the water's flow path. This decreases the interface between the bacteria and the solution, and favors biofilm development by enhancing microorganism survival. This biofilm development causes a sharp change in the flow rate and CV.

Chemical precipitation also has an effect on the dripper flow rate and the performance of micro-irrigation systems but no study has been done using treated wastewater. The fouling of the micro-irrigation systems due to the precipitation of the minerals was done either with drilling water and spring water (Hills et al., 1989[128]; Hadfi et al., 2011[125]) or with saline water (Lili et al., 2016[174]).

In the work of Hadfi et al., (2011)[125], only chemical precipitation and more precisely calcium carbonate was investigated in irrigation systems. The origin of the water comes from wells, and that is why a high concentration in calcium and magnesium can be observed. The hardness of water reached 118°F (1°F corresponding to $4\ mg/L$ of Ca^{2+} ions). According to Nguyen, (1996)[210] when the hardness exceeds 25°F, chemical clogging may occur. Water temperature and pH was measured at the outlet of the well. The temperature varied between 22 and 50° C, and pH varied between 6.68 and 7.3.

Samples of fouling were collected from irrigation pipes. Their identification was carried out on the basis of their chemical analysis and their X-ray diffraction (XRD) examination. The ion calcium is the major element, and it is present in the sample at 39.2%. If the fouling consists of a pure phase of $CaCO_3$, the theoretical content of Ca^{2+} would be 40.04%. Therefore, the sample is at 98% of calcium carbonate. The X-ray diffraction spectrum (Figure I.16) shows the presence of calcite and quartz in the sample.

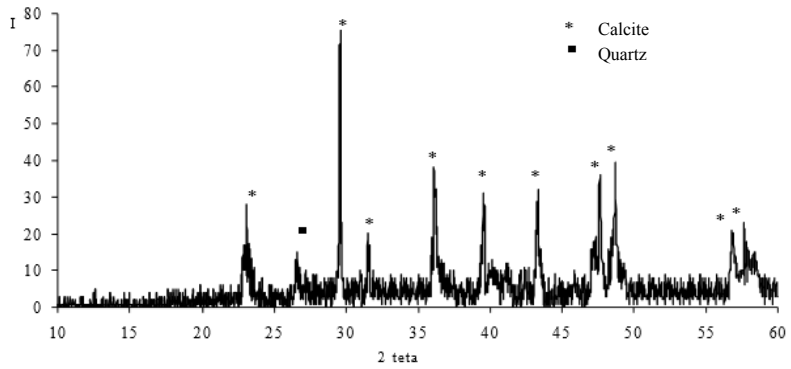

Figure I.16: X-ray diffraction of the fouling collected from irrigation pipes (Hadfi et al., 2011[125]).

Lili et al., (2016)[174] also found that the dominant material associated with chemical clogging was calcium carbonate ($CaCO_3$) when using saline water for micro-irrigation. The dripper clogging parameter (discharge ratio variation (Dra) and coefficient of uniformity (CU)) showed a significant positive relationship between the calcium and magnesium carbonate content (%) but a negative correlation with quartz. The higher the inorganic precipitation, the more serious is dripper chemical clogging.

Some studies have focused on the interaction between biofilm development and inorganic precipitation. No studies have focused on this interaction in micro-irrigation condition using treated wastewater, but a link can be made between those works and the present work concerning the quality of water and the operating conditions. Most water sources contain carbonates and bicarbonates, which can serve as inorganic energy sources for certain slime forming autotrophic bacteria. Several types of slime-forming organisms can deposit onto the tubing walls and contribute to clogging, particularly in the presence of Fe^{2+} and H_2S (Nakayama et al., 2007[208]). Several factors can bacterially induce calcium carbonate precipitation, such as carbon source, nitrogen source, pH and EPS (Obst et al., 2009[216]; Chahal et al., 2011[56]; Priya et al., 2016[233]). But the mechanisms of carbonate nucleation and growth via microorganisms are, however, not yet fully understood.

Some bacteria can increase the pH of their micro-environment and lead to calcium carbonate precipitation. For example, Chahal et al., (2011)[56] shows that ureolytic bacteria influence calcium carbonate precipitation by the production of urease enzyme which catalyzes the hydrolysis of urea to CO_2 and ammonia, resulting in an increase of the pH. Kah and Riding, (2007)[141] proved that photosynthesis done by cyanobacteria result in a rise of the pH in the micro-environment of the cells, which leads to significant $CaCO_3$ supersaturation followed by $CaCO_3$ precipitation.

The composition of media, regarding carbon and nitrogen sources, plays an important role in calcium carbonate precipitation. According to Priya et al., (2016)[233], glucose, lactose, beef extract and peptone showed higher growth rate of calcium carbonate precipitation than sucrose and yeast extract for both *Bacillus sp* and *Pseudomonas sp*. These bacteria are known for their ability to precipitate calcium

carbonate.

Macromolecules present on the surface of bacteria, in EPS, have anionic functional groups and negative charged ions also play an important role in $CaCO_3$ precipitation (Fortin et al., 1997[104]). It favors the adsorption of divalent cations such as Ca^{2+} making microorganisms' cell walls act as crystal nucleation sites (Douglas and Beveridge, 1988[86]; Rivadeneyra et al., 1998[245]).

Obst et al., (2009)[216] developed a model of the temporal and spatial evolution of calcite precipitation mediated by cyanobacteria of the strain *S. leopoliensis* PCC 7942. Two layers of EPS are observed (Figure I.17). A thin layer closely bound to the cell surface form a capsular-like structure and a second layer of loosely bound EPS (Figure I.17.a). In their model Ca^{2+} ions adsorb onto both layers of EPS preferentially to the closely bound type (EPS) (Figure I.17.b). The nucleation of amorphous aragonite-like $CaCO_3$ starts before the nucleation of calcite and the nucleation is within the first EPS layer (Figure I.17.c). Once calcite nucleates and starts precipitating, the aragonite-like $CaCO_3$ is no longer stable and dissolve (Figure I.17.d).

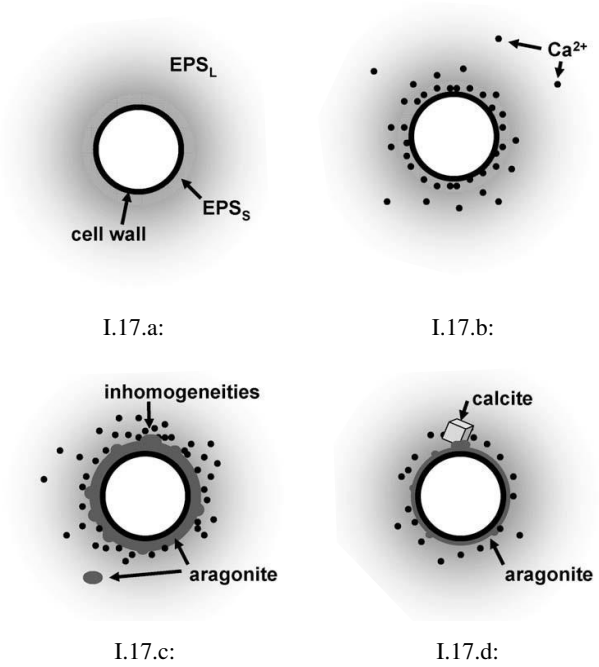

I.17.a: I.17.b:

I.17.c: I.17.d:

Figure I.17: Schematic outlining proposed model of the temporal evolution of calcite nucleation on the surface of *S. leopoliensis* PCC 7942 (Obst et al., 2009[216]).

This model proves that even the bacteria were exposed to shear stress and that a fraction of EPS and Ca^{2+} were ripped off, a lower area of EPS still remaining at the surface. The remaining EPS still have an embedded aragonite-like $CaCO_3$ which is a reversible precipitation mechanism once the supersaturation drops due to the abiotic precipitation of calcite.

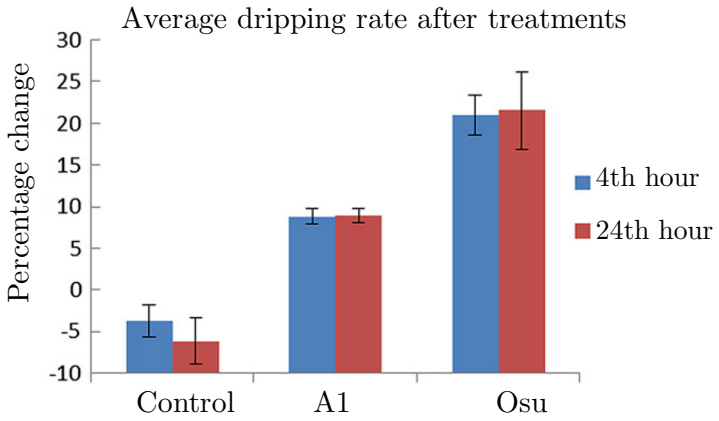

Figure I.18: Average flow rates of clogged drippers after 4h and 24h of treatment with two bacterial strains (A1) and (Osu). The columns represent the mean values and the error bars represent the standard error of the mean (SEM) (Eroglu et al., 2012[96]).

Eroglu et al., (2012)[96] developed a method with two bacterial strains to dissolve $CaCO_3$ and unclog the drippers clogged with calcium carbonate precipitation. After 4h and 24h of flushing, flow rates decreased 5% in the negative control but increased 10% for *Lactococcus garvieae* strain (referred to as A1) and increased 20% for *B. subtilis* OSU-142 (referred to as OSU). Results are illustrated in Figure I.18. There are no significant differences between 4h and 24h.

Conclusion and thesis objectives

The reuse of treated wastewater in micro-irrigation seems to be a good solution to fight water scarcity. Treated wastewater contains a multitude of elements that may be beneficial or harmful to the soil and the environment. Standards have been developed to regulate the discharge of these waters into the nature and their reuse for irrigation. Even if standards are generally respected, the risk of pipes and irrigation drippers clogging is always high. Water contains nutrients and dissolved salts that under favorable pH and temperature conditions may lead to biofilm development and mineral precipitation. Understanding the mechanisms of biofilm formation and chemical precipitation can help us to avoid biological and chemical fouling in irrigation systems when using treated wastewater. According to the state of art some minerals, dissolved in water will react and precipitate following a change in operating parameters. These elements in the dissolved or precipitated form can interact with the biofilm development and depending on the case either favor or disfavor their development. On the other hand several parameters are involved in biofilm colonization and development, such as water quality, environmental factors, hydrodynamic conditions, properties of the surface, etc.

The objective of this thesis is to bring new elements on the reuse of treated wastewater in micro-irrigation. Many researchers are interested in this field and a lot of study with treated wastewater in the laboratory or in the field has been made. What is new in this study is that for the first time a Taylor-Couette reactor will be used to reproduce shear stress found in drippers and pipes using real treated wastewater. The aim is to follow in the same time biofilm development, chemical precipitation and the interaction between them. Interaction between biofilm and chemical precipitation using treated wastewater under micro-irrigation condition is very little argued in the literature. So we found it interesting to develop it in this thesis especially that the research team where the work were done work on irrigation materials. Therefore finding methods and solutions to limit or avoid clogging of drippers is in their greatest interest.

In addition a geochemical model will be used also for the first time as a chemical precipitation indicator to be able to predict the quantity and the quality of mineral deposition. The new numerical methods will be validated thru laboratory experience.

The originality of this work is also based on the study of calcium carbonate and its interaction with biofilm. Several biomineralization studies have been carried out on the biofilm's ability to precipitate calcite but no study has been done on the effect of calcium carbonate on the development of biofilms in pipes and drippers.

Chapter II

Materials and Methods

Introduction

In this materials and methods chapter, the objective is to present the different setups and analysis in order to understand and identify the parameters that affect chemical precipitation, biofilm development, and their interaction in irrigation systems using TWW. These two phenomena contribute to the clogging of drippers and fouling of pipes which cause decreased micro-irrigation performance.

The first part of this chapter focuses only on mechanisms that influence chemical precipitation in irrigation. Temperature, pH and CO_2 partial pressure were investigated. Laboratory experiments were done in batch reactors by varying water pH and temperature to induce precipitation of dissolved compounds. X-ray diffraction (XRD) and thermo-gravimetric analysis (TGA) are used to qualify the precipitate. Knowing the composition of chemical deposits helps to manage and reduce the chemical clogging problem. PHREEQC as a geochemical software was used to predict the quantity and the quality of chemical precipitation according to the interaction of different parameters such as water quality, pH, temperature, concentration of dissolved carbon dioxide, etc. The correlation between modeling and laboratory experiments is meant to validate PHREEQC as an accurate model for predicting chemical clogging under micro-irrigation conditions.

The second part of this chapter focuses on biofilm development under different shear stresses encountered in irrigation systems. The possible presence of chemical precipitation with biofilm development was also investigated. A Taylor-Couette reactor (TCR) was designed and built in the laboratory to reproduce the range of shear stress found in irrigation pipes and drippers channel. The advantages of TCR are that it is relevant for hydrodynamics studies. Shear stresses and flows can be accurately determined and controlled, which is difficult to assess inside drippers or pipes. Fouling will be easier to retrieve and enough to characterize since they are formed on large detachable plates. Total solids (TS) and volatile solids (VS) were measured in order to quantify the biofilm. X-ray diffraction (XRD) and thermo-gravimetric analysis (TGA) were used to determine possible chemical precipitation and biofilm sample contents.

The third part of Chapter II focuses on the study of the interactions between biofilm development and chemical precipitation. According to the results of Chapter III, calcium carbonate was found to be the must abundant precipitate when using treated wastewater for irrigation. The effect of calcium carbonate on biofilm development was studied inside pipes and drippers. Two synthetic effluents were used, one with and the other without calcium carbonate. TS, VS, XRD and TGA were used to characterize the fouling inside the pipes. To monitor the clogging inside drippers, continuous measurements of their flow rate was done. Optic microscopy was at the end used to identify the location of the fouling inside the drippers in order to find a link between drippers' geometry and fouling emplacement.

Part II.1

Characterization of chemical precipitation by laboratory experiments and modeling

The objective of Part I is to determine the quality and quantity of chemical precipitation under micro-irrigation conditions using TWW. The water quality used for all the experiments was invariable (section II.2.7) so studying the factors that affect the precipitation remains essential. In micro-irrigation, the temperature, pH and CO_2 partial pressure are the main factors of precipitation mechanisms. The pH can change due to water CO_2 concentration, microbial degradation (fermentation, photosynthesis, etc.) and fertilizer injection (acid or alkaline) (Imas and Cohen, 2009[136]). Temperature can increase according to the season and to irrigation schedule. It can reach 50°C at midday during the summer inside black PE pipes. CO_2 partial pressure can be related to temperature and to the way in which irrigation occurs. Irrigation water can be pumped directly into the distribution system, which does not have contact with the atmosphere. In this case equilibrium with CO_2 is not included. Irrigation water was set in a reservoir or at the outlet of a dripper where water was open to the atmosphere. In this case, equilibrium with atmospheric CO_2 is included which means that [PCO_2] is constant. Another point is that micro-irrigation systems work under pressure (Annex A.5) which affects water CO_2 solubility and hence the solubility of the chemical elements. So understanding the operating mode of each parameter is paramount in order to be able to limit or avoid chemical fouling.

In an open system, mineral precipitation will be made in batch reactors by varying pH and temperature. The precipitate will then be quantified and qualified. The results will be used to validate and calibrate a numerical method. Once the calibration and validation of the model is done, other simulations will be made. Mineral precipitation will be done in a closed system, and the results will be compared. The use of PHREEQC (Parkhurst and Appelo, 1999[219]) aims to predict chemical precipitation using a specified water quality under different environmental conditions.

II.1.1 Chemical precipitation in batch reactors

To study the precipitation of the dissolved component of wastewater, a series of analyses have been done in the laboratory. In the experimental studies, the temperature and pH effects were the only two parameters that were analyzed. The experiments were done in open batch reactors where the water is in equilibrium with the atmosphere and the partial pressure of CO_2 is constant.

The precipitation test consists of filling clean transparent beakers with one liter of pre-filtered Mauguio wastewater (II.2.7.1). The filtration at 0.45 μm is used to eliminate all suspended solids and most of the bacteria. Four pHs at two temperatures will be tested. For this reason, eight experiments will be done. Four of the eight beakers were at room temperature (22°C), and the others at 55°C obtained using a thermostatic bath. The initial pH was 7.8 (II.2.7.1) and the studied pH were 8, 8.5, 9 and 9.5. These pH were chosen to provide a wide range study in the condition of irrigation.

When the water reached the desired temperature, a solution of sodium hydroxide (NaOH) at 0.1 M was used to trigger precipitation using a micropipette of 1 ml. The volume of added NaOH was noted. When adding NaOH and since the precipitation begins the pH of the solution decreases (section III.1.4). The solution was considered stable without pH decreasing by monitoring a constant value of pH for 2h (Spanos and Koutsoukos, 1998 a[258]). After 24h, when the equilibrium reaction has been achieved (Figure II.1.a) the water is filtered using a vacuum pump and glass microfiber filter paper with $0.45\ \mu m$ pore diameter (Fisher brand) in order to quantify the precipitate. This filter paper is then passed in an oven for 24h at 105°C to remove all traces of water and then weighed with an electronic balance (precision $0.1\ mg$) (Figure II.1.b). Glass microfiber filter weight was previously verified to be invariable even at temperature equal to 105°C.

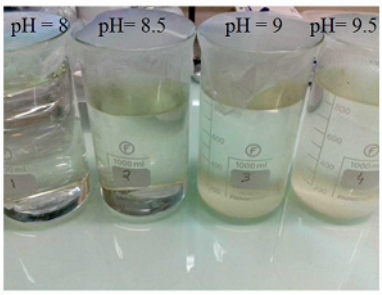

II.1.a:

II.1.b:

Figure II.1: Observed Precipitation at the bottom of the beakers after 24h for pH 8, 8.5, 9 and 9.5 at 55°C (a), filter papers after filtration and desiccation of the eight experiments (b).

Figure II.1.a shows four of the eight beakers after 24h of adding NaOH. The precipitation is visible at the bottom especially for pH 9 and 9.5. Figure II.1.b shows the filter paper after their passage to the oven (105°C for 24h).

To better understand the steps followed, Figure II.2 shows the approach which was done to induce precipitation.

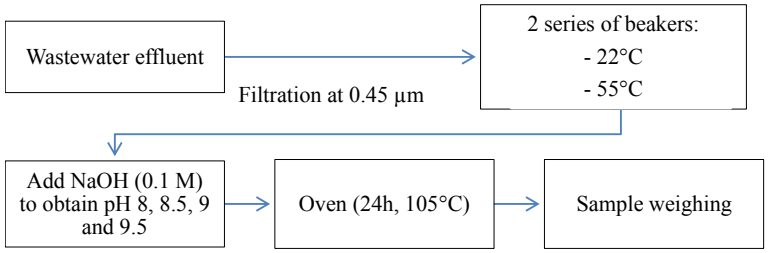

Figure II.2: The followed process that has been done to induce precipitation.

Experiments were repeated four times to analyze the chemical precipitation variation. The studied effluents were collected between March and May 2015.

The samples then underwent a characterization of their composition using XRD and TGA to highlight the presence of crystallized and non-crystallized form of chemical precipitation. More details can be found in annex A.4.

The experimental results were used to validate and calibrate a numerical model. The aim is to predict which elements will be formed and what their quantity is for water quality in an irrigation condition. In this case, the same parameters used in the laboratory experiments (water quality, pH and temperature) will be introduced in the geochemical model (PHREEQC). To have the results given by the model close to those of the laboratory, a good knowledge of the model and chemical equilibrium is required.

II.1.2 Precipitation modeling with PHREEQC

The main objective of this part is to introduce the basics of chemical equilibrium and thermodynamics to be able to model chemical precipitation, using treated wastewater in a context of reuse in irrigation. Depending on water qualities, the clogging of drippers due to the precipitation of initially dissolved minerals in water can be affected by different factors (pH, temperature, partial pressure of CO_2. The modelling objective is to accurately predict which minerals are likely to precipitate using such water quality in such conditions and the amount of those in prevention and /or treatment purposes.

The mathematical formulation of the model was established using PHREEQC, a program of thermodynamic-based equilibrium calculation for geo- and hydrochemistry developed by the USGS. In the literature, the studies are mainly based on the ground water and the precipitation of minerals in the soil (Chapelle, 2001[57]; Barry et al., 2002[27]). No study has been done with PHREEQC on treated wastewater and the precipitation of minerals inside pipes and micro-irrigation drippers.

Numerical simulation under PHREEQC requires a description of the solutions and operating conditions that will be used (composition and concentration, temperature, pH, pe). A thermodynamic database including all the chemical and thermodynamic characteristics (equilibrium constants, reaction heats, etc.) of elements, mineral phases and reactions is essential for the simulation. Four databases are provided with PHREEQC, but users are free to modify or compile a "personal" base. In this work, PHREEQC interactive is used and the simulations are run with the default database phreeqc.dat.

In an aqueous solution, PHREEQC enables estimation of the evolution of a system from its initial state to its thermodynamic equilibrium state. This is done by calculating the distribution of the elements between their different potential chemical forms (solid, liquid, gaseous, adsorbed, etc.), known as "speciation". This calculation is based on mass balance (chemical elements, electrical neutrality, etc.), mass action laws (representative of thermodynamic equilibrium) and the possibly kinetic reaction law (Zhu and Anderson, 2002[307]). If the reactions are considered instantaneous and systems go directly from their initial state to their equilibrium state, it is called an equilibrium model. If the kinetic reactions are taken into account, the mass action laws are then supplemented by kinetic laws (Peyronnard, 2008[225]).

II.1.2.1 Numerical variation of pH

Experimentally, increasing water pH was done by adding a solution of NaOH (0.1M). To increase the pH calculated by the model, Na_2O was used instead of NaOH. The same numbers of moles (volume of added NaOH$\times$ 0.1 M) used in the experiments were applied in the model. For PHREEQC it is easier and more accurate to use Na_2O because its thermodynamics is better known than NaOH. Na_2O reacts with water to give sodium hydroxide. 1 mole of Na_2O is equivalent to 2 moles of NaOH according to the following reaction:

$$\mathrm{Na_2O_{(cr)} + H_2O \longrightarrow 2\,NaOH_{(aq)}} \qquad \text{(Reaction.II.1)}$$

So that the addition of NaOH is formally equivalent to dissolution of Na_2O.

II.1.2.2 Equilibrium chemistry

a) The law of mass action: The equilibrium between a salt having A_nB_m as formula and the aqueous phase is obtained when the water is saturated with respect to salt. The equilibrium is maintained from the moment when solution and precipitation occur in the same amount equally. This balance is represented with the laws of mass action (Eq.II.1) which establish a relationship between the quantities of products and the reagents of a reaction. The contents of the species involved in the equilibrium are expressed by their activity (a_i) (Appelo and Postma, 2005[19]). For the case of a reversible reaction

$A_nB_{m\,\text{solide}} \longleftrightarrow nA^{m+} + mB^{n-}$ the law of mass action is:

$$K_{A_nB_m} = \frac{[\gamma A^{m+}]^n\,[\gamma A^{n-}]^m}{[\gamma A_nB_m]} \tag{II.1}$$

In which K is the equilibrium constant, whereas γ_i is the coefficient of activity of compound i.

The temperature variations have effect on the values of the mass action constant while pressure has little effect on it. So the Van't Hoff equation is usually used to calculate the variation of mass action constants with temperature (Appelo and Postma, 2005[19]).

$$\frac{d\,lnK}{dT} = \frac{\Delta H}{RT^2} \tag{II.2}$$

Where ΔH is the reaction enthalpy, or the heat lost or gained by the chemical system, R is the gas constant ($8.3144\ J/Kmol$), and T is the temperature in Kelvin.

b) Concentration and activity: The activity equals the concentration in an infinite dilute solution where the interactions among the ions are close to zero and the activity coefficient is equal to one (Merkel, 2005[192]). In this case, the solution is called ideal. The activity of the species a_i is related to the molal concentration C_i (mol/l) by an activity coefficient (γ_i) (Eq.II.3) (Stumm and Morgan, 1996[266]), which corrects for non-ideal behavior. The activity and the activity coefficient are dimensionless.

$$a_i = \gamma_i C_i \tag{II.3}$$

The activity coefficients can be calculated from the ionic strength I by the relation (Apello and Postma, 2005[19]):

$$log(\gamma_i) = f(I) \tag{II.4}$$

where

$$I = \frac{1}{2}\sum_{i=1}^{M} m_i Z_i^2 \tag{II.5}$$

M is the number of species in the solution mixture, z_i^2 is the charge number of ion i, and m_i is the molality of ion i. Strictly, I is defined in molal rather than molar concentrations, but in dilute solutions the difference is insignificant.

In a dilute solution where all concentrations are sufficiently low giving an ionique strength lower than 0.005 $(I < 0.005)$, the coefficient activity is calculated by the Debye-Hückel limiting law (Eq.II.6), for $I < 0.1$ the extended version of the Debye-Hückel equation will be used (Eq.II.7) (Appelo and Postma, 2005[19]). For more saline waters, other equations like Davies equation (Eq.II.8) or Pitzer expressions (Pitzer, 1979[231]) are used in the case where $I = 0.5$ and $I = 1$, respectively. The Davies

equation and Pitzer expressions do not pertain to this work because such salinities are not encountered in treated wastewater.

$$log[\gamma_i) = -0.5 z_i^2 \sqrt{I} \tag{II.6}$$

$$log[\gamma_i) = -\frac{A z_i^2 \sqrt{I}}{1 + B\dot{a}_i \sqrt{I}} \tag{II.7}$$

$$log[\gamma_i) = -A z_i^2 \left[\frac{\sqrt{I}}{1 + \sqrt{I}} - 0.3I \right] \tag{II.8}$$

Where A and B are temperature dependent constants, $(\dot{a}_i)$ is the empirical ion-size parameter, z_i^2 is the charge number of ion i (valence) and I is the ionic strength.

c) Calculation of saturation states The saturation states Ω' (Eq.II.9) may be expressed as the ratio between the analogue product of the activities derived from water analyses, which is often termed as the Ion Activity Product (IAP) and the equilibrium constant K (Eq.II.1).

$$\Omega' = \frac{\text{IAP}}{K} \tag{II.9}$$

Thus for $\Omega' = 1$, there is equilibrium, $\Omega' > 1$ indicates supersaturation and $\Omega' < 1$ subsaturation. For larger deviations from equilibrium, a logarithmic scale can be useful given by the saturation index (SI) (Eq.II.10) (Appelo and Postma, 2005)[19].

In PHREEQC, the SI can be defined in the input file for selected species, and will also be shown in the output file for the referring species.

$$\text{SI} = log\left(\frac{\text{IAP}}{K}\right) \tag{II.10}$$

SI $= 0$ reflects equilibrium between the mineral and the solution, and SI > 0 reflects supersaturation. The reaction proceeds to precipitate the mineral. At SI < 0, the solution is subsaturated and proceeds to dissolve the salt (Appelo and Postma, 2005, p. 131[19]).

In Chapter III, the value of SI will define whether, in certain operating conditions of pH, temperature and partial pressure of CO_2, there will be salt precipitation or not. The results of Chapter III put into evidence the presence of calcium carbonate precipitate in all water samples. For that reason, calcium carbonate was chosen as a parameter to ascertain any effect between its presence and the biofilm development.

Part II.2

Effect of shear stress on biofilm development kinetics and chemical precipitation

The objective is to study the effect of shear stress on biofilm development kinetics and possible presence of chemical precipitation. Since the present study is on micro-irrigation, the selected conditions of shear stresses are those found in irrigation pipes and drippers. To understand better how shear stress influences biofilm development, the best approach is to use laboratory-scale systems simulating environmental conditions under different levels of experimental control.

In the literature, various large- and small-scale laboratory designed systems were found to investigate biofilm development. Among them, Taylor-Couette reactors (TCR) have been suggested to study the effects of shear stress change on biofilm development in turbulent regime (Gagnon and Slawson, 1999[109]; Tsai et al., 2004[279]; Rochex et al., 2008[246]; Paul et al., 2012[220]; Pechaud et al., 2012[221]; Derlon et al., 2013[79]).

The liquid phase is located between two cylinders, and the biofilm grows on plates placed on one of the cylinders. A wide range of support materials for biofilm development can be tested. Plates are easily removed without biomass contact, and can be easily observed by microscopy. A more complete description of this type of reactor is made in sections II.2.1 and II.2.4. First, general information will be given about the TCR and the flows that may be encountered. A second experimental set-up and analysis done on the fouling will be developed.

II.2.1 Taylor-Couette Reactor generalities

Taylor-Couette reactors are characterized by a flow between two concentric cylinders an inner cylinder driven in rotation and a fixed external cylinder. This type of reactor derives from the original device developed by Couette in 1923 (Liu et al., 1999[175]; Coufort, 2004[70]) which could rotate its two cylinders in the same direction or in the opposite direction. There are several geometries of the reactor: Co-axial or conical (figure II.3) (Characklis and Marshall, 1990[60]; Noui-Mehidi et al., 2005[215]).

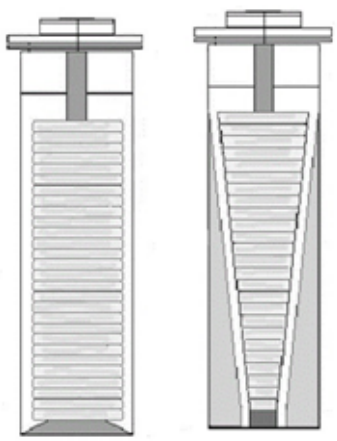

II.3.a: II.3.b:

Figure II.3: Scheme of co-axial (a) and conical (b) Taylor-Couette reactors (Rochex et al., 2008[246]).

Co-axial Taylor-Couette reactors provide a constant wall shear stress distribution on surfaces and are suitable for the cultivation of biofilms in turbulent flowing environments. Conical Taylor-Couette reactors allow the simultaneous generation of different shear rates along the inner cylinder on the same inoculating population (Willcock et al., 2000[293]).

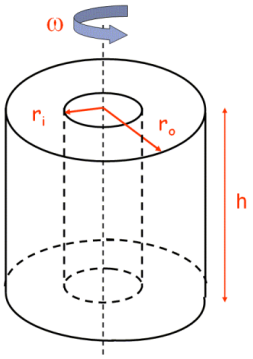

Figure II.4: Sketch of a Taylor-Couette reactor with inner rotating cylinder (Krivilyov et al., 2006[158]).

In our research we will use a co-axial reactor to analyze the effect of a constant shear stress. Figure II.4 shows a scheme of a co-axial annular reactor. R_1 and R_2 are the radii of the two cylinders (outer radius of inner cylinder and the inner radius of the outer cylinder). "h" represents the height of the two cylinders in meters. The angular velocity of the inner cylinder "Ω" is measured in radians per second. The gap (e) corresponds to the space between the two cylinders (e = R_2-R_1). The fixed cylinder is called a "stator", and the rotating cylinder is called a "rotor" (Annachhatre and Bhamidimarri, 1992[18]). Shear stresses depend on the cylinder's rotation velocity and the gap (e). Table II.1 shows the parameters of the Taylor-Couette Reactor (TCR) that will be used in this study.

Table II.1: Parameters of the Taylor-Couette reactor (TCR).

Taylor-Couette dimension parameters	
Dimensions of the reacteur	**Value (units)**
Inner radius (R_1)	0.1065 (m)
Outer radius (R_2)	0.1195 (m)
Gap (e)	0.013 (m)
Height of the cylinders (h)	0.2 (m)
$\eta\,(R_1/R_2)$	0.89121339
$\Gamma(h/e)$	15.384

These parameters are important in calculating the hydrodynamic conditions and the flow regime inside the TCR and to calculate the transitions from one regime to another (figure II.5).

II.2.2 Hydrodynamic conditions inside TCR

Hydrodynamic conditions and mainly the flow velocity and the resulting forces strongly influence the structure and morphology of the biofilm, its activity (exopolymer and metabolite production) and the distribution of micro-colonies (Stoodley et al., 1997[262]; Costerton, 1999[68]; Busscher and Van der Mei, 2006[50]). Understanding and mastering TCR hydrodynamic conditions facilitates biofilm development.

In a Taylor-Couette reactor, the rotation speed of the inner cylinder and the radii of the two cylinders define the regime flow. The flow is characterized by a dimensionless number called Reynolds number (Re). The Reynolds number is the ratio of inertia forces and viscous forces. It is expressed in the case of a co-axial reactor, as follows:

$$Re = \frac{\Omega R_1 \left(R_2 - R_1\right)}{\nu} \tag{II.11}$$

Where ν is the kinematic viscosity of fluid ($1.00 \times 10^{-06}\ m^2/s$ in the case of water) and Ω is the angular velocity (rad/s).

The characterization of the flow in the annular space of the two cylinders is also carried out via the dimensionless number of Taylor (Ta). The Taylor number allows characterization of the hydrodynamic regime specifically in the TCR. It is characterized by the ratio of the centrifugal forces over the viscous forces (Duvet, 1935[**?**]). The centrifugal force is greater near the inner cylinder than in the external cylinder. While the expression of the Taylor number can take many forms, the relation presented by Racina and Kind, 2006[238] was adopted:

$$Ta = \frac{\Omega R_1^{0.5} e^{1.5}}{\nu} \tag{II.12}$$

The Taylor number depends on the rotational speed of the inner cylinder. Coufort 2004[70] distinguish six flow regimes in the reactor annulus (from stable flow to fully turbulent flow), as summarized in figure II.5. More details on the determination and description of the regimes are provided in Annex A.5.

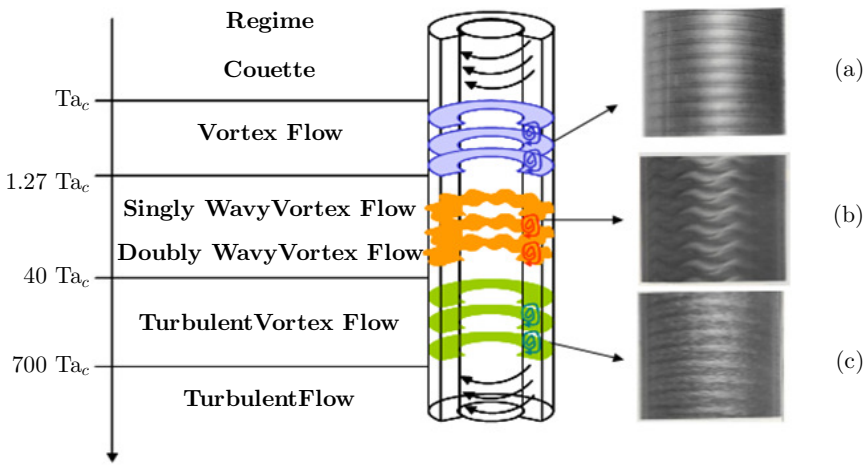

Figure II.5: Transitions in a Taylor-Couette reactor (Coufort 2004[70]).

Figure II.5 shows the various regimes and transitions based on a critical value of Taylor number Ta_c. Ta_c is determined by a critical angular speed Ω_c (Eq.II.15) of the inner cylinder corresponding to the occurrence of instabilities of the fluid in the gap.

The passage from one regime to another is marked by a change in the fluid flow due to the increase of the internal cylinder speed. Each modification is called instability and can be determined by the Ta_c.

The critical Taylor number corresponds to the appearance of the instabilities. Since many empirical or analytical correlations have been proposed to determine that threshold, the Ta_c used by Mehel,

2006[188] will be used in this work:

$$Ta_c = Re_c\sqrt{\frac{e}{R_1}} \tag{II.13}$$

To be able to calculate the Ta_c in (Eq.II.13), the critical Reynolds number Re_c must be determined. The most used equation was proposed by Esser and Grossmann, 1996[97] defined by:

$$Re_c = \frac{1}{\alpha^2}\frac{(1+\eta)^2}{2\eta\sqrt{(1-\eta)(3+\eta)}} \tag{II.14}$$

with $\alpha = 0,1556$ and $\eta = R_1/R_2$

To attribute the value of the Ta_c to the TCR, the inner cylinder must rotate at a speed corresponding to the critical angular speed Ω_c. The critical rotation speed of the inner cylinder was taken from the thesis of Coufort, 2004[70], defined by:

$$\Omega_c = \frac{41.3\,\nu}{R_2^{0.5}\,(R_2 - R_1)^{1.5}} \tag{II.15}$$

Given the TCR parameters that will be used in this study, the values of Re_c, Ta_c and Ω_c are 127.39, 44.505 and $0.08\ rad/s$, respectively.

Two geometric parameters in TCR are particularly important considering the fact that they directly affect the critical Taylor number Ta_c and the multiplicity of flow statements. One is a form ratio (η) and the other is an aspect ratio (Γ) which is defined as follows:

$$\eta = \frac{R_1}{R_2} \tag{II.16}$$

$$\Gamma = \frac{h}{e} \tag{II.17}$$

The interest of determining Ta_c and Re_c is to know when the flow passes from a laminar regime to a turbulent regime. In irrigation, the flow in the pipes and the drippers is under a turbulent regime but the value is not the same depending on whether it was in a dripper or in a pipe. In a circular pipe, the ow is laminar for $Re \leq 2000$ and turbulent for $Re \geq 4000$ (Eq .II.21). For drippers, Re_c can range from 100 to 700 depending on the geometry of the labyrinth (Eq.A.3) (Harley et al., 1995[127]; Kandilikar et al., 2003[144]).

In order to ensure the presence of a turbulent regime in the TCR, a bibliographic study was carried out to collect the various Ta and Re data for these transitions (Annex A.6) since in the literature different values of Re_c, Ta_c and Ω_c can be found. Turbulent flow regime will be used in this work since in the drippers, particle aggregation or biofilm formation occurs in these hydrodynamic conditions.

The aim of this study is to grow biofilm under micro-irrigation conditions in a turbulent flow and to see the effect of the shear stress on its development. For this, it is necessary to determine the rotational

speed which enables us to obtain the shear stress. The shear stress, which is mainly applied to the surface of the inner and outer cylinder, is connected to the tangential flow, itself linked to the rotation of the rotor. This shear stress is generated by the velocity gradient near the surface of the reactor. It is uniform over the internal and external cylinders. Different correlations have been established to estimate the shear stress (τ) on the inner cylinder surface in this TCR geometry. The expressions used in this work are those proposed by Racina and Kind, 2006[238] which are based on the concept of Wendt, 1933[291]:

$$\tau = 2.13 \frac{\left(R_1/\left(e+R_1\right)\right)^{3/2}}{\left(e/\left(e+R_1\right)\right)^{7/4}} Re^{1.445} \frac{\rho\nu^2}{2\pi R_1^2} \qquad \text{for } Re > 8\times 10^2 \tag{II.18}$$

$$\tau = 0.113 \frac{\left(R_1/\left(e+R_1\right)\right)^{3/2}}{\left(e/\left(e+R_1\right)\right)^{7/4}} Re^{1.764} \frac{\rho\nu^2}{2\pi R_1^2} \qquad \text{for } Re > 10^4 \tag{II.19}$$

Where τ: the shear stress expressed in pressure units ($kg/s^2/m$ or N/m^2 or Pa); ρ: the studied fluid density (1000 kg/m^3 for water); ν: the kinematic viscosity of the studied fluid (1.00×10^{-06} m^2/s for water).

The aim is to be able to determine the angular velocity of the rotor in order to have the desired shear stress. A backward step was made. The shear stress was selected (more details are provided in section II.2.3) and then the Reynolds number was determined according to equations II.18 and II.19. At the end, the value of Re was introduced in Eq.II.11 to determine the angular velocity.

II.2.3 Choice of the shear stress

Since this study is on the effect of shear stress found in irrigation on biofilm development, the selected conditions of shear stresses are those found in irrigation pipes and drippers. Every shear stress corresponds to a rotational speed of the cylinder. It will be seen hereinafter how the shear stress and the corresponding speed of the reactor were calculated.

Three shear stresses will be studied: one found in the irrigation pipes and two found in the drippers.

II.2.3.1 Shear stress found in irrigation pipe:

A 16 mm diameter polyethylene (PE) pipe with a flow velocity of 0.4 m/s was used for the calculation of one condition of shear stress. The wall shear stress was 0.7 Pa, calculated from the formula

of Blasius (Chadwick and Morfett, 1993[55]):

$$\tau = 0.0395 Re^{-0.25} \rho V^2 \tag{II.20}$$

with: τ: wall shear stress (N/m^2 or Pa); Re: Reynolds number inside the pipe; ρ: water density (1000 kg/m^3); V: flow velocity (m/s).

The formula of Blasius is used in the case of a circular pipe. The Re inside a pipe is calculated following equation (Eq.II.21):

$$Re = \frac{V D_h}{\nu} \tag{II.21}$$

where D_h: Hydraulic diameter which characterize the system geometry (m)

This velocity or shear stress was chosen mainly because in the work of Gamri, 2014[112], several velocities were studied for the same pipe. The initiation phase of biofilm development is faster for 0.4 m/s (10 days) than for higher velocity (21 days for 1.2 m/s corresponding to a shear stress of 4.9 Pa). Hydrodynamic conditions inside the pipe are presented in Table II.2.

Table II.2: Hydrodynamic conditions inside the pipe.

Conduct	PE
Flow speed (m/s)	0,4
Outer diametre (mm)	16
Inner diametre (mm)	12,7
Reynolds number	5700
Shear stress (Pa)	0,7

II.2.3.2 Shear stress found inside drippers:

The shear stresses inside drippers are related among others on the geometry of the latter. Labyrinth-channel geometry can control and change hydrodynamic conditions and may have an influence on the clogging properties of the drippers. Since the trapezoidal geometry is the most used, it is considered a valid geometry that gives turbulent flow and a good performance with anti-clogging properties Al-Muhammad et al., 2016[10]).

This geometry is also the basic unit of a Gr type integrated dripper with non-uniform section Figure II.6. This dripper is the most widespread industrially in micro-irrigation. The shear stresses calculated inside a dripper with specific geometry and flow rate are 2.2 and 4.4 Pa (more details of the calculation of the shear stress can be found in Annex A.7).

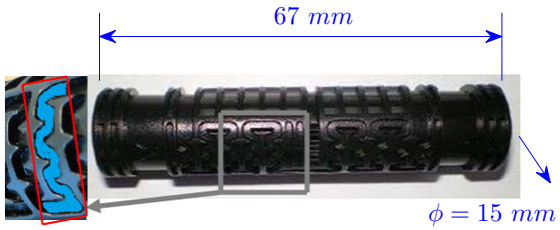

Figure II.6: Gr type integrated dripper with non-uniform section (industrial geometry) (Al-Muhammad et al., 2016[10]).

II.2.4 TCR speed rotation and parameters

As the aim was to study biofilm development under different shear stress, it was necessary to determine the rotational speed from which the desired shear stress is ensured. Wall shear stress (τ) is directly related to the torque on the inner cylinder of the TCR. Since the shear stresses are 0.7 Pa, 2.2 Pa and 4.4 Pa, Eq.II.18 and Eq.II.19 were used to estimate the Reynolds number. Since the Re was higher than 10^4, Eq.II.19 was used. The values were introduced in Eq.II.11 to calculate the speed rotation Ω of the reactor. Table II.3 shows the calculation of the strain rate obtained from Eq.A.4 and Figure A.2. The corresponding shear stress is obtained from Eq.A.5. The Reynolds numbers were calculated from Eq.II.19. The angular velocities were calculated from Eq.II.11. The Taylor numbers were calculated from Eq II.12, and the Ta/Ta_c were calculated from Eq.A.4 and Eq.A.5. The rotation speeds were calculated py multiplying the angular velocity by $60/2\pi$.

Table II.3: Calculation of strain rate, shear stress, Re, Ta, Ta/Ta_c and rotational speed of the inner cylinder.

Strain rate (s^{-1})	Shear stress (Pa)	Re Couette	Taylor	Ta/Ta_c	rad/s	Rotation speed (RPM)
$7.05E+02$	0.704	$9.71E+03$	$3.39E+03$	76.22	7.012	67
$2.21E+03$	2.206	$1.86E+04$	$6.51E+03$	146.18	13.449	128.5
$4.42E+03$	4.418	$2.76E+04$	$9.64E+03$	216.71	19.939	190.5

The inner cylinder is connected to a motor which allows it to rotate. Its speed is adjustable from 15 to 240 rotations per minute (rpm). This allows development of biofilm at different shear stresses which have been chosen for this study to be 0.7, 2.2 and 4.4 Pa, corresponding to rotational speeds of the inner cylinder equal to 67, 128.5 and 190.5, respectively.

II.2.5 TCR experimental set-up

In order to study the impact of shear stress on biofilm development kinetics, the Taylor-Couette reactor (TCR) was used. A study of biological and chemical fouling, and their proportions regarding Mauguio water quality (section II.2.7.1) was also conducted. Three different shear stresses were operated 0.7, 2.2 and 4.4 Pa. The water temperature inside the reactor was kept at $21°C \pm 1°C$ using a thermostatic bath. A peristaltic pump delivering a fixed flow rate of $1.38\ ml/min$ was used for supplying water to the reactor with a residence time of water inside the reactor equal to 24h. This time was chosen to allow attachment and development of biofilm over the plates and to minimize suspended cell growth (Rochex et al, 2008[246]). The reactor specific charge is $0.049\ mg/day/cm^2$. The experiments were run in an open system, the water surplus was sent as an overflow to another tank where the water was then discarded (Figure II.7). Figure II.7 shows from left to right the tank containing Mauguio's effluent, the peristaltic pump, the TCR with the motor and a drainage system. Then comes the overflow system and the thermostatic bath.

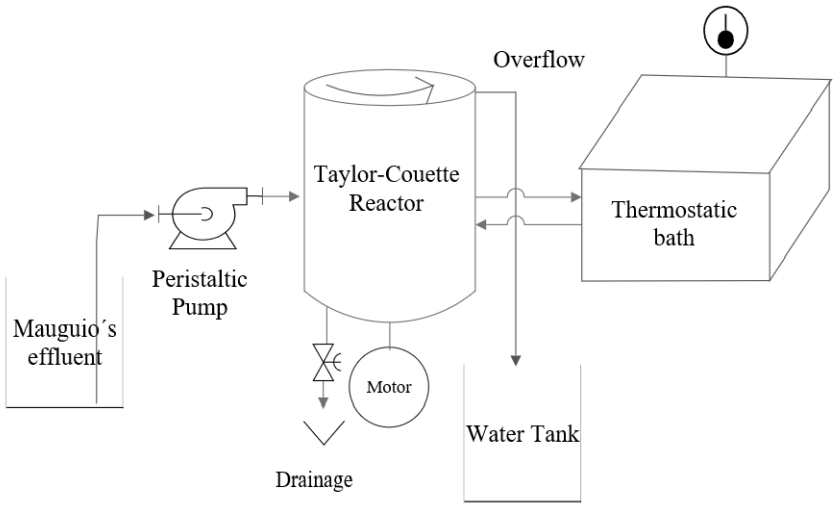

Figure II.7: Schematic representation of the experimental set-up.

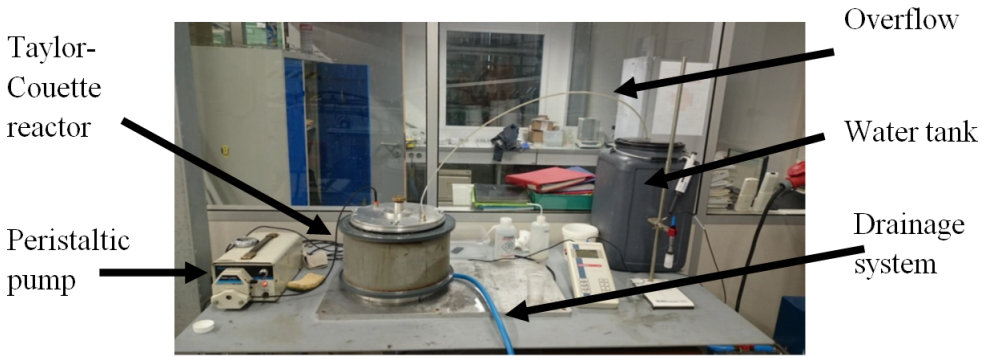

Figure II.8: Experimental set-up.

The inner cylinder of the TCR ((a) in Figure II.9) was surrounded by five removable polyvinyl chloride (PVC) strips (green) with five low density polyethylenes (LDPE) on which the biofilm will grow. PVC was chosen as a rigid and light support for a better fixation of the plate and to minimize friction at the bottom of the reactor. The plastic material studied is LDPE, which is the most used in the assembly of micro-irrigation systems. The PE plates are fixed by six screws at the ends in such a way as to fit as perfectly as possible their location on the cylinder (in Figure II.9 only one plate is shown (b)). Thus the perturbations of the liquid phase flow due to geometrical irregularities are minimized. The design was conceived this way for a better observation and analysis of biofilm developement. The parameters of the TCR are presented in Table II.1.

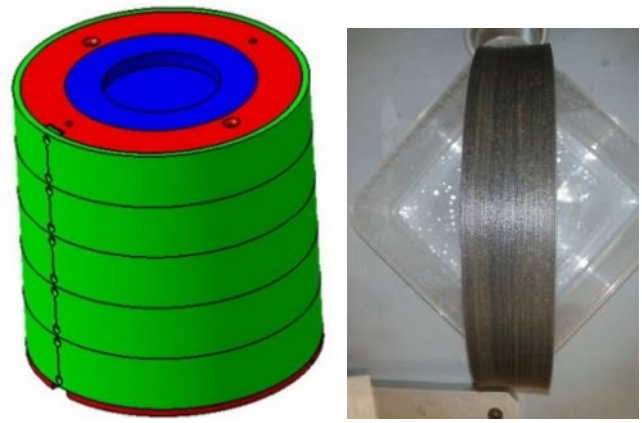

II.9.a: II.9.b:

Figure II.9: (a) Inner cylinder showing the five strips and (b) LDPE plate fixed on one strip.

II.2.6 Experimental protocol

To study the biofilm development under 0.7, 2.2 and 4.4 Pa and its evolution over time, every experience, which represents one shear stress, runs continuously over a total period of 8 weeks. The development of the biofilm over a period of 8 weeks has been found sufficient to allow identification of the different stages of biofilm development (section I.3.3 in Chapter I). The time required to reach biomass peaks is usually 4 to 6 weeks, but it also depends on the environmental factors (pH, temperature, nutrient concentration, etc.) and composition of the biofilm (bacterial strains, algae, fungi, etc.) (Dorigo et al., 2007[84], Paul, 2012[220]).

Each experience was interrupted at weeks 2, 3, 4, 5 and 6 to study the evolution of biofilm development in time. Plates 1, 2, 3, 4 and 5, respectively, are removed, scraped to collect the fouling and cleaned for a second use. Two repetitions are made for each plate. At week 8, all the plates are removed and scraped to collect the fouling. They will represent the second repetition of the experiment. Table II.4 shows the planning of the experiment for repetitions 1 and 2.

Table II.4: Experiment schedule over the eight weeks for repetition 1 where the plates are scraped and changed (green) and repetition 2 where the plates are only scraped (blue).

Weeks / Plate	2	3	4	5	6	7	8
1	2	1	2	3	4	5	6
2	2	3	1	2	3	4	5
3	2	3	4	1	2	3	4
4	2	3	4	5	1	2	3
5	2	3	4	5	6	1	2

The hydrodynamic conditions as shear stress effect are the main parameter and will be varied in this chapter. The pH, temperature, conductivity, chemical oxygen demand (COD) and dissolved oxygen were continuously followed to ensure the same operating conditions for the 3 shear stresses from the beginning to the end of the experimentation. The plate preparation and sampling and explained in Annex A.8.

II.2.7 Wastewater Treatment Plant (WWTP) of Mauguio

Treated wastewater used in the experiments comes from the outlet of a tertiary treatment (section I.4 Chapter I) of Mauguio's WWTP. Mauguio's WWTP is an activated sludge type and has a capacity of 24000 population equivalent. It meets the demographic and activity trends of the cities of Mauguio and Mudaison (Hérault, France). In 2014, the maximum input charge was 23020 population equivalent

and the average inflow was 2903 m^3/day. Wastewater passed through several treatment stages (section I.4 Chapter I), from the pretreatment (screening, degritting and degreasing) to biological treatment (secondary treatment). An advanced treatment of nitrogen and phosphorus is required (tertiary treatment) to preclude the eutrophication of the pond (Etang de l'Or). The effluent from the clarifier is discharged in old lagoons rehabilitated in an environmental transition zone.

II.2.7.1 Water quality

Independently of the work of this thises, the quality of the effluent is monitored once to twice a month on a sample representing the average of many small samples for 24h. The objective is to make sure that the WWTP produces all over the year water quality that satisfies the recommendation criteria and the discharge standards (section I.4 in Chapter I). The homogeneity of the water is also highlighted so the date of water sampling for chemical precipitation (part II.1 in this chapter) and biofilm development (part II.2 in this chapter) will have no effect on the results. The physicochemical characteristics of the effluent are listed in Table II.5.

According to Ayers and Westcot, (1985)[22], treated effluents at the Mauguio plant fall within the normal range of water quality recommended to preclude clogging of micro-irrigation drippers except for hardness and complete alkalimetric title (CAT), whose values are higher than the recommended one (Dey et al., 2007[80]). The acceptable range of hardness is between 60 and 120 mg/l and the recommended range for (CAT) is between 120 and 200 mg/l. As important parameters to follow, for example, the sulfate concentration should not exceed 100 mg/l, otherwise creating poisoning problems in the anaerobic digestion process. Conductivity which is rather related to salinity must have a value below 1500 $\mu S/cm$ (20°C) to ensure that the effluent is suitable for irrigation in accordance with the standards defining the thresholds for treated wastewater intended for agricultural reuse (El Haité, 2010[93]).

Table II.5: Physicochemical characteristics of the effluent from Mauguio's WWTP

Parameters	**values**	**Parameters**	**values**
T (°C)	17	N Kjeldhal (mg Ntot/ L)	2,31
Turbidity	2,03	Fluorine (mg/L)	< 0,50
pH	7,8	Aluminium (µg/L)	< 20
Conductivity (µS/cm)	1270	Br (mg/L)	0,18
TDS (mg/L)	1241,7	B (mg/L)	0,14
Hardness (mg/L)	223	Ba (mg/L)	<0,05
Alkalinity (mg/L)	< 20	Cd (mg/L)	<0,005
CAT (mg/L)	261	Cu (mg/L)	<0,02
Ammonium (mg/L)	0,37	Fe (mg/L)	<0,05
Nitrates (mg/L)	9,8	Mn (mg/L)	0,03
Nitrites (mg/L)	0,17	Li (mg/L)	<0,02
Phosphorus (mg Ptot/ L)	0,17	Pb (mg/L)	<0,05
Mg (mg/L)	7	Si (mg/L)	12
Ca (mg/L)	133	Sr (mg/L)	0,39
Na (mg/L)	119	Zn (mg/L)	0,03
Cl (mg/L)	171	COD (mg/L)	< 30
K (mg/L)	18,1	TOC (mg/L)	6,8
Sulfates (mg/L)	109	Total TSS (mg/L)	5

To highlight the homogeneity of the discharged water, two parameters were followed. Suspended solids (SS) and chemical oxygen demand (COD) were monitored daily as a routine measurement for the WWTP. Figure II.10 shows the evolution of suspended solids (SS) and chemical oxygen demand (COD) in mg/l from June 2013 untill April 2015.

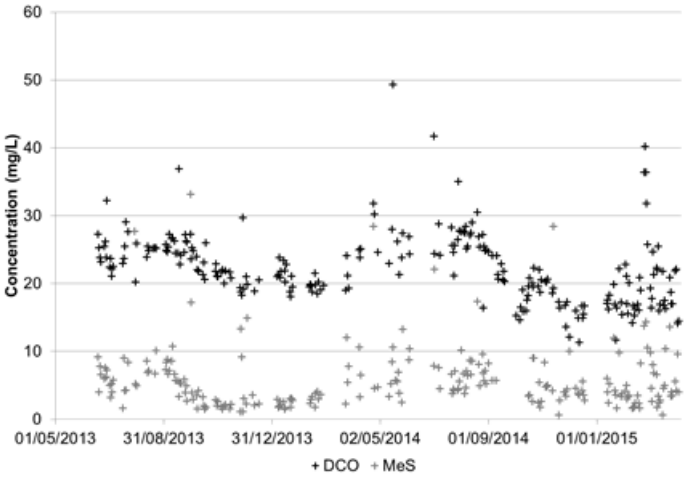

Figure II.10: Variation of the concentration in mg/l of the COD and SS in the same period

Figure II.10, shows that during the year some fluctuation may be encountered regarding the water parameters but these fluctuations are so minimal that the quality of the water is considered to be constant. The concentration of COD varies in general between 20 to 30 mg/l (average value 22.3 ± 8.6). A drop in the COD concentration is noticeable from October to December 2013 and for the same period in 2014.

The concentration drops below 20 mg/l and can reach 12 mg/l in December 2013. Since Mauguio is located in the south of France, this dilution is due to the high precipitation in this period of the year in this region. The same is true for SS (average value 5.6 ± 5.1), where a drop in the concentration is observed at the same period especially in 2013 where the concentration of SS decreased from 10 mg/l in August 2013 to 3 mg/l in November 2013. It can be said that the quality of the effluent is constant throughout the year with low seasonal effect. The average and standard deviation of the other measurements of the water quality at the outlet of Mauguio WWTP obtained from the same period can be found in Annex A.9.

The monitoring and analysis of the water quality were also done inside the TCR during the experiments of biofilm development to ensure the same conditions over all eight weeks and for the three shear stresses. In these conditions, only the shear stress will affect biofilm development and not the water quality.

II.2.8 Analyzing the water quality inside the TCR

For each shear stress, the duration of the experiment was 8 weeks. The effluent was collected every two weeks from the sewage treatment plant and is stored in a PVC container at 4°C in the refrigerator to help maintain sample integrity (USGS 2006). The Taylor-Couette reactor is fed continuously using a peristaltic pump and a water container positioned upstream the TCR (Figure II.7). Every 53h (3 times per week) the water container is filled with fresh wastewater from the refrigerator. During the experiments, temperature, conductivity, dissolved oxygen concentration and pH were measured using a digital multi meter for mobile measurement (WTW multi 3430 set F). Chemical oxygen demand (COD) was measured using a WTW kit reagent for photometer (Cat.No.109772). The COD measurements are detailed in Annex A.10

The water which is inside the refrigerator and inside the container that fed the TCR (Figure II.7) is also analyzed. The purpose is to put into evidence the stability of the water quality during the 2 weeks in the refrigerator and between two water renewals (53h).

Part II.3

Effect of calcium carbonate on biofilm development

Our objectives are to study the effect of calcium carbonate on biofilm development inside irrigation pipes and on the clogging of drippers. Calcium carbonate ($CaCO_3$) was chosen because it was the most abundant precipitate when using treated wastewater (Schwankel and Prichard, 1990[252]) and it was also detected in the results of Chapter III. An irrigation set-up consisting of pipes with drippers was installed. Two series of experiments have been made to compare the development of biofilm with and without calcium carbonate. For this purpose, synthetic wastewater was used. In order to make clear the fouling kinetics along the micro-irrigation system, the study is divided into two parts: in the pipe and in the drippers.

II.3.1 Experimental set-up

The experimental study was carried out in the laboratory using an irrigation set-up system (Figure II.11) with controlled flow conditions (Section II.3.2). It is composed of two independent parts which enable a simultaneous study of biofilm development with (tank 2) and without (tank 1) calcium carbonate. Each part operates in a closed circuit and includes an opaque tank of 60 liters and a pump (Figure II.12) for supplying the pipes. The tanks are opaque to preclude exposure of the solution used lighting, which limits the development of algae in the system.

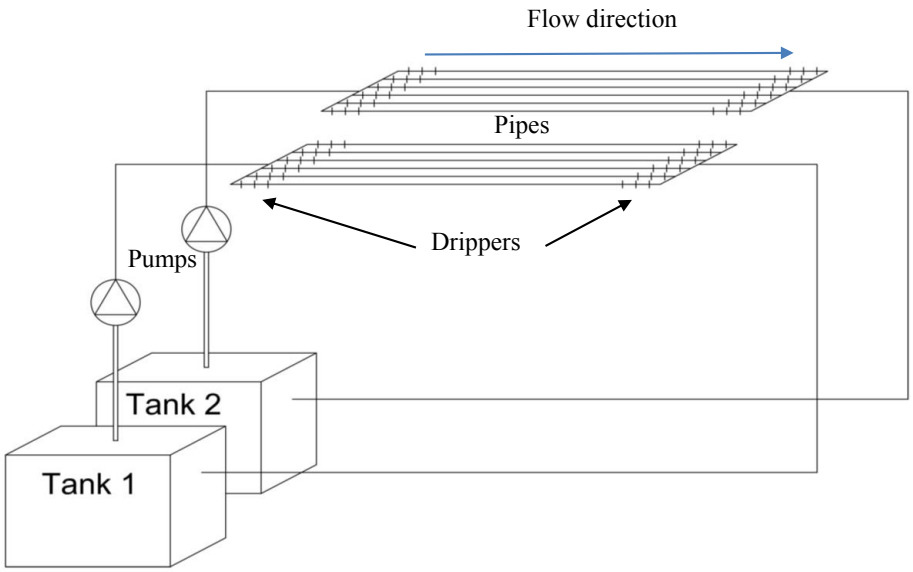

Figure II.11: Schematic of experiment of the irrigation system.

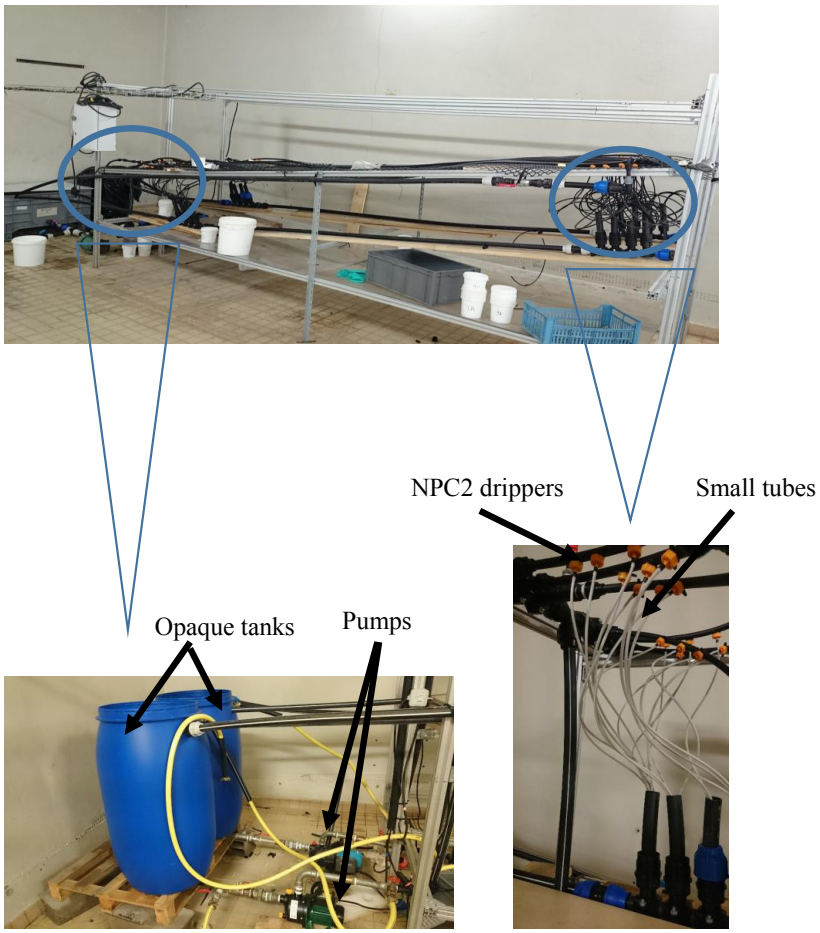

Figure II.12: Experimental set-up

Tank 1 and tank 2 contain synthetic wastewater without and with calcium carbonate respectively. Each configuration is composed of 6 pipes $4\ m$ long installed in parallel with a slope of 10% to preclude

any entrapment of the air in the pipes. This is the same type of pipes used in the TCR (LDPE Φ 16mm), having an internal diameter equal to 12.7. The purpose is to be able to compare the fouling developed in the pipes and in the TCR under the same operating condition but with different water quality. Every side of the pipe will be named ”line” designated by the letter ”L” Figure II.13. The flow direction goes from the beginning of the line to the end of the line. 50 cm on each side of the pipes were intended to install 3 drippers, which makes 6 drippers per pipe. This is a good way to compare dripper fouling in the beginning and at the end of the line. The drippers are designated by the letter ”D” and are named as follows Figure II.13.

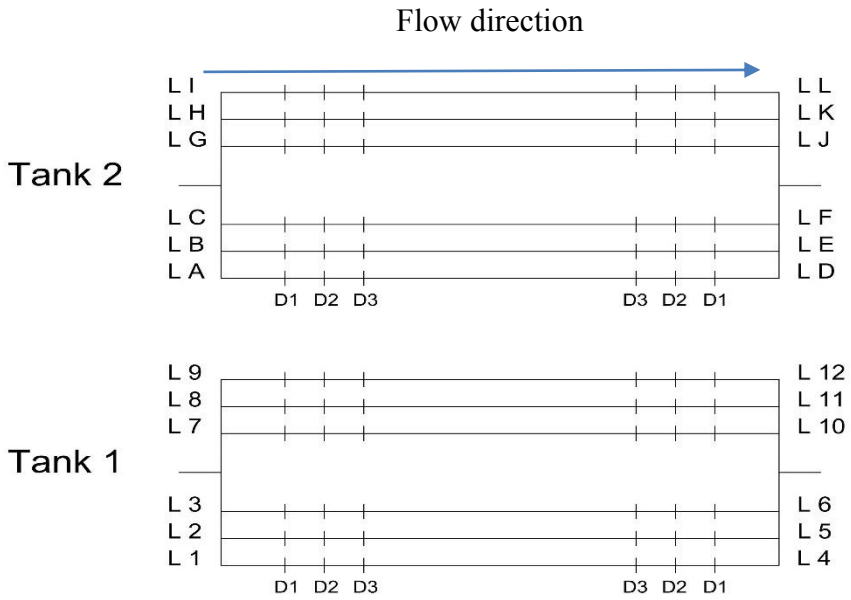

Figure II.13: Designation of drippers and pipes

Figure II.13 will be used to better explain dripper clogging in the Chapter IV of this thesis.

II.3.2 Method of fouling analysis

The effect of calcium carbonate on the biofilm development was divided into two steps. The first examined the biofilm development in pipes as a function of time. The second consisted in following the clogging in the drippers.

a) Biofilm development in pipes as a function of time The velocity was set at $0.4\ m/s$. According to the formula of Blasius (Chadwick and Morfett, 1993[55]) (Eq.II.20), the shear stress applied for biofilm development is equal to 0.7 Pa. The choice of this velocity or shear stress is explained in section II.2.3 of Chapter II.

The flow velocity in the pipes is regulated by calibrated nozzles used on Komet IWT sprinklers (Gamri, 2014[112]). They have been installed downstream of each pipe in polyethylene (PE) or polyvinyl chloride (PVC) fittings and have been attached with seals to ensure watertightness. The Komet IWT nozzles are selected to a fixed flow rate value for a measured pressure of 1 bar. This pressure was maintained at a constant rate during all the experimentation and was monitored using a manometer at the beginning and at the end of each line.

The experimental set-up runs for a period of seven weeks using the synthetic effluent described in paragraph II.3.3. It operates four hours per day divided into two hours in the morning and two hours in the afternoon for three reasons: i) to be as close as possible to the real conditions of irrigation; ii) to not overheat the system, the temperature should not exceed 25°C especially when powerful pumps are used; and (iii) to be able to develop biofilm in a limited time. According to Dorigo et al., (2007)[84] and Paul, (2012)[220], a period of seven weeks is sufficient for optimal biofilm development.

Biofilm development was followed every week by collecting the fouling that develops in the system. Every week, one pipe is analyzed and then replaced by a new one to have two repetitions for each measurement.

b) Monitoring of the clogging in the drippers Non pressure compensating drippers delivering 2 L/h (NPC2) at 1 bar pressure were used. NPC was shown to be less sensitive to clogging than pressure compensating drippers (PC) (Gamri et al., 2013[111]). They were also used also because they are one of the most used in micro-irrigation. The monitoring of the dripper clogging was done by measuring the flow rate at the output of drippers three times per week for all the drippers in the system (72 drippers).

Drippers drip into small tubes that are connected to the system and will be used to facilitate flow rate measurement (Figure II.12). The flow rate is measured by collecting in a bucket an amount of water at the outlet of each dripper over a period of 10 minutes and then weighed. The flow rate is then evaluated in terms of volume per time unit.

Every week when the pipes are removed and changed the drippers are changed too and replaced by new ones. This allows to have two measurements of flow rates for each biofilm age. For the two measurements only 12 drippers will reach the end of the experiment.

II.3.3 Synthetic effluent quality

The experimental setup is fed with a synthetic effluent with a concentration of 200 mg/L of COD, and the composition of the water is described in Table II.6. The components described in Table II.6 are diluted with demineralized water. The use of demineralized water allows limitation of the interaction

between the biofilms and the ions present in the water.

Table II.6: synthetic water quality of tank 1 (without calcium carbonate) and tank 2 with calcium carbonate.

	Components	Concentrations (mg/L)
Tank 1 and tank 2	Glucose	200
	Ammonium chloride	16.28
	Phosphoric acid	2.05
Only tank 2	Calcium chloride	369
	Sodium bicarbonate	443.3

The concentrations were chosen to be as close as possible to Mauguio's water quality. All year around, the average ammonium concentration is $4.26\ mg\ N/L$ and that of phosphorus is $0.65\ mg\ P/L$. For sodium bicarbonate, this was calculated according to the concentration of water alkalinity in French degree. For calcium chloride, the concentration was based on the Ca^{2+} concentration in water and was $133\ mg/L$ (Table II.5). Sodium bicarbonate and calcium chloride are precursors for calcium carbonate formation (Declet et al., 2016[76]).

The use of a high concentration of COD (two to four times the WWTP output concentration) allows promotion of the bacterial development in the system and thus to obtain quantities of measurable biofilm. The solution is renewed every week to ensure a constant supply of nutrients and calcium carbonate for bacteria.

The objectives of this work are to quantify the fouling that develops on the walls of the pipes and inside the drippers without being too interested in its activity. The quantification of this fouling as a function of time will allows establishment of a link between the presence of the calcium carbonate and the development of the biofilm in the pipes and in the drippers. In the case where the development of the biofilm in the pipes is monitored as a function of time, a measurement of the total solids (TS) and volatile solids (VS) matter has been made.

II.3.4 Characterization of the fouling material

The fouling collection was done with an elastomeric membrane fixed to the end of a metal rod. This makes it possible to scrape the inside of the pipe without abrading it. The characterization of fouling will be the same as for TCR.

The objective of the characterization is to determine the composition of the fouling and the proportion of each constitute.

Many investigative techniques have been developed to characterize the physical, morphological,

mechanical, chemical, and microbial properties of biofilm. Simple techniques provide access to a macroscopic quantification of biomass colonizing a surface. Some of these global techniques are based on the determination of chemical oxygen demand (COD) or total organic carbon (TOC) as well as thickness, density, porosity and surface roughness of the biofilm. More simply, the biofilm is also characterized by the determination of the total solids (TS) and the volatile solids (VS) (Annex A.4). From these weights, it is also possible to find the density and thickness of the biofilm (Horn and Hempel, 1997b[130]). Thermogravimetric analysis (TGA) and X-ray diffraction (XRD) (Annex A.4) were also used to characterize fouling. They put into evidence the chemical precipitation that occurred with biofilm development by determining the quality of the precipitate. XRD characterizes the crystallography of the chemical precipitation, and TGA can determine the non-crystalized precipitate form and the proportion of each one. Techniques for identification and characterization of fouling and chemical precipitation will be the same as used for all experiments.

Chapter III

Characterization of chemical precipitation by laboratory experiments and modeling

Introduction

Chemical precipitation in drippers and pipes depends largely on water quality. The solubility of a given material in water is controlled by variations in temperature, pressure, pH, redox potential, and the relative concentrations of other substances in solution. In order to predict what might cause chemical plugging of micro irrigation system drippers, the process of mineral deposition must be understood.

The objective of this study is to determine which elements precipitate and cause chemical clogging when using treated wastewater (TWW) effluent in a micro-irrigation system, to evaluate the effect of pH, temperature and CO_2 partial pressure on chemical precipitation and to use a geochemical model to quantify and qualify chemical precipitation when using TWW.

The results are divided into two categories: experimental and modeling.

Experimental precipitation will be done in the laboratory. In a batch chemical process, two temperatures (22°C and 55°C) and four pH (8, 8.5, 9 and 9.5) are tested to analyze the quantity of precipitates and their crystalline nature. Water temperature can reach 50°C in summer inside black pipes (Gamri et al., 2016[113]). High pH can be due to water CO_2 concentration, to microbial degradation or to fertilizer injection (Haman, 1990[126]). Precipitates and crystalline phase are weighted and then analyzed using thermogravimetric analysis (TGA) and X-ray diffraction (XRD) .

Experimental results allow validation and calibration of the model in order to predict chemical precipitation. All of it was done with the intent to prefigure suitable measures to take to preclude/limit chemical clogging. Modeling was done using the code PHREEQC (Parkhurst and Appelo, 1999[219]) to do a speciation calculation under different environmental conditions (temperature, pH and CO_2 partial pressure). The values of pH and temperature were the same as in laboratory experiments. For CO_2 partial pressure, two situations have been taking into account: water does not have any contact with the atmosphere, which is considered as a closed system (e.g., water pumped from water tables), and water has contact with the atmosphere, which is considered as an open system (e.g., water taken from an open reservoir). In the case of treated wastewater we are rather in the second case. These results will allow a widening of perspective about other water qualities.

Part III.1

Experimental characterization of chemical precipitation using TWW

Chemical precipitation using treated wastewater was monitored in beakers in the laboratory by varying pH and water temperature. The aim is to know the quantity and quality of the precipitate obtained using TWW in an irrigation system. The precipitate was quantified by the measurement of its mass in function of an increase in pH and temperature. Thermogravimetric analysis (TGA) and X-ray diffraction (XRD) were used to qualify the crystallography and composition of the precipitate. The results allowed a study of the chemical precipitation according to two parameters.

III.1.1 Chemical precipitation

Treated effluents were collected between March and May 2015 from Mauguio wastewater treatment plant. Four water samples were used for the precipitation experiments. The repetition allows verification of homogeneity of Mauguio's water quality over time. Figure V.1 shows the average of precipitate mass and corresponding NaOH-added volumes with their standard deviations (SD) at different pH for 22°C and 55°C. SD was calculated from the four repetitions in the same conditions. The choice of pH and temperature is explained in Chapter II. These results are also summarized in Table III.1.

According to Figure V.1 and Table III.1 the difference between the repetitions is negligible for all the studied pH and temperature. For example the precipitate average mass and standard deviation was 140.75 ± 16.51 mg, 109.3 ± 17.1 mg and 294.25 ± 6.98 mg respectively at pH 9.5, 22°C, pH 8.5, 55°C and pH 9, 55°C. This underlines the homogeneity of the water quality.

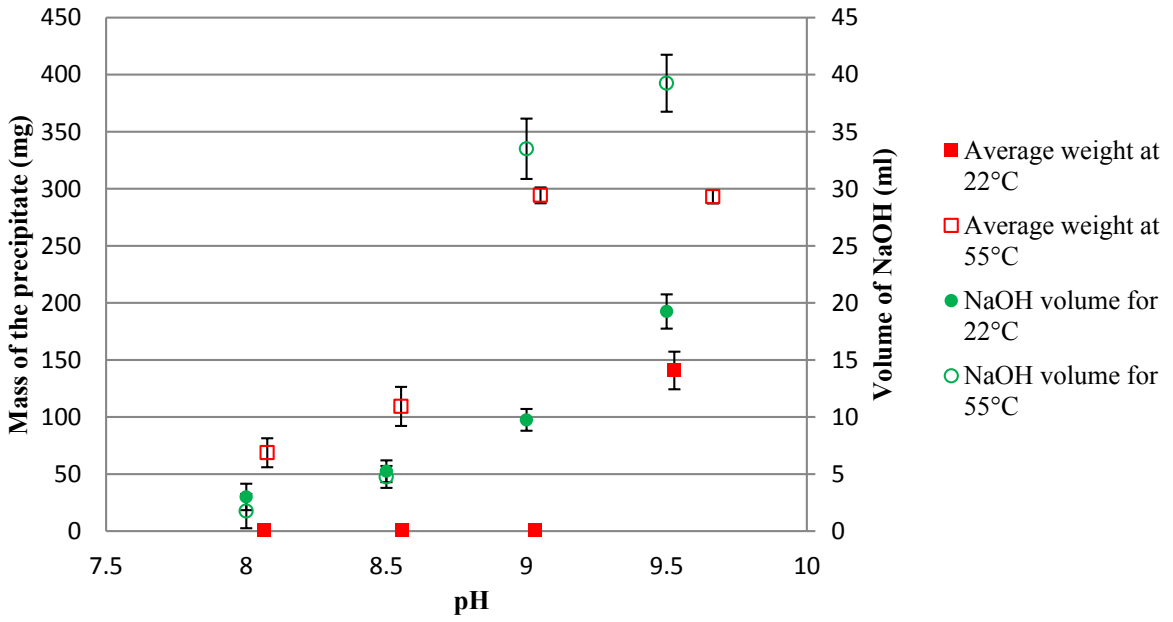

Figure III.1: Evolution of average precipitate mass and volume of added NaOH in function of pH and temperature.

Table III.1: Average precipitate mass and volume of added NaOH with their SD for pH 8, 8.5, 9 and 9.5 at 22 and 55°C.

Average NaOH volume, pH and precipitate mass at 22°C			Average NaOH volume, pH and precipitate mass at 55°C		
Average volume of added NaOH (ml)	Average measure of the pH	Average mass of the precipitate (mg)	Average volume of added NaOH (ml)	Average measure of the pH	Average mass of the precipitate (mg)
3 ± 1.15	8.06	0.675 ± 0.09	1.75 ± 1.5	8.07	68.75 ± 12.69
5.25 ± 0.96	8.55	0.625 ± 0.15	4.75 ± 0.96	8.55	109.35 ± 17.1
9.75 ± 0.96	9.03	1.325 ± 0.8	33.5 ± 2.65	9.05	294.25 ± 6.98
19.25 ± 1.5	9.53	140.75 ± 16.51	39.25 ± 2.5	9.66	293.025 ± 5.92

Concerning the behavior of precipitation in function of pH and temperature, it is shown that at 22°C for pH lower than or equal to 9, the mass of precipitation is equal 0.87 ± 0.35 mg. When the temperature increases from 22 to 55°C, precipitation occurred even at pH 8 (68.7 ± 12.7 mg). The variation of the precipitate mass as a function of the pH is mainly driven by temperature. It increases from 68.7 ± 12.7 mg at pH 8 until 109.3 ± 17.1 mg at pH 8.5 for a temperature equal to 55°C. At this temperature for pH 9 and 9.5 the same quantity of precipitate is formed and the mass is 293.6 ± 6.45 mg. It can be said that at 55°C and from pH 9 all compounds precipitate.

The volume of NaOH also varied not only by increasing the pH but also by increasing the temperature. For a definite value of pH, the volume of NaOH added to reach this same value at 22°C is not the same at 55°C. For example for a pH of 9 the added volume to reach this pH is 9.75 ± 0.95 ml at 22°C. This volume increases to 33.5 ± 2.6 ml at 55°C. This difference is greater as the mass of precipitate

is important. For a temperature equal to 22°C, the volume of NaOH increases from 9.75 ± 2.6 ml to 19.25 ± 2.5 ml, giving a precipitate mass of 1.3 ± 0.8 mg and 140.75 ± 16.5 mg, respectively. For a temperature equal to 55°C, the volume of NaOH increases from 4.75 ± 0.95 ml to 33.5 ± 2.64 ml, giving a precipitate mass of 109.3 ± 17.1 mg and 294.2 ± 6.98 mg, respectively. To better explain the precipitation process and the link between pH, temperature and mass of the precipitate, XRD and TGA are used to characterize the precipitate type and crystalline form.

III.1.2 Precipitate characterization by X-ray diffraction (XRD)

X-ray diffraction (XRD) was used to analyze crystalline form in the precipitate. Six different samples from the four different precipitation conditions were tested for XRD analysis: pH 8.5 and 9.5 at 22°C and 55°C. For pH = 8.5 at 55°C and for pH = 9.5 at 22°C, two samples were taken to evaluate the repeatability. The objective was to know whether the pH and temperature also affect the crystalline form or composition of the precipitate. Figure III.2 shows the result of XRD analyses. Figure III.2.a corresponds to precipitate from pH 8.5; temperature 22°C. Figure III.2.b corresponds to precipitate from pH 9.5; temperature 55°C. Figures III.2.c and III.2.d correspond to precipitates from pH 8.5; temperature 55°C. Figures III.2.e and III.2.f correspond to precipitate from pH 9.5; temperature 22°C. In Figure III.2.a no peaks were observed due to the insufficient quantity of sample or calcium carbonate ($CaCO_3$) in the amorphous form Amorphous Calcium Carbonate (ACC) and did not crystallize. In the other Figures III.2.b, III.2.c III.2.d III.2.e III.2.f, XRD signals indicate the presence of crystallized calcium carbonate in calcite form (number 1 above peaks). The most representative peak of calcite is observed for $2\theta = 34$ (blue arrow). Vaterite and aragonite, which are two other crystalline forms of calcium carbonate, were also detected (Gabrielli et al., 1999[108]). Vaterite (number 2 above peaks) is observed in 60% of the crystallized samples. Its peaks are perfectly observed in Figure III.2.b. In Figure III.2.d vaterite peaks are also observed and even less in Figure III.2.f. Aragonite (number 3 above peaks in Figure III.2.d) is only observed in one sample of one experience. The presence of vaterite and/or aragonite is observed together or separately but always with calcite.

From the results of scanning electron microscopy and transmission electron microscopy Gabrielli et al., 1999[108], have shown three crystallographic varieties of calcium carbonate precipitation. Their presence (solubility properties) depends on the experimental conditions of precipitation kinetics and temperature. The three polymeric forms are: calcite (cubic), aragonite (needle-shaped) and vaterite (spherically-shaped). It has been shown that at ambient temperature and over a temperature range between 0°C and 90°C, calcite is the preponderant precipitate which explains why it is found in all the samples.

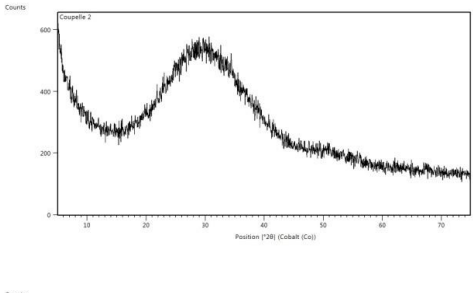

III.2.a: pH 8.5; temperature 22°C

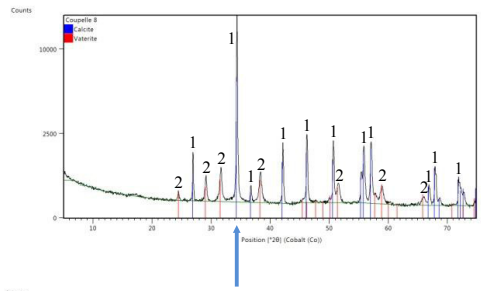

III.2.b: pH 9.5; temperature 55°C

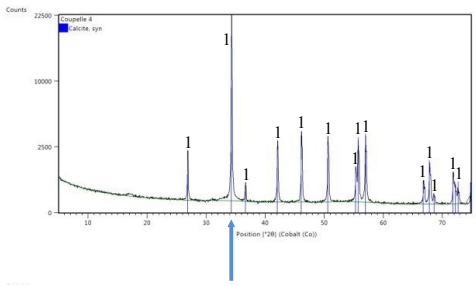

III.2.c: pH 8.5; temperature 55°C

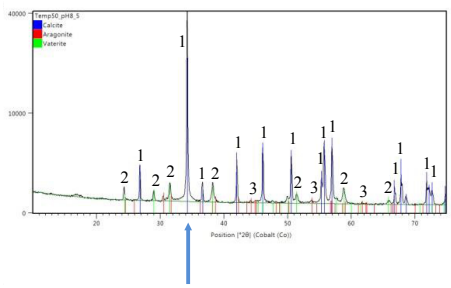

III.2.d: pH 8.5; temperature 55°C

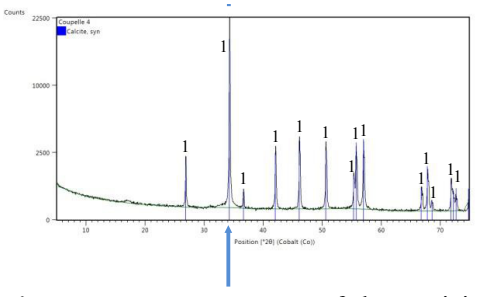

III.2.e: pH 9.5; temperature 22°C

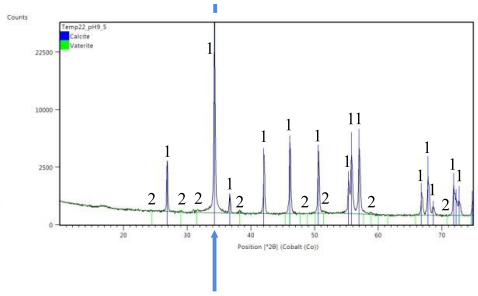

III.2.f: pH 9.5; temperature 22°C

Figure III.2: XRD pattern of the precipitate. Calcite (number 1 above peaks). Vaterite (number 2 above peaks) and aragonite (number 3 above peaks only in d).

Calcite is the preponderant precipitate because it is the least soluble phase and the most thermodynamically stable crystal structure form of calcium carbonate, while vaterite is the most soluble phase and the least thermodynamically stable (Muryanto, 2014[202]). The increase in pH and especially in temperature favors the simultaneous formation of aragonite and especially of vaterite. The peaks of vaterite are more visible at pH 9.5; temperature 55°C (Figure III.2.b), than at pH 8.5 temperature 55°C (Figure III.2.d), and less visible at pH 9.5; temperature 22°C (Figure III.2.f). Note that XRD is a qualitative and not a quantitative analysis and that the peaks area does not refer to the quantity of the elements. The peaks area indicates rather the degree of crystallization. Rogriguez-Blanco et al., 2011[249] showed that first precipitation is in amorphous form (ACC) and then crystallizes to calcite via vaterite which is the least stable (Jzotzi, 2007[140]). In this case, the presence of vaterite in the samples especially in the case of Figure III.2.b is due to a fast precipitation process where vaterite did not have enough time to

be transformed into calcite. Spanos and Koutsoukos, (1998 a)[258] found a linear dependence of calcite content in the precipitate as a function of time.

The increase of calcite quantity means a decrease in the vaterite quantity. In the same study and in another study made but by the same authors (Spanos and Koutsoukos, 1998 b[259]), they put into evidence that calcium carbonate precipitation kinetics is linked more to the supersaturation ratio or saturation index (Eq.III.1) than to pH for pH 9.0 and 10.0 at 25°C or to temperature 25 - 45°C. They underline that a very high supersaturation (1.5 - 1.9) in which the solid phase is formed affects the transformation of vaterite into calcite. But this supersaturated solution can be obtained by increasing temperature for the same water quality (Larson and Buswell, 1942[163]). In this study, increasing pH and temperature lead to a very high supersaturation ratio. More details can be found in the modeling (part III.2 of this chapter). The equation of the supersaturation ratio or saturation index is presented below.

$$S = \frac{\left[Ca^{2+}\right]\left[CO_3^{2-}\right]}{C_{KS}} \qquad \text{and} \qquad \text{Log S=SI} \qquad \text{(Eq.III.1)}$$

where [Ca^{2+}] and [$CO_3{}^{2-}$] are the concentrations (mol/L) of calcium and carbonate ions, c_{K_s} is the concentration solubility product constant of calcium carbonate, and SI is the saturation index.

Sabbides et al., (1992)[250] state that aragonite may also be stabilized depending on the temperature of the supersaturated solutions and on the concentration of foreign ions present in water (Mg^{2+}, oxalate anions, etc.). When the magnesium concentration exceeds 12.97 mol/L, aragonite phase was found while below this concentration calcite was the only phase forming. Ghorbel et al., (2001)[116] tested 57 sources of irrigation water, and the result is that the deposition formed at the level of the drippers fed by these waters is mainly formed of calcite and aragonite accompanied by traces of gypsum. In the work of Tarchitzky et al., (2013)[271], several qualities of treated wastewater were studied to determine fouling in irrigation systems. The fouling layers sampled in the drippers' lateral were subjected to elemental analysis using Scanning Electron Microscopy equipped with Energy Dispersive X-Ray Spectroscopy (SEM-EDAX). The plots selected for analysis contain inorganic and organic matter (IM and OM) in the fouling but with two different proportions (20% and 80% of IM). In both cases, inorganic matter includes the same elements but in a different ratio due to the inorganic nature of the fouling. The material contains most probably insoluble precipitates of calcium phosphates and carbonates, as well as of iron and magnesium. This underlines that the use of treated wastewater promotes calcium precipitation in different forms, mostly in calcium carbonates form.

III.1.3 Precipitate characterization by thermogravimetric analysis (TGA)

In order to complete XRD results, to detect amorphous phases and to qualify the precipitation TGA was used. Thermogravimetric analysis (TGA) studies the evolution of a sample mass in function of an increase of temperature inside a furnace (Annex A.4). The decomposition temperature, the amount of mass loss, and the number of mass variation can give information about the sample composition. The information that can be added to the XRD using TGA is the non-crystallized part of the sample that cannot be detected by the XRD. Figure III.3 shows mass variation of a sample taken randomly from one experience (pH 9.5 temperature 55°C).

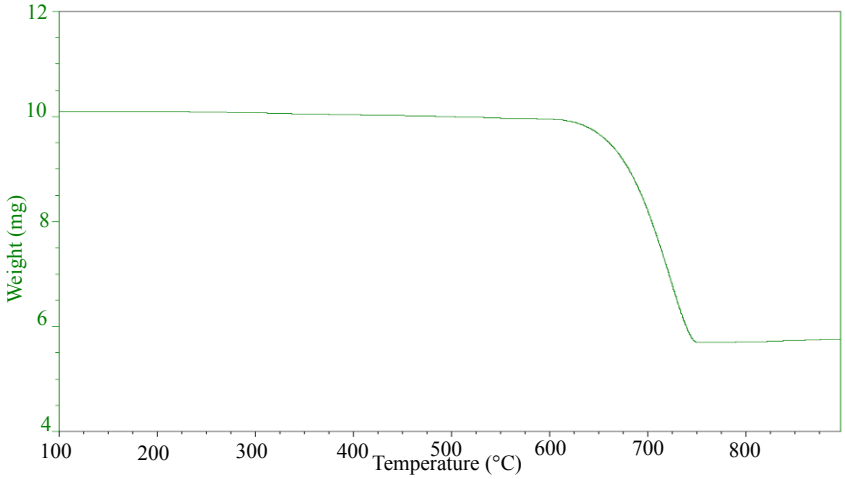

Figure III.3: Mass loss of a sample precipitate (pH 9.5; temperature 55°C) in function of temperature

The descending TGA thermal curve indicates one large mass loss. It occurs between 600 and 750°C. The percentage of this mass loss is 44% from the initial mass. This put into evidence the unique presence of calcium carbonate in the sample. The 44% value represents the mass of CO_2 which is released from the sample. The remaining 56% corresponds to CaO according to the reaction Reaction.III.1:

$$CaCO_3 \longrightarrow CaO + CO_2 \qquad \text{(Reaction.III.1)}$$

In theory, the molar mass of $CaCO_3$ is 100.08 g/mol with 44.01 g/mol for the CO_2. When the CO_2 is released, 43.97% of mass loss occurs, which confirms the results. Li et al., (2013)[172], confirm that during thermal decomposition of a pure phase of $CaCO_3$ one mass loss is observed between 600-850°C, representing 43.8% from the initial mass.

III.1.4 Effect of pH and temperature on calcium carbonate precipitation

Calcium carbonate was identified as the constituent of the precipitate using TWW. The effect of pH and temperature on its formation is essential to understanding chemical fouling when using treated effluents in irrigation. In this study, the precipitation of calcium carbonate is induced by heating and by adding an NaOH solution to water (0.1M) (Reaction.III.2). Carbon dioxide is a very important gas in determining the solubility characteristics of water so in the precipitation of carbonates (Reaction.III.3) (Haman, 1990[126]).CO_2 partial pressure, is interlinked with pH and temperature and the modification of one may entail the modification of the other. To better understand the mechanisms of precipitation and the links between the factors here are the reactions that comes in:

$$OH^- + H^+ \longleftrightarrow H_2O \quad \text{, NaOH is added to the water} \tag{Reaction.III.2}$$

$$CO_2(g) \longleftrightarrow CO_2(aq) + H_2O \quad \text{,} CO_2 \text{ equilibrium} \tag{Reaction.III.3}$$

$$CO_2(aq) + H_2O \longleftrightarrow H_2CO_3 \quad \text{, Carbonic acid} \tag{Reaction.III.4}$$

$$H_2CO_3 \longleftrightarrow HCO_3{}^- + H^+ \quad \text{, Bicarbonate} \tag{Reaction.III.5}$$

$$HCO_3{}^- \longleftrightarrow CO_3^{2-} + H^+ \quad \text{, Carbonate} \tag{Reaction.III.6}$$

$$Ca^{2+} + 2\,HCO_3{}^- \longleftrightarrow CaCO_3 + CO_2 + H_2O \quad \text{, Calcium carbonate precipitation} \tag{Reaction.III.7}$$

III.1.4.1 Effect of pH on calcite precipitation

Calcite precipitation could be momentarily observed when fertigation is performed with high pH fertilizers. As NaOH is added to the water, OH^- neutralises H^+ in Reaction.III.2. This removes H^+ from Reaction.III.5 and Reaction.III.6 which causes these reactions to shift to the right, generating more free $HCO_3{}^-$ in solution. As more NaOH is added, this process continues with accompanying pH increase until enough free $HCO_3{}^-$ is present to exceed the solubility of $CaCO_3$ that results in its precipitation. In Figure V.1, it can be observed that increases only of pH do not induce precipitation especially at 22°C since the precipitation begins after pH 9. This is due to the CO_2 equilibrium since the experiment was done in an open system (in equilibrium with the atmosphere). The more the H^+ is consumed by adding a base, the more Reaction.III.5 will consume H_2CO_3. Reaction.III.4 will also shift to the right as well as Reaction.III.3. Atmospheric CO_2 will dissolve in water to balance the lack of bicarbonate ($HCO_3{}^-$), which causes the precipitation to delay. Two ascertainments were observed in the Figure V.1, which will

be explained below.

a) Analysis of the high volume of added NaOH In Figure V.1, for example for pH 9 at 22°C no precipitation is produced. The volume of NaOH added to reach this pH is 10 ml. For the same pH at 55°C, 293 mg of calcium carbonate precipitate. The volume of NaOH added to maintain the pH at 9 is 34 ml. A higher quantity of NaOH volume must be added to maintain the same pH when precipitation occurs. This phenomenon occurs because between pH 8 and 9.5, HCO_3^- is the predominant carbonate ion (Suarez, 1983[267]). For these conditions, the calcite precipitation reaction can be written as in Reaction.III.7. Reaction.III.7 shows that as $CaCO_3$ is formed, free HCO_3^- is removed from solution; this troubles the equilibrium of Reaction.III.5. To restore the needed balance, reaction shifts to the right to generate more free HCO_3^- and, at the same time, creates additional H^+. The presence of additional H^+ lowers the pH. It is this sequence which causes the pH to decrease as more NaOH is added.

b) Stabilization of calcite mass In Figure V.1, a stabilization of the calcium carbonate mass is observed at 55°C from pH 9 with 293 mg for both pH 9 and 9.5. In Mauguio's water, the calcium concentration is 133 mg/l. Calcium (M = 40.078 g/mol) is a limiting reagent with respect to the carbonates which are always in excess and forms as long as there is equilibrium with the atmospheric CO_2 (Reaction.III.3 till Reaction.III.6). It is considered that all Ca^{2+} is associated with HCO_3^- to form calcium carbonate (M = 100.0869 g/mol) in solid form. The theoretical mass of calcium carbonate ($CaCO_3$) that can be formed with this initial concentration of calcium is 332.5 mg. For Dey et al., (2007)[80], pH and carbonic acid concentration (H_2CO_3) play an important role in the precipitation of $CaCO_3$. Calcium, which is linked to carbonate (carbonate hardness), can be precipitate by the addition of hydroxide ions (OH^-) having a pH above 10. The remaining calcium, i.e., non-carbonate hardness, cannot be removed by simple adjustment of pH. Therefore, soda ash (sodium carbonate) must be externally added to precipitate this remaining calcium. This can explain the difference between the experimental mass of calcium carbonate and the theoretical mass which was based on the total calcium concentration in the water.

III.1.4.2 Effect of temperature and CO_2 partial pressure on calcite precipitation

In field situations, scale deposits are mainly governed by thermal effects (Hui and Lédion, 2002[133]). Heating of the water in the pipes exposed to sunlight results in a decrease in carbon dioxide solubility. The decrease of CO_2 solubility causes the release of CO_2 in the atmosphere (degassing). The release of CO_2 in the atmosphere by heating drives reactions (Reaction.III.3, Reaction.III.4, Reaction.III.5 and Reaction.III.6) to the left, which induces a consumption of H^+ and thus to a rise in pH (Hui and Lédion,

2002[133]). The rise of pH and the presence of calcium ions and carbonic species induce calcium carbonate precipitation (Reaction.III.7) (Hui and Lédion, 2002[133]). In Figure V.1, the increase of pH has more effect on calcite precipitation at 55°C and began even at pH 8.

III.1.4.3 Effect of calcite saturation index on calcite precipitation

As stated earlier, calcium carbonate precipitation kinetics is linked more to the supersaturation ratio or saturation index (SI) (Eq.III.1) than to pH and temperature. In Figure V.1, calcium carbonate precipitation is related to temperature and pH and rise when both are increased. According to Panthi, (2003)[218], taking from Larson and Buswell, (1942)[163], the solubility product (Ksp), which is the same as the equilibrium constant in the case for a solid substance dissolving in an aqueous solution (Eq.II.2), of $CaCO_3$ is related to the temperature and drops when temperatures rise. In the Eq.III.2, T refers to the temperature in °C:

$$\mathrm{p}K_{sp} = 0.001183T + 8.03 \qquad \text{(Eq.III.2)}$$

Pepe et al., 2009[222] state that the saturation index of calcite is related to the pH and rises when pH increases:

$$\text{Log (SI calcite)} = 1.0997pH - 8.0632 \qquad \text{(Eq.III.3)}$$

Wojtowicz, (2001)[296] underlines that a positive saturation index (SI) does not result in calcium carbonate precipitation until a certain certain degree of supersaturation is reached. A supersaturated solution can be obtained by increasing temperature and pH for the same water quality or by increasing water alkalinity and calcium content (Larson and Buswell, 1942[163]).

The experimental results aim to calibrate and validate a model in order to predict which elements will precipitate and what their quantities are without going through laboratory tests every time. Calcite saturation index was found to be the most concerned for the precipitation of calcite which is related on pH and temperature. PHREEQC will calculate the saturation index of calcite, which will induce precipitation when increasing pH and temperature. Two cases of figures will also be taken into account: Water in equilibrium with the atmosphere, and water without equilibrium with the atmosphere.

Part III.2

Numerical characterization of chemical precipitation using TWW

In order to widen the exploratory parameters of temperature and pH and to be able to introduce the partial pressure of CO_2, PHREEQC will be used. PHREEQC is a geochemical model that calculates equilibrium composition in a batch of water-containing reactants. It will be used to model mineral precipitation using TWW under micro-irrigation conditions. This helps to define the limits of water quality and water supply that can be accepted in irrigation systems.

III.2.1 Treated wastewater speciation

The water quality parameters (Table II.5) are introduced in the software. Only elements capable to generate a precipitate were taken into account. Trace elements (concentration below $0.05\ mg/l$), non-dissolved elements (ex TSS) and non-mineral elements (ex N Kjeldahl) (Table II.5) have not been introduced. All concentrations were converted into $mmol/L$ for a better speciation calculation since PHREEQC calculates everything in moles. Activities, molatities and saturation indexes (SI = log IAP – log K) (Section II.1.2.1) were computed using phreeqc.dat database, and activity coefficients were computed with Debye-Hückel (Eq.III.4), as ionic strength (Eq.III.4) is small enough ($I < 0.1M$) (Bourrié et al., 2013[42]). In Mauguio's effluent, the calculated ionic strength is equal to 0.01 M.

$$ln\gamma_i = -\frac{Az_i^2\sqrt{I}}{1 + B\dot{a}_i\sqrt{I}} \qquad \text{(Eq.III.4)}$$

where γ_i is the activity coefficient (dimensionless), A and B are temperature dependent coefficients, ($\dot{a}_i$) is the empirical ion-size parameter and I ionic strength (Appelo and Postma, 2005[19]).

Table III.2 shows the initial saturation index of the elements which are formed according to the quality of the water and the possibility of their dissolution / precipitation. pH 7.8 was taken as the initial pH and 22°C as the initial temperature. According to Table III.2, water is supersaturated, at these conditions, with respect to aragonite, calcite, chalcedony, dolomite, hydroxyapatite, quartz and talc ($SI > 0$). The list of elements proposed by PHREEQC must be coherent with the experimental results. Calcite was the only element selected since it was also the most preponderant element in the samples (Figure III.2).

Table III.2: Saturation indices and formula of the different mineral species

Mineral species	SI	Formula
Anhydrite	-1.74	$CaSO_4$
Aragonite	0.67	$CaCO_3$
Calcite	0.82	$CaCO_3$
Celestite	-3.21	$SrSO_4$
Chalcedony	0.22	SiO_2
Chrysotile	-3.91	$Mg_3Si_2O_5(OH)_4$
Dolomite	0.66	$CaMg(CO_3)_2$
Gypsum	-1.41	$CaSO_4 : 2\,H_2O$
Halite	-6.27	NaCl
Hydroxyapatite	3.38	$Ca_5(PO_4)\,3\,OH$
Quartz	0.65	SiO2
Sepiolite	-2.35	$Mg_2Si_3O_7 \cdot 5\,OH : 3\,H_2O$
Smithsonite	-2.06	$ZnCO_3$
Strontianite	-2.25	$SrCO_3$
Sylvite	-6.64	KCl
Talc	0.18	$Mg_3Si_4O_{10}(OH)_2$
Willemite	-1.98	Zn_2SiO_4

III.2.2 Calcite saturation index in function of pH and temperature

The saturation index (SI) (Eq.II.10) is only an indicator of precipitation of calcium carbonate. The calcite saturation index in Mauguio water is 0.82 for a pH of 7.8 and a temperature of 22°C (Table III.2). As seen in III.1.4.3, SI is pH and temperature dependent. As the temperature and pH rises, the saturation index increases. Figure III.4 shows the different SI of calcite as a function of the temperature at different pH. Calcite SI was calculated in an open system which mean in equilibrium with the atmospheric CO_2 since laboratory precipitation was done in beakers. The aim is to calibrate and validate the numerical results from the laboratory experiments. By varying the temperature, the pH of water can change. To

simplify the interpretation the pHs was fixed at 7.8, 8, 8.5, 9 and 9.5 in Figure III.4. The two blue vertical lines in Figure III.4 indicate the temperatures that were tested in the laboratory which are 22 and 55°C.

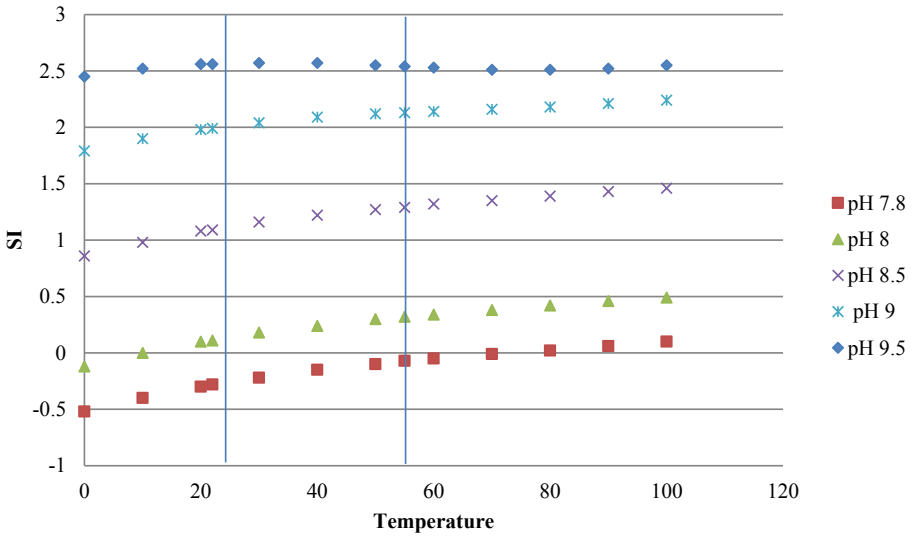

Figure III.4: Saturation indices of calcite at different pH and temperature in an open system.

The initial water pH is 7.8 and pH 8, 8.5, 9, 9.5 represents pH after basifying the water. At pH 7.8, the calcite is under-saturated at any temperature below 80°C and then in equilibrium up to 100°C where the saturation index reaches 0.1. At pH 8, the calcite is supersaturated from 22°C (SI = 0.11), whereas from pH 8.5 for any temperature the saturation index is always higher than 0.86. This value is reached at pH 8.5 for a temperature of 0°C. It can be observed that SI is more related to pH than to temperature. At pH 8, for example, SI increased from 0.18 at 30°C to 0.49 at 100°C while it increased to 1.16 at pH 8.5 for 30°C. Similarly, at pH 9.5 there was no change in the saturation index over the entire temperature range (0 to 100°C). It went from 2.45 to 2.55 at 0°C and 100°C, respectively. This may correspond to the maximum supersaturation value that the calcite can reach for this water quality. But it will be seen hereafter that, although SI is greater than zero ($SI > 0$), calcite will not precipitate.

III.2.3 Experimental and numerical calculation of pH and SI

The aim is to validate the model threw comparisons between numerical, experimental and theoretical pH and between numerical and theoretical SI. Organogram presented in Figure III.5 shows the approach which was followed. The blue arrows indicate the parameters that will be compared.

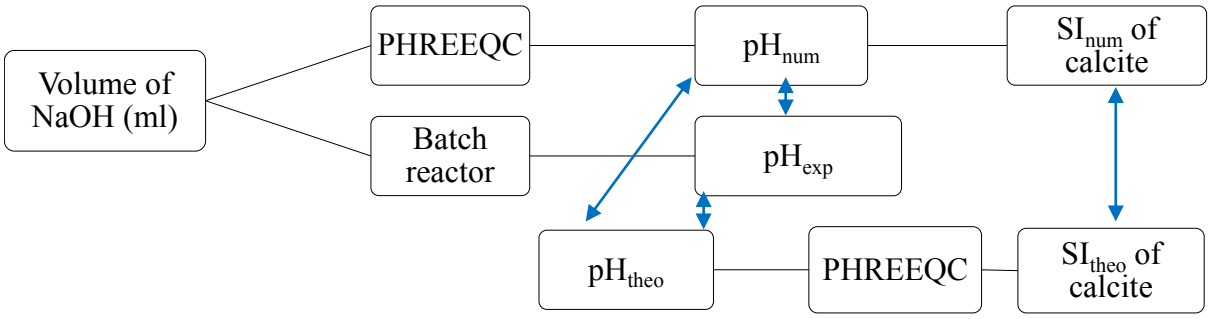

Figure III.5: The process followed which shows the different stages of the modeling allowing to calculate the pH and SI.

PHREEQC calculates pH of the effluent and SI of calcite for each volume of added NaOH. The volumes of NaOH are presented in Table III.1. The values of SI and pH are numerical values (pH_{num} and SI_{num}). The pH measured in batch reactors will be called experimental pH (pH_{exp}). The theoretical values of pH are 8, 8.5, 9 and 9.5 (pH_{theo}). The theoretical pH is the pH we are trying to achieve in our experiments. The values of numerical, experimental and theoretical pHs will be shown in Table III.3 and compared. The theoretical values of the saturation index (SI_{theo}) of calcite was calculated with PHREEQC according to the theoretical values of pH (pH_{theo}). Numerical and theoretical values of calcite SI will also be shown in Table III.3 and compared.

The goal is to predict the precipitation of the calcite according to the values of the saturation index calculated with PHREEQC. The precipitation experiments (Section III.1.1) enables to know at which pH and temperature precipitation begins and the quantity of precipitate at each parameter. For the precipitation experiments, the calculation of calcite SI is impossible (SI_{exp}). PHREEQC will calculate calcite SI based on the pH_{num} and pH_{theo} (Figure III.5). The validation of the model is based on the fact that pH_{num} is very close or equal to pH_{exp} both based on pH_{theo}. In this case the value of SI_{exp} is known and it is the same or very close to SI_{num} and SI_{theo}.

Table III.3 shows the values of pH_{exp}, pH_{num} and SI_{num} after adding the corresponding volume of NaOH for a temperature of 22°C (Table III.3.a) and 55°C (Table III.3.b). pH_{theo} and SI_{theo} are also presented only for a comparative purpose. The volume of NaOH corresponds to the amount of sodium hydroxide added in ml during the laboratory experiments in order to have a theoretical pH equals to 8, 8.5, 9 and 9.5. The experimentally measured pH values are also shown in the table. PHREEQC calculates the pH (pH_{num}) based on the added NaOH volume and the calcite SI (SI_{num}) corresponding to each pH. Another calculation of the calcite SI (SI_{theo}) with PHREEQC was done based on the theoretical pH (pH_{theo}). Table III.3 allows a clearer comparison of the numerical and experimental values.

Table III.3: Comparison between pH_{exp}, pH_{num} and pH_{theo} and between SI_{num} and SI_{theo} at 22°C (a) and 55°C (b).

III.3.a:Comparison between pH_{exp}, pH_{num} and pH_{theo} and between SI_{num} and SI_{theo} at 22°C

Volume of NaOH (ml)	pH_{exp}	pH_{num} calculated after NaOH add	SI_{num} of calcite calculated after NaOH add	pH_{theo}	SI_{theo} of calcite
3	8.06	8.39	1.39	8	1.01
5.25	8.55	8.68	1.65	8.5	1.46
9.75	9.03	9.03	1.93	9	1.85
19.25	9.53	9.47	2.22	9.5	2.12

III.3.b:Comparison between pH_{exp}, pH_{num} and pH_{theo} and between SI_{num} and SI_{theo} at 55°C

Volume of NaOH (ml)	pH_{exp}	pH_{num} calculated after NaOH add	SI_{num} of calcite calculated after NaOH add	pH_{theo}	SI_{theo} of calcite
1.75	8.07	8.03	1.43	8	1.38
4.75	8.55	8.34	1.69	8.5	1.77
33.5	9.05	9.54	2.35	9	2.05
39.25	9.66	9.7	2.39	9.5	2.19

From the results of Table III.3 it can be seen that:

- At 22°C (Table III.3.a) at high pH (pH values obtained after adding 9.75 and 19.25 ml of NaOH), there is no difference between pH_{exp} and pH_{num} values. For example, for a volume of NaOH equal to 9.75 ml, the pH is 9.03 for both measurements. Whereas at lower pH (pH values obtained after adding 3 and 5.25 ml of NaOH), the difference is greater. For a volume of added NaOH equal to 3 ml, pHexp is equal to 8.06 while pH_{num} is equal to 8.39.

- At 55°C (Table III.3.b) this difference is mainly observed for a volume of NaOH equal to 33.5 ml. pH_{exp} is equal to 9.05 while pH_{num} is equal to 9.54. These differences may be due to the buffering effect of water that has been underestimated by the software.

- For the saturation index values, the difference between the numerical values after adding NaOH (SI_{num}) and the theoretical values (SI_{theo}) is that for SI_{theo} the pH has been fixed at 8, 8.5, 9 and 9.5. The largest difference of calcite SI values observed between the numerical and the theoretical at 22°C is for a pH of 8 where SI_{num} is equal to 1.39 and SI_{theo} is equal to 1.01.

- At 55°C, the largest difference is observed for a pH of 9 where $SI_{num}$is equal to 2.35 and SI_{theo} is equal to 2.05. For the other pH values, the difference is smaller (Table III.3).

According to Figure III.4 and Table (III.3), the saturation index of calcite is mainly linked to pH. In

Table (III.3) if the values of SI_{theo} are compared at pH 9.5 for example, the SI increases from 2.12 for a temperature of 22°C to 2.19 for a temperature of 55°C. While it increases from 1.01 for a pH of 8 at 22°C up to 2.12 for a pH of 9.5 at the same temperature. The difference between the values of SI_{num} and SI_{theo} in Table (III.3) is due to the variation between the values of pH_{num} and pH_{theo}. For this reason a very accurate pH measurement seems necessary in order to determine the SI of the calcite in the solution. PHREEQC has been validated for the calculation of pH and SI. It can subsequently be used in the calculation of the calcite precipitation.

III.2.4 Numerical precipitation of calcite

The objective is to simulate calcite precipitation under micro-irrigation conditions. To do so, the pH and temperature that were used for batch reactor precipitation were introduced in PHREEQC. Temperature, pH and CO_2 partial pressure were the environmental conditions that have been modulated. In paragraph III.2.3 experimental and numerical values of pH and SI were calculated and compared. In this paragraph, calcite mass and the variation of pH and SI before and after precipitation will be followed. According to Figure III.4, starting from pH 8.5 the calcite is always supersaturated at any temperature ($SI > 0$). For a pH of 8, it is supersaturated from 20°C. According to laboratory experiments, for the same conditions calcite does not precipitate even if the water is supersaturated with respect to calcite ($SI > 0$). To calibrate the model in order to be able to simulate calcite precipitation, numerical mass and experimental mass of calcite must be the same. To do so SI_{num} was introduced by trial and error to meet this objective. Organogram presented in Figure III.6 shows the approach used to allow validation of the numerical calculation of calcite precipitation based on experimental results.

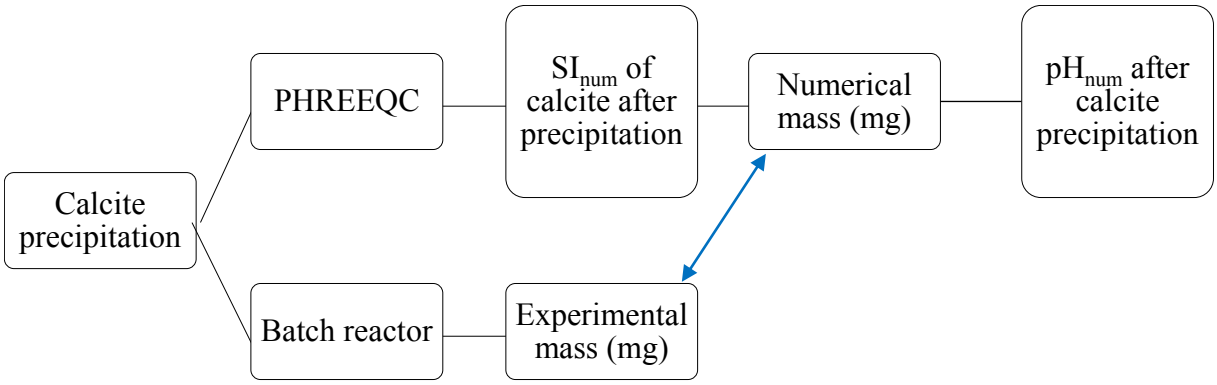

Figure III.6: The process followed which shows the different stages of the modeling allowing to calculate the mass of calcite and the saturation index after precipitation.

The precipitation of the calcite was taken up by the software by introducing the saturation indices of the calcite allowing a mass of precipitate close or equal to that obtained in experimentation. For example, for pH 8 at 22°C the experimental mass of calcite is $0.67 \pm 0.31mg$ (Table III.1). The numerical value for the same conditions (pH 8 at 22°C) is 0.42 mg (Table III.4). The validation of the model was carried out under the same operating conditions as the experiment (pH, temperature and atmospheric CO_2). Table III.4 shows the results of the different values of SI, pH and mass of calcite calculated by PHREEQC after precipitation for 22 and 55°C.

Table III.4: SI and pH values after precipitation under the same operating conditions as the experiment with the corresponding mass of calcite at 22 and 55°C.

SI, pH, and mass of calcite after precipitation occurs at 22°C			SI, pH, and mass of calcite after precipitation occurs t at 55°C		
pH_{num} after calcite precipitation	SI_{num} of calcite after precipitation	Mass of calcite (mg)	pH_{num} after calcite precipitation	SI_{num} of calcite after precipitation	Mass of calcite (mg)
8.87	1.78	0.42	8.84	1.81	68.68
8.88	1.805	0.47	8.81	1.685	108.91
8.91	1.849	1.37	8.78	0.85	295.59
8.8	1.42	141.64	8.85	0.98	294.59

At 22°C according to Table III.3 and Table III.4 precipitation begins when after adding NaOH, the SI of calcite is between 1.93 and 2.22 (Table III.3.a). It corresponds to a pH between 9 and 9.5. The corresponding experimental calcite weight is 1.3 mg and 140.1 mg respectively (Table III.1). For the first two volumes of added NaOH (3 and 5.25 ml) (Table III.3.a), the pH after precipitation increases (Table III.4). It goes from 8.4 and 8.7 to 8.8 in both cases, and the same goes for the values of SI. SI increases from 1.39 to 1.78 for the first volume and from 1.65 to 1.8 for the second one. No precipitation occurred to reduce these values and overcome the added NaOH. When precipitation occurred even in very small quantities (1.3 mg of calcite), the pH and SI began to decrease. pH dropped from 9.03 to 8.91 and SI from 1.93 to 1.849 for a volume of 9.75 ml of NaOH.

At 55°C, precipitation begins following the first volume of added NaOH (1.75ml). The pH is 8 and the mass of calcite is $68.75 \pm 12.69\ mg$ (Table III.1). The value of SI after adding 1.75 ml ofNaOH is 1.43 (Table III.3). The values of pH and SI began to decrease compared to the values before precipitation since a volume of added NaOH is equal to 33.5 ml (Table III.4). The high quantity of precipitation overcomes the high quantity of added NaOH. Before this value, the volume of NaOH takes over. The numerical pH after adding 33.5 ml of NaOH is 9.54 and it decreases to 8.87 after precipitation. For SI, it was 2.35, decreasing to 0.85. At these values of NaOH (33.5 and 39.25 ml) and temperature (55°C), the precipitation is almost complete. The saturation index drops to nearly that of the calcite in the initial state (initial SI = 0.8). The drop in SI is due to the decrease in the concentration of Ca^{2+} and HCO_3^- linked to

precipitation and not to the pH. For all the values of NaOH added and calcite mass, the pH after precipitation is invariable in 22°C and 55°C even with a high rate of precipitation. It is due to the equilibrium of the carbonic system since the water is in equilibrium with the atmospheric CO_2. Maximum pH was 8.9 and minimum pH was 8.7. A certain supersaturation value must be achieved, which is not the same at 22 or at 55°C. At 22°C, precipitation begins for an $SI >$ than 1.99 while at 55°C the precipitation is already detectable from SI = 0.32.

According to Table III.4, it can be seen that in an open system (in equilibrium with atmospheric CO_2) the pH values after precipitation are invariable. So a follow-up of the water pH alone does not allow prediction or detection of any calcite precipitation. The follow-up of the saturation index of calcite seems a more efficient and accurate tool. This was also suggested by Hills et al., in 1989 [128]. Table III.5 shows the different saturation index values of calcite at different temperature and pH. The red rectangle (round dots) surrounds the saturation indices of the calcite where there was precipitation for a temperature equal to or higher than 55°C. The blue rectangle (square dots) surrounds the saturation indices of the calcite where there was precipitation for a temperature equal to or higher than 22°C. The green triangles (solid line) surrounds the saturation indices of the calcite where there may be precipitation.

Table III.5: Values of calcite SI at different pH and temperature. The round dots (red) and square dots (bleu) rectangles surround calcite SI where there was precipitation for a temperature equal to or higher than 55°C and 22°C, respectively. The solid line triangles (green) surrounds the saturation indices of the calcite where there may be precipitation.

Fix pH / **T °C**	**8**	**8.5**	**9**	**9.5**
0	0.68	1.15	1.57	1.9
10	0.84	1.3	1.71	2.02
20	0.98	1.44	1.83	2.11
22	1.01	1.46	1.85	2.12
30	1.11	1.56	1.93	2.17
40	1.23	1.67	2.01	2.22
50	1.34	1.76	2.07	2.25
55	1.39	1.8	2.1	2.26
60	1.45	1.85	2.13	2.27
70	1.55	1.92	2.17	2.29
80	1.64	1.99	2.22	2.31
90	1.74	2.07	2.26	2.34
100	1.83	2.14	2.32	2.38

Based on PHREEQC analysis and laboratory experiments, the results show a very close relationship in the case of limestone water. The calcite precipitation can be predicted from Table III.5. For example, for a temperature equal to 10°C the saturation index of calcite even if it is equal to 1.3 at pH 8.5 there will be no precipitation. The risk of precipitation starts once the water reaches 30°C. This table can be used for water qualities close to those of Mauguio. For very different water qualities, other validation must be done.

III.2.5 Effect of CO_2 partial pressure on calcite precipitation

The partial pressure of the CO_2 can play a very important role on the dissolution / precipitation of calcite (paragraph III.1.4). This parameter is introduced to PHREEQC, with the pH and temperature, to see its effect on calcite precipitation in micro-irrigation condition. In micro-irrigation, it can be considered that the water inside the pipes is not in equilibrium with the atmosphere (closed system). The time the water takes passing through the pipe to the dripper and the pressure applied in the irrigation system influences the partial pressure of the CO_2 as well as precipitation. Sherlock et al., (1995)[254] pointed out that the absence or presence of carbon dioxide strongly influences the solubility of calcite. Table III.6 shows the results of the different values of SI, pH and mass of calcite calculated by PHREEQC after precipitation for 22 and 55°C in a closed system (without equilibrium with atmospheric CO_2).

Table III.6: SI and pH values after precipitation under the same operating conditions as the experiment with the corresponding mass of calcite at 22 and 55°C without equilibrium with the atmosphere.

SI, pH, and mass of calcite after precipitation occurs at 22°C			SI, pH, and mass of calcite after precipitation occurs at 55°C		
pH_{num} after calcite precipitation	SI_{num} of calcite after precipitation	Mass of calcite (mg)	pH_{num} after calcite precipitation	SI_{num} of calcite after precipitation	Mass of calcite (mg)
8.43	1.43	0.31	7.32	0.6	55.63
8.71	1.67	0.81	7.1	0.25	102.3
9.05	1.94	1.45	8.94	0.95	295.4
8.19	1.5	143.54	9.37	1.2	295.8

Calcite SI and pH in Table III.6 were calculated in the same way like in Table III.4 but without equilibrium with atmospheric CO_2. At 22°C, SI_{num} and pH_{num} increase until precipitation occurs. The pH decreases from 9.05 to 8.19, and SI decreases from 1.94 to 1.5. Contrary to Table III.4, the SI values are related to the pH and temperature values rather than to the concentration of Ca^{2+} and HCO_3^- in the solution. At 55°C, the relationship between calcite SI and pH is also observed. The mass of calcite does

not affect the values of SI. Calcite SI and pH follow the same trend, when pH decreases, SI decreases and vice-versa. For a pH of 7.32, SI is 0.6. The pH decreases to 7.1 due to an increase of precipitation. Calcite SI decrease to 0.25, and calcite mass increases from 55.6 to 102.3 mg. When a higher volume of NaOH is added, an increase of precipitation is also observed (295 mg). Even if the precipitation is almost total it does not overcome the hight volume of added NaOH. pH increases to 8.94, and SI increases to 0.95, as well. Calcite precipitation is more difficult in an open system than in a closed system especially at high pH for both temperatures. The SI values at high pH in Table III.4 are lower than the one in the same conditions in Table III.6. The lower the saturation index, the harder it is for calcite to precipitate. For example, for the third volume of added NaOH the calcite SI at 22°C is 1.849 and 1.94 in an open and closed system, respectively. At 55°C the calcite SI is 0.85 in an open system and 0.95 in a closed one.

Precipitation of calcite is greater in a closed system especially at high pH for both temperature. In irrigation, even at low temperatures, water that is equilibrated with the atmosphere in reservoirs before supplying the irrigation system will be subject to less chemical precipitation.

Conclusion

Chemical precipitation using treated wastewater under micro-irrigation conditions was studied and monitored in batch reactors. Laboratory experiments were conducted to validate and calibrate PHREEQC. The purpose of PHREEQC model is to predict the quantity and quality of mineral precipitation using TWW without going through laboratory tests. The influence of temperature, pH, and the presence or absence of atmospheric CO_2 equilibrium on the precipitation of dissolved salts was the key of the study. Characterization of chemical precipitation was done using XRD and TGA.

Precipitations was carried out at pH 8, 8.5, 9 and 9.5 at 22 and 55°C. This pH is the theoretical pH that we are trying to achieve, it will be defined as pH_{theo}. In the batch reactors, the precipitations was done in an open system (with equilibrium with the atmospheric CO_2). Increasing the pH and temperature of Mauguio's TWW induce an increase of the precipitation. Temperature was increased using a thermostatic bath. The pH was increased using a solution of NaOH (0.1M) the pH obtained was defined as experimental pH (pH_{exp}). Calcium carbonate in calcite form was found to be the most predominant and stable precipitate. All dissolved calcium precipitates in combination with the carbonates from pH 9 at 55°C.

The parameters of the water quality used in the laboratory test was introduced to PHREEQC. PHREEQC calculates the saturation index of all the elements able to be formed. We were interested only in calcite based on the laboratory results and because PHREEQC also showed that calcite is the most abundant precipitate using Mauguio's TWW quality. The SI of calcite was equal to 0.82. Even if the value is positive no precipitation is formed. The model provided proof that calcite precipitates at a given degree of supersaturation, which can be achieved by increasing pH and temperature.

The increasing of pH was done by introducing to PHREEQC the same quantity of OH^- used in the laboratory test. The obtained pH was defined as numerical pH (pH_{num}). For each value of pH_{theo} and pH_{num} a SI_{theo} and SI_{num} was calculated. To validate the model pH_{theo}, pH_{num} and pH_{exp} was compared as well for SI_{num} and SI_{theo}. The values were very close in most cases (for example at 22°C for a pH_{theo} equal to 9.5, pH_{exp} = 9.53 and pH_{num} = 9.47 for the saturation index of calcite SI_{theo} is equal to 2.12 while SI_{num} is equal to 2.22). This proof the efficiency of PHREEQC to be used as a tool to calculate

calcite precipitation under micro-irrigation conditions.

The calculation of calcite precipitation was done by calibrating the saturation index of calcite to obtain the same mass of calcite as in the laboratory experiment. The values of SI when the precipitation occurs was higher than 0.82. At a high temperature (55°C) the value of SI_{theo} that led to calcite precipitation was 1.39 above a pH of 8, while it was 2.12 at 22°C at pH 9.5. According to that, a grid was done to estimate the values of SI that lead to calcite precipitation in function of temperature and pH (Table III.5).

To enlarge more the modeling experiments and to be in a real case of micro-irrigation condition the effect of CO_2 partial pressure was also investigated. CO_2 partial pressure has an effect on calcium carbonate precipitation since it is involved naturally in the control of the pH. CO_2 water concentration change depending on the water temperature. So the pH, temperature and CO_2 partial pressure are interlinked and can affect the SI of calcite. In an open system, i.e., in equilibrium with CO_2, the solubility of calcite increased due to a constant supply of CO_2 (SI_{num} = 1.78 in an open system at 22°C while it is equal to 1.43 in a closed system for the same temperature). To minimize calcite precipitation in irrigation, water should be stored in open reservoirs at a low temperature and a low pH.

Chemical precipitation in micro-irrigation conditions will be studied in parallel with biofilm development in the Chapter IV of this work.

Chapter IV

Characterization of biological fouling and its interaction with chemical precipitation

Introduction

According to chapter III which was dedicated solely to chemical fouling, we were interested in this chapter on the biofilm development and its interaction with chemical precipitation using treated wastewater (TWW). We decided to focus our study on the parameters affecting the clogging of the drippers and the fouling of the pipes being the major problems encountered in irrigation using TWW.

Shear stresses are among the major parameters affecting biofilm development, we will centered this study on those encountered inside drippers and pipes. Plus, from the results of chapter III calcium carbonate was the major element found in the precipitate. On this, the effect of calcium carbonate on biofilm development will be studied. In this chapter the experiments will be divided into two parts:

The first part will be dedicated to study the impact of shear stress on fouling evolution and on biofilm development inside a Taylor-Couette Reactor (TCR) using TWW. The values of shear stresses were chosen based on those calculated in drippers (2.2 and 4.4 Pa) and pipes (0.7 Pa) (paragraph II.2.3). The TCR was used as a tool for the biofilms development because the shear stresses are well controlled. Fouling, developed on polyethylene plate made from an irrigation pipe, was monitored over a period of eight weeks to study the evolution of fouling and biofilm development in function of time. The results between the different shear stresses were then compared.

The second part of this chapter is focused more on the effect of calcium carbonate on biofilm development inside pipes and drippers. To do so, an irrigation set-up fed with two different water qualities was implemented. One water quality contains a solution of calcium carbonate formation precursors ($CaCl_2$ and $NaHCO_3$) and the other does not contain this solution. The goal was to be able to study the effect of $CaCO_3$ on biofilm development. Fouling inside pipes and drippers was monitored over time (seven weeks) for the two water qualities. Drippers' flow rates were also monitored to determine whether $CaCO_3$ has a positive or negative effect on drippers' biological fouling and clogging. Electronic microscopy was used to detect the general appearance of the fouling and to observe the preferential zones, inside the dripper, of biofilm growth during the experimental studies.

Fouling was quantified and qualified the same way in TCR and in the irrigation pilot plant: A measure of total solids (TS) and volatile solids (VS) to see the ratio between organic and inorganic matter, X-ray diffractometry (XDR) and thermogravimetric analysis (TGA) to analyze the precipitate and its crystalline phase. As the TCR resumes the same shear stresses inside the pipes and drippers a comparison of its results will be made with the one of the irrigation set-up.

Part IV.1

Effect of shear stress on biofilm development and chemical precipitation inside Taylor-Couette Reactor when using treated wastewater.

As seen in chapter I, shear stress is a parameter that influences the growth, the agglomeration mechanisms, and the detachment of biofilm and has an impact on biofilms bacterial composition and structure (Stoodley et al., 1999[263]; Rochex et al., 2008[246]). In micro-irrigation many shear stresses values can be encountered whether inside the pipes or inside the drippers. The effect of shear stress on biofilm development will be studying using a Taylor-Couette Reactor (TCR).

IV.1.1 Validation of the protocol for monitoring the biofilm development kinetics

To be able to use the TCR as a tool to develop and to follow the biofilm over time it is necessary to ensure that the growth of the biofilm is independent on the position of the plate. Three experiments, for repeatability, were carried out with a shear stress of 2.2 Pa over a period of 2 weeks in order to demonstrate the homogeneity of the biofilm development over the 5 plates.

After 2 weeks of growth the five plates were removed in the same time to examine spatial variation of the fouling. The fouling was collected and weighted. It is measured by the quantity of total solids

(TS) in mg (Annex A.4) over the surface of each plate (243.2 cm^2). Figure IV.1 shows the average of the fouling over the three experiments. The error bars corresponds to the standard error of the mean (SEM) which is calculated by dividing the standard deviation (SD) by the square root of the sample number (here 5).

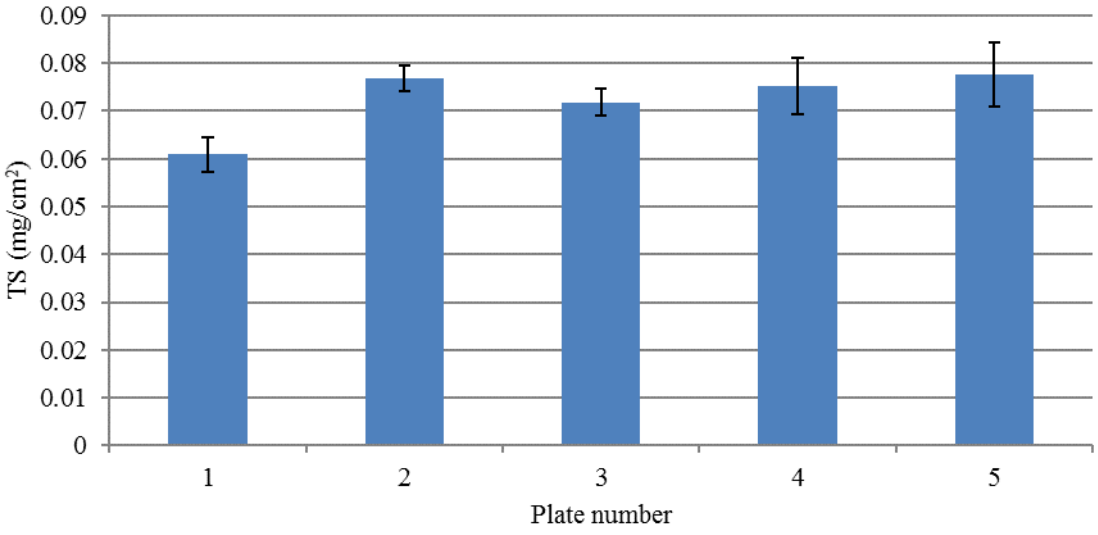

Figure IV.1: Average of the fouling for the three experiments measured in total solids (TS) for the 5 plates. The error bars correspond to the SEM.

In Figure IV.1, it can be observed that over the five plates the fouling was almost the same. Since the collected quantity is very low, the difference between the samples can be related to the measurement error (Error related to the operator + error related to the balance + error related to the surface of each plate). The quantity of the fouling vary from 0.061 ± 0.003 mg/cm^2 for the first plate to 0.077 ± 0.006 mg/cm^2 for the plate number 5. Once the hydrodynamic conditions are well controlled and the homogeneity of the latter are verified over the entire height of the reactor the experiences can begin.

IV.1.2 Evolution of the fouling in the TCR

In order to analyze the effect of shear stress on biofilm development, the TCR run for a period of eight weeks. Shear stresses found in irrigation pipes (0.7 Pa) and in drippers (2.2 Pa and 4.4 Pa) (section II.2.4) were studied.

The biofilm was characterized by the measurement of its total solids (TS) (figure IV.2) and volatile solids (VS) (figure IV.4) masses in mg over a plate surface in cm^2. The results allowed characterization of the biofilm development as a function of shear stress and time.

Figure IV.2 presents the variation of TS which is the dry matter mass in mg / plate surface in cm^2

over eight weeks of experiment for shear stresses of 0.7, 2.2, and 4.4 Pa. As previously described in chapter II, the values presented in figure IV.2 correspond to sampling performed at one week interval except for the first sampling. The first measurement was made after two weeks of experiment operation in order to allow the biofilm to initiate and develop. The dashed lines represent the time in weeks where biofilm was collected, which also represent the age of the biofilm. Over eight weeks of operation, the maximum age of the biofilm was six weeks. Figure IV.2 represent the mean of the TS mass/cm^{2}of the two repetitions, and errors bars represent their standard error of the mean (SEM).

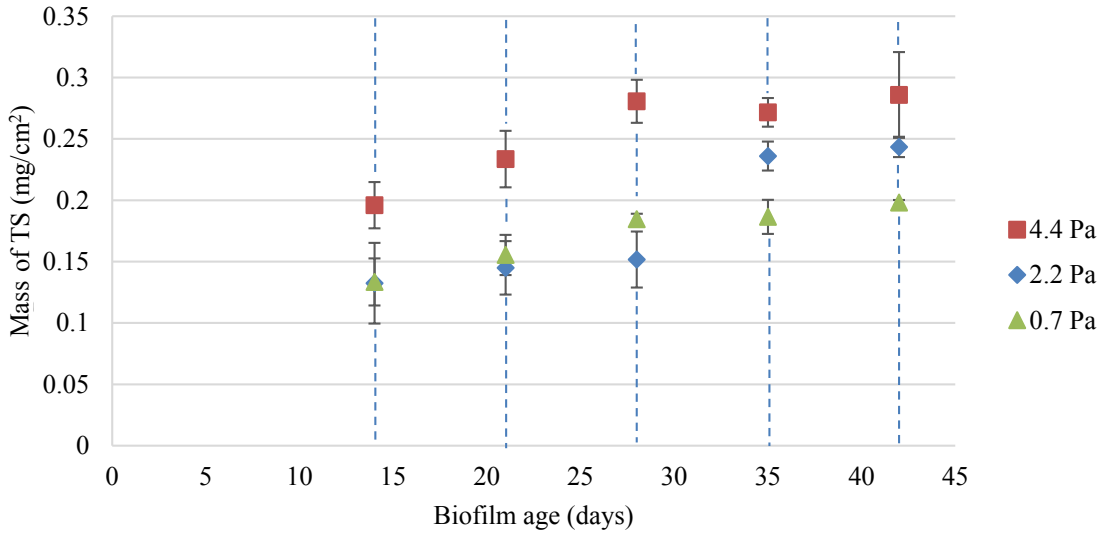

Figure IV.2: Evolution of the amount of total solids obtained in the TCR over time for 0.7, 2.2 and 4.4 Pa.

The initiation of the biofilm which normally occurs during the first 2 weeks of development of biofilm could not be measured and demonstrated in this study due to the impossibility of collecting very small quantities of fouling. This phase, which takes in general 10 days, corresponds to the latency phase in which the fixation of the bacteria to the support is initiated (Characklis, 1981)[59]. During this phase, the microorganisms are not firmly attached so they can be easily detached from the support by the hydrodynamic conditions (Characklis, 1981)[59].

In figure IV.2 it can be observed that after 14 days, whatever the shear stress, the evolution of the fouling follows the same trend. In all three cases of shear stress the curves can be divided into two parts: a first part that would be between 14 and 28 days of biofilm age and a second part that would be between 28 and 42 days of biofilm age.

For 0.7 and 2.2 Pa the quantity of total solids (TS) per unit area is the same at 14 days (0.13 mg/cm^2 error $\pm$ 0.025). For a shear stress of 2.2 Pa the quantity of TS increase between 28 and 35 days from 0.15 mg/cm^2 $\pm$ 0.02 to 0.23 mg/cm^2 $\pm$ 0.01, respectively. At 42 days the curve returns to a plateau with an amount equal to 0.24 mg/cm^2 $\pm$ 0.008. For 0.7 Pa it is also observed that the curve

has two shapes. The quantity of TS increases between 14 and 28 days, from 0.18 mg/cm^2 $\pm$ 0.01 to 0.2 mg/cm^2 $\pm$ 0.002, respectively. Then a stabilization phase occurs between 28 and 42 days.

For a shear stress equal to 4.4 Pa, the curve shape in figure IV.2 follows the same trend as that of 0.7 Pa but the quantities are higher. An increase in the quantity of TS from 0.19 mg/cm^2 $\pm$ 0.01 to 0.28 mg/cm^2 $\pm$ 0.01 is observed between 14 and 28 days, respectively. From 28 days a plateau is observed where the quantity stabilizes up to 42 days, also with a value of 0.28 mg/cm^2 $\pm$ 0.03.

Some knowledge of the amount of organic matter (OM) in the fouling is necessary to explain the development of the biofilm in function of time and the applied shear stresses. The OM refers to the quantity of biofilm developed, and it is obtained after taking the samples from one repetition of each experiment and passing it in an oven at 550°C for 2 hours (Annex A.4).

Figure IV.3 shows the amount of organic matter (OM) in percentage with respect to the TS in function of the biofilm age in days for different shear stresses.

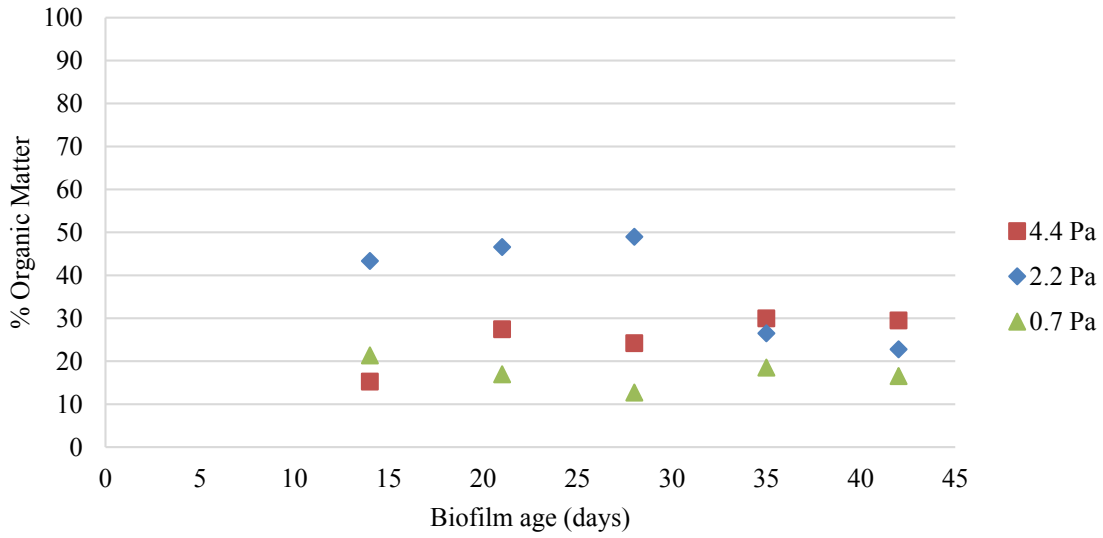

Figure IV.3: Evolution of the amount of organic matter expressed in percentage as a function of time in days for each shear stress

Figure IV.3 put into evidence the dominant mineral composition of the samples. For the three shear stresses the percentage of organic matter is less than 50% throughout the experiment. The average percentage of organic matter for a shear stress of 0.7 Pa is 17.2%, and the standard error of the mean is $\pm$ 1.26. For a shear stress of 2.2 Pa the value is 37.6 $\pm$ 4.84% and for 4.4 Pa it is 25.3 $\pm$ 2.42%. The most important point in figure IV.3 is that at the end of the experiment (after day 28) the percentage of organic matter accumulated for a shear stress at 4.4 Pa is greater than the one at 2.2 Pa which is greater than the one at 0.7 Pa. The values for day 42, for example, are 29.5%, 22.7% and 16.5%, respectively. For 2.2 Pa, the decrease in the percentage of organic matter from 50% to 30% between day 28 and day 35 is not due to a detachment of the organic matter (figure IV.4) but rather to an increase in the chemical

precipitation produced during this period. Since the sample is mainly formed with IM (Figure IV.3), the effect of shear stress on biofilm development must be followed on the organic part of the fouling. The quantity of volatile solids (VS) which is the same as the quantity of OM is represented in figure IV.4.

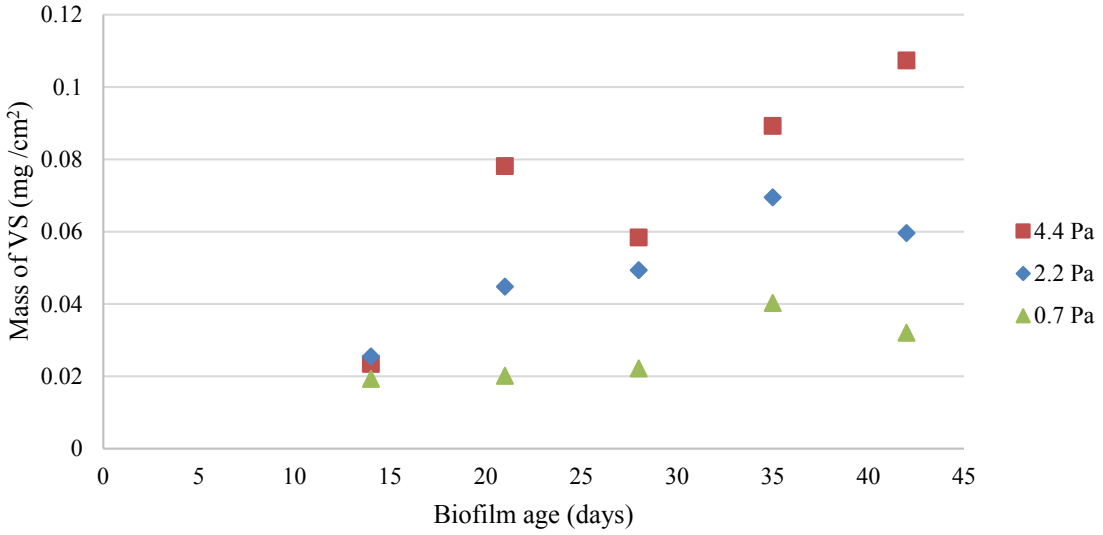

Figure IV.4: Evolution of the amount of volatile solids (VS) in TCR over time for 0.7, 2.2 and 4.4 Pa.

Figure IV.4 represents the evolution of volatile solids (VS) in mg over the surface of the plate in cm2 in function of the age of biofilm for 0.7, 2.2 and 4.4 Pa. It highlights the effect of shear stress on biofilm development.

At the beginning, the amount of biofilm measured at 14 days of experimentation is on the order of 0.02 mg/cm^2 for the three shear stresses. From 20 days of experimentation, a difference is observed between the quantities of biofilm developed for the three operating conditions. In fact, the amount of biofilm obtained with a shear stress of 4.4 Pa appears to be 1.5 to 3 times greater than that obtained with a shear stress of 2.2 or 0.7 Pa, respectively. For 4.4 Pa the mass of the VS over the surface of the plate is 0.078 mg/cm^2. This value is equal to 0.044 mg/cm^2 for a shear stress of 2.2 Pa and 0.02 mg/cm^2 for a shear stress of 0.7 Pa.

For 0.7 Pa it can be observed that the latency phase is prolonged until 28 days. After 28 days the amount of biofilm is increased from 0.022 mg/cm^2 to 0.04 mg/cm^2 at day 35 then decreased (20%) at the end of the experiment to 0.032 mg/cm^2 at day 42. For 2.2 Pa no latency phase is detectable. The exponential phase begins from day 14 until day 35 where the amount of biofilm increases to 0.069 mg/cm^2. After day 35, a decrease (15%) is also observed at the end of the experiment where the amount of VS per unit of surface area is 0.059 mg/cm^2.

Generally speaking, the quantity of biofilm for a shear stress of 4.4 Pa constantly increased except at day 28 where there was a decrease of 25% in the amount of VS. The value decreased from 0.078

mg/cm^2 to 0.058 mg/cm^2 in one week. Belkhadir et al., (1988)[30] observed that the growth kinetics of biofilms are divided into several phases described by a sigmoid curve. The growth of the bacteria begins with a latency phase. It is followed by an exponential growth phase of the bacterial population where the biofilm develops rapidly and grows in thickness. Then comes a stage where the development slows down to achieve the stage of maturation and then detachment.

A short latency phase like in the case of 2.2 and 4.4 Pa can be explained by the high shear stress generated by high velocities. It reduces the thickness of the diffuse layer which promotes the more rapid adhesion of the bacteria (Liu and Tay, 2002[176]; Vrouwenvelder et al., 2010[286]). This induces the production of exopolymers and more particularly polysaccharides in higher quantity than for lower sheer stresses, ensuring a more rigid structure with a greater cohesion between the cells (Decho, 2000[75]).

In figure IV.4 it is observed that when the shear stress increases the attachment and the development of biofilm increases too. The amount of biofilm thats develops at 4.4 Pa is higher than the one developed at 2.2 Pa and even higher than the one at 0.7 Pa. Wasche et al., (2002)[287] observed the impact of hydrodynamic conditions on biofilms development. The increase in hydrodynamic conditions in a range of Reynolds numbers from 650 to 6000 leads to an increase in biofilm density. In order to resist the strong hydrodynamic conditions, biofilms must develop a denser structure (Kwok et al., 1998 [161]; Picioreanu et al., 2001[228]). Melo and Vieira, (1999)[190] have also shown that for turbulent flows (between 4200 and 12000), high flow velocities favor the development of a more compact and stable biofilm that is more resistant to detachment, which explains probably our results.

The works cited above suggest that the increase in hydrodynamic conditions favors the supply of substrate in biofilms, and consequently their development. Moreover, high flow velocities favor biofilm resistance by modifying their structure (Melo and Vieira, 1999[190]; Wasche et al., 2002[287]). In this study, the Reynolds number were greater than in the studies cited above especially for 4.4 Pa ($Re = 27605$) and 2.2 Pa ($Re = 18621$). In figure IV.4, a decrease in the amount of biofilm at day 28 for 4.4 Pa and at day 42 for 2.2 and 0.7 Pa is observed. This decrease is probably due to the biofilm detachment on the basis of two hypothesis: either the biofilm has become quite thick or old enough to detach.

According to section II.2.2 in chapter II all the experiments, for the three shear stresses, were conducted under turbulent regime. The difference in the results in figure IV.4 is only due to change in shear stress. We can conclude that shear stress appears to be a parameter that promotes biofilm development. Due to a lack of data on the density and thickness of the biofilms during their development phases for each shear stress, the hypothesis concerning the effect of hydrodynamic conditions on the structure of the biofilm and its detachment could not be confirmed.

In figure IV.4, a reflection could be made concerning the reduction of the quantity of biofilm at the fourth week for 4.4 Pa. During biofilm collection the reactor is stopped to allow removal of the

corresponding plate and then immediately restarted. The sudden changes in hydrodynamic conditions like the abrupt increase in the rotational speed from 0 to 190 rpm ($Re = 0$ to $Re = 27605$) may have caused this decrease. Knowing that each week the reactor is stopped and then restarted, the decrease in the amount of biofilm in the middle of the experiment was observed only for a shear stress of 4.4 Pa at 28 days of biofilm age. This may be due to the very rapid growth that is produced at the beginning of the experiment between week 2 and week 3. This rapid increase probably produces a hardly compact and fragile biofilm towards a change in hydrodynamic conditions.

The effect of the sudden change in hydrodynamics conditions on the biofilm development has also been observed in the works of Horn et al., (2003)[131]. In their study, Horn et al., (2003)[131] characterized the detachment of biofilm by measuring the suspended solids at the outlet of a biofilm tube reactor after applying a high shear stress. After increasing the flow velocity from 0.6 m/s to 1.2 m/s, 50 to 70% of the biomass was detached after 10 seconds. The thickness of the biofilm decreased from 1200 to 600 μm.

In figure IV.4, after the decrease of the amount of biofilm that occurred at week 4 a multiplication of biofilm is observed which is produced up to week 6. This phenomenon was also observed in the work of Choi and Morgenroth, (2003)[62]. They observed that an increase of shear stress from 1.1 Pa to 3.1 Pa induces within seconds a significant increase in effluent suspended solids (SS) concentration due to detachment. The concentration of SS in the effluent was 10 mg/ℓ, and it increased to 600 mg/ℓ instantaneously then decreased quickly to 1 mg/ℓ due to a washout of detached particles. After two hours the concentration of SS increased from 1 mg/ℓ to return to the steady state value of 10 mg/ℓ. This shows that the biofilm even after detachment or reduction of its concentration or quantity due to any perturbation can recover and return to its equilibrium value.

For 4.4 Pa (figure IV.4), the biofilm not only returned to its equilibrium value but continued to develop. Among several reasons is that biofilm developed under constant high shear stress becomes denser and more resistant to shear stress (Wasche et al., 2002[287]).

In order to highlight the TCR performance and the biomass production the yield rate (Y) was calculated. Figure IV.5, shows the yield rate production of biofilm, corresponding to the variations in the cellular material generated represented by the amount of VS (in mg) (values in figure IV.4 $\times$ the surface of the plate). This yield rate is obtained by linking the amount of biofilm produced weekly (in mg) for a shear stress of 4.4 Pa to the quantity of chemical oxygen demand (COD) consumed (in mg) during the same period (one week) (Eq.IV.1). The calculation is detailed in Annex A.10. For the other shear stresses, yield rate could not be calculated due to a lack of data concerning COD.

$$\text{Yield rate} = \frac{\mathrm{m_b}}{\mathrm{m_{COD}}} \tag{IV.1}$$

With m_b: mass of biofilm that develops on all the plates at a period t (mg) and m_{COD} : consumed COD corresponding to the same period t (mg)

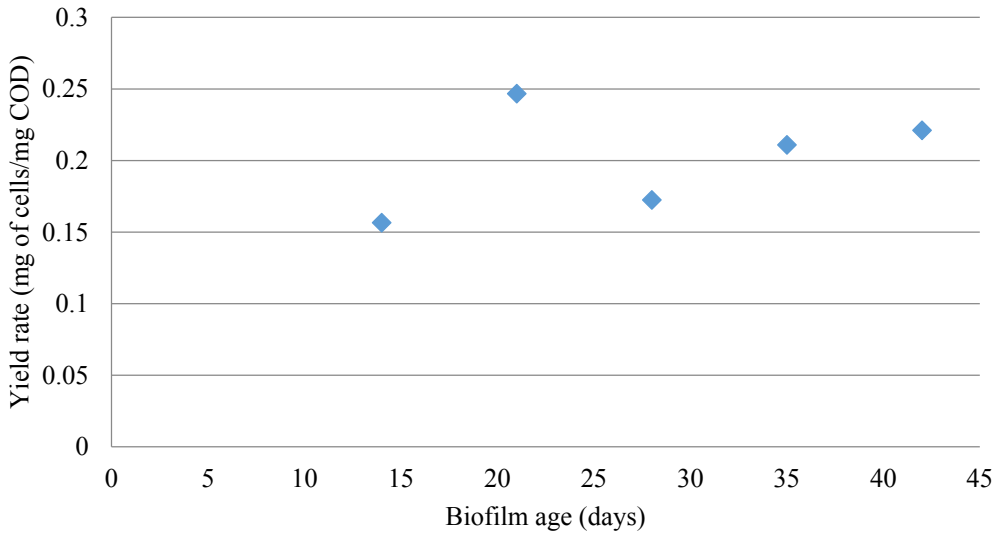

Figure IV.5: Yield rate corresponding to the total mass of biofilm for each week over consumed COD corresponding to the same period at a shear stress equals to 4.4 Pa.

According to figures IV.4 and IV.5, the mass of the volatile solids and the yield rate growth follow the same curve. They increase from days 14 to days 21, decrease to day 28 and then to increase again. A stabilization of the yield is observed from day 35 (figure IV.5) where the values at days 35 and 42 are 0.21 and 0.22, respectively. The variation on the yield rate values over time are due to the quantity of biofilm variation measured rather than to the amount of COD consumed. The values of COD are detailed in Annex A.10.

IV.1.3 Characterization of fouling chemical composition inside the TCR

According to the results of figure IV.3, the fouling is mainly composed of mineral matter ($>$ 73%). Therefore, some knowledge of the chemical composition of the fouling is important to establish a link between the biological and chemical clogging according to the hydrodynamic conditions and the wastewater quality. Two methods have been used here for the chemical characterization of the fouling: X-ray diffractometry (XRD) and thermogravimetric analysis (TGA). (Annex A.4). For each shear stress, as explained above, two repetitions were made. One was used for the identification of TS, VS (IM), XRD and TGA and the second one only TS, XRD and TGA.

Figure IV.6 shows how the procedures were done. For each shear stress, fouling collected from

the five strips was mixed together first, to have a sufficient quantity for XRD and TGA analysis and second, to eliminate the parameter age of biofilm in the analysis and focused only on shear stress effect.

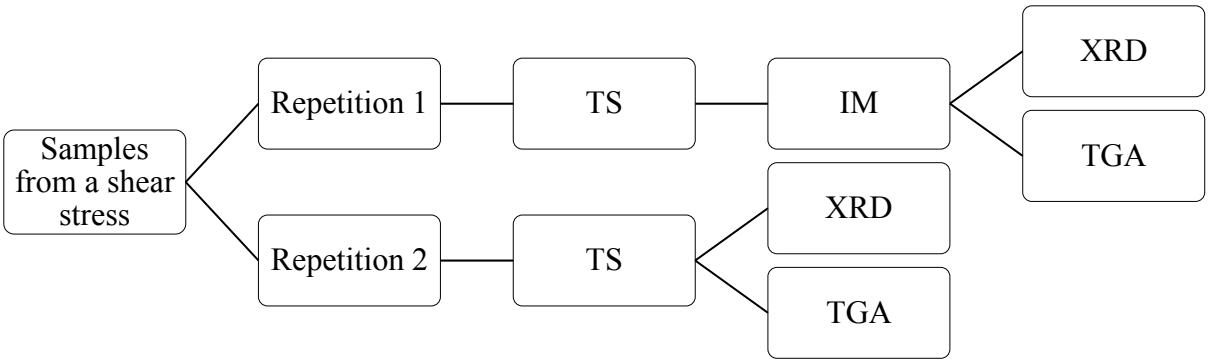

Figure IV.6: The process followed that shows how mineral characterization was done on each sample of repetitions 1 and 2 for each shear stress.

IV.1.3.1 X-ray diffraction (XRD) analysis of the fouling inside TCR:

X-ray diffraction (XRD) was used to determine the mineralogy and the crystalline form of the chemical precipitation which is produced at the same time as the biofilm development using Mauguio's wastewater effluent. Figure IV.7 shows the diffraction pattern of the fouling obtained for a shear stress of 4.4 Pa in the Taylor-Couette reactor. Figure IV.7.a shows diffraction peaks of the total solids (TS), and figure IV.7.b shows diffraction peaks of the inorganic matter (IM) obtained after TS calcination (Annex A.4).

In these two figures three characteristic peaks were highlighted. The most intense peak of calcite ($CaCO_3$) is at 29.5 in 2θ position and the second that follows is at 23 in 2θ position (number 1 above peaks). The most intense peak of silicon oxide (SiO_2) is at 26.5 in 2θ position and the second that follows is at 21 in 2θ position (number 2 above peaks). The presence of SiO_2 (quartz) is due to small particles of sand and sandstone present in the effluent water and which have been trapped by the biofilm matrix. The third interesting peak is that of hematite (Fe_2O_3) (number 3 above peaks) where the most intense one is at 36 in 2θ position. Hematite is a compound constituting sedimentary rocks and some fine particles can be found also in wastewater.

In figure IV.7.b, a fourth interesting peak is observed in the IM sample which is that of calcium oxide (CaO). The difference between the TS sample and the M sample is that TS was obtained after desiccation of the sample at 105°C and IM was obtained after passing TS in the oven at 550°C for 2 hours. CaO was produced inside the oven since in TS, no CaO peaks were detected (figure IV.7.b). CaO presence is due to the decomposition of calcium carbonate (calcite) which is already present in TS due to calcination (Reaction.III.3).

In the IM sample (figure IV.7.b), there is always calcite, which proves that the whole calcium

carbonate has not been calcinated as the temperature is only raised to 550°C to eliminate the organic matter. The decomposition of calcium carbonate (calcination) takes place at higher temperature (500°C-1000°C), which demonstrates the presence of both calcite and calcium oxide in the sample. For the other shear stresses the results of the XRD were similar to those presented here and they can be found in Annex A.11. The pics area of each constituents do not represent the quantity of the elements since the XRD is a qualitative and non-quantitative method.

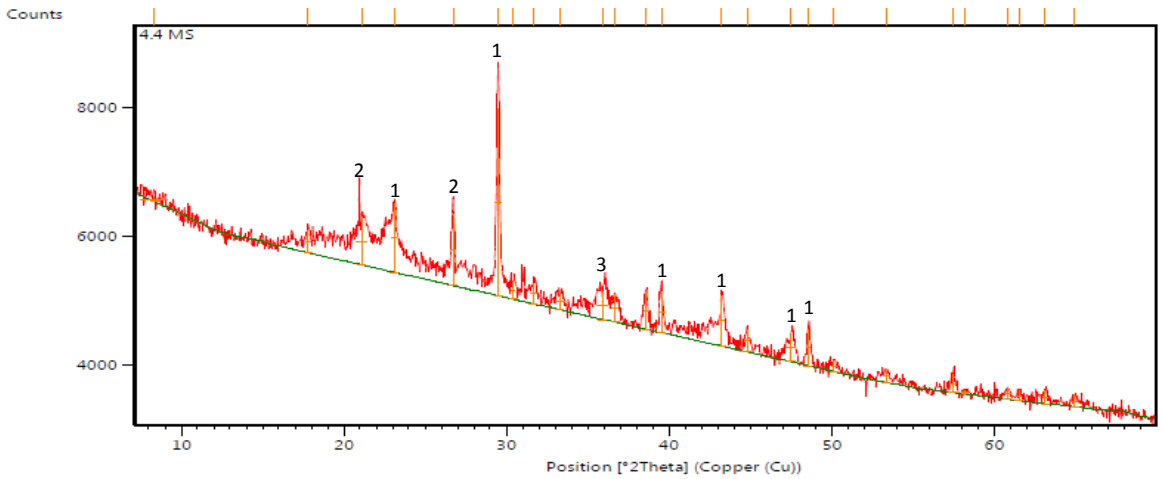

IV.7.a: XRD pattern of total solids (TS) sample for a shear stress of 4.4 Pa. Number 1 above peaks represents diffraction peaks of calcite, number 2 represents diffraction peaks of quartz, and number 3 represents diffraction peaks of hematite.

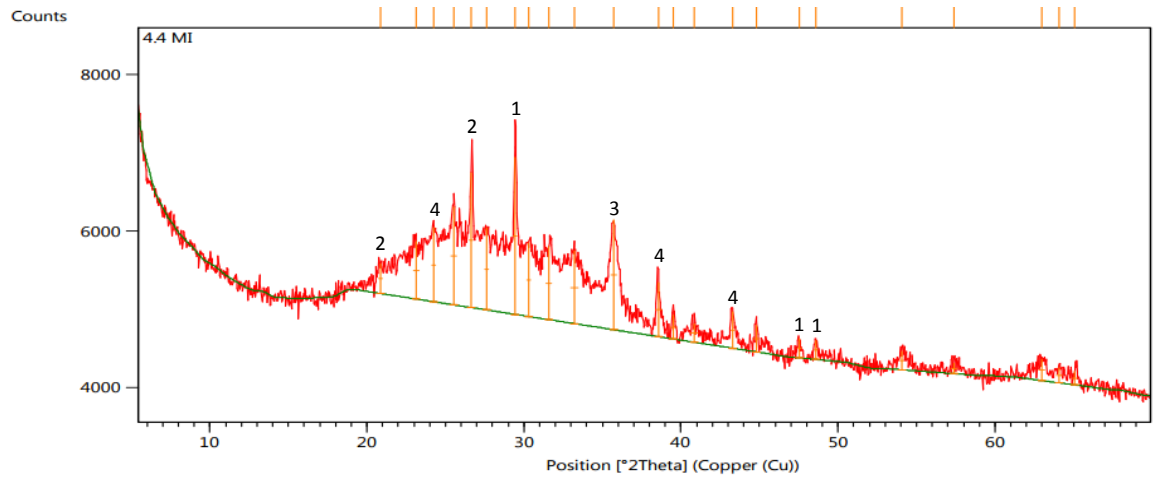

IV.7.b: XRD pattern of inorganic matter (IM) sample after TS calcination for a shear stress of 4.4 Pa. Numbers 1, 2 and 3 represent the same thing as in figure IV.7.a. Number 4 represents diffraction peaks of calcium oxide.

Figure IV.7: XRD pattern of TS (a) and IM (b) fouling. Number 1 above peaks is for calcite. Number 2 above peaks is for quartz. Number 3 above peaks is for hematite and number 4 above peaks is for calcium oxide.

According to the precipitation results in chapter III, the most abundant constituent found in the precipitate was the calcite. Calcite was also found (Figure IV.7) inside the fouling obtained in a TCR using treated wastewater. Since these experiments were carried out at ambient temperature and pH both

not exceeding 25°C and pH8, respectively, the presence of calcite could be detected contrary to the results of Chapter III. This demonstrates the possible interaction between the biofilm and the Ca^{2+} in the wastewater to induce precipitation. Tourney and Ngwenya (2009)[277] found that EPS release dissolved organic carbon (DOC) which complexes Ca^{2+} ions in solution, favoring calcite precipitation by reducing the calcium carbonate saturation.

Other elements have also been detected by the XRD as feldspars and clays which are essential constituents of rocks and soils. The detection of these elements in the samples is due to their presence in the effluent and not to the interaction between biofilm and minerals. Thermogravimetic analysis (TGA) will be used not only to detect amorphous elements which are impossible with XRD but also to establish a link between the percentage of OM and calcite precipitation.

IV.1.3.2 Thermogravimetric analysis (TGA) of the fouling inside TCR:

Thermogravimetric analysis (TGA) was used to detect amorphous structure by studying the decomposition of the sample as a function of an increase in temperature. In this study, an expectation of the percentage mass of calcium carbonate constituting each sample will also be made by TGA Table IV.1. Table IV.1 shows the total solids (TS) mass loss in percentage for a shear stress of 0.7, 2.2 and 4.4 Pa. The study of the mass loss was divided into 2 parts: from 0°C to 550°C and from 600°C to 850°C. From 0°C to 550°C the mass losses the percentage of organic matter (OM) present in the sample. From 600°C to 850°C, the values represents the mass losses occurred in percentage after calcium carbonate decomposition. The percentage of calcium carbonate in the sample was calculated based on Li et al., (2013)[172] works. According to their works, the mass loss of a pure sample (100%) of calcium carbonate is 43.8%(Section III.1.3). Based on the results of the DRX regarding the mineral elements found in the samples, only calcium carbonate decomposes at this temperature. Therefore, any mass loss is assumed to be due to this element decomposition.

Table IV.1: Mass loss in percentage between 0°C - 550°C, 600°C - 850°C for the three shear stresses and an estimation of the percentage of calcium carbonate in each sample.

Samples	Mass loss % (0°C - 550°C)	Mass loss % (600°C - 850°C) from total Mass	Percentage of calcium carbonate in the sample
0.7 Pa TS	48.3%	6%	13.69%
2.2 Pa TS	25.2%	2.2%	5%
4.4 Pa TS	35.3%	2.9%	6.6%

In Table IV.1, the percentages of organic matter (mass loss between 0°C and 550°C) in the total solids (TS) obtained for shear stresses of 0.7, 2.2 and 4.4 Pa are 48.3, 25.2 and 35.3 %, respectively.

Note that the samples used for the measurements of organic matter (OM) in TGA are not the same as those presented in figures IV.3 (organogram presented in figure IV.6). In addition, the conditions of degradation in an oven and in a TGA are not the same. In the oven, a reaction of combustion occurs (presence of air) while in the TGA it is a reaction of pyrolysis (presence of argon). Pyrolysis is the chemical decomposition of organic materials by heating in the absence of oxygen or any other reagents. The comparison between the percentages of organic matter values here and in figure IV.3 is impossible but in both cases samples contain more mineral matter. According to Table IV.1 the maximum percentage of OM was found for a shear stress of 0.7 Pa and it represents 48.3%, while according to figure IV.3 the maximum average percentage of OM was found for a shear stress of 2.2 Pa and it represents $37.6 \pm 4.84\%$. TGA graphs can be found in the Annex A.12.

The main purpose of Table IV.1 is to show the relationship between the percentage of organic matter and the estimated mass percentage of calcium carbonate. The more organic matter in the sample, the more calcium carbonate precipitation increases. For the percentages of OM equal to 48.3, 35.3 and 25.2%, the percentage of calcium carbonate in the sample is equal to 13.69, 6.6 and 5%, respectively, which enables to calculate a very strong positive correlation ($y = 0.3841x - 5.5007$, $R^2 = 0.925$) between the percentages of OM and the calcium carbonate in the sample. This has also been observed by Obst et al., (2009)[216] (paragraph I.4) where an extensive production of EPS has been demonstrated to be the main factor to accelerate carbonate mineralization.

Many researchers have been working on the process of biomineralization, especially with respect to calcium carbonate precipitation (Benzerara et al., 2006[34]; Wei et al., 2015[289]). This process is often related to microbial cell surface structures and metabolic activities. Microbial extracellular polymeric substances (EPS) play a very important role in the morphology and mineralogy of calcium carbonate precipitation. EPS can trap and bind remarkable quantities of calcium to facilitate precipitation (Arp et al., 1999[21]; Dupraz et al., 2005[88]; Braissant et al., 2007[43]).

This might be of interest as an approach in the clogging of drippers with TWW. However, studies must be carried out in depth to detect the interaction between biofilm and chemical elements under micro-irrigation conditions.

IV.1.4 Conclusion

The effect of the shear stresses encountered in irrigation on the evolution of fouling and the development of biofilm using treated wastewater was studied in this section of the chapter IV. A Taylor-Couette reactor (TCR) was used to reproduce these shear stresses since it is a good tool for the biofilms development because the shear stresses are well controlled. The values of shear stresses were chosen

based on those calculated in drippers (2.2 and 4.4 Pa) and pipes (0.7 Pa). For each shear stress a quantity of fouling was obtained. The amount of total solids (TS), organic matter (OM) and inorganic matter (IM) of each fouling obtained from each shear stress were quantified and qualified. X-ray diffraction (XRD) was used to determine the mineralogy and the crystalline form of the chemical precipitation which is produced at the same time as the biofilm development using TWW. Thermogravimetric analysis (TGA) was used to detect amorphous structure and a quantitative measure of precipitated calcite. Several important results have been obtained:

- The quantity of biofilm development, which is represented by the OM or the volatile solids (VS), is greater at a shear stress of 4.4 Pa compared to 2.2 Pa and 0.7 Pa.

- An analysis of the percentage of OM/IM shows that all the samples are mainly composed of IM.

- The higher the shear stress is, the greater the amount of fouling is. The quantity of TS at 4.4 Pa is higher than 2.2 Pa which is higher than 0.7 Pa throughout the duration of the experiment. This proof that en parallel of the increasing of the quantity of OM there is an increasing of the quantity of IM.

- Using XRD, the calcite was detected in all the samples.

- TGA highlight the presence of calcium carbonate and its relation with the quantity of OM. The more the sample contains OM, the more it can precipitate calcium carbonate.

According to the results of TS and VS, biofilm development is influenced by shear stress. As the shear stress increases, so does the amount of biofilm in mg/cm^2. High shear stress gives a denser and more rigid biofilm that withstands strong hydrodynamics conditions. An interaction between the quantity of biofilm and the quantity of calcium carbonate was highlighted from the results of TGA and TS. The effect and interaction between calcium carbonate and biofilm must be studied deeper. In the second part of this chapter, biofilm will be developed with and without calcium carbonate to better understand the link between them.

Part IV.2

Effect of calcium carbonate precipitation on biofilm development on fouling of irrigation pipes and drippers

According to chapter III and the part IV.1 of chapter IV, calcium carbonate ($CaCO_3$) was found to be the most abundant mineral compound using TWW. In part I of this chapter, it was demonstrated that the quantity of organic matter and calcium carbonate is proportional. In this second part of chapter IV the objective is to see the effect of the presence and absence of calcium carbonate on biofilm development inside irrigation pipes and drippers. An irrigation setup was implemented to study the development of biofilm and the irrigation water uniformity with and without $CaCO_3$. Two experiments run in parallel for a period of seven weeks. In order to enhance biofilm development and to study the effect of calcium carbonate on it, the first experiment is fed with synthetic effluent without $CaCO_3$ and the second experiment is fed with the same synthetic effluent but with $CaCO_3$ (paragraph II.3.1).
The study will be divided into two parts:

- Quantifying and qualifying the fouling inside the pipes and comparing it with the results of TCR since the shear stress applied is equal to 0.7 Pa.

- Follow the clogging of drippers by flow rate measurements and microscope visualization. The shear stress inside drippers, even if the geometry is not the same, is close to those studied in the first part (between 2.2 and 4.4 Pa).

IV.2.1 Interaction between calcium carbonate precipitation and biofilm development in irrigation pipes.

Biofilm inside irrigation pipes was developed under a constant shear stress of 0.7 Pa (paragraph II.2.4) and flow rate ($0.05\ m^3/s$). As in the TCR, biofilm was characterized by the measurement of its total solids (TS) and volatile solids (VS) masses. These measurements enable us to quantify the fouling and calculate the ratio between organic and inorganic matters (OM and IM).

Thermogravimetric analysis (TGA) and X-ray diffraction (XRD) were also used to detect a crystalline form of mineral precipitate and highlight calcite precipitation in function of the quantity of organic matter. Figure IV.8 shows the evolution of the fouling calculated in total solids (TS) in mg/cm^2 for the two experiments without $CaCO_3$ (T1) and with $CaCO_3$ (T2). Every week, fouling was collected from one pipe of each experiment (with and without $CaCO_3$). Every week corresponds to the age of biofilm development. Each pipe was then replaced by a new one to have a repetition. The TS values represented in figure IV.8 are the average of two repeatability, and the error bars correspond to the standard error of the mean (SEM).

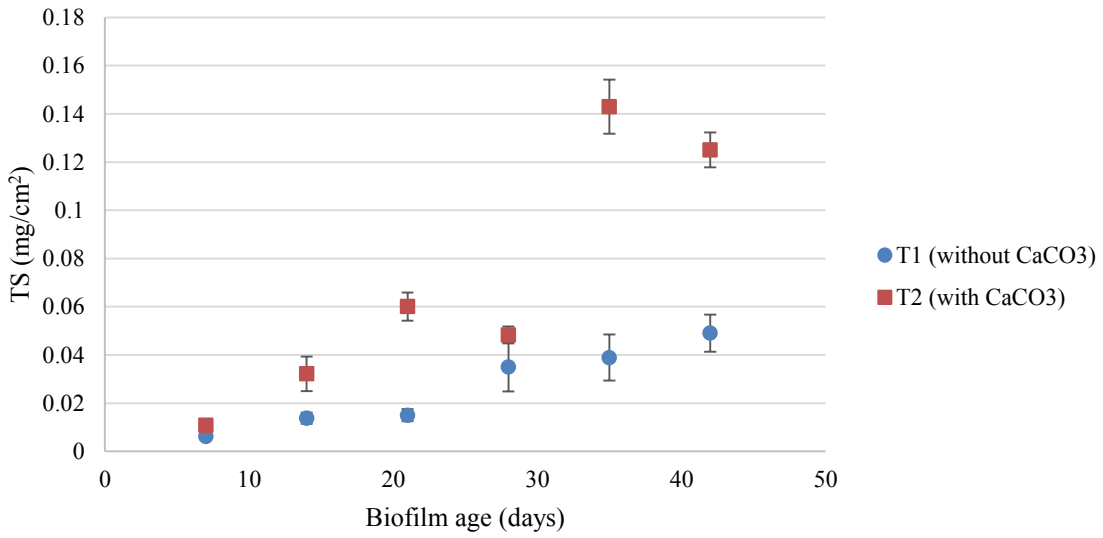

Figure IV.8: Fouling expressed by its total solids in mg/cm^2 for the experiment without $CaCO_3$ (T1) and with $CaCO_3$ (T2) as a function of the biofilm age in days.

In the figure IV.8 it is observed that the results can be divided into two parts: from day 7 to day 28, and from day 28 to day 42. After seven days of biofilm development the amount of TS in T1 and T2 is very close. From day 14, the difference between the two experiments is clear. For T1, the amount of TS is equal to $0.014 \pm 0.002\ mg/cm^2$, and for T2 it is equal to $0.03 \pm 0.007\ mg/cm^2$. This difference continued to be emphasized until the end of the experiment. The highest difference of TS between T1 and T2 was observed after day 28. An exponential increased in the amount of TS is observed for T2. The

values increased from $0.05 \pm 0.003\ mg/cm^2$ at day 28 to $0.143 \pm 0.001\ mg/cm^2$ at day 35. In one week, the value increased by 300%. This is in contrast to T1, where stabilization is observed after day 28. The amount of TS was $0.035 \pm 0.01\ mg/cm^2$, $0.039 \pm 0.009\ mg/cm^2$ and $0.05 \pm 0.007\ mg/cm^2$ for days 28, 35 and 42, respectively.

The difference observed between T1 and T2 especially at day 35 and 42 (figure IV.8) is due to the precipitation of inorganic matter (IM) which has been demonstrated in figure IV.9. A low percentage in OM means a high percentage in IM (100 - %OM = %IM). One repetition of TS of each experiment was analyzed for the percentage of OM. Figure IV.9 shows the evolution of the percentage of OM for T1 and T2 in function of biofilm age in days.

In figure IV.9, As in figure IV.8, the amounts of organic matter (OM) are close at day 7 for T1 and T2 (around 15%). The low percentage in OM at day 7 for both experiments indicates the initiation of biofilm. From day 14 for T1 the percentage of OM increased to reach 75% at day 35. For T2, fouling is mostly made of IM and the percentage did not change throughout the experiment. At day 14, TS was made of 15% of OM, and the same percentage was found at days 28, 35 and 42. The increase of TS in figure IV.8 in the experiment with calcium carbonate is due mainly to mineral precipitation. Since the percentage of organic matter did not change (figure IV.9), it means that the amount of biofilm was increasing too.

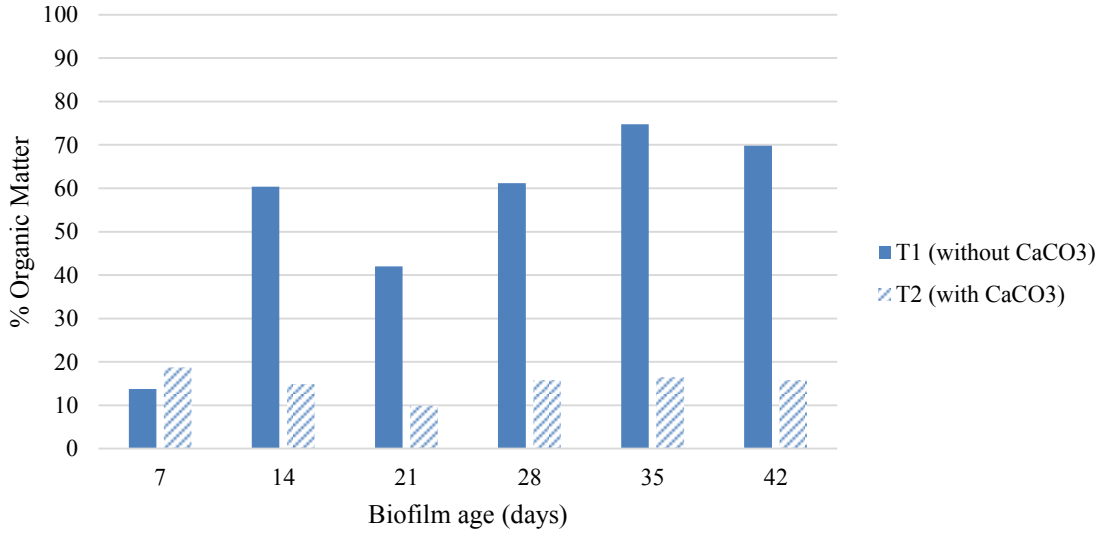

Figure IV.9: Evolution of the percentage of organic matter (OM) in TS samples in function of biofilm age in days for the experiments without $CaCO_3$ (T1) and with $CaCO_3$ (T2).

So the fouling obtained with water without calcium carbonate (T1) is mostly formed of organic matter (OM) whereas that obtained with water with calcium carbonate (T2) is mostly formed of inorganic matter (IM). To compare the development of biofilm with and without calcium carbonate, it is necessary to follow the evolution of the quantity of volatile solids (VS) in mg/cm^2 which represents the quantity of biofilm in the sample. Figure IV.10 shows the amount of VS contained in the total solids (TS) for

experiments T1 and T2 according to biofilm age in days.

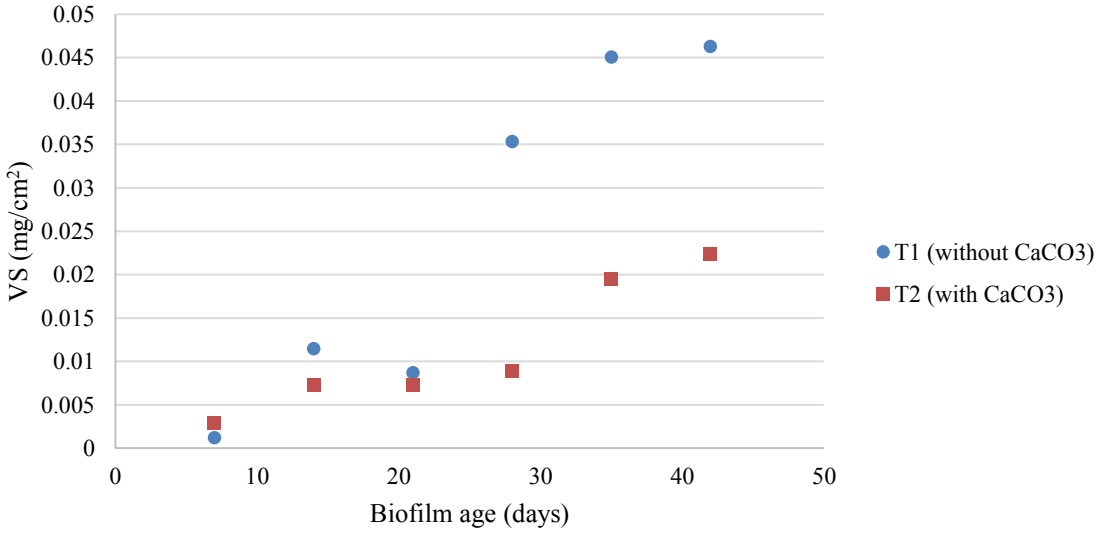

Figure IV.10: Quantity of volatile solids (VS) contained in the total solids (TS) for experiments T1 and T2 according to the biofilm age in days.

In the figure IV.10 as in figure IV.8 it is observed that the results can be divided into two parts. In figure IV.10 the two part are from day 7 to day 21, and from day 21 to day 42. During the 42 days of experience the curves of VS for T1 and T2 follow the same trend (increase in VS values, stabilization, etc.). From day 7 until day 21, the amount of VS was even very close (at day 21 the values of VS is 0.008 mg/cm^2 for T1 and 0.007 mg/cm^2 for T2) (figure IV.10).

It can be considered that this period of 21 days corresponds to the initiation phase of the biofilm. The same period has also been demonstrated for the TCR experiments at the same shear stress (0.7 Pa) (figure IV.4). But in the TCR this period was a little longer (28 days) knowing that it is not the same amount of COD that is used in the 2 experiments (here 200 mg /l in the TCR experiments around 30 mg / l) (section II.2.7.1 and section II.3.3).

After 21 days in both experiments, an exponential phase of the biofilm development is observed. The exponential phase initiates between day 21 and day 28 for the experiment without $CaCO_3$ (T1), and the amount of VS increased from 0.008 mg/cm^2 to 0.03 mg/cm^2 respectively. For the experiment with $CaCO_3$ (T2), the exponential phase comes after or, put differently, the initiation phase is longer than in T1. The exponential increasing of the amount of VS initiates between day 28 and day 35, and the value of VS increases from 0.009 mg/cm^2 to 0.019 mg/cm^2, respectively. The extension of the initiation phase in T2 may be due to the large amount of mineral material present in the sample. But in all cases from day 21 until the end of the experiment, the quantity of organic matter in T1 becomes much greater than that in T2. At day 42, the amount of VS for T1 is 0.046 mg/cm^2, whereas for T2 it is 0.022 mg/cm^2, or almost double. From day 35 in both experiments with calcium carbonate (T2) and without calcium

carbonate (T1), a stabilization of biofilm development is observed. This shows perfectly the sigmoid curve of biofilm kinetics growth described by Belkhadir et al., (1988)[30].

In order to explain this difference according to biofilm development, a measurement of the COD concentration was carried out 3 times per week (COD graphs can be found in Annex A.13). It can be confirmed that the difference between the two experiments is not due to the amount of carbon oxygen demand (COD) (explications can be found in the Annex A.13).

The only explanation is, that calcium carbonate precipitation has a negative effect on biofilm development. Apparently, once precipitated, calcium carbonate acts as mineral particles in suspension. Several studies have worked on the effect of mineral particles on biofilm development (Gjaltema et al., 1997 a-b[120]-[121]; Derlon et al., 2008[78]). The reduction of biofilm development when adding particles is probably due to the abrasion phenomenon and/or to the presence of particles within the biofilm which makes it less likely to attach to the surfaces.

Gjaltema et al., (1997 a-b)[120] [121] found that abrasion of the biofilm surface is caused by its collisions with particles and that the abrasion rate and particle size are proportional. Derlon et al., (2008)[78] exposed colonized straps to particle abrasion tests. Only the surface of biofilm was influenced, with a significant decrease of the total solids concentration.

In this study, the operating conditions did not allow calcium carbonate to attach to the walls of the pipes or drippers and to improve biofilm development. A calculation of the yield rate (Figure IV.11) may also explain the curves in figure IV.10. The COD values allow us to calculate the yield rate (Eq.IV.1). The calculation of the yield rate (Y) Figure IV.11 shows the yield rate production of biofilm linking the amount of biofilm produced weekly (in mg) to the quantity of chemical oxygen demand consumed (in mg) during the same period (one week).

For the first experiment, in which there is no calcium carbonate (T1) the yield rate increases from 0.002 at day 7 to 0.051 at day 28. From day 28, a stabilization of the yield rate is observed. The values for days 35 and 42 are equal to 0.051 and 0.048, respectively. For the second experiment where there is calcium carbonate (T2), the yield rate increases from 0.007 at day 7 to 0.02 at day 14. From day 14, a stabilization of the yield rate is observed but with significant fluctuations. Y is between 0.018 and 0.027. At the beginning of the experiments (day 7 and day 14) no significant difference is observed. From day 21, the yield rate in T2 was around 50% less than T1. Since the consumed quantity of COD was the same in both experiments, the difference is only due to the quantity of biofilm which is produced.

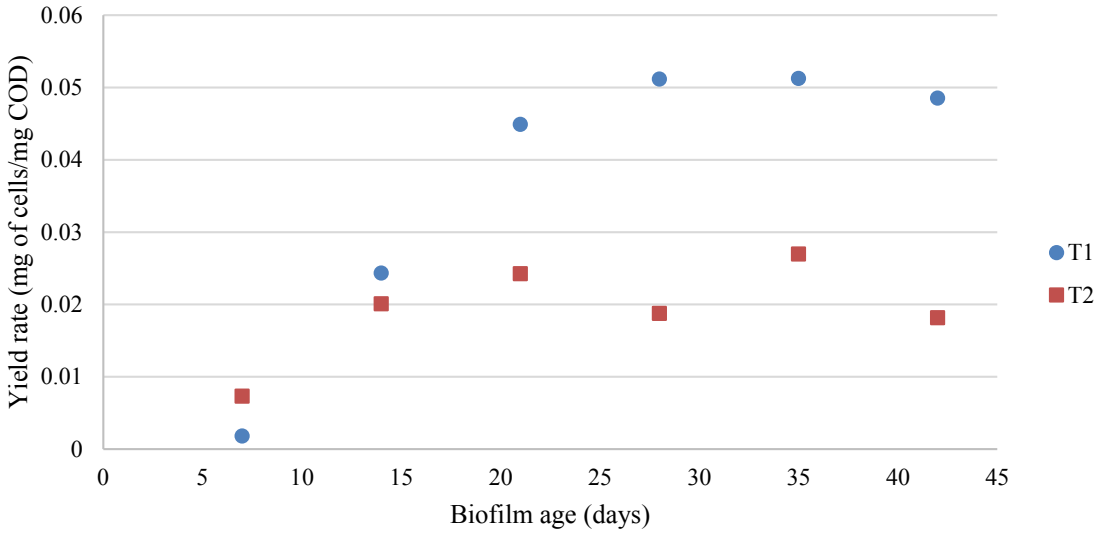

Figure IV.11: Yield rate corresponding to the amount of biofilm produced weekly over the quantity of chemical oxygen demand consumed during the same period in the case of T1 and T2.

IV.2.2 Characterization of the fouling by DRX and TGA.

X-ray diffraction (XRD) is used to detect any possible mineral precipitation in T1 and in T2 to detect the crystalline form of calcium carbonate precipitation. Thermogravimetric analysis (TGA) is used to ascertain whether, as previously, there is a link between the amount of organic material formed and the amount of precipitated calcium carbonate.

The procedures done to characterize the fouling by XRD and TGA were the same as in figure IV.8. The measurements of volatile solids (VS) show that fouling developed from the experiment without calcium carbonate (T1) contains a majority of organic matter (OM) while the fouling developed from the experiment with calcium carbonate (T2) contains more inorganic matter (IM).

From each experiment, four samples of fouling were analyzed: total solids (TS) and inorganic matter (IM) samples at the age of biofilm of 1 and 4 weeks.

Results from DRX highlight the presence of calcium carbonate in the form of calcite from the first week in all the samples even from fouling developed without calcium carbonate (DRX graphs are found in Annex A.14).

Knowing that the solution is only formed of demineralized water, glucose, phosphoric acid and ammonium chloride (section II.3.3), calcium carbonate could be formed and precipitated by the bacteria in the form of calcite. The conductivity of the demineralized water is not zero ($0.5\ \mu S/cm$), and it always contains calcium and dissolved carbonate ions in trace elements.

According to the results, these ions even at very low concentrations can precipitate as calcium

carbonate. As already observed in Taylor-Couette reactor (TCR) (part IV.1 of this chapter), calcium ions can be trapped in the matrix of the biofilm, which facilitates its precipitation.

The DRX being a qualitative and a non-quantitative method, the area of the peak is not proportional to the amount of calcite present in the sample. It is rather proportional to the crystallization rate which is much more pronounced in week 4 (Figure IV.12). Figure IV.12 shows diffraction peaks of TS sample obtained from experiment without calcium carbonate at an age of biofilm of 1 week (figure IV.12.a) and 4 weeks (figure IV.12.b).The most intense peak of calcite is at 29.5 in 2θ position (number 1 above peak).

Knowing that at week 4 the quantity of biofilm is higher than at week 1 (figure IV.10), a link can be established between the quantity of organic matter (OM) and the quantity of precipitated calcium carbonate.

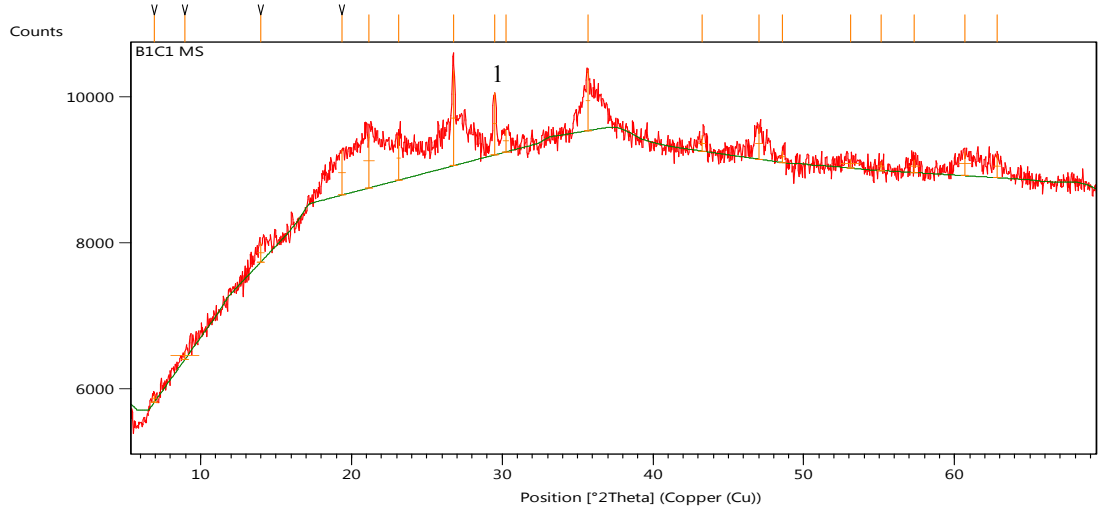

IV.12.a: at week 1

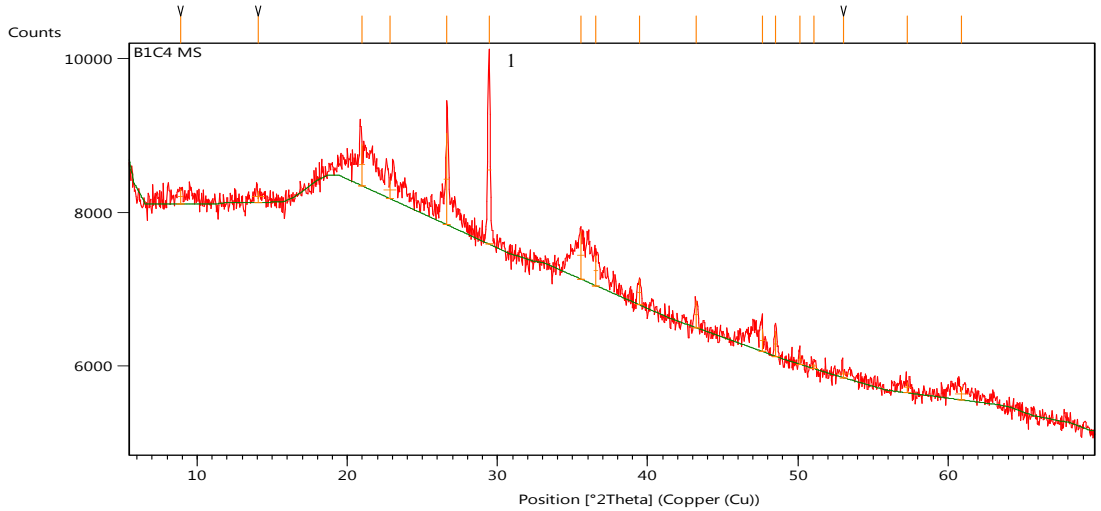

IV.12.b: at week 4

Figure IV.12: Diffraction peaks of sample total solids (TS) from experiment without $CaCO_3$ at week 1 (a) and at week 4 (b).

To better underline this link, TGA is made on the same samples and on samples from the experiment with $CaCO_3$.

Table IV.2 shows TGA results for the total solids (TS) of the experiment without calcium carbonate (T1) and with calcium carbonate (T2) at one week and four weeks of biofilm age. As for table IV.1, the study of the mass loss was divided into 2 parts: from 0°C to 550°C where the mass losses represent the percentage of organic matter (OM) present in the sample and from 600°C to 850°C where the values in percentage represent the mass losses that occurred after calcium carbonate decomposition. The percentage of calcium carbonate in the sample was calculated as in table IV.1.

For the interpretation of table IV.2 it is better only to compare between the percentage of OM and the percentage of calcium carbonate because since the water quality is not the same (with and without calcium carbonate) it is sure that the percentage of OM will not be the same.

For the experiment without calcium carbonate, the percentage of OM at week 1 is equal to 49.72% while it is equal to 48% at week 4. For the experiment with calcium carbonate the percentage of OM at week 1 is equal to 9% while it is equal to 7.5% at week 4. No explanation can be given concerning the percentage of OM for week one and week 4 since in figure IV.10 at week 4 the percentage is higher than at week 1. The percentage of OM cannot be compared between table IV.2 and figure IV.9 for the same reason explained in paragraph IV.1.3.2.

What is most important to see is that there is a big difference in the values of OM between T1 and T2, and the percentage of calcium carbonate is proportional to the quantity of OM for each experiment:

- For TS sample without calcium carbonate:
  - At week 1: the percentage of calcium carbonate corresponding to 49.72% of OM is 19.84%;
  - At week 4: the percentage of calcium carbonate corresponding to 48% of OM is 15.9%.
- For TS sample with calcium carbonate:
  - At week 1: the percentage of calcium carbonate corresponding to 9.15% of OM is 87.99% ;
  - At week 4: the percentage of calcium carbonate corresponding to 7.48% of OM is 87.17%.

Table IV.2: Mass loss in percentage between 0°C- 550°C, 600°C- 850°C for fouling at age one and 4 weeks fed from tanks 1 and 2, and an estimation of the percentage of calcium carbonate in each sample.

TS samples	Mass loss % (0°C- 550°C)	Mass loss % (600°C- 850°C) from total mass	Percentage of calcium carbonate in the sample
Without calcium carbonate at week 1	49.72	8.69	19.84
Without calcium carbonate at week 4	48	7	15.9
With calcium carbonate at week 1	9.15	38.54	87.99
With calcium carbonate at week 4	7.48	38.18	87.17

The percentage of calcium carbonate in the sample was calculated based on Li et al., (2013)[172] (see paragraph IV.1.3.2). TGA was also used on the inorganic matters (IM) after passing the total solids (TS) in an oven at 550°C for 2h (Annex A.4).

The analyzed sample is taken from the experiment with calcium carbonate at 6 weeks of biofilm age. The objective is to detect the release of CO_2 due to the decomposition of calcium carbonate in the temperature range of 600°C - 800°C. Since the molar mass of CO_2 is equal to 44, TGA thermal curve and chromatogram show the characteristic peak for the ion having a specific mass-to-charge ratio (m/z) or Thomson equal to 44 figure IV.13. According to Basler and Morill, (1998)[255], CO_2 is one of the most common elements that have an m/z = to 44. In this figure, the peak is clearly observed at 775°C. The arrow shows the corresponding peak.

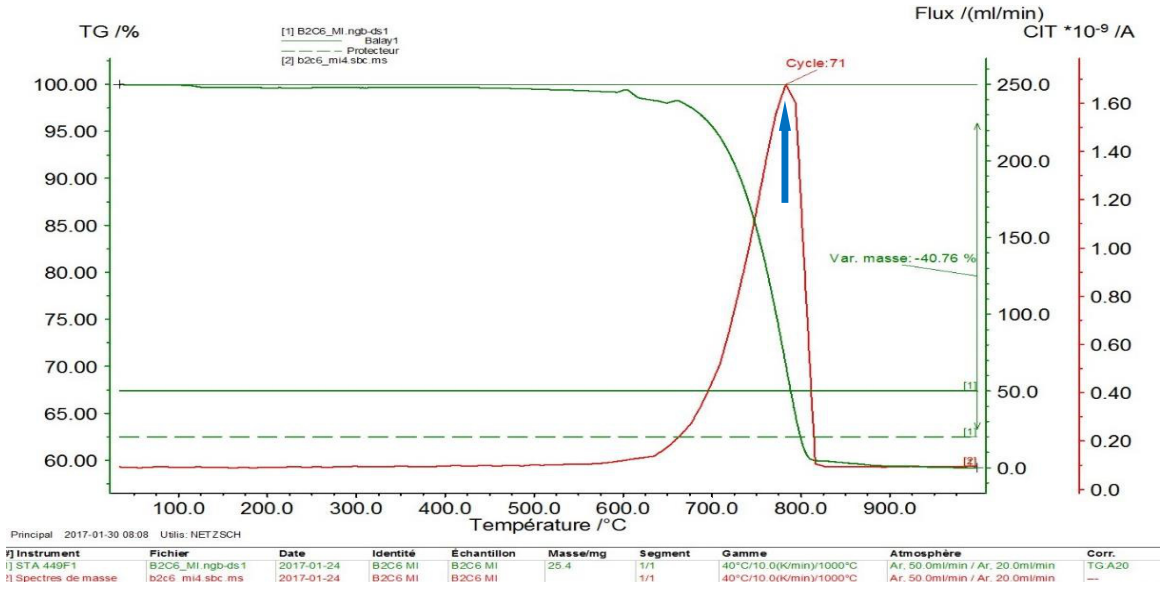

Figure IV.13: Simultaneous TGA/MS thermal curves of the IM of for tank with calcium carbonate at an age of 6 weeks.

Since an IM sample is formed solely from inorganic matters (IM), it is possible to take into consideration the mass loss carried out over the entire temperature range (600°C -800°C). The mass loss being 40.76%, it can be deduced that the T2P6 IM sample contains 93% of calcium carbonate. This has also been confirmed by XRD (figure IV.14) where only the diffraction peaks of calcite is observed. For the other samples, the results of the DRX and TGA can be found in Annex A.14 and Annex A.15, respectively.

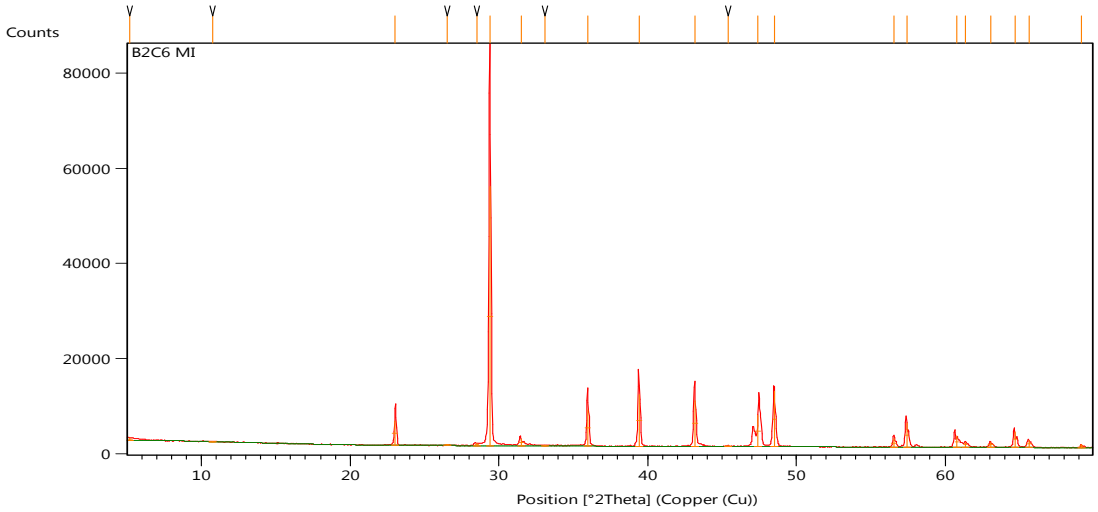

Figure IV.14: Diffraction peaks of the inorganic material (IM) for experiment with calcium carbonate at a biofilm age of 6 weeks.

It has been seen that calcium carbonate, once precipitated, has a negative effect on the biofilm development inside pipes due to its behavior like mineral particles and which may have an abrasive effect. While precipitation of calcium carbonate is favored by the presence of organic matter (OM) and the calcium ions which are already in the water even at very low concentrations and can be trapped by EPS. In the following section, the effect of precipitation of calcium carbonate on biofilm development will be studied at the level of drippers.

IV.2.3 Effect of calcium carbonate precipitation on biofilm development and dripper clogging.

In complement of the first study which were focused on pipe fouling analysis, in this paragraph the objective is to study the effect of the presence and absence of calcium carbonate on biofilms development and on the rate of fouling in drippers. The drippers used are NPC2 (chapter II) having a nominal flow rate of ($2\ l/h$) under a working pressure of 1 bar. Each week one pipe of each experiment was removed for biofilm collection and then replaced with a new one. Each pipe has 6 drippers, which were also replaced by new ones. In this case, two repetitions were made for each experiment. Each experiment work with 36 drippers but not all the 36 reach the end of the experiment (chapter II). Table IV.3 shows for each biofilm age how many drippers have been measured. For two repetitions, the number is multiplied by 2.

Table IV.3: Total number of drippers measured at each biofilm age in days for one repetition of one experiment.

Age of biofilm in days	7	14	21	28	36	42
Total number of drippers	36	30	24	18	12	6

The two repetitions will be represented at the same time, which means that for each experiment 72 drippers were followed over 7 weeks but for a different biofilm age. Only 12 drippers in each experiment will reach 42 days of biofilm age. The dripper flow rates were measured 3 to 4 times per week making a total of 705 ± 12 measurements for each experiment. Over the 705 measurements, 31 ± 1 measurements were less than $1.4\ \ell/h$ in both cases, giving a percentage equal to 4.2%. A dripper is considered to be clogged if the flow rate is less than 70% of the initial flow rate (Gilbert et al; 1979[117]), i.e. if a dripper drops $1.4\ \ell/h$ or less.

IV.2.3.1 Irrigation uniformity

At the level of an irrigation plot, what really interest the farmer in terms of irrigation performance, is the uniformity of distribution. It is affected among others by dripper discharge coefficient of variation (CV) which can be expressed in percentage:

$$CV(\%) = 100 \times \frac{\sigma}{\overline{X}} \tag{IV.2}$$

With σ: standard deviation of dripper flow rate at a specific time (t) and $\overline{X}$: average flow rate at the same time (t).

In this study the statistical uniformity (SU) will be used and it is expressed as follow (Mansour and Pibras 2015[272]):

$$SU = 100\,(1 - CV) \tag{IV.3}$$

Figure IV.15 shows the statistical uniformity for the experiments without (T1) and with (T2) calcium carbonate as a function of the biofilm age. The two repetitions are represented at the same time on the same graph.

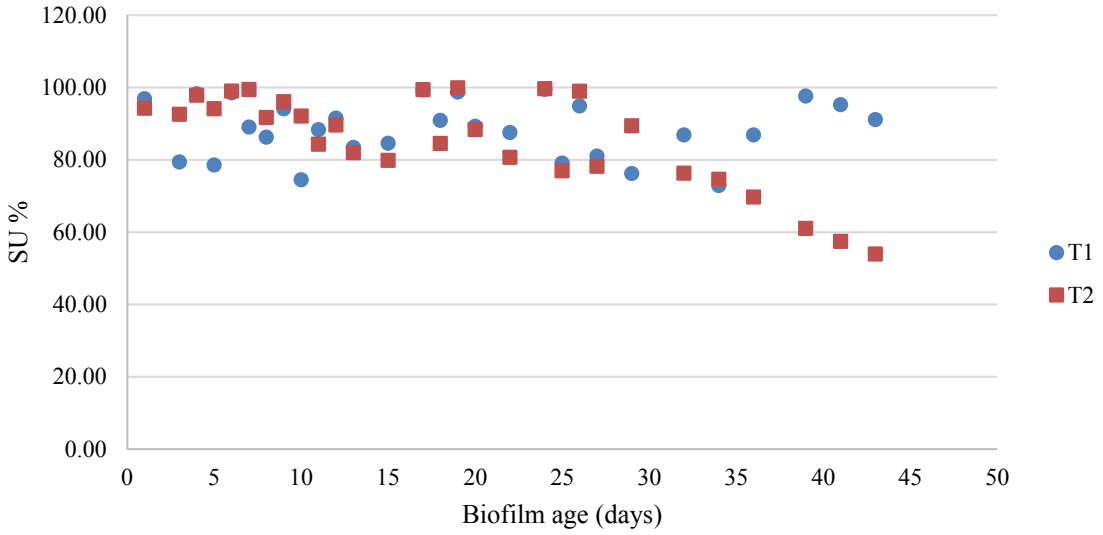

Figure IV.15: Statistical uniformity in % as a function of the biofilm age for the experiments without (T1) and with (T2) calcium carbonate.

According to Figure IV.15, results can be divided into two parts: i) From day 0 until day 20 and ii) from day 20 until day 42.

i) Large fluctuation due to clogging which is fragile and can be driven out by the starting cycles,

ii) Much more fluctuation and a significant decrease in the percentage of SU which is due to clogging.

Figure IV.15 shows that the coefficient of uniformity represented by the statistical uniformity is more affected by the presence of calcium carbonate especially at the end of the experiment. A deeper study of the flow rate and a optical observation of the drippers is a must to confirm the results.

IV.2.3.2 Flow rate and optical observation of the drippers

The measurement of the flow rate was made according to the method explained in section II.3.2. The observation of fouling with a microscope is very important and constitutes a step in the analysis and characterization of clogging. Nine drippers from each experiment were visualized. Drippers were opened and the deposits were observed using an Olympus BX43 microscope using a 10X magnification. In this study only four will be discussed and analyzed. The other pictures and discussions can be found in Annex A.16.

Figure IV.16 shows the evolution of the flow rate of each dripper in scatter as a function of the biofilm age for the experiment without calcium carbonate (T1) and with calcium carbonate (T2) figure IV.19. Drippers with different marker shapes are those which have been observed under an optical

microscope. The results will be divided into 2 sections. Those that have been done without calcium carbonate and those that have been done with calcium carbonate.

Experiments run without calcium carbonate:

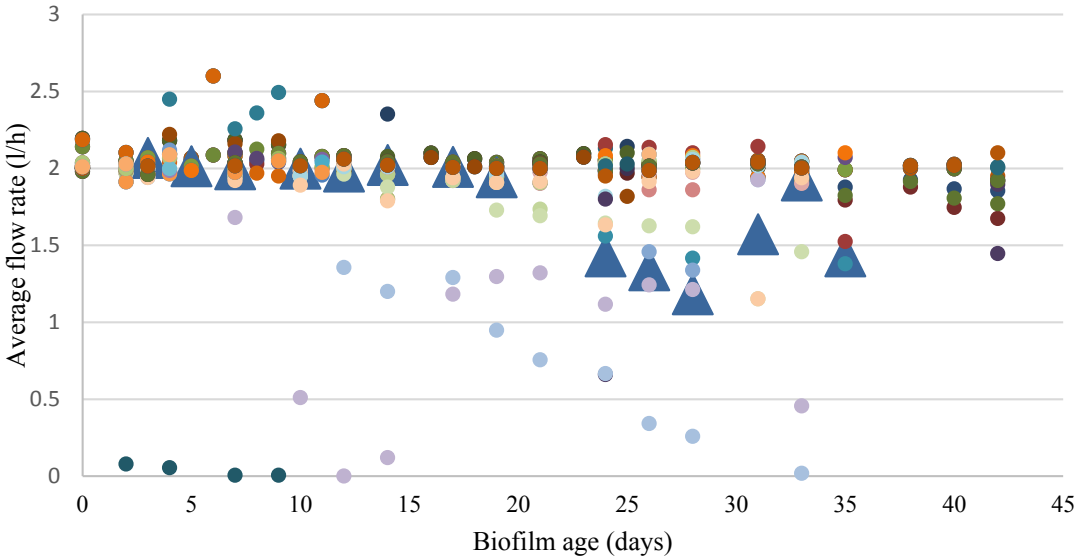

Figure IV.16: Evolution of dripper flow rate as a function of time for the experiment without calcium carbonate (T1).

In figure IV.16, it can be observed that over 42 days of biofilm age only 7 drippers over 72 drippers had an average flow rate less than $1.4\ \ell/h$. Only one dripper totally clogged (average flow rate = $0\ \ell/h$) since day 2 probably due to physical clogging. For the others, the average flow rate began to decrease since day 7. Two of them ended up with a flow rate of $0\ \ell/h$ one at day 12 and the other at day 33. After day 35, no dripper had a flow rate below $1.4\ \ell/h$.

Figure IV.17 shows the dripper with triangle marker (Figure IV.16) observed with an optical microscope. This dripper has an average flow rate equal to $1.428\ \ell/h$ at the end of the experiment (35 days). It is observed that biofilm is accumulated in the central zone (a and b) with strong biofilm development in the first baffle (c). Few biofilm accumulation is observed at the labyrinth exit (d).

IV.17.a:

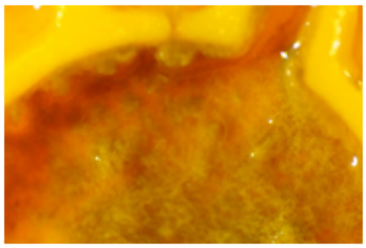

IV.17.b:

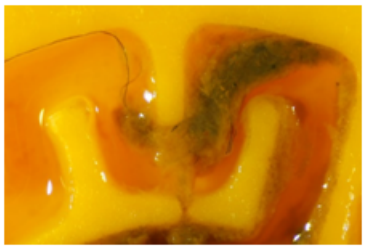

IV.17.c:

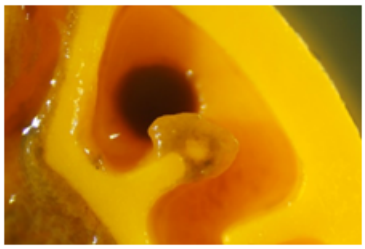

IV.17.d:

Figure IV.17: Photos of the dripper with a triangle marker shapes showing the location of fouling inside dripper.

Another dripper having an average flow rate of $1.854\ \ell/h$ was also observed (figure IV.18). Figure IV.18 shows that biofilm development was only in the central zone of the dripper and no biofilm was found on the first baffles.

IV.18.a:

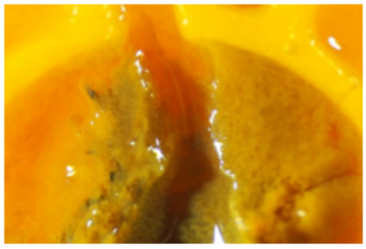

IV.18.b:

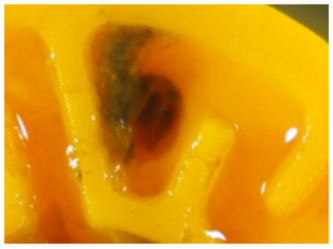

IV.18.c:

Figure IV.18: Biofilm development at the center of the dripper (a), preferred furrow / flow within the mass of biofilm formed in the central zone (b), presence of biofilm in the exit channel of the labyrinth (c).

In both cases (figure IV.17 and figure IV.18), biofilm development was observed in the central zone of the dripper. The difference between these two figures is the presence of biofilm in the first baffles. This caused the difference between the flow rate ($1.854\ \ell/h$ for the dripper presented in Figure IV.18 and $1.428\ \ell/h$ for the one presented in Figure IV.17).

It was found that the drippers are mostly vulnerable to clogging in the rst bafes where the turbulence quantities are weak especially in the vortex region where the velocity of the fluid is low (Gamri et al., 2013[111]; Al Muhammad 2016[10]). Gamri et al., (2013)[111] studied the same dripper type (NPC2) and they highlight that the areas with low velocity correspond to those where the biofilm begins

to develop. In NPC2 drippers biofilm begins to develop essentially on the central circles, this has also been observed in our results.

Experiments runs with calcium carbonate:

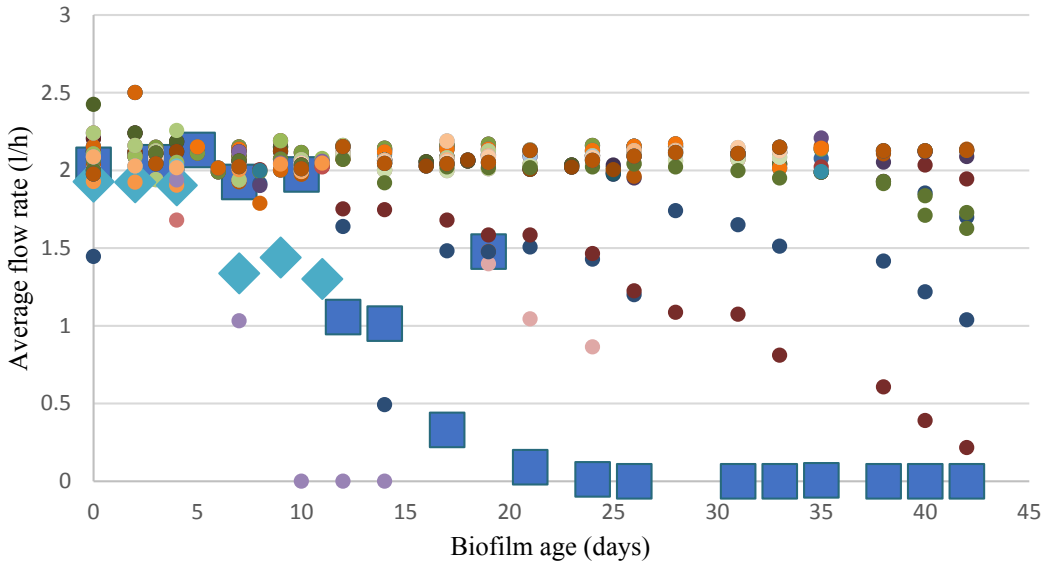

Figure IV.19: Evolution of dripper flow rate as a function of time for the experiment with calcium carbonate (T2).

In figure IV.19 drippers do not follow the same trend as in figure IV.16 (experience without $CaCO_3$). No drippers was totally clogged before day 10, this shows that initiation and development of biofilm takes longer in the presence of calcium carbonate. After 10 days, three drippers were totally clogged (average flow rate = 0 ℓ/h). Over 42 days of biofilm age only six drippers over 72 had an average flow rate less than 1.4 ℓ/h.

First observation: The number of drippers clogged in the experiment with calcium carbonate (6 drippers) and without calcium carbonate (7 drippers) can be considered as being the same, however, the decrease in the percentage of SU (Figure IV.15) has been shown more clearly in the case where there is calcium carbonate.

According to Table IV.3, the number of drippers decreases each week to arrive at the end of the experiment with 12 drippers (adding the two repetitions together). Which means that the clogged dripper in the experiment with calcium carbonate almost all reached age 42, which means that the ratio of clogged dripper / not clogged dripper in the experiment with calcium carbonate is higher than the ratio obtained without calcium carbonate.

Two clogged dripper were opened and observed with an optical microscope. The dripper with a diamond marker shapes has a flow rate of 1.302 ℓ/h at the end of the experiment (day 7) will be shown in Figure IV.20. The dripper with a square shapes has a flow rate of 0 from day 19 until the end of the

experiment will be shown in Figure IV.21.

Drippers in Figure IV.20 and Figure IV.21 both are clogged and no biofilm was detected in the central zone. Biofilm accumulation was only detected with chemical precipitation at the 1st and 2nd baffle of the labyrinth (whitish biofilm with a granular appearance). This underline also which was deduced in the case of the drippers of Figure IV.17 and Figure IV.18. Which says that the decrease of the dripper flow rate, even up to a total obstruction, is due to the presence of biofilm only in the first baffles.

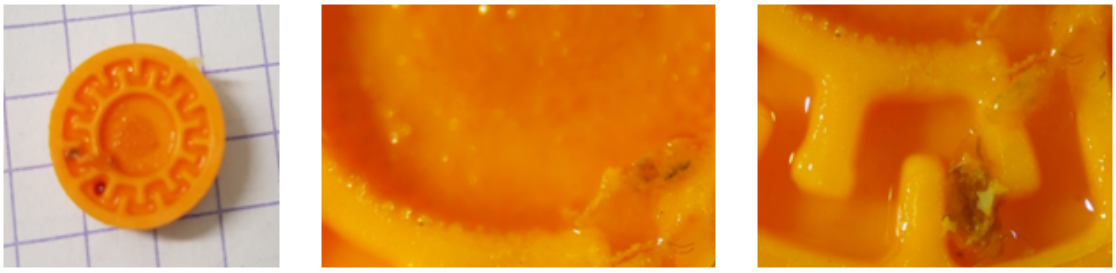

IV.20.a: IV.20.b: IV.20.c:

Figure IV.20: Global view of the dripper with a diamond marker shapes (a), presence of whitish granular fouling in the central zone (b), residue at the 1st baffle (c).

IV.21.a: IV.21.b: IV.21.c:

Figure IV.21: Global view of the dripper with a square marker shapes where no biofilm is found in the central zone (a), presence of biofilm in the 2nd baffle (b), calcium carbonate precipitation in the 8th baffle (c).

Second observation: The absence of biofilm in the central zone in the presence of calcium carbonate.

As seen above (section IV.2.1), calcium carbonate acts like mineral particles and has an effect on the abrasion of the biofilm. Biofilm tends to develop firstly in the central zone. The unique presence of the biofilm with calcium carbonate in the first baffle is probably due to the abrasive effect of the calcium carbonate. $CaCO_3$ detached biofilm from the central zone. The biofilm is then stuck in the small cross section of the labyrinth causing its clogging. So the clogging of drippers is mainly due to the presence of biofilm but the presence of calcium carbonate in this case aggravated the situation.

Concerning the interaction between mineral particles, biofilms and detachment Moinul Hosain et al., (2014)[196] emphasize the fact that EPS has the ability to accumulate mineral particles. This increases the volume of biomass. When the size increases the hydrodynamic forces of the water also increase until part of the biomass is detached. After losing some of its parts, the biofilm biomass regrows again until a substantial biomass blocks the dripper flow. This study validate our results but there is no other work focusing on this subject which remains an important perspective to exploit.

Third observation: The presence of the calcium carbonate in parallel with the biofilm in a dripper creates fluctuations in the flow rate (only one case will be presented).

The dripper presented in figure IV.21 works for 42 days and its flow rate decreases from day 10. The value of the flow rate decreased from 1.97 ℓ/h at day 10 until 0.33 ℓ/h at day 17. Then it increased to 1.47 ℓ/h at day 19 and decreased to 0 ℓ/h until the end of the experiment.

According to figures IV.16 and IV.19, there are more flow rate fluctuations in the case of the experiment with calcium carbonate. This is due to the fact that dripper can be clogged at a time and then be unclogged due to a change of fouling location inside the dripper due to calcium carbonate particles.

IV.2.4 Conclusion

In this part IV.2 of the chapter IV, an irrigation set-up was implemented to develop biofilm inside LDPE pipes under a shear stress of 0.7 Pa and NPC2 drippers under a shear stress between 2.2 and 4.4 Pa. Two series of experiments were followed in parallel in the same conditions but having different water quality. In order to study the effect of calcium carbonate ($CaCO_3$) on biofilm development, one series runs with a synthetic water containing a solution of calcium carbonate formation precursors ($CaCl_2$ and $NaHCO_3$) and the other does not contain this solution. Table IV.4 contains some important points revealed in this part of the chapter depending on whether the fouling is inside a dripper or a pipe and according to whether the fouling is developed with calcium carbonate or not.

Table IV.4: Summary of the calcium carbonate /biofilm interaction study in pipes and drippers when using synthetic effluent with and without $CaCO_3$.

Pipes			**Drippers**		
With $CaCO_3$		Without $CaCO_3$	With $CaCO_3$		Without $CaCO_3$
TS	$>$	TS	Flow fluctuation	$>$	Flow fluctuation
%OM	$<$	%OM	Flow rate	$>$	Flow rate
VS	$<$	VS	# of clogged drippers	$<$	# of clogged drippers
Y	$<$	Y	SU	$<$	SU
			Labyrinth		Central zone
			Clogging (time)	$<$	Clogging (time)

Taking into account the results of Table IV.4, the most important conclusion is that calcium carbonate has a negative effect on the biofilm development:

- Concerning the pipes part: calcium carbonate particles play an abrasive role, and influence the attachment of the biofilm to the support (lower percentage in OM and in the mass of VS comparing to the ones with $CaCO_3$.

- Fluctuation of the flow rate and the delay in the clogging of drippers is observed in the presence of calcium carbonate.

At the level of drippers, several contradiction can be emphasized especially concerning data between:

i) Flow rate and location of the fouling: it has been demonstrated that the fouling located in the labyrinth decrease more the flow rate than the fouling located in the central zone. The few drippers totally clogged due to the presence of biofilm in their labyrinth does not affect the general flow rate.

ii) Statistical uniformity and number of clogged drippers: The drippers that have been clogged from the 10^{th} day of experimentation (figure IV.19) are those that have remained until the end. At the end of the experimentation the total number of drippers decreased from 72 until 12 which affect the value of SU (%).

The whole plot must be looked at in order to study the performance of an irrigation system. According to the results, water irrigation uniformity is better with biofilm clogging than with biofilm and chemical precipitation but several repetitions must be done to confirm the results.

Conclusion and perspectives:

The objective of this thesis study is to contribute to the understanding of the mechanisms that induce chemical precipitation and biofilm development using treated wastewater for micro-irrigation. The impact of the pH, temperature and partial pressure of CO_2 on chemical precipitation, the effect of shear stress on biofilm development and the effect of calcium carbonate on pipes fouling and drippers clogging was particularly studied in this work.

Different experimental and numerical approaches have been realized in order to characterize the chemical precipitation and to be able to couple the various parameters that can influence the solubility of the salts in water. The first part of the work consisted in characterizing experimentally the chemical precipitation from a qualitative and quantitative point of view. The effect of pH and temperature on chemical precipitation will be also studied. Precipitation experiments were carried out in batch reactors using filtered treated wastewater. Thus, the influence of suspended solids on precipitate weight is eliminated. When the temperature and pH increased the mass of the precipitate increases too. The analyzing of the precipitate using the DRX and the TGA highlight the presence of calcium carbonate in the form of calcite. It was being the most abundant precipitate found in all the precipitate samples.

The results and data of the chemical precipitation allows to validate and calibrate a geochemical software. PHREEQC enables us to predict the quantity and the quality of chemical precipitation for a water quality under different operating conditions without passing each time through laboratory experiments. Using PHREEQC software, the effect of partial pressure of CO_2 on the precipitation of calcite could be studied. Experimentally, following and studying this parameter was difficult for us to do it as for the saturation index which can only be calculated by a software. All PHREEQC calculations are based on the saturation index value of each element using the Debye Huckel equation since the ionic strength (I) is less than 0.01M.

If the SI is positive the element has the ability to precipitate. PHREEQC also showed that calcite is the most abundant precipitate using Mauguio WWTP effluent. The saturation index of calcite was calibrated to obtain the same weight of calcite as in the laboratory experiment.

According to the results, calcite begins to precipitate when the value of SI exceeds a certain pos-

itive threshold value. This value can be reached more easily in a closed system where the water is not in equilibrium with atmospheric CO_2, and also by increasing pH and temperature. The effect of atmospheric CO_2 was also investigated. In an open system, i.e., in equilibrium with CO_2, the solubility of calcite increased due to a constant supply of CO_2. To minimize calcite precipitation in irrigation, water should be stored in open reservoirs at a low temperature and a low pH.

The second part of this thesis work involved in the implementation of experimental set-ups in order to study: i) in a Taylor-Couette reactor, the effect of shear stress on biofilm development in parallel with the chemical precipitation using real TWW and ii) inside pipes and drippers the interaction of calcium carbonate on the biofilm development using a synthetic wastewater.

The Taylor-Couette reactor (TCR) is known to give well-controlled shear stress values. According to the results the more the shear stress increases the more biofilm development is advantageous. Three shears stresses found in micro-irrigation system were studied. 0.7 Pa is a shear stress that can be found in pipes and 2.2 and 4.4 Pa are shears stresses that can be found in drippers. By increasing the shear stress biofilm becomes denser and more compact so it can resists to hydrodynamic conditions changes. From the measurements of the XRD and the TGA the biofilm has the ability to precipitate calcium carbonate and the more the fouling contain organic matter the more precipitation is promoted.

The effect of calcium carbonate on pipes fouling and drippers clogging was demonstrated using an irrigation set-up. Two synthetic wastewater was used. The difference between these two waters quality is that in one of them calcium carbonate was added. The fouling inside pipes in the presence of calcium carbonate is much higher than in the case where there is no calcium carbonate. An analysis of the fouling composition put into evidence the higher quantity of organic matter in the sample developed without calcium carbonate.

The presence of calcium carbonate as a precipitate in large quantities has a negative effect on biofilm development. The calcium carbonate particles can play an abrasive role and influence the attachment of the biofilm to the support. This can be also observed at the level of drippers. At the beginning of the experiments, calcium carbonate also does not favor the biofilm development and induces fluctuations in the drippers flow rate. The biofilm began to develop mainly in the central zone of the dripper. When a detachment occurs biofilm settles in the baffles and obstructs water passage. The biofilm wedged in the baffles will favor the accumulation of calcium carbonate which will aggravate more the clogging. According to the results, water irrigation uniformity is better with one type of clogging and not two.

Further experiments carried out with other water qualities seem necessary in order to better calibrate the modeling done with PHREEQC. The study could serve as a database for farmers to check whether their water is likely to be used for irrigation and whether there is a risk of chemical precipitation. In this case, necessary measures could be programmed like for example, acidification in order to lower the saturation index below the precipitation threshold without acidifying too much the irrigation

water and harmful the soil and plants.

In bioprocesses, modeling of biofilm development is generally based on substrate concentration, often based on the Monod equation, which is the oldest model (Monod, 1958)[198] and the most widely used. The Monod equation can thus be modeled by PHREEQC. An interesting case of study would be to investigate the modeling of biofilm growth with chemical precipitation by varying the operating conditions. In this study, the novelty is the studying of biofilms development in a Taylor-Couette reactor using real wastewater. Experimentally studying the effect of pH and temperature in a TCR would be an innovative and interesting idea to compare with numerical modeling.

Further experiments using the confocal laser scanning microscope, and/or Optical Coherence Tomography (OCT) seem to be necessary to pursue the development of the biofilm closely regarding biofilm thickness, density and structure and to be able to detect and to understand the chemical precipitation. It would also be interesting to follow as closely as possible the interaction between biofilm and chemical precipitation by visualizations using cameras on transparent drippers for example taking care not to develop algae.

The path leading to the understanding of all the interactions involved in the clogging of drippers and fouling of pipes using treated wastewater remains long despite extensive studies in this field. Our experiments have brought very interesting results which can be used for other studies on the reuse of wastewater in irrigation, a subject which is becoming more and more useful to study given the hydro-ecological and biodemographic problems which become more widespread over time and affect more than half of the planet.

Chapter V

Résumé détaillé en Français

Part V.1

Contextes et Objectifs de la thèse:

La micro-irrigation est la technique la plus adaptée dans le contexte de la réutilisation en irrigation des eaux usées traitées. Dans les pays arides, semi-arides et en voie de développement l'utilisation de ces eaux pour l'agriculture semble être une alternative efficace face au problème de la pénurie en eau. Dans le monde environ 70% des eaux usées traitées sont utilisées pour l'agriculture (Kalavrouziotis et al., 2011[145]). Mais avant toute utilisation des réglementations internationales et nationales ont été mises en place pour limiter le risque sanitaire lié à l'utilisation des eaux résiduaires urbaines traitées pour l'irrigation de cultures et d'espaces verts (Directives de l'Organisation Mondiale de la Santé pour l'utilisation sans risques des eaux usées, 2006).

D'autres recommandations et normes sont aussi à prendre en compte concernant la qualité des eaux pour une utilisation en micro-irrigation. Même si la micro-irrigation offre plusieurs avantages tant de point de vue économique et que de celui environnemental, ceci n'empêche pas la présence de certains inconvénients tels le colmatage des goutteurs et l'encrassement des conduites d'irrigation. Nakayama and Bucks, 1980[204] ont établi une grille pour lier la qualité de l'eau au risque de colmatage. Dosoretz et al., 2011[85] ont identifié trois types de colmatages des goutteurs qui sont liés ou non entre eux.

Il est cependant clair que le colmatage physique est dû à l'accumulation de matière en suspension, le colmatage biologique au développement de biofilms et celui chimique à la précipitation de composés chimiques présents dans l'eau.

Le colmatage des goutteurs est directement lié à plusieurs paramètres dont la qualité de l'eau, les conditions hydrodynamiques à l'intérieur du goutteur et les conditions opératoires. En particulier des concentrations élevées de matières en suspension, de nutriments (carbone, azote, phosphore, etc.) et de certains ions (Ca^{2+}, Mg^{2+}, $Mn^{2+}\dots$) peuvent, sous des conditions de pH et de température déterminées engendrer les développements de biofilms et la précipitation de sels (Adin et Sacks, 1987[5]). La géométrie des goutteurs a aussi un effet remarquable sur le colmatage de ceux-ci (Taylor et al., 1995[273]).

De même les conditions hydrodynamiques, comme la vitesse d'écoulement et les contraintes de cisaillement ont un effet notable sur le développement des biofilms (Ravina et al., 1992[240]).

La température, le pH et la pression partielle en CO_2 sont les principaux facteurs physico-chimiques rencontrés en micro-irrigation. Des variations de température de l'eau peuvent atteindre 50°C pendant les jours d'été à l'intérieur des conduites noires en polyéthylène (PE) (Qian et al., 2017[237]). Le changement du pH sont tributaires de la concentration en CO_2 dans l'eau, de la dégradation microbienne (fermentation, photosynthèse ...) et aussi de l'injection de fertilisants dans l'eau (Imas and Cohen 2009[136]), tandis que la pression partielle en CO_2 dans l'eau est directement liée à la température (Loi de Henry). Plus la température augmente plus la solubilité du CO_2 diminue ce qui induit une augmentation du pH. Ceci prouve que le pH, la température et la pression partielle en CO_2 sont liés et affectent les mécanismes de précipitation chimique. La pression partielle du CO_2 dans l'eau et son effet sur les mécanismes de précipitation, est liée aussi à la pression qui est exercé sur cette eau (système d'irrigation sous pression i.e. micro-irrigation) elle dépend aussi du système dans lequel cette eau se trouve: Système fermé (eau non en équilibre avec le CO_2 atmosphérique) ou système ouvert (eau en équilibre avec le CO_2 atmosphérique).

Quand l'eau d'irrigation est directement pompée dans le système de distribution elle se trouve dans un système fermé. Par contre si elle sort du goutteur ou qu'elle soit mise avant utilisation dans des réservoirs, elle se trouve dans un système ouvert.

L'objectif principal de cette thèse consiste à apporter de nouveaux éléments sur le colmatage des goutteurs et sur l'encrassement des conduites à l'échelle du laboratoire, dans des conditions bien contrôlées dans l'objectif de la réutilisation des eaux usées traitées en irrigation.

Le travail a été réalisé au sein de l'Institut national de Recherche en Sciences et Technologies pour l'Environnement et l'Agriculture (IRSTEA) (UMR Geau) et au laboratoire M2P2 (Mécanique, Modélisation et Procédés Propres, AMU-CNRS) afin d'étudier les mécanismes du colmatage chimique et biologique et leurs interactions en micro-irrigation.

Le travail est divisé en trois parties : La première partie aborde la problématique des bancs d'essais et des conditions d'expérimentation qui ont été prises en compte dans cette étude. La deuxième porte sur les résultats expérimentaux et numériques quant à la précipitation chimique en utilisant une eau usée traitée. Et enfin la troisième partie se concentre sur le développement du biofilm et l'interaction de celui-ci avec la précipitation du carbonate de calcium.

Part V.2

Matériels et méthodes

Dans ce chapitre l'objectif est de présenter les différentes démarches et analyses dans le but de comprendre et d'identifier et de caractériser les paramètres qui affectent précipitation chimique, développement des biofilms et l'interaction entre les deux avec l'utilisation d'une eau usée traitée pour satisfaire les conditions d'emploi en micro-irrigation, une série d'expérimentation sur banc d'essai a été faite.

Qualité de l'eau

L'eau usée traitée utilisée provient de la sortie d'un traitement tertiaire de la station d'épuration des eaux usées de Mauguio. Les paramètres physicochimiques de l'effluent sont listés dans le tableau V.1.

Précipitation chimique au laboratoire

L'objectif est de déterminer la quantité et la qualité de la précipitation chimique sous des conditions de micro-irrigation en utilisant l'effluent de la STEP de Mauguio.

Une précipitation chimique au laboratoire utilisant l'eau citée a été faite dans des séries de réacteurs ouverts à l'air libre avec la possibilité d'augmenter température et pH. L'eau a été au préalable filtrée à $0.45\ \mu m$ afin d'éliminer toutes les matières en suspension et la plupart des bactéries. Quatre valeurs de pH (8, 8.5, 9, 9.5) et deux températures (22°C et 55°C) ont été testées. Une solution d'hydroxyde de sodium 0.1M fut utilisée pour augmenter le pH. L'augmentation de la température fut réalisée à l'aide

d'un bain réglé au thermostat.

Table V.1: Paramètres physicochimiques de l'effluent de la STEP de Mauguio.

Paramètres	**valeurs**	**Paramètres**	**valeurs**
T (°C)	17	N Kjeldhal (mg Ntot/ L)	2,31
Turbidité	2,03	Fluore (mg/L)	< 0,50
pH	7,8	Aluminium (µg/L)	< 20
Conductivité (µS/cm)	1270	Br (mg/L)	0,18
TDS (mg/L)	1241,7	B (mg/L)	0,14
Dureté (mg/L)	223	Ba (mg/L)	<0,05
Alcalinité (mg/L)	< 20	Cd (mg/L)	<0,005
TAC (mg/L)	261	Cu (mg/L)	<0,02
Ammonium (mg/L)	0,37	Fe (mg/L)	<0,05
Nitrates (mg/L)	9,8	Mn (mg/L)	0,03
Nitrites (mg/L)	0,17	Li (mg/L)	<0,02
Phosphores (mg Ptot/ L)	0,17	Pb (mg/L)	<0,05
Mg (mg/L)	7	Si (mg/L)	12
Ca (mg/L)	133	Sr (mg/L)	0,39
Na (mg/L)	119	Zn (mg/L)	0,03
Cl (mg/L)	171	DCO (mg/L)	< 30
K (mg/L)	18,1	COT (mg/L)	6,8
Sulfates (mg/L)	109	MES (mg/L)	5

Pour récupérer le précipité, l'eau est filtrée sous vide sur du papier filtre à base de microfibres de verre. Pour mesurer la masse du précipitât, les papiers filtres sont mis dans une étuve à 105°C, pendant 24h, afin d'éliminer toute trace d'eau et puis pesés à l'aide d'une balance électronique de précision (0.1 mg).

Modélisation de la précipitation avec PHREEQC

Les résultats expérimentaux ont été utilisés pour valider et calibrer un modèle numérique qui permettra par la suite de prédire les quantités et qualités de la précipitation chimique suite à l'utilisation d'une eau usée traitée pour satisfaire les conditions d'emploi en micro-irrigation.

Le but est de pouvoir prendre les mesures nécessaires pour éviter ou limiter le colmatage des goutteurs et l'encrassement des conduites par la précipitation chimique. Les paramètres physicochimiques de l'eau sont précisés dans la base de données du logiciel PHREEQC. Dans celui-ci le calcul de l'indice de saturation (SI) (Eq.V.1) de chaque élément s'effectue en utilisant la relation dite de Debye-Huckel étendue (V.1) (pour une force ionique ¡ à 0.1M) la force ionique (I) de l'eau étant égale à 0.01M :

$$\mathrm{SI} = log\left(\frac{\mathrm{IAP}}{K}\right) \tag{V.1}$$

$$ln\gamma_i = -\frac{Az_i^2\sqrt{I}}{1 + B\dot{a}_i\sqrt{I}} \tag{V.2}$$

Avec A et B constantes dépendantes de la température, ($\dot{a}_i$) paramètre empirique de taille ionique, z_i^2 la valence, I la force ionique, IAP produit d'activité ionique et K constante d'equilibre.

SI = 0 reflète l'équilibre entre le minéral et la solution, SI > 0 reflète la sursaturation et la capacité de précipitation du minéral. Si SI <0, la solution est sous-saturée ce qui provoque la dissolution du sel (Appelo and Postma, 2005)[19].

Effet de la contrainte du cisaillement sur le développement du biofilm

Un réacteur de Taylor-Couette (RTC) a été utilisé pour étudier le développement du biofilm sous différentes contraintes de cisaillement contrôlées, caractéristiques des écoulements dans les goutteurs en régime turbulent. La hauteur du cylindre (h) est de 20 cm, l'entrefer (e) est de 1.3 cm, le rayon interne R_1 est de 10.65 cm et le rayon externe R_2 est de 11.95 cm. Le support sur lequel le biofilm se développera est constitué de plaques de polyéthylène de faible densité (LDPE) (Φ 16 mm). Cinq plaques sont utilisées pour suivre le développement du biofilm en fonction du temps, chaque plaque occupe une surface de 243.2 cm^2. Les contraintes de cisaillement sélectionnées sont les mêmes rencontrées en micro-irrigation. Dans une conduite de LDPE de diamètre 16 mm la contrainte de cisaillement rencontrée est de 0.7 Pa pour une vitesse de l'eau égale à 0.4 m/s (Gamri, 2014[112]). Dans les goutteurs les contraintes de cisaillement rencontrées sont en général comprises entre 2.2 et 4.4 Pa (Al-Muhammad, 2016[10]).

Les expériences ont été faites en circuit ouvert sur une durée de 8 semaines. La température de l'eau a été réglée au thermostat à 21°C, le temps de séjour de l'eau dans le réacteur est de 24h maintenu à l'aide d'une pompe péristaltique délivrant un débit de 1.38 ml/min. La charge spécifique du réacteur est de 0.049 mg/jour/cm2. Chaque semaine une plaque est retirée du RTC et son encrassement raclé à l'aide d'une membrane élastomère puis mis dans des coupelles en céramique pour mesures.

Effet du carbonate de calcium sur le développement du biofilm

Un banc d'irrigation pilote formé de 12 conduites en LDPE (Φ 16 mm) a été mis en place pour étudier l'effet du carbonate de calcium sur le développement du biofilm dans les conduites et dans les goutteurs. La vitesse de l'eau est de 0.4 m/s ce qui donne une contrainte de cisaillement de 0.7 Pa. Chaque conduite est alimentée séparément à partir d'un réservoir contenant une eau usée artificielle. L'eau utilisée dans ces expérimentations est une eau déminéralisée dont les composants cités dans le tableau V.2 y ont été dissous. Le tableau V.2 résume la qualité des eaux utilisées dans ces expérimentations.

Table V.2: Composition de l'eau synthétique dans le réservoir 1 (sans carbonate de calcium) et dans le réservoir 2 (avec carbonate de calcium).

	Composants	**Concentrations (mg/L)**
Réservoir 1 et réservoir 2	Glucose	200
	Chlorure d'ammonium	16.28
	Acide phosphorique	2.05
Seulement réservoir 2	Chlorure de calcium	369
	Bicarbonate de sodium	443.3

L'expérience fut réalisée durant 7 semaines et chaque semaine une conduite de chaque série était retirée et remplacée par une neuve pour avoir deux répétitions. L'encrassement est raclé à l'aide d'une membrane élastomère fixée à l'extrémité de l'éprouvette par un fil métallique. L'encrassât est ensuite mis dans des coupelles en céramique pour mesures. Chaque conduite contient 6 goutteurs de type NPC2 montés en dérivation délivrant un débit de 2 L/h sous une pression de 1 bar. Le suivi du colmatage des goutteurs se fait par mesure du volume délivré sur une période de 10 minutes.

Caractérisation de l'encrassement

L'encrassement récupéré du RTC et des conduites du banc d'irrigation pilote fut caractérisé par des mesures sur la matière sèche (MS) et la matière sèche volatile (MVS). La mesure sur la matière sèche (MS) est faite en faisant passer à l'étuve les coupelles pendant 24h à 105°C. La matière sèche volatile (MVS) est obtenue en faisant passer au four les coupelles pendant 2h à 550°C (matière inorganique MI). Afin d'identifier les phases cristallines dans l'échantillon une mesure de diffraction aux rayons X (DRX) a été utilisée. Dans le cas de phases amorphes et de quantification entre matière organique et non organique l'analyse thermogravimétrique (ATG) a été utilisée.

L'encrassement des goutteurs du banc d'irrigation pilote a été visualisé par un microscope optique. La localisation du colmatage que ce soit dans la zone centrale du goutteur ou dans les chicanes (première, dernière...) ou à la sortie du labyrinthe fournit des informations très importantes pour l'optimisation de l'écoulement dans le goutteur. Un changement des conditions hydrodynamiques à l'intérieur du goutteur par un changement de sa géométrie peut être une solution anti-colmatage (Wei et al., 2006[288]).

Part V.3

Caractérisation de la précipitation chimique par des expériences au laboratoire et numérique

L'objectif de cette étude est de déterminer quelles sont les éléments susceptibles de précipiter et d'engendrer un colmatage chimique en utilisant une eau usée traitée en micro-irrigation et d'évaluer l'effet du pH, température et pression partielle du CO_2 sur la précipitation chimique et d'utiliser un model géochimique pour quantifier et qualifier cette précipitation.

Précipitation chimique au laboratoire

La précipitation chimique a été induite en augmentant le pH et la température de l'eau. L'analyse du précipité avec la DRX et la TGA montre qu'il est formé principalement de carbonate de calcium sous forme de calcite. Plus la température et le pH augmente plus la masse du précipité augmente. Le pH et la température jouent un rôle important sur la solubilité de la calcite et du CO_2 dissous dans l'eau. Plus la température augmente plus la solubilité du CO_2 diminue ce qui engendre une augmentation du pH de l'eau. Plus le pH augmente plus la solubilité de la calcite diminue d'après l'équation V.3 (Pepe et al., 2009[222]) de même plus la température (T) augmente plus le produit de solubilité de la calcite diminue (équation V.4 (Panthi 2003)[218].

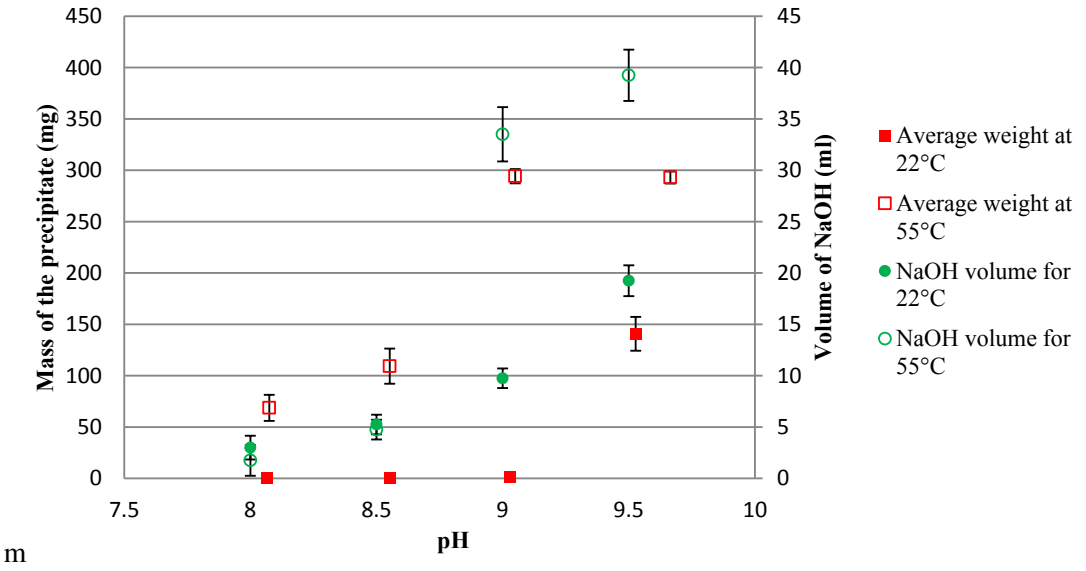

m

Figure V.1: Evolution de la masse du précipité en fonction du pH et de la température

$$\text{Log (SI calcite)} = 1.0997pH - 8.0632 \tag{V.3}$$

$$\text{p}K_{sp} = 0.001183T + 8.03 \tag{V.4}$$

Caractérisation numérique de la précipitation chimique

Les modélisations réalisées avec PHREEQC ont montré que la calcite est l'élément prépondérant. L'indice de saturation (SI) de la calcite dans l'eau de Mauguio pour un pH de 7.8 et une température de 17°C quoique supérieur à 0 (SI calcite = 0.82) n'entraine pas de précipitation de calcite. La calcite précipite pour une certaine sursaturation qui ne peut être atteinte que par l'augmentation du pH et de la température. Le même volume de base (NaOH) et les mêmes températures (22°C et 55°C) qui ont été utilisés pour la précipitation chimique au laboratoire ont été introduits dans PHREEQC. L'objectif a été d'induire la précipitation numérique de la calcite en calculant le pH et l'SI correspondant, et comparer les résultats avec ceux expérimentaux. Le but était de pouvoir valider et calibrer le modèle.

Les résultats montrent que les valeurs entre les pH et les SI sont très voisins et en conséquence le modèle peut être utilisé pour calculer et estimer les précipitations de la calcite sur les plateformes réelles.

Des valeurs de l'indice de saturation de la calcite ont été introduites dans le logiciel pour faire précipiter la même quantité de calcite comme dans les expérimentations. Les résultats montrent que pour un pH de 8 à 55°C l'indice de saturation à partir duquel on observe une précipitation est égal à 1.39

tandis que pour un pH de 9.5 à 22°C l'indice de saturation est égal à 2.12.

Pour étudier l'influence d'autres paramètres que ceux des températures et pH, l'effet de la pression partielle du CO_2 sur la précipitation de la calcite a été modélisée par PHREEQC. On remarque que l'indice de saturation est plus élevé en absence d'équilibre avec le CO_2 atmosphérique que ce soit à 22°C ou à 55°C. Pour un volume ajouté de NaOH égal à 9.75 ml et une température de 22°C le SI de la calcite est égal à 1.849 dans un système ouvert et 1.94 dans un système fermé. La précipitation de la calcite est plus élevée dans un système fermé que dans un système ouvert surtout pour un pH et température élevés.

Part V.4

Caractérisation du colmatage biologique et son interaction avec le colmatage chimique

Les objectifs de cette partie sont d'étudier l'effet des contraintes de cisaillement rencontré en irrigation sur le développement du biofilm et l'effet du carbonate de calcium sur le développement du biofilm dans les conduites et les goutteurs.

Développement du biofilm en fonction des contraintes de cisaillement

Pour pouvoir suivre l'évolution du développement du biofilm en fonction du temps et des contraintes de cisaillement la MVS qui n'est autre que la matière organique (MO) a été prise en compte. La figure V.2 montre la masse de cette MVS pour différentes contraintes de cisaillement de 0.7, 2.2 et 4.4 Pa. On peut voir que plus la contrainte est élevé plus le développement du biofilm est favorisé. Ceci est dû à la formation d'un biofilm plus dense et plus rigide qui résiste mieux aux fortes contraintes de cisaillement (Decho, 2000[75]).

La caractérisation de l'encrassement avec la DRX montre la présence de calcite dans les échantillons. La précipitation de la calcite a été faite dans des conditions où la température ne dépasse pas les 25°C et le pH ne dépasse pas 8. Dans ces mêmes conditions, en utilisant l'eau usée traitée de Mauguio, lors des expériences de précipitation au laboratoire, la calcite n'a pas pu être détectée. Ceci met en évidence la possibilité d'interaction entre le biofilm et les ions Ca^{2+}. A l'aide de la TGA on a pu mettre en évidence que plus on a de biofilm plus la précipitation de la calcite est favorisée ce qui confirme les résultats. Ceci est dû aux propriétés de l'EPS qui entoure les biofilms (Tourney and Ngwenya, 2009[277]).

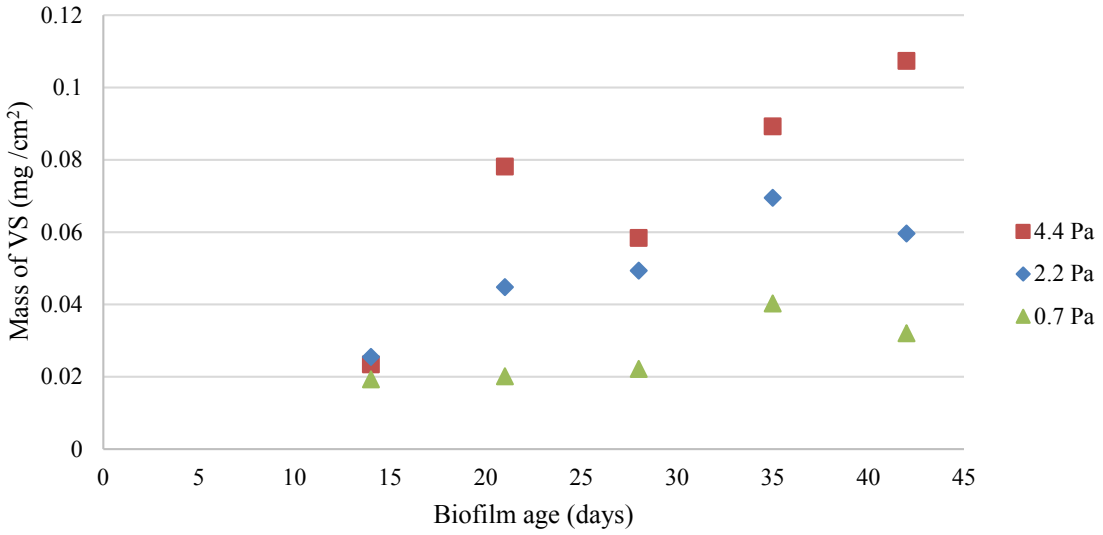

Figure V.2: Evolution de la masse du biofilm dans le RTC en fonction du temps à 0.7, 2.2 et 4.4 Pa

Interaction entre carbonate de calcium et développement du biofilm

Le carbonate de calcium a été choisi parce qu'il a été identifié comme étant l'élément le plus abondant dans les expérimentations précédentes. La figure V.3 montre le développement du biofilm dans les conduites en fonction du temps dans le cas du bidon 1 (T1) (sans carbonate de calcium) et le bidon 2 (T2) (avec carbonate de calcium).

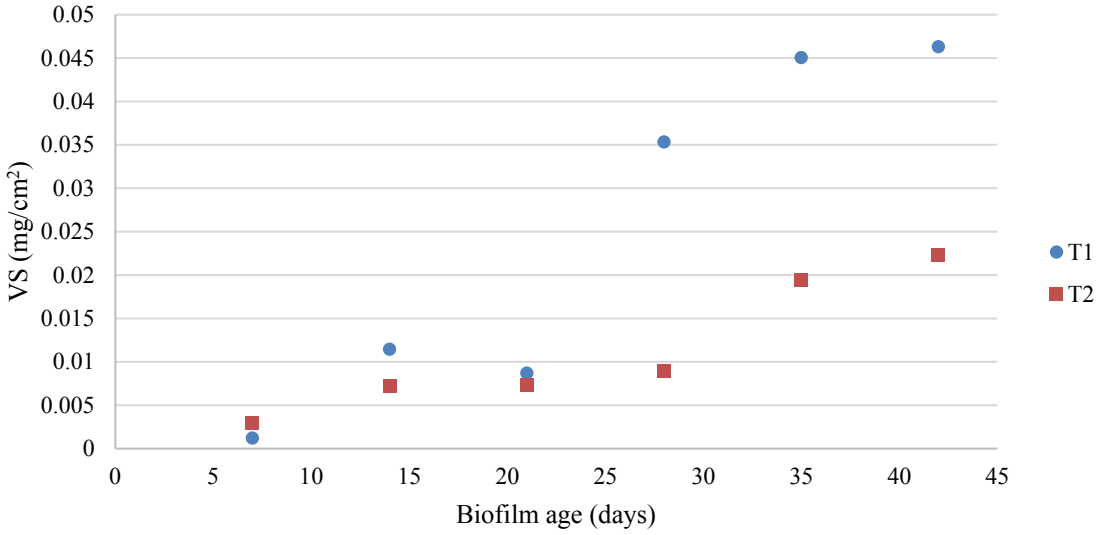

Figure V.3: Evolution de la quantité du biofilm dans les conduites en présence (T1) ou pas (T2) de carbonate de calcium.

On remarque que la présence du carbonate de calcium affecte la croissance du biofilm à partir du 21ème jour. A partir de cette date la quantité de précipité devient assez suffisante pour jouer le rôle de matière en suspension qui ont un effet abrasif sur le biofilm (Derlon et al., 2008[78]).

L'analyse de l'encrassement avec la DRX montre la présence de calcite même sans carbonate de calcium. Ceci met en évidence que le biofilm a la capacité de faire précipiter la calcite et ce même avec la présence de traces de calcium. Les résultats obtenus sur la TGA mettent aussi en évidence le fait que plus il y a de matière organique dans l'échantillon plus le pourcentage en carbonate de calcium dans cet échantillon augmente.

Dans les goutteurs, le carbonate de calcium a aussi retardé l'apparition du biofilm et a créé plus de fluctuations dans les mesures des débits. A partir des observations au microscope et au suivi des débits en fonction de l'âge de biofilm on peut noter qu'un développement du biofilm dans la zone centrale du goutteur n'affecte pas le débit. Par contre, la présence du biofilm dans les premières chicanes fait chuter directement celui-ci. La présence de biofilm dans les chicanes peut être due à un détachement de celui-ci de la zone centrale. La chute du débit est surtout due au développement du biofilm. Le calcul de la valeur de l'uniformité statistique (SU) est plus faible dans le cas de la précipitation chimique avec le développement du biofilm qu'avec le biofilm tout seul. Une fois le biofilm formé le carbonate de calcium est surement piégé dans les EPS ce qui aggrave la situation.

Conclusion et perspectives

L'étude réalisée dans le cadre de ce travail de thèse a pour objectif de contribuer à la compréhension des mécanismes qui induisent la précipitation chimique et le développement du biofilm en utilisant une eau usée traitée pour l'emploi en micro-irrigation.

Différentes approches expérimentales et numériques ont été réalisés dans le but de caractériser la précipitation chimique et de pouvoir coupler les différents paramètres qui puissent influer sur la solubilité des sels dans l'eau. La première partie du travail consistait à caractériser expérimentalement la précipitation chimique du point de vue quantitatif et qualitatif et de voir l'effet du pH et de la température sur celle-ci. Les résultats obtenus par les analyses et par la DRX et la TGA ont permis d'identifier le carbonate de calcium sous forme de calcite comme étant le précipité le plus abondant. Grace au données et aux résultats du travail expérimental la validation et la calibration de PHREEQC a pu être réalisée. PHREEQC nous permet de prédire la quantité et la qualité de la précipitation chimique sans passer chaque fois par des expériences au laboratoire. A l'aide de ce logiciel géochimique, l'effet de la pression partielle du CO_2 sur la précipitation de la calcite a pu être étudié. Expérimentalement, l'étude de ce paramètre nous était difficile à suivre. L'indice de saturation lui aussi ne peut être calculé que par le moyen d'un logiciel. Il en ressort que la calcite ne précipite que lorsque la valeur du SI dépasse un certain seuil. Ce seuil peut être atteint plus facilement dans un système fermé qui n'est pas en équilibre avec le CO_2 atmosphérique et aussi par augmentation de la température et du pH.

La seconde partie du travail de thèse a porté sur la mise en œuvre de bancs d'essais dans le but de suivre le développement du biofilm en parallèle avec la précipitation chimique et l'interaction du carbonate de calcium sur le biofilm en utilisant une eau usée traitée réelle et une eau usée synthétique. Un réacteur de type Taylor-Couette a été mis en place afin de suivre l'effet du cisaillement sur le développement du biofilm en utilisant une eau usée réelle. Un développement plus important dû à un biofilm plus dense et plus rigide a été observé pour une contrainte de cisaillement élevée (4.4 Pa) contrairement à ceux développés à des contraintes de cisaillement plus faible (0.7 et 2.2 Pa). Une seconde expérimentation avec des eaux usées synthétiques a permis de mettre en évidence l'effet du carbonate de calcium sur le développement du biofilm dans les conduites et goutteurs. Dans un premier point le

carbonate de calcium a un effet négatif sur le développement du biofilm dans les conduites d'irrigation. La quantité de matière sèche volatile s'est avérée inférieure dans l'encrassement formé avec le carbonate de calcium. Ceci pourrait être dû à l'effet abrasif du précipité. L'effet du carbonate de calcium ($CaCO_3$) sur le développement du biofilm dans les goutteurs suit un peu la même tendance où le colmatage et plus précisément l'apparition du biofilm prend plus de temps en présence de $CaCO_3$.

Des expériences supplémentaires menées avec d'autres qualités d'eau nous semblent nécessaires afin notamment de mieux calibrer la modélisation réalisée sous PHREEQC. L'étude pourrait servir de base de données pour les agriculteurs qui souhaitent vérifier si leur eau est susceptible d'être utilisée en irrigation et s'il y a un risque de précipitation chimique. Dans ce cas des mesures nécessaires pourraient être programmées comme par exemple l'acidification dans le but de faire abaisser l'indice de saturation en dessous du seuil de précipitation sans rendre l'eau très acide et néfaste pour le sol et les plantes. En bioprocédés, la modélisation du développement du biofilm est généralement basée sur la concentration en substrat souvent basée sur l'équation de Monod qui est le modèle le plus ancien (Monod, 1958[198]) et le plus utilisé. L'équation de Monod peut être ainsi modélisée par PHREEQC.

Un cas intéressant à étudier serait d'approfondir la modélisation de la croissance du biofilm avec la précipitation chimique en variant les conditions opératoires. Dans notre étude la nouveauté consistait à étudier le développement des biofilms dans un réacteur couette en utilisant une eau usée réelle. Etudier expérimentalement l'effet du pH et de la température dans un réacteur couette serait une idée innovante et intéressante à comparer avec les modélisations informatiques.

Des expériences supplémentaires menées à l'aide du microscope confocal à balayage laser nous semblent nécessaires pour poursuivre de tout près le développement du biofilm et de pouvoir détecter si possible la précipitation chimique. Il serait aussi intéressant de suivre au plus près l'interaction entre le biofilm et la précipitation chimique par des visualisations à l'aide de cameras sur des goutteurs transparents par exemple en faisant attention de ne pas développer des algues.

Le chemin menant à la compensation de toutes les interactions qui rentrent en jeu dans le colmatage des goutteurs et l'encrassement des conduites utilisant des eaux usées traitées reste encore long malgré les études approfondies dans ce domaine.

Nos expérimentations ont ramené des résultats très intéressants pouvant servir à d'autres études sur la réutilisation des eaux usées en irrigation, sujet qui devient de plus en plus utile à étudier étant donné les problèmes hydro-écologiques et biodémographiques qui s'aggravent avec le temps et qui touchent plus que la moitié de la planète.

List of Figures

List of Tables

References

[1] 2030 Water resources Group. (2009). Charting our water future: Economic frameworks to inform decision-making. Washington, dC, 2030 WRG.

[2] Abrahamson, M., Lewandowski, Z., Geesey, G., Skjak-Braek, G., Strand, W., Christensen, B. E. (1996). Development of an artificial biofilm to study the effects of a single microcolony on mass transport. Journal of Microbiological Methods. 26(1-2): 161-169.

[3] Abusam, A., Al-Anzi, B. (2011). Comparison between the irrigation qualities ofconventional tertiary and UF + RO advanced treated wastewaters. Agric. Sci. 2:526–532.

[4] Adin, A., Alon, G. (1986). Mechanisms and Process Parameters of Filter Screens. Journal of Irrigation and Drainage Engineering. 112(4):293-304.

[5] Adin, A., Sacks, M. (1987). Water quality and emitter clogging relationship in wastewater irrigation. In: Proceedings of Water Reuse Symposium IV , American Water Work Association Research Foundation: Denver, Colo.

[6] Adin, A., Elimelech, M. (1987). Particle Filtration for Wastewater Irrigation. Journal of Irrigation and Drainage Engineering. 115(3):474-487

[7] Adin, A., Sacks, M. (1991). Dripper Clogging Factors in Wastewater Irrigation. Journal of Irrigation and Drainage Engineering. 117(6):813-826.

[8] Addiscott, T. M., Whitmore, A. P., Powlson, D. S. (1991). Farming, fertilizers and the nitrate problem. CAB International (CABI).

[9] Ahmad Aali, K. A., Liaghat, A., Dehghanisanij, H. (2009). The effect of acidification and magnetic field on emitter clogging under saline water application. Journal of Agricultural Science. 1(1):132-141.

[10] Al-Muhammad, J., Tomas, S., Anselmet, F. (2016). Modeling a weak turbulent flow in a narrow and wavy channel: cas of micro irrigation. Irrigation Science. 34(5):361-377.

[11] Almuktar, S. A. A. A. N., Scholz, M., Al-Isawi, R. H. K., Sani, A. (2015). Recycling ofdomestic wastewater treated by vertical-flow wetlands for irrigating chilliesand sweet peppers. Agric Water Manage. 149:1–22.

[12] Almuktar, S. A. A. A. N., Scholz, M. (2016). Mineral and biological contamination of soiland capsicum annuum irrigated with recycled domestic wastewater. Agric Water Manage. 167:95–109.

[13] Alnouri, S. Y., Linke, P., El-Halwagi, M. M. (2015). A synthesis approach for industrial city water reuse networks considering central and distributed treatment systems. Journal of Cleaner Production. 89:231-250.

[14] An, Y. H., Friedman, R. J. (1997). Laboratory methods for studies of bacterial adhesion. J Microbiol Meth. 30:141-152.

[15] Andersson, S. (2009). master report - Characterization of bacterial biofilms for wastewater treatment. Royale Istitute of Technology, school of Biotechnology: Stocholm.

[16] Andritsos, N., Karabelas, A. J. (1999). The influence of particulates on $CaCO_3$ scale formation. ASME J. Heat Transfer. 121:225-227.

[17] Andereck, C. D., Liu, S. S., Swinney, H. L. (1986). Flow regimes in acircular Couette system with independently rotating cylinders. J. Fluid Mech. 164:155-183.

[18] Annachhatre, A. P., Bhamidimarri, S. M. R. (1992). Microbial attachment and growth in fixed-film reactors: process startup considerations. Biotechnol Adv. 10:69–91.

[19] Appelo, C. A. J., Postma, D. (2005). Geochemistry, groundwater and pollution, Second Edition. (CHEMLIBnetBASE.) Leiden: Balkema.

[20] Applegate, DH., Bryers, J. D. (1991). Effects of carbon and oxygen limitations and calcium concentrations on biofilm removal process. Biotechnol Bioeng 37:17-25

[21] Arp, G., Thiel, V., Reimer, A., Michaelis, W., Reitner, J. (1999). Biofilm exopolymers control microbialite formation at thermal springs discharging into the alkaline Pyramid Lake, Nevada, USA. Sedimentary Geology. 126:159-176.

[22] Ayers, R. S., Westcot, D. W. (1985). Water Quality for Agriculture, Food and Agriculture Organi-

zation of the United Nations. Rome.

[23] Ayer, R. S., Westcot, D. W. (1988). qualité de l'eau d'irrigation et du drainage. bulletin FAO, 29, pp.174.

[24] Bagatin, R., Klemes, J.J., Reverberi, A.P., Huisingh, D. (2014). Conservation and improvements in water resource management: a global challenge. J. Clean. Prod. 77:1-9.

[25] Bauder, T. A., Waskom, R.M., Sutherland, P.L., Davis, J. G. (2014). Irrigation Water Quality Criteria, fact sheet No.0.506, Colorado State University Extension, USA.

[26] Bakke, R. (1986). Biofilm detachment. Ph.D. thesis. Montana State University.

[27] Barry, D. A., Prommer, H., Miller, C. T., Engesgaard, P., Brun, A., Zheng, C. (2002). Modelling the fate of oxidisable organic contaminants in groundwater. Adv. Water Resour. 25:945–983.

[28] Batarseh, M. I., Ioannis, K. K., Prodromos, K. H., Rawajfeh, A. (2011). Treated municipal wastewater irrigation impact on olive trees (Olea Europaea L.) at Al-Tafilah, Jordan. Water, Air, & Soil Pollution, 217(1-4), 185-196.

[29] Battin, T. J., Kaplan, L. A., Newbold, J. D., Hansen, C. M. E. (2003). Contributions of microbial biofilms to ecosystem processes in stream mesocosms. Nature 426:439–442.

[30] Belkhadir, R,., Capdeville, B., Roques H. (1988). Etude descriptive fondamentale et modelisation de la croissance d'un film biologique Etude descriptive fondamentale de la croissance d'un film biologique. Water Research, 22(1):59-69.

[31] Beloin, C., Roux, A., Ghigo, J. M. (2008). Escherichia coli biofilms. Curr. Top. Microbiol. Immunol. 322:249–289

[32] Bendinger B, Rijnaarts HHM, Altendorf K, Zehnder AJB. (1993). Physicochemical cell-surface and adhesive properties of coryneform bacteria related to the presence and chain-length of mycolic acids. Appl Environ Microbiol 59:3973–3977.

[33] Benitez, E., Romero, M., Gomez, M., Gallardolaro, F., Nogales, R. (2001). Biosolid and biosolid ash as sources of heavy metals in plant-soil system. Water Air Soil Pollut. 132:75–87.

[34] Benzerara, K., Menguy, N., López-García, P., Yoon, T. H., Kazmierczak, J., Tyliszczak, T. (2006). Nanoscale detection of organic signatures in carbonate microbialites. Proc. Natl. Acad. Sci. U.S.A. 103:9440–9445

[35] Beyenal, H., Lewandowski, Z. (2002). Internal and External Mass Transfer in Biofilms Grown at Various Flow Velocities. Biotechnol Progress. 18: 55–61

[36] Bliefert, C., Perraud, Robert. (2001). Chimie de l'environnement: Air, Eau, Sols, Déchets. Paris: DeBoeck Université.

[37] Blumenthal, U., Mara, D., Peasey, A., Ruiz-Palacios, G., Stott, R. (2000). Guidelines for microbiological quality of treated wastewater used in agriculture: recommendations for revising WHO guidelines. Bulletin of World Health Organization. 78 (9): 1104–1116.

[38] Blumenthal, U., Peasey, A. (2002). Critical Review of Epidemiological Evidence of the Health Effects of Wastewater and Excreta Use in Agriculture. London School of Tropical Medicine, London.

[39] Boman, B.J. (1990). Clogging characteristics of various microsprinkler designs in mature citrus grove. Proc.Fla. State Hort. Soc. 103:327-330

[40] Bounoua, S. (2010). Étude du colmatage des systèmes d'irrigation localisée. Thèse, Aix Marseille Université. 109p.

[41] Bounoua, S., Tomas, S., Labille, J., Molle, B., Granier, J., Haldenwang, P., Izzati, S. N. (2016). Understanding physical clogging in drip irrigation: in situ, in-lab and numerical approaches. Irrigation Science. 34(4):327–342.

[42] Bourrie, G., Trolard, F., Chanzy, A., Ruget, F., Lecerf, R., Charron, F. (2013). Sustainable intensive agriculture: evidence from equeous geochemistry, Procedia Earth and Planetary Science, 7, 93-96.

[43] Braissant, O., Decho, A. W., Dupraz, C., et al. (2007). Exopolymeric substance of sulfate-reducing bacteria: interactions with calcium at alkaline pH and implication for formation of carbonate minerals. Geobiology. 5:401–411.

[44] Briandet, R., Meylheuc, T., Maher, C., Bellon-Fontaine, M. N. (1999). Listeria monocytogenes Scott A: Cell Surface Charge, Hydrophobicity, and Electron Donor and Acceptor Characteristics under Different Environmental Growth Conditions. Applied and Environmental Microbiology, 65(12), 5328–5333.

[45] Bucks, D. A., Nakayama, F. S., Gilbert R. G. (1979). Trickle irrigation water quality and preventive maintenance. Agricultural Water Management. 2(2): 149-162.

[46] Bucks, D.A., Nakayama, F.S. (1982). Principles and potentialities of trickle (drip) irrigation. In Advances in Irrigation. 1:219-298.

[47] Bucks, D.A., and Nakayama, F.S. (1984). Problems to avoid with drip/trickle irrigation systems. Proceedings of the American Society of Civil Engineers Specially Conference on Irritation and Drainage Division, 24-84.

[48] Burt, C. M., Styles, S. W. (1994). Drip and microirrigation for trees, vines, and row crops. Irrigation Training and Research Center. California Polytechnic State University. San Luis Obispo, CA. 261 p.

[49] Burt, C. M., O'connor, K., Ruehr, T. (1995). Fertigation. Irrigation Training and Research Center. California Polytechnic State Univ. San Luis Obispo, CA. 295 p.

[50] Busscher, H.J., van der Mei, H.C., Clin. Microbiol. Rev.19, 127–141 (2006).

[51] Bryers, J., Characklis, W. G. (1981). Early fouling biofilm formation in a turbulent flow system: Overall kinetics. Water Res. 15: 483–491.

[52] Carpa, A., Scicolone, B. (1998). Water quality and distribution uniformity in drip/trickle irrigation systems. Journal of Agricultural Engineering Research, 70(4),355–365.

[53] Carpa, A., Scicolone, B. (2004). Emitter and filter tests for wastewater reuse by drip irrigation. Agricultural Water Management, 68, pp. 135-149.

[54] Carpa, A., Scicolone, B. (2005). Assessing dripper clogging and filtering performance using municipal wastewater. Irrigation and drainage, 54, pp. 71-79.

[55] Chadwick, A., Morfett, J. (1993). Hydraulics in civil and environmental engineering. Chapman and Hall. 2nd edition.

[56] Chahal, N., Rajor, A., Siddique, R. (2011). Calcium carbonate precipitation by different bacterial strains. African Journal of Biotechnology 10(42): 8359-8372.

[57] Chapelle, F.H. (2001). Ground-water microbiology and geochemistry. 2nd ed. John Wiley Sons, New York.

[58] Characklis, W. G. Attached microbial growths-II. Frictional resistance due to microbial slimes Water Research, 1973, 7, 1249 - 1258

[59] Characklis, W. G. (1981), Bioengineering report: Fouling biofilm development: A process analysis. Biotechnology and Bioengineering, 23(9):1923-1960.

[60] Characklis, W.G., Marshall, K.C. (1990). Biofilms. John Wiley and Sons.

[61] Chen, M., Zhang, Z., Bott, T. Effects of operating conditions on the adhesive strength of Pseudomonas fluorescens biofilms in tubes Colloids and Surfaces B: Biointerfaces , 2005, 43, 61 - 71

[62] Choi, Y.C., Morgenroth, E. (2003). Monitoring biofilm detachment under dynamic changes in shear stress using laser-based particle size analysis and mass fractionation Water Sci. Technol., 47:69–76

[63] Christou, A., Maratheftis, G., Eliadou, E., Michael, C., Hapeshi, E., Fatta-Kassinos, D. (2014). Impact assessment of the reuse of two discrete treated wastewaters forthe irrigation of tomato crop on the soil geochemical properties, fruit safetyand crop productivity. Agric. Ecosyst. Environ. 192:105–114.

[64] Clutterbuck, AL., Cochrane, CA., Dolman, J., Percival, SL. (2007). Evaluating antibiotics for use in medicine using a poloxamer biofilm model. Ann Clin Microbiol Antimicrob. 6, 2-5.

[65] Compaore, M. L. (2006). Panorama des techniques d'irrigation et éléments de choix. In : Tiercelin J.-R. Vidal A., eds. Traité d'irrigation. 2^e éd. Paris : Lavoisier, 489-512.

[66] Costerton, J. W., Geesey, GG., Cheng, K-J. (1978). How bacteria stick. Sci. Am.238:86–95

[67] Costerton, J. W., et al., Annu. Rev. Microbiol.49, 711(1995).

[68] Costerton, J. W.; Stewart, P. S., Greenberg, E. P. (1999) Bacterial Biofilms: A Common Cause of Persistent Infections Science, American Association for the Advancement of Science. 284: 1318-1322.

[69] Costerton, J. W. (2004). Short History of the Development of the Biofilm Concept Microbial Biofilms, American Society of Microbiology. 4-19

[70] Coufort, C. (2004). Analyse expérimentale de la floculation en réacteur de Taylor-Couette : Influence de l'hydrodynamique sur les phénomènes d'agglomération et de rupture. INSA Toulouse.

[71] Couture, I., (2004). Principaux critères pour évaluer la qualité de l'eau en micro-irrigation.https://www.agrireseau.net/horticulture-pepiniere/documents/Couture$_Isabelle.pdf$

[72] Cuenca, R.H. (1989). Irrigation System Design, an Engineering Approach. Prentice Hall, Inc., Englewood Cliffs, NJ, 552 pp.

[73] Dazhuang, Y., Peiling, Y., Shumei, R., Yunkai, L., Tingwu, X. (2007). Numerical study on flow property in dentate path of drip emitters. New Zealand Journal of Agricultural Research. 50:705-712.

[74] De Beer, D., Stoodley, P., Roe, F., Lewadowski, Z (1994). Effects of biolm structures on oxygen distribution and mass transport. Biotechnol Bioeng 43: 1131–1138.

[75] Decho, A.W. (2000). Microbial biofilms in intertidal systems: an overview. Cont. Shelf Res.20: 1257 – 1273.

[76] Declet, A.; Reyes, E.; Suárez, O.M. Calcium carbonate precipitation: A review of the carbonate crystallization process and applications in bioinspired composites. Rev. Adv. Mater. Sci. 2016, 44, 87–107.

[77] DehghaniSanij, H., Yamamoto, T., Rasiah, V., Utsunomiya, J., Inoue, M. (2004). Impact of biological clogging agents on filter and emitter discharge characteristics of microirrigation systems. Irrigation and drainage. 53(4):363-373.

[78] Derlon, N., Massé, A., Escudié, R., Bernet, N., Paul, P. Stratification in the cohesion of biofilms grown under various environmental conditions, Water Research. 42(8–9):2102-2110

[79] Derlon, N., Peter-Varbanets, M., Scheidegger, A., Pronk, W., Morgenroth, E. (2012). Predation influences the structure of biofilm developed on ultrafiltration membranes. Water Research. 46:3323–3333.

[80] Dey, D., Herzog, A., Srinivasan, V. (2007). Chemical precipitation : water softening. report ENE 806,Michigan State University East Lansing.

[81] DiPrima, R. C., Eagles, P. M., Ng, B. S. (1984). The effect of radius ratio on the stability of Couette flow and Taylor vortex flow. Phys. Fluids 27:2403–2411.

[82] Domingez-Lerma, M. A., Ahlers, G., Cann Ell, D. S. (1984). Marginal stability curve and linear growth rate for rotating Couette–Taylor flow and Rayleigh–Bénard convection. Phys.Fluids:27, 856–860.

[83] Donlan, RM., Costerton, JW. Biofilms: survival mechanisms of clinically relevant microorganisms. Clin Microbiol Rev 2002; 15:167–93.

[84] Dorigo, U., Leboulanger, C., Berard, A., Bouchez, A., Humbert, JF., Montuelle, B. Lotic biofilm community structure and pesticide tolerance along a contamination gradient in a vineyard area. Aquat. Microb. Ecol. 2007;50:91–102.

[85] Dosoretz, C., Tarchitzki, J., Katz, I., Kenig, E., Chen, Y. (2011). Development and effects of fouling layer in distribution and irrigation systems applying treated wastewater effluents. In: Levy G, Fine P,

Bar-Tal A (eds) Use of treated sewage water in agriculture: impacts on crops and soil environment. Blackwell Publishing, Oxford, pp 328–350.

[86] Douglas, S., Beveridge, T. J. (1998). Mineral formation by bacteria in natural microbial communities. FEMS Microbiol. Ecol. 26, 79–88

[87] Dunglas, J. (2014). La réutilisation des eaux usées. Académie d'Agriculture de France.

[88] Dupraz, C., Visscher, PT. (2005). Microbial lithification in marine stromatolites and hypersaline mats. Trends Microbiol. 13:429–438.

[89] Duran-Ros, M., Puig-Burgués, J., Arbat, G., Barragán, J., Cartagena, FR. (2009). Effect of filter, emitter and location on clogging when using effluents. Agric Water Manag 96(1):67–79.

[90] Duràn-Àlvarez, J.C., Jiménez-Cisneros, B. (2014). Beneficial and negative impacts on soil by the reuse of treated/untreated municipal wastewater for agricultural irrigation — a review of the current knowledge and future perspectivesM.C. Hernández-Soriano (Ed.), Environmental risk assessment of soil contamination, InTech, Rijeka. pp. 137-198

[91] Eberl, H.J., Picioreanu, C., Heijnen, J.J., Van Loosdrecht, M.C.M. (2000). A three-dimensional study on the correlation of spatial structure, hydrodynamic conditions, and mass transfer and conversion in biofilms. Chemical Engineering Sciences, 55: 6209-6222.

[92] El-Berry, A.M., Bakeer, G.A., Al-Weshali, A.M., (2003). The effect of.water quality and aperture size on clogging of emitters. In: Proceedings of International Workshop on Improved Irrigation Technologies and Methods: Research, Development and Testing, Montpellier.

[93] El Haite, H. (2010). Traitement des eaux usées par les réservoirs opérationnels et réutilisation pour l'irrigation. Thèse Doctorat, Ecole Nationale Supérieure des Mines de Saint-Etienne, France. 214p [in French].

[94] El Samrani, A.g., Lartiges, B. S., Ghanbaja, J., Yvon, J., et Kohler, A. (2004). Trace element carriers in combined sewer during dry and wet weather: an electron microscope investigation. Water Research, 38, 2063-76.

[95] Enciso, J., and D. Portar, (2005). Basics of microirrigation.Publications of Texas Cooperative Extension, Texas AM University, Weslaco and Lubbock.

[96] Eroglu, S.; Sahin, U.; Tunc, T. Sahin, F. Bacterial application increased the flow rate of CaCO3-clogged emitters of drip irrigation system Journal of Environmental Management, 2012, 98, 37 -

42.

[97] Esser, A., Grossmann, S. (1996). Analytic expression for Taylor–Couette stability boundary. Phys. Fluids 8, 1814–1819.

[98] FAO (1985) Water Quality for Agriculture. FAO Irrigation and Drainage Paper 29 (Rev. 1), R.S. Ayers and D.W. Westcot (Eds), Food and Agriculture Organization of the United Nations, Rome, Italy.

[99] Flemming, H. C., Wingender, J., Griebe, T., Mayer, C. (2000). Physico-chemmical properties of Biofilms. Biofilms: Recent advances in their study and controle. L. V. Evans, Harwood Academic Publishers.

[100] Flemming, H. C., Neu, T. R., Wozniak, D. The EPS matrix: the house of biofilm cells. J. Bacteriol. 189, 7945–7947 (2007).

[101] Flemming, H. C., Wingender, J. (2010). The biofilm matrix. Nat Rev Microbiol 8: 623–633

[102] Fletcher, M. (1979). The attachement of bacteria to surfaces in aquatic environments. Adhesion to Microorganisms to Surfaces. D. C. Ellwood, J., Melling P. Rutter, Academic Press.

[103] Fletcher, M. (1988). Attachment of Pseudomonas fluorecens to Glass and Influence of Electrolytes on Bacterium-Substratum Separation distance. Journ of Bacteriology 170 (5); 2027-2030

[104] Fortin, D., Ferris, F. G., Beveridge, T. J. (1997). Surface-mediated mineral development by bacteria. Rev. Mineral. 35, 161–180

[105] Fox, P., Abbaszadegan, M. (2013). Impact of Scale Formation on Biofilm Growth in Premise Plumbing. Retrieved from:http://www.saltinstitute.org/wp-content/uploads/2014/01/Fox-Final-Report-UAZ.pdfhttp://www.saltinstitute.org/wp-content/uploads/2014/01/Fox-Final-Report-UAZ.pdf

[106] Friedel, J. K., Langer, T., Siebe, C., and Stahr, K. (2000). Effects of long-term waste water irrigation on soil organic matter, soil microbial biomass and its activities in central Mexico. Biol. Fert. Soils. 31:414–421.

[107] Friese, K., Mages, M., Wendet-Potthoff, K., Neu, T.R. (1997). Determination of heavy metals in biofilms from the River Elbe by total-reflection X-ray fluorescence spectrometry. Spectrochimica Acta Part B: Atomic Spectroscopy, 52(7): 1019-1025.

[108] Gabrielli, C., Maurin, G., Poindessous, G., Rosset R. (1999). Nucleation and growth of calcium carbonate by an electrochemical scaling process. Journal of Crystal Growth 200: 236-250.

[109] Gagnon, G. A., Slawson, R. M. (1999). An efficient biofilm removal method for bacterial cells exposed to drinking water in Journal of Microbiological Methods 34(3):203-214.

[110] Gal, J.-Y.; Fovet, Y., Gache, N. Mechanisms of scale formation and carbon dioxide partial pressure influence. Part I. Elaboration of an experimental method and a scaling model Water Research , 2002, 36, 755 - 763.

[111] Gamri, S., Soric, A., Tomas, S., Molle, B., Roche, N. (2013). Biofilm development in microirrigation emitters for wastewater reuse. Irrigation Science. 32 (1):77-85.

[112] Gamri, S. (2014). Réutilisation des eaux usées traitées en irrigation localisée : impacts des conditions d'écoulement et des matériaux sur le développement de biofilm . Université d'Aix Marseille. p178

[113] Gamri, S., Soric, A., Tomas, S., Molle, B., Roche, N. (2016). Effects of pipe materials on biofouling under controlled hydrodynamic conditions. Journal of Water Reuse and Desalination, 6(1):167-174.

[114] Gauthier, P. M., Szerlip, H. M. (2002). Metabolic acidosis in the intensive care unit. Critical care clinics, 18(2), 289-308.

[115] Gebara, F., Activated sludge biofilm wastewater treatment system, Water Research, Volume 33, Issue 1, January 1999, Pages 230-238,

[116] Ghorbel, A., Tlili, M.M., Walha, K., Ben Amor, M. & Rosset, R. (2001). Étude du phénomène de colmatage chimique des distributeurs d'eaux utilisés en microirrigation. Cahiers de l'association Scientifique Européenne pour l'Eau et la Santé 6(1), 31-38.

[117] Gilbert, R.G., Nakayama F.S., Bucks. D. A. (1979). Trickle irrigation: prevention of clogging. Trans. ASAE. 22: 514-519.

[118] Gilbert, R. G., Nakayama, F. S., Bucks, D. A., French, O. F., Adamson, K. C. (1981). Trickle irrigation: emitter clogging and other flow problems. Agricultural Water Management. 3(3):159-178.

[119] Ginn, T.R., Wood, B.D., Nelson, K.E., Scheibe, T.D., E.M. Murphyc, T.P. Clement Processes in microbial transport in the natural subsurface Adv. Water Resour., 25 (2002), pp. 1017–1042

[120] Gjaltema, A., van der Marel, N., van Loosdrecht, M.C.M., Heijnen, J.J. (1997a). Adhesion and biofilm development on suspended carriers in airlift reactors: Hydrodynamic conditions versus surface characteristics. Biotechnol. Bioeng. 55:880 – 889.

[121] Gjaltema, A., Vinke, J.L., van Loosdrecht, M.C.M., Heijnen, J.J. (1997b). Abrasion of suspended biofilm pellets in airlift reactors: Importance of shape, structure, and particle concentrations. Biotechnol. Bioeng. 53: 88 – 99

[122] Goller, C. C., Romeo, T., Romeo, T. (Ed.) Environmental Influences on Biofilm Development Bacterial Biofilms, Springer Berlin Heidelberg, 2008, 37-66

[123] Gordon, A.S., Gerckakov, S.M., and Udey, L.R., (1981). The effect of polarization on the attachment of marine bacteria to copper and platinum surfaces. Can. J. Microbial., 27: 698-703.

[124] Guyon, E., Hulin, J. P., Petit, L. and Mitescu, C. D. (2001). Physical Hydrodynamics, Oxford University Press.

[125] Hadfi, A., Eddaoudi, H., El Hadek, M., Ghorbel, A., Driouiche, A. (2011). CHARACTERIZATION OF SCALE-FORMING POWER OF IRRIGATION WATER THE AGRICULTURAL REGION OF LARGE AGADIR. Physical and Chemical News 57:44-50

[126] Haman, D. Z. (1990). Causes and Prevention of Emitter Plugging In Microirrigation Systems, BUL258, Agricultural and Biological Engineering Department, UF/IFAS Extension.

[127] Harley, J. C., Huang, Y., Bau, H., Zemel, J. (1995). Gas flow in micro-channels. Journal of Fluid Mechanics. 284:257-274.

[128] Hills, D. J., Nawaar, F. M., Waller, P. M. (1989). Effects of chemical clogging on drip-tape irrigation uniformity, Trans of the ASAE 32(4),1202-1206.

[129] Hogt, A. H., DANKERT, J., DE VRIES, J. A., FEIJEN, J. (1983). Adhesion of coagulase-negative staphylo- cocci to biomaterials. Journal of General Microbiology 129, 2959-2968.

[130] Horn, H., and Hempel, D. C. (1997b). Growth and decay in an auto-/heterotrophic biofilm.Wat. Res. 31(9):2243-2252.

[131] Horn, H., Reiff, H., Morgenroth, E. (2003). Simulation of growth and detachment in biofilm systems under defined hydrodynamic conditions. Biotechnology and Bioengineering. 81(5): 607-617.

[132] Houhou, J., Lartiges, B. S., Sieliechi, J., Ghanbaja, J., et Kohler, A. (2009). Sources, nature, and fate of heavy metal-bearing particles in the sewer system. The Science of the total environment, 407, 6052- 6062.

[133] Hui, F., Lédion, J. (2002). Evaluation methods for the scaling power of water, European Journal of Water Quality, 33(1);41-52.

[134] Hunt, S; M., Werner, E. M., Huang, B., Hamilton, M. A., Stewart, PS. (2004). Hypothesis for the role of nutrient starvation in biofilm detachment. Appl Environ Microbiol 70:7418-7425

[135] Hussain, I., L. Raschid, M.A. Hanjra, F. Marikar, W., van der Hoek. (2001). A framework for analyzing socioeconomic, health and environmental impacts of wastewater use in agriculture in developing countries: Working Paper 26. Colombo, Sri Lanka: International Water Management Institute. IWMI.

[136] Imas, P., Cohen, A. (2009) Improving the ph of irrigation waters with acidic fertilizers. The Proceedings of the International Plant Nutrition Colloquium XVI. P4.

[137] Ivleva, NP., Wagner, M., Horn, H., Niessner, R. Haisch, C. Raman microscopy and Surface-Enhanced Raman Scattering (SERS) for in situ analysis of biofilms. J Biophotonics. 2010;3:548–556

[138] IWMI, (2007). Agricultural use of marginal-quality water-opportunities and challenges. Coord. Lead author: M. Qadir, chap. 11, part 4.

[139] Jiménez, B., and Asano, T. (2008). Water reclamation and reuse around the world. In Water reuse: An international survey of curre nt practice, issues and needs. London: IWA Publishing

[140] Jzotzi, C., Pahia dak, T., Yiantsios, S.G., Kacabetas, A.J., Andritsos, N. (2007). A study of $CaCO_3$ scale formation and inhibition in RO and NF membrane processes, J.Membr. Sci. 296:171–184.

[141] Kah, L.C., Riding, R. Geology 35, 799 (2007)

[142] Kalavrouziotis, I. K., Kostakioti, E., Koukoulakis, P. H., Papadopoulos, A. H., Leotsinidis, M., Sakazli, E. (2011). The impact of ClxCd Interrelationship on planning wastewater reuse in cabbage. Water, Air, and Soil Pollution, 214, 565–573.

[143] Karmeli, D. (1977). Classification and flow regime analysis of drippers. Journal of Agricultural Engineering Research. 22: 165-173.

[144] Kandilikar, S. G., Joshi, S., Tian, S. (2003). Effect of surface roughness on heat transfer and fluid flow character at low Reynolds numbers in small diameter tubes. Heat Transfer Eng. 24(3):4–16.

[145] Kalavrouziotis, I. K., Arambatzis, C., Kalfountzos, D., Varnavas, S. P. (2011). Wastewater reuse planning in agriculture: the case of Aitoloakarnania, Western Greece. Water, 3(4), 988-1004.

[146] Karaca, O. F., Uçan, K. (2013). Elimination of lime causing clogging in emitters by chemical methods in drip irrigation . African journal of agricultural research 8(13),1136-1143.

[147] Kataoka, K., (1986). Taylor Vortices and instabilities in Circular Couette Flows. Encyclopedia of Fluid Mechanics, edited by N.P. Cheremisinoff. 1:236-274.

[148] Katz, S., Dosoretz, C., Chen, Y., Tarchitzky, J., (2014). Fouling formation and chemical control in drip irrigation systems using treated wastewater. Irrig. Sci. 32, 459 – 469.

[149] Kemp, p.h. (1971) chemistry of natural waters–i fundamental relationships. water research persamon press 1971. 5: 297-311.

[150] Keller, J., Bliesner, R.D. (1990). Sprinkler and Trickle Irrigation. New York: Van Nostrand Reinhold.

[151] Kellis, M., Kalavrouziotis, I. K., Gikas, P. (2013). Review of wastewater reuse in the Mediterranean countries, focusing on regulations and policies for municipal and industrial applications. Global Nest Jour., 15 (3): 333-350.

[152] Khalizadeh, P. (2009). Formation de Biofilm à Pseudomonas aeruginosa: évaluation d'inhibiteurs potentiels du quorum sensing. Microbiologie. Toulouse, Université de Toulouse. Ecole doctorale SEVAB.

[153] Khan, S., Cao, Q., Zheng, Y. M., Huang, Y. Z., Zhu, Y. G. (2008). Health risks of heavy metals in contaminated soils and food crops irrigated with wastewater in Beijing, China. Environmental pollution, 152(3), 686-692.

[154] Khurana, M.P.S., Singh, P. (2012). Waste water use in crop production: a review. Resour. Environ. 2:116–131.

[155] Kiziloglu, M., Turan, F. M., Sahin, U., Angin, I., Anapali, O., Okuroglu, M. (2007) Effects of wastewater irrigation on soil and cabbage-plant (brassica olerecea var. capitate cv. yalova-1) chemical properties. J. Plant Nutr. Soil Sci. 170(1):166–172.

[156] Klapper, I., Rupp, CJ., Cargo, R., et al. Viscoelastic fluid description of bacterial biofilm material properties. Biotechnol Bioeng. 2002;80:289–96

[157] Kokare, CR., Chakraborty, S., Khopade, AN., Mahadik KR. Biofilms: importance and applications. Ind J Biotechnol 2009;8:159–168.

[158] Krivilyov, M., Detandt, Y., Abeele, D.V., Degrez, G., Fransaer, J. (2006) Direct numerical simulations of Taylor–Couette flow using a hybrid spectral/finite element approach. in: Proc. of the 7th National Conference on Theoretical and Applied Mechanics, Mons, Belgium. 6p.

[159] Kujundzic, E. A., Cristina Fonseca, E. A., Evans, M., Peterson, A. R., Greenberg, Hernandez, M. (2007). "Ultrasonic monitoring of early-stage biofilm growth on polymeric surfaces." Journal of Microbiological Methods 68(3): 458-467.

[160] Kukul, Y. S., Çalışkan, A. D. Ü., Süer, A. N. A. Ç. (2007). Arıtılmış atık suların tarımda kullanılması ve insan sağlığı yönünden riskler. Ege Üniversitesi Ziraat Fakültesi Dergisi, 44(3).

[161] Kwok, W., Picioreanu, C., Ong, S., Van Loosdrecht, M., Ng W., Heijnen, J. (1998). Influence of biomass production and detachment forces on biofilm structures in a biofilm airlift suspension reactor. Biotechnology and Bioengineering, 58(4): 400-407.

[162] Lamm, F.R., Camp, C.R., Subsurface drip irrigation. Microirrigation for crop production. Amsterdm: Elsevier, 2007. chap. 13, p. 473–551.

[163] Larson, T. E., and Buswell, A. M. (1942). Calcium Carbonate Saturation Index and Alkalinity Interpretations." Journal of the American WaterWorks Association 34(11): 1667–1684

[164] Lazarova, V., Manem, J. (1995). Biofilm characterization and activity analysis in water and wastewater treatment. Water research 29, 2227–2245.

[165] Lazarova, V., Bahri, A. (2005). Water Reuse for Irrigation: Agriculture, Landscapes, and Turf Grass, Water reuse for irrigation, CRC press.

[166] Lazarova, V., Brissaud, F., (2007). Intérêt, bénéfices et contraintes de la réutilisation des eaux usées en France, L'eau, l'industrie, les nuisances, n°299, p. 29-39. http://www.ecoumenegolf.org/XEauXLAZAROVA.pdf

[167] Lehtola, M J., Miettinen, I T., Keinanen, M M., et al. (2004). Microbiology, chemistry and biofilm development in a pilot drinking water distribution system with copper and plastic pipes. Water Res 38: 3769–3779.

[168] Levy, G., Fine, P., Bart-Tal, A. (2011). Treated Wastewater in Agriculture: Use and impacts on the soil environments and crops. Wiley-Blackwell.446 p.

[169] Lewandowski, I., Clifton-Brown, J. C., Scurlock, J. M. O., Huisman, W. (2000). Miscanthus: European experience with a novel energy crop. Biomass Bioenergy 19 209–227

[170] Li, G.B., Li, Y.K., Xu, T.W., Liu, Y.Z., Jin, H., Yang, P.L., Yan, D.Z., Ren, S.M., Tian, Z.F. (2011). Effects of average velocity on the growth and surface topography of biofilms attached to the reclaimed wastewater drip irrigation system laterals. Irrig. Sci. 30:103–113.

[171] Li, Y., Zhou, B., Liu, Y., Jiang, Y., Pei, Y., Shi, Z. (2012). Preliminary surface topographical characteristics of biolms attached on drip irrigation emitters using reclaimed water. Irrigation science. Published online.

[172] Li, X.-G., Lv, Y., Ma, B.-G., Wang, W.-Q.. & Jian, S. W. (2013). Decomposition kinetic characteristics of calcium carbonate containing organic acids by TGA, Arabian Journal of Chemistr. Available online 21 September 2013.

[173] Liang, X., van Dijk, M.P., (2010). Financial and economic feasibility of decentralized wastewater reuse systems in Beijing Water Sci. Technol., 61:1965–1973.

[174] Lili, Z., Yang, P., Ren, S., Li, Y., Liu, Y., Xia, Y. (2016). Chemical clogging of emitters and evaluation of their suitability for saline water drip irrigation. Irrigation and Drainage, 65:439-450.

[175] Liu, Z. (1999). The three-dimensional structure of the HRDC domain and implications for the Werner and Bloom syndrome proteins. Structure 7(12):1557-66

[176] Liu, Y., Tay, J.-H. (2002). The essential role of hydrodynamic shear force in the formation of biofilm and granular sludge. Water Research. 36(7):1653-1665.

[177] Liu, H. S., Li, Y. K., Liu, Y. Z., Yang, P. L., Ren, S. M., Wei R. J., Xu, H. B. (2010). Flow characteristics in energy dissipation units of labyrinth path in the drip irrigation emitters with DPIV technology. Journal of Hydrodynamics, Ser. B 22(1):137-145.

[178] Loosdrecht, V. M. C., M., Lyklema, J., Norde, W., Schraa, G., Zehnder, A. J. B. (1987). "Electrophoretic mobility and hydrophobicity as a measure to predict the initial steps of bacterial adhesion."Appl. Envir. Microbiol., 53, 1898–1901.

[179] Loosdrecht, V. M. C., Lyklema, J., Norde, W., Zehnder, A. J. (1989). Bacterial adhesion: A physicochemical approach. Microb Ecol. Jan; 17(1): 1–15.

[180] Loosdrecht V. M. C., Norde, W., Zehnder, A. (1990). Physical chemical description of bacterial adhesion. J. Biomater. Appl. 5, 91–106

[181] Loosdrecht, V. M. C., Heijnen, JJ., Eberl, HJ., Kreft, JU., Picioreanu, C. (2002). Mathematical modelling of biofilm structures. Antonie van Leeuwenhoek 81:245–256.

[182] Loubier, S., Declercq, R. (2014). Analyses coûts-bénéfices sur la mise en œuvre de projets de réutilisation des eaux usées traitées (REUSE) Application à trois cas d'études Français. Final Report (in French)- Onema – Irstea, 37pp. Retrieved from http://www.onema.fr/IMG/pdf/2014$_0$25.*pdf* [Google Scholar].

[183] MacAdam, J., Parsons, S. A. (2004). Calcium carbonate scale formation and control Re/Views in Environmental Science Bio/Technology, , 3, 159-169

[184] Magesan, G.N., Williamson, J.C., Yeates, G.W., Lloyd-Jones, A.R. (2000). Wastewater C:N ratio effects on soil hydraulic conductivity and potential mechanisms for recovery. Bioresource Technology, 71 (1): 21-27.

[185] Mahfoud, C., El Samrani, AG., Mouawad, R., Hleihe, l. W., El Khatib, R., Lartiges, BS., Ouaini, N. (2009). Disruption of biofilms from sewage pipes under physical and chemical conditioning. Journal of environmental sciences. 21:1-8.

[186] Mapanda, F., Mangwayana, E.N., Nyamangara, J., Giller, K.E. (2005). The effect of long-term irrigation using wastewater on heavy metal contents of soils under vegetables in Harare, Zimbabwe. Agric. Ecosyst. Environ. 107(2–3):151–165.

[187] Maukonen, J., Matto, J., Wirtanen, G., Raaska, L., Mattila-Sandholm, T., Saarela, M. (2003). Methodologies for the characterization of microbes in industrial environments: a review. J Ind Microbiol Biotechnol 30:327–35.

[188] Mehel, A., Gabillet, C., Djeridi, H.(2006) Bubble Effect on the structures of Weakly Turbulent Couette Taylor Flow. J. Fluid Eng. 128 (4):819-831

[189] Mekonnen, M. M., Hoekstra, A. Y. Four billion people facing severe water scarcity Science Advances, American Association for the Advancement of Science, 2016, 2

[190] Melo, L., Vieira, M. (1999). Physical stability and biological activity of biofilms under turbulent flow and low substrate concentration. Bioprocess Engineering. 20(4):363-368.

[191] Mengel, K. (1994). Iron availability in plant tissues - iron chlorosis on calcareous soils Plant and

Soil 165: 275-283.

[192] Merkel, B.J., Planer-Friedrich, B. (2005). Groundwater Geochemistry. Springer Verlag, Berlin, Heidelberg 200.

[193] Metcalf, Eddy. (1991). Wastewater Engineering; Treatment, Disposal and Reuse. 3rd edition. McGraw-Hill Int. Ed., Singapore.

[194] Molle, B., Audouard, M., Gamri, S., Carette, M. C. (2012). rapport de recherche. utilisation de l'irrigation goutte à goutte avec des eaux usées traitées. pp. 15.

[195] Molle, B., Tomas, S., Huet, L., Roudil, A., Granier, J., Audouard, M., Dimaiolo, P., Rosa, C. (2012). Rapport de recherche. Evaluation du risque de dispersion d'aérosols biologiques par aspersion d'eaux usées traitées pp. 23.

[196] Moinul Hosain, O. M .D, Hewa, G. A., Pezzaniti, D. (2014). Predicting emitter sensitivity to clogging: a focus on the biological component .2014 Irrigation Show and Education Conference. 118-127.

[197] Monod, J. (1949). The growth of bacterial cultures. Annu Rev Microbiol. 3:371–394.

[198] Monod, J. (1958). Recherches sur la croissance des cultures bacteriennes. Hermann Parisp

[199] Morvay, A. A.; Decun, M.; Scurtu, M.; Sala, C.; Morar, A., Sarandan, M. (2011). Biofilm formation on materials commonly used in household drinking water systems Water Science and Technology: Water Supply, IWA Publishing. 11:252-257

[200] Mueller, R.F. (1996). Bacterial transport and colonization in low nutrient environments. Water Research, 30(11): 2681-2690.

[201] Murgel, G. A., Lion, L.W., Acheson, C., Shuler, M.L., Emerson, D. and Ghiorse, W.C. (1991). Experimental apparatus for selection of adherent microorganisms under stringent growth conditions. Applied and Environmental Microbiology. 57:1987-1996.

[202] Muryanto, S., Bayuseno, A., Ma'mun, H., Usamah, M. Jotho (2004) Calcium Carbonate Scale Formation in Pipes: Effect of Flow Rates, Temperature, and Malic Acid as Additives on the Mass and Morphology of the Scale. Procedia Chemistry. 9:69-76

[203] Muyen, Z., Moore, G.A., Wrigley, R.J. (2011). Soil salinity and sodicity effects of wastewater irrigation in South East Australia. Agricultural Water Management. 9:33–41.

[204] Nakayama, F. S., Bucks, D. A. (1980). clogging effects on emitter discharge rate and trickle irrigation uniformity. Trans ASAE. In press.

[205] Nakayama, F. S., Bucks, D. A. (1981). Emitter clogging effects on trickle irrigation uniformity. Trans American Society of Agricultural and Biological Engineers. 24(1):77-80.

[206] Nakayama, F. S., Bucks, D. A. (1986). Trickle Irrigation for Crop Production Design, Operation and Management, Developments in Agricultural Engineering 9. Elsevier. New York., NY. 383 pp.

[207] Nakayama, F. S., Bucks, D. A. (1991). Water quality in drip/trickle irrigation: a review. Irrigation Science. 12(4):187-192.

[208] Nakayama, F. S., Boman, B. J., Pitts, D. J. (2007). Maintenance, in: Lamm, F.R., Ayars, J.E., Nakayama, F.S. (Eds.), Microirrigation for Crop Production. Design,operation, and Management. Elsevier, Amsterdam, the Netherlands, pp. 389 – 430.

[209] Nasr Abroug, S. (2014). Traitement et reutilisation des eaux uses traitées en Tunisie, ONAS. ONAS (2014). Rapport annuel 2014. 41 p.

[210] Nguyen, F. "Contribution à l'étude de procédés inhibiteurs de l'entartrage : Procédés chimiques, procédés physiques par microélectrolyse", Thèse de doctorat. Doct., (1996). Univ. Paris 6.

[211] Nicolella, C., van Loosdrecht, M.C.M., and Heijnen, J.J. (2000) Wastewater treatment with particulate biofilm reactors. Journal of Biotechnology, 80, 1-33

[212] Nishimura, T., Ohori, Y., Kawamura, Y. (1984). Flow characteristics in a channel with symmetric wavy wall for steady flow. Journal of Chemical Engineering of Japan. 17:466-471.

[213] Noguera, D. R., Pizarro, G., Stah, D. A., Rittmann, BE. (1999). Simulation of multispecies biofilm development in three dimensions. Water Sci Technol 39: 503–510.

[214] Norton-Brandao, D., Scherrenberg, S.M., van Lier, J.B. (2013). Reclamation of used waters for irrigation purposes: A review of treatment technologies. J. Environ. Mgt. 122:85–98.

[215] Noui-Mehidi, M.N., Ohmura, N., Kataoka, K. (2005) Dynamics of the Helical Flow between Rotating Conical Cylinders. Journal of Fluids and Structures. 20(3):331-344.

[216] Obst, M., Dynes, J., Lawrence, J., Swerhone, G., Benzerara, K., Karunakaran, C., Kaznatcheev, K., Tyliszczak, T., Hitchcock, A.P. (2009). Precipitation of amorphous $CaCO_3$ (aragonite-like) by cyanobacteria: a STXM study of the influence of EPS on the nucleation process. Geochim. Cos-

mochim. Acta 73:4180–4198.

[217] Ohmura, N., Kataoka, K., Shibata, Y., Makino, T. Effective mass diffusion over cell boundaries in a Taylor-Couette flow system, Chemical Engineering Science, Volume 52, Issue 11, 1997, Pages 1757-1765

[218] Panthi, S.R. (2003). Carbonate chemistry and calcium carbonate saturation state of rural water supply projects in Nepal. Seventh International Water Technology Conference Egypt 1-3 April 2003

[219] Parkhurst, D. L., Appelo, C.A.J. (1999). "User's guide to PHREEQC (Version 2): a computer program for speciation, batch-reaction, one-dimensional transport, and inverse geochemical calculations, Water-Resour. Invest. Rep. 99-4259. US Geol. Surv. Denver, Colorado.

[220] Paul, E., Ochoa, J.C., Pechaud, Y., Liu, Y., Liné, A. (2012). Effect of shear stress and growth conditions on detachment and physical properties of biofilms. Water research 46:5499-5508.

[221] Pechaud, Y., Marcato-Romain, C.E., Girbal-Neuhauser, E., Queinnec, I., Bessiere, Y., Paul, E. (2012). Combining hydrodynamic and enzymatic treatments to improve multi-species thick biofilm removal. Chemical Engineering Science. 80:109–118

[222] Pepe, M., Gaillard, A., Pétré, M. A., Harrault, L., Groleau, A., Benedetti, M. F. (2009). Les métaux dissous, la matière organique et les carbonates en Seine : Variabilité temporelle et spatiale près de Paris. Programme PIREN-Seine : Les Métaux dissous et les carbonates en Seine près de Paris

[223] Pereira, A.R.; Green, S.; Villa Nova, N. A. (2006) Penman-Monteith reference evapotranspiration adapted to estimate tree transpiration. Agricultural Water Management. 83:153-161.

[224] Perez-Paricio, A. (2000). Integrated modelling of clogging processes in artificial groundwater recharge. PhD Technical University of Catalonia, Barcelona. 105p.

[225] Peyronnard, O. (2008). Apports méthodologiques pour la modélisation du comportement à la lixiviation de résidus minéraux. Application aux solidifiats de boues d'hydroxydes métalliques. Thèse de l'INSA de Lyon, 29-31p, 75-76p, 95-98 p, 101-102p, 107p.

[226] Pfahler, J., Harley, J., Bau, H. H., Zemel, J. (1990). Liquid and gas transport in small channels. AMSE DSC. 19:149-157.

[227] Picologlou, BF., Zelver, N., Characklis, WG. (1980). Biofilm growth and hydraulic performance. J Hyd Div ASCE 106:733–746.

[228] Picioreanu, C., Van Loosdrecht, M. C., Heijnen, J. J. (2001). Two-dimensional model of biofilm detachment caused by internal stress from liquid flow. Biotechnology & Bioengineering. 72(2):205-218.

[229] Pirt, (1985). Principles of microbe and cell cultivation. Oxford: Blackwell Scientific; p. 274.

[230] Pitts, D. J., Haman, D. Z., Smajstria, A. G. (1990). Causes and prevention of Emitter plugging in Mico irrigation Systems. Bulletin 258. Florida Cooperative Extension Service. Institute of Food and Agricultural Sciences. University of Florida.

[231] Pitzer, K.S. (1979). Activity coefficients in electrolyte solutions. p. 157–208. In R.M. Picowicz (ed.) Ac-tivity coefficients in electrolyte solutions. CRC Press, Boca Raton, FL.

[232] Plauborg, F., Andersen, M. N., Liu, F., Ensin, J.K., Ragab, R. (2010). Safe and high quality food production using low quality waters and improved irrigation systems and management: SAFIR. Agric. Water Manage. 98:377–384.

[233] Priya, N. J., M. Kannan, P.Priyanka and Vergin Mary, S. 2016. A Study on Characterization of EPS and Media Optimization for Bacterial Calcium Carbonate Precipitation-Int.J.Curr.Microbiol.App.Sci. 5(4): 590-595.

[234] Puig-Bargues, J., Arbat, G., Barragan, J., Ramirez de Cartagena, F. (2005). Hydraulic performance of drip irrigation subunits using WWTP effluents. Agricultural Water Management. 77(1-3):249–262.

[235] Puig-Bargués, J., Arbat, G., Elbana, M., Duran-Ros, M., Barragán, J., Ramírez de Cartagena, F., Lamm, F.R. (2010). Effect of flushing frequency on emitter clogging in microirrigation with effluents. Agricultural Water Management, 97 (6), 883-891

[236] Qin, Z., Berliner, PR., Karnieli, A. (2005). Ground temperature measurement and emissivity determination to understand the thermal anomaly and its significance on the development of an arid environmental ecosystem in the sand dunes across the Israel–Egypt border. J Arid Environ. 60:27–52

[237] Qian, J., Shen, M., Wang, P., Wang, C., Li, K., Liu, J., Lu, B., Tian, X. Perfluorooctane sulfonate adsorption on powder activated carbon: Effect of phosphate (P) competition, pH, and temperature Chemosphere , 2017, 182, 215 - 222

[238] Racina, A., Kind, M. (2006). Specific power input and local micro mixing times in turbulent Taylor–Couette flow. Exp. Fluids 41: 513–522.

[239] Rattan, R.K., Datta, S.P., Chhonkar, P.K., Suribabu, K., Singh, A.K. Long-term impact of irrigation with sewage effluents on heavy metal content in soils, crops and groundwater—a case study. Agric. Ecosyst. Environ. 2005;109(3–4):310–322.

[240] Ravina, I., Paz, E., Sofer, Z., Marcu, A., Shisha, A., Sagi, G. (1992). Control of emitter clogging in drip irrigation with reclaimed wastewater. Irrigation Science. 13(3):129-139.

[241] Rav-Acha, C., Kummel, M., Salamon, I., Adin, A. (1995). The effect of chemical oxidants on effluent constituents for drip irrigation. Water Research, 29, 1, pp. 119-129.

[242] Ravina, I., Paz, E., Sofer, Z., Marm, A., Schischa, A., Sagi, G., Yechialy, Z., Lev, Y. (1997). Control of clogging in drip irrigation with stored treated municipal sewage effluent. Agricultural Water Management. 33(2):127-137.

[243] Ricci, J. E. (1952). Hydrogen 1on Concentration. Princeton University Press.

[244] Rijnaarts, H. H. M. Ph.D. Thesis, Wageningen Agricultural University, Wageningen, The Netherlands, 1994.

[245] Rivadeneyra, M. A. G., Delgado, A., Ramos-Cormenzana Delgado R. (1998). Biomineralization of carbonates by Halomonas eurihalina in solid and liquid media with different salinities: crystal formation sequence. Res. Microbiol. 149, 277–287

[246] Rochex, A., Godon, J.-J., Bernet, N., Escudié, R. (2008). Role of shear stress on composition, diversity and dynamics of biofilm bacterial communities. Water Research. 42(20):4915-4922.

[247] Rogers, J., Dowsett, AB., Dennis, PJ., Lee, JV., Keevi, CW. (1994). Influence of plumbing materials on biofilm formation and growth of Legionella pneumophila in potable water systems. Appl Environ Microbiol 60:1842–51.

[248] Rogers, ME., Grieve, CM., Shannon, MC. (2003) Plant growth and ion relations in Lucerne (Medicago sativa L.) in response to the combined effects of NaCl and P. Plant Soil 253:187–194

[249] Rodriguez-Blanco, J. D., Shaw, S., Benning, L.G. (2011). The kinetics and mechanisms of amorphous calcium carbonate (ACC) crystallization to calcite, via vaterite. Nanoscale, 3, 265-271.

[250] Sabbides, T., Giannimaras, E., Koutsoukos, P. G. (1992). The precipitation of calcium carbonate in artificial seawater at sustained supersaturation. Environmental Technology 13(1):73-80.

[251] Saur, T., Morin, E., Habouzit, F., Bernet, N., Escudie,R. (2017). Impact of wall shear stress on ini-

tial bacterial adhesion in rotating annular reactor. PLoS ONE 12(2): e0172113. doi:10.1371/journal.pone.0172113

[252] Schwankl, L., Prichard, T. (1990). Clogging of buried drip irrigation systems. Calif Agr 44(1):16-17.

[253] Sehar, S. and Iffat Naz, (2016). Role of the Biofilms in Wastewater Treatment, Microbial Biofilms - Importance and Applications, Dr. Dharumadurai Dhanasekaran (Ed.), InTech. Available from: https://www.intechopen.com/books/microbial-biofilms-importance-and-applications/role-of-the-biofilms-in-wastewater-treatment

[254] Sherlock, E. J., Lawrence, R. W., Poulin, R. Geo. (1995). On the neutralization of acid rock drainage by carbonate and silicate minerals. Environmental Geology, 25(1),43-54.

[255] Silvertsein R. M., Basler C.G., Morill C.T. (1998). Identification spectrométrique de composés organiques, De Boeck (ed.), p 26.

[256] Simoes, R. R., Poirel, L., Da Costa, P. M., Nordmann, P. (2010). Seagulls and beaches as reservoirs for multidrug-resistant Escherichia coli. Emerging Infect. Dis. 16, 110–112

[257] Skillman, JB., Garcia, M., Winter, K. (1999). Whole-plant consequences of Crassulacean acid metabolism for a tropical forest understory plant. Ecology 80,1584–1593.

[258] Spanos, N., Koutsoukos, P. G. (1998). The transformation of vaterite to calcite: effect of the conditions of the solution in contact with the mineral phase. J Crystal Growth 191,783-790.

[259] Spanos, N., Koutsoukos, P. G. (1998). Kinetics of precipitation of calcium carbonate in alkaline pH at constant supersaturation. Spontaneous and seeded growth J. Phys. Chem. B 1998, 102, 6679–6684

[260] Stevenin, C. (2012). Etude de l'atomisation d'un jet haute vitesse : application à l'irrigation par aspersion et à la pulvérisation. Thèse, Ecole Centrale de Marseille. 144p.

[261] Stevenin, C., Tomas,S., Vallet, A., Amielh, M., Anselmet, F. Flow characteristics of a large-size pressure-atomized spray using DTV. International Journal of Multiphase Flow, Elsevier, 2016, 84, pp.264-278.

[262] Stoodley, P., Cargo, R., Rupp, C. J., Wilson, S., Klapper, I. (2002). Biofilm material properties as related to shear-induced deformation and detachment phenomena. Journal of Industrial Microbiology and Biotechnology, 29(6), 361-367.

[263] Stoodley, P., Lewandowski, Z., Boyle J. D., Lappin-Scott, H. M. (1999), Structural deformation of bacterial biofilms caused by short-term fluctuations in fluid shear: An in situ investigation of biofilm rheology. Biotechnology and Bioengineering. 65(1): 83-92.

[264] Stoodley, P., Sauer, K., Davies, D.G., and Costerton, J.W. (2002). Biofilms as complex differentiated communities. Annu. Rev. Micro-biol.56, 187–209.

[265] Stryker, J. (2001). Drip irrigation design guidelines (Emitters). http:// www.Irrigation Tutorials.com

[266] Stumm, W., Morgan, J. J. (1996). Aquatic Chemistry: Chemical Equilibria and Rates in Natural Waters , third ed. John Wiley & Sons, New York, 1022 p.

[267] Suarez, D. L. (1983). Prediction of major ion concentrations in arid land soils using equilibrium and kinetic theories, in ARS Modeling Symposium, Rep. USDA-ARS-30:170-175. Pingree Park, Colo.

[268] Sutherland, IW. The biofilm matrix—an immobilized but dynamic microbial environment.Trends Microbiol 2001;9:222–7

[269] Syron, E., Casey, E. (2007). Membrane-aerated biofilms for high rate biotreatment: Performance appraisal, engineering principles, scale-up, and development requirements. Environmental Science Technology 42, 1833–1844.

[270] Szekut, F. D., Delfran Batista do Santos, Carlos Alberto Vieira de Azevedo, Márcio Roberto Klein, Maycon Diego Ribeiro, Salomão de Sousa Medeiros. (2015). Emitter clogging in drip irrigation using treated domestic wastewater. Journal of Food, Agriculture and Environment.13 (3-4):60-66.

[271] Tarchitzky, J., Rimon, A., Kenig, E., Dosoretz, C. G., Chen, Y. (2013). Biological and chemical fouling in drip irrigation systems utilizing treated wastewater. Irrigation Science, 31(6), 1277–1288.

[272] Tayel, M.Y., H. A. Mansour, and Sabreen Kh. Pibars. (2015) Effect of Two Sprinkler Irrigation Types on Coefficient of Variation (CV) and Some Quality Properties of Grain Wheat. Global Advanced Research Journal of Agricultural Science. 4(7):353-360,

[273] Taylor, HD., Bastos, RKX., Pearson, HW., Mara, DD. (1995). Drip irrigation with waste stabilization pond effluents: solving the problem of emitter fouling. Water Science and Technology 29 (4): 1069–1078.

[274] Telgmann, U., Horn, H., Morgenroth, E. (2004). Influence of growth history on sloughing and

erosion from biofilms. Water Res 38:3671–3684

[275] Tiercelin, J.R. (1998). Traité d'irrigation. LAVOISIER / TEC ET DOC.

[276] Tolker-Nielsen, T., Molin, S. (2000) Spatial Organization of Microbial Biofilm Communities Microbial Ecology. 40:75-84.

[277] Tourney, J., Ngwenya, B.T. (2009). Bacterial extracellular polymeric substances (EPS) mediate $CaCO_3$ morphology and polymorphism. Chemical Geology 262 :138–146.

[278] Trulear, M. G., Characklis, W. G. Dynamics of biolm pro cesses. Journal WPCF, 54(9):12881301, Sept. 1982.

[279] Tsai, HF., et al. (2004). Candida glabrata erg1 mutant with increased sensitivity to azoles and to low oxygen tension. Antimicrob Agents Chemother 48(7):2483-9

[280] http://unesdoc.unesco.org/images/0012/001295/129556e.pdf [Accessed June 2017].

[281] Van der Kooij, S., Zwarteveen, M., Boesveld, H., Kuper, M. (2013). The efficiency of drip irrigation unpacked. Agricultural Water Management, 123: 103–110.

[282] Van der Kooij, D.; Veenendaal, H. R., Scheffer, W. J. Biofilm formation and multiplication of Legionella in a model warm water system with pipes of copper, stainless steel and cross-linked polyethylene Water Research, 2005, 39, 2789 - 2798

[283] Veolia Water Technologies. (2006). Multiple Effect Distillation: Processes for Sea Water Desalination.

[284] Verheye, W. (2009). Soils of Arid and Semi-Arid Areas. In: Verheye, W, editor. Land cover and soil sciences – volume VII: soils and soil sciences. Oxford: EOLSS Publications/UNESCO; p. 248.

[285] Verrier, D., Mortier, 6. 81 Albagnac, G. (1987). Initial adhesion of methanogenic bacteria to polymers. Biutechnod Lett 9:735-740.

[286] Vrouwenvelder, J.S., Buiter, J., Riviere, M., van Der Meer WGJ, Loosdrecht, V. M. C., Kruithof, JC. (2010). Impact of flow regime on pressure drop increase and biomass accumulation and morphology in membrane systems. Water Res. 44:689–702.

[287] Wäsche, S., Horn, H., Hempel, D. C. (2002). Influence of growth conditions on biofilm development and mass transfer at the bulk/biofilm interface. Water Research. 36(19):4775.

[288] Wei, Q., Shi, Y., Dong, w., Lu, G., Huang, S. (2006). Study on hydraulic performance of drip emitters by computational fluid dynamics. Agricultural Water Management. 84(1-2):130-136.

[289] Wei, S., Cui, H., Jiang, Z., Liu, H., He, H., Fang, N. (2015). Biomineralization processes of calcite induced by bacteria isolated from marine sediments. Braz. J. Microbiol. 46:455–464.

[290] Wei, Z., Cao, M., Liu, X., Tang, Y., Lu, B. (2012). Flow behaviour analysis and experimental investigation for emitter micro-channels. Chinese Journal of Mechanical Engineering. 25(4):729-737.

[291] Wendt, F. (1933) Turbulente Strömungen zwischen zwei rotierenden Zylindern. Ingenieurs-Archiv. 4:577–595.

[292] World Health Organization (1989) Health guidelines for the use of wastewater in agriculture and aquaculture, Report of a WHO Scientific Group. WHO Technical report series 778. World Health Organization, Geneva, Switzerland.

[293] Willcock, L., Gilbert, P., Holah, J., et al. (2000). A new technique for the performance evaluation of clean-in-place disinfection of biofilms. J Ind Microbiol Biot 25:235–41.

[294] Wimpenny, J., Manz, W., Szewzyk, U. (2000). Heterogeneity in biofilms. FEMS microbiology reviews, 24, 5, pp. 661-671.

[295] Wijeyekoon, S., Mino, T., Satoh, H., Matsuo, T. (2004), Effects of substrate loading rate on biofilm structure. Water Research, 38, 10, pp. 2479-2488.

[296] Wojtowicz, J. A. (2001). Calcium Carbonate Precipitation Potential. Journal of the Swimming Pool and Spa Industry, 2, 23–29.

[297] Wu, F., Fan, Y.S., Li, H., Guo, Z.X., Li, J.S., Li, W.C. (2004). Clogging of emitter in subsurface drip irrigation system. Transactions of the CSAE. 20: 80–83.

[298] Xanthoulis, A. (2006). Complete Cytoreduction Combined with Early Postoperative Intraperitoneal Chemotherapy for Ovarian Carcinosarcoma https://www.karger.com/Article/Abstract/92855

[299] Xanthoulis, D. (2006). Réutilisation agricole des eaux usées In: Traité de l'irrigation 2ème édition. Lavoisier ed., pp. 737-768.

[300] Xavier, JB., Picioreanu, C., Loosdrecht, V. M. C. (2005). A general description of detachment for multidimensional modelling of biolms. Biotechnol Bioeng 91: 651–669.

[301] Yan, D., Bai, Z., Mike, R., Ren, S., Yang, P. (2009). Biofilm structure and its influence on clogging in drip irrigation emitters distributing reclaimed wastewater. J Enviro Sci. 21(6):834–84.

[302] Yohannes, E., Barnhart, DM., Slonczewski, JL. (2004) pH-dependent catabolic protein expression during anaerobic growth of Escherichia coli K-12. J Bacteriol. 186:192–199.

[303] Yu, J., Kim, D., Lee, T. (2010), Microbial diversity in biofilms on water distribution pipes of different materials. Water Science and Technology, 61, pp. 163-171.

[304] Zhang, J., Zhao, W., Wei, Z., Tang, Y., Lu, B. (2007). Numerical investigation of the clogging mechanism in labyrinth channel of the emitter. International Journal for Numerical Methods in Engineering. 70:1598-1612.

[305] Zhang, T. C., Bishop, P. L. Density, porosity, and pore structure of biofilms Water Research, 1994, 28, 2267 - 2277

[306] Zhang, X., Bishop, P. L. (2003) Biodegradability of biofilm extracellular polymeric substances. Chemosphere. 2003 Jan;50(1):63-9.

[307] Zhu, C., Anderson, G. Environmental applications of geochemical modelling. Cambridge, UK: Cambridge University Press; 2002.

Annex

A.1 Standards of wastewater used in irrigation

In the World Health Organization guideline (WHO, 1989[292]) for the microbiological quality of treated wastewater used in agriculture revised in 2000 the limit for fecal coliform bacteria in irrigation (where crops are likely to be eaten uncooked) is valid from 0 to 1000 fecal coliform bacteria/100 ml. When adult farm workers are exposed to spray irrigation, $\leq 10^5$ fecal coliform bacteria/100 ml is recommended. A limit of $\leq 10^3$ fecal coliform bacteria/100 ml is recommended if flood irrigation is used or children are exposed. For nematode eggs for both types of irrigation (flood irrigation and spray irrigation), it must be ≤ 1 egg$/l$ and reduced to ≤ 0.1 egg$/l$ if children are exposed. Macronutrients are normally at a concentration of 1000 ppm in plants while micronutrients are found in rates up to 500 ppm. However, concentrations of nutrients must be regularly monitored to offset any nutritional imbalances and avoid pollution of soil and ground water by nitrates (Addiscott et al., 1991[8]) plus high concentrations of these micronutrients can be toxic to the crops. The Food and Agriculture Organization (FAO) has also published recommendations on the physico-chemical quality of the treated wastewater to be reused in agriculture. Its evaluations are based on a number of parameters such as total suspended solids (TSS), pH, salinity, trace elements, etc. As mentioned above pollution (soil, crops, groundwater, etc.) depends not only on the quality of water, but also on the quantity of water applied to soil, the irrigation method and the type of crop. A summary of all these recommendations is provided in Table A.1.

Table A.1: Recommended microbiological and physico-chemical quality guidelines for wastewater use in agriculture (FAO 1985[98]; French Minestry of Health 2010)

		Surface irrigation	**Sprinkler irrigation**	**Micro-irrigation**
Microbiological recommendation	*Intestinal nematodes*	≤ 1 egg per litre		Not applicable if exposure to people does not occur
	Faecal coliforms	≤ 1000 per 100 ml	≤ 10^5 bacteria/100 ml	
Physico-chemical recommendation	*Conductivity (dS/m)*	< 3		
	TDS (mg/l)	< 2000		
	Sodium Absorption Ratio (SAR)	< 9	-	-
	Sodium (Na) (meq/l)	-	< 3	-
	Chloride (Cl) (meq/l)	< 10	< 3	-
	Boron (Br) (meq/l)	< 3		
	Nitrate (NO_3-N) (mg/l)	< 30		
	Bicarbonate (HCO_3^-)	< 8.5		
	pH	Normal Range 6.5 – 8.4		

A.2 Composition and structure of the biofilm

While an essential component of the biofilm, bacteria are only about 15 to 25% of its total composition. The remainder is held by EPS (matrix they synthesize) which contains water (main component), nutrients and also polysaccharides, proteins, lipids and nucleic acids (DNA and RNA). Water causes the hydrophilic property of biofilm (Flemming and Wingender, 2010[101]) and maintains the microorganisms in a moist environment favorable to their survival and protection against dehydration (Lewandowski, 2000[169]). Initially, bacteria cling irreversibly and colonize surfaces in the free-floating mode called planktonic form (minority form) (Clutterbuck, 2007[64]). This lifestyle allows bacterial colonies to persist at a given location, without proliferating. The C / N ratio of a biofilm is five times higher than for a suspension of planktonic bacteria, this being due to the dominance of the matrix composed mainly of water and organic matter (Flemming and Wingender, 2010[101]). A biofilm may be composed of one or more species of micro-organisms homogeneous or heterogeneous biofilms, respectively (Tolker-Nielsen, 2000[276]). Most biofilms are heterogeneous. The presence of a microorganism species or another

species within the biofilm is dependent on environmental conditions. For example, biofilms illuminated by sunlight are mainly composed of phototrophic organisms, such as algae or cyanobacteria, leading to photosynthesis and production of biomass from inorganic carbon. Biofilms formed in the absence of light mainly consist of heterotrophic (degradation of organic matter) and chemotrophic (transformation of mineral substances) bacteria. The development of techniques for the study of biofilms such as microscopy and microelectrodes (Zhang and Bishop, 1994[305]; Costerton et al., 1995[67]; Wimpenny et al., 2000[294]) has highlighted the heterogeneous structure of biofilms.

The heterogeneity of biofilms is observed at several levels: physical, chemical and biological. The physical (density, porosity, permeability, etc.) and chemical (substrate concentration gradients and oxygen (Beyenal and Lewandowski, 2002[35])) properties vary with the depth of biofilms.The deeper we go, the more transfer mechanisms and diffusion decrease Zhang and Bishop, (1994)[305].

A.3 Extracellelar polymeric substances (EPS)

As mentioned above, bacteria form a small part of the biofilm. Exopolymers (EPS) dominate its composition with about 70 to 98% in the case of biofilms developed from wastewater (Ivleva et al., 2010[137]; Liang et al., 2010[173]; Simoes et al., 2010[256]). EPS are produced by the bacteria, whether they are in suspension or adherent to biofilms. Quantity, form, properties, and chemical compositions of the EPS are determined by factors such as age of the biofilm, type of bacteria, concentration and bioavailability of nutrients, hydrodynamic conditions and temperature (Lazarova and Manem, 1995[164] Flemming et al., 2000[99]; Ivleva et al., 2010[137]). Exopolymers play a key role in the biofilm formation process, including ensuring irreversible adhesion of bacteria on the solid support and maintaining consistent microcolonies, facilitating interaction and cell-cell communication (Stoodley, 1997[262]; Tolker-Nielsen, 2000[276]; Flemming and Wingender, 2010[101]). EPS allow microorganisms associated in biofilm to be more resistant to chemical attack (De Beer et al., 1994[74]), hydrodynamic stresses and disinfectants, including those based on chlorine (Characklis, 1973[58]). The exopolysaccharide matrix also plays an important role in the antimicrobial properties of biofilms by directly binding to anti-microbial agents and preventing them from penetrating the biofilm (Maukonen et al., 2003[187]; Simões et al., 2010[256]) and as a protective barrier against bacteriophages (Donlan, 2002[83]). Generally, morphological and physicochemical properties of biofilms such as porosity, density, roughness, elasticity, mechanical stability, architecture and biofilm activity, are defined by the nature and composition of the EPS (Fletcher, 1979[102]; Flemming et al., 2000[99]. Lewandowski, 2000[169]; Klapper et al., 2002[156]; Kokare et al., 2009[157]; Liang et al., 2010[173]).

A.4 COD/ TS/VS/DRX/TGA

A.4.1 COD measure

Measurements of the oxidizable organic material can also be applied to the characterization of biofilms (Bryers and Characklis, 1981[51]; Murgel et al., 1991[201]). In their work, Murgel et al., (1991)[201] estimate that one microequivalent of COD corresponds to three micrograms of carbon. COD is the amount of oxygen required to chemically oxidize the reducing substances contained in a solution. The soluble COD was measured by oxidation with potassium dichromate. To perform the assay, the HACH method (1996-2000) was used. WTW kits were used. Two ml of the filtered sample is introduced into a tube containing potassium dichromate solution. Blank is carried out the same way, but the sample is replaced by distilled water. The tubes are heated for 2h at 150°C and after cooling the reading is done by spectrophotometry at the wavelength of 620 nm.

A.4.2 Total Solids (TS) and Volatile Solids (VS)

To determine the weight of the biological material attached to the surface, the biofilms are mechanically detached from the plates by scraping with a ruler having elastomeric ends. Biofilms are then recovered into ceramic cups previously weighed (M_0) with a precision balance (Denver instrument S-64) (precision 0.1 mg). The assembly was then placed in an oven for 24h at 105°C so that the water evaporated completely, and then weighed again (M_1) after cooling in a desiccator. The difference between the two weighings corresponds to the total solids. The cups can be placed in an oven for 2h at 550°C before a final weighing (M_2) to determine volatile solids. The following equations give the masses of TS and VS, and the result is expressed in mg/cm^2 IV.1.1:

$$TS = M_1 - M_0 \tag{A.1}$$

$$VS = M_1 - M_2 \tag{A.2}$$

Lazarova and Manem, (1995)[164] estimate that the measure of TS and VS includes, in addition to active organisms, inert matter, exo-polymers and adsorbed organic matter.

A.4.3 X-ray diffraction (XRD)

X-ray diffractometry allows the identification of more or less crystalline phases present in a solid matrix and the characterization of their crystalline structure. For example, it can provide information about their texture and their degree of crystallinity. The presence of amorphous phases in the material results in a deformation of the background noise of the diffraction pattern: large and diffuse peaks. The identification by XRD is limited to a majority of well-crystallized phases in the matrix. Nevertheless, in some cases, deformation of the background noise can be exploited for the identification of partially crystalline phases.

Two diffractometers were used for this work. For the chemical precipitations in Chapter III, chemical characterization was performed at CEREGE Aix-en-Provence on powder samples with a $\theta - \theta$ analytical X'Pert Pro diffractometer running at $40kV$ and $40\ mA$ using Co $k\alpha$ radiation ($\lambda = 1.79\mathring{A}$) with a linear X'Celerator detector and a secondary flat monochromator. The 2θ range was $10 - 75°$ with a step size of $0.033°$ and a counting time of $3s$ per step.

For the chemical characterization in Chapter IV, analysis was performed at the institute of Charles Gerhardt Montpellier 2. Powder patterns were recorded on a PHILIPS X'Pert MPD $\theta - \theta$ diffractometer equipped with the X'Celerator detector with Cu $k\alpha$ radiation ($\lambda = 1.5418\mathring{A}$) and nickel filter. The 2θ range was $5 - 70°$ with a step size of $0.033°$ and a counting time of 3s per step.

In all cases, samples were finely ground in an agate mortar and deposited onto low-background silicon plates with a drop of ethanol to get a homogeneous and thin layer of powder.

A.4.4 Thermo gravimetric analyzer (TGA)

TGA allows identification of non-crystalline forms of chemical precipitation and can be used contrary to the XRD, which is a qualitative and not quantitative method, to determine the proportion of each constituent. It can also be used to quantify the composition of organic and inorganic materials of a sample.

TGA is a technique that consists in measuring the mass change of a sample as a function of temperature and time. The quantifiable applications are usually done upon heating. The mass of the sample is monitored during the experiment. A sample purge gas controls the sample environment.

TGA studies were made in the institute of Charles Gerhardt Montpellier 2 on a Netzsch STA 449 F1. The system was purged with an inert gas which is argon and heated at a rate of 10°C/min, from room temperature to 1000°C. Both TGA and its derivative (DTG) were simultaneously plotted versus temperature. This system was also coupled with a mass spectrometer (TG-MS) to be able to analyze gases and, in particular, volatile decomposition products of thermal analysis. This allows identification

of the escape of CO_2 in the analysis of calcium carbonate. These details and the results are presented in Chapter IV.

A.5 Determination and description of the different regimes

To be able to visualize the modification of the flow (instabilities) and to determine the different regimes inside the TCR, many studies have been dedicated since Taylor's work in 1923 to the identification and mapping of the instabilities of Taylor-Couette flow. Many instruments were used for the experimental investigation of fluid flow and the detection of various regimes from the first instability to a turbulent regime. Laser Doppler Velocimetry (LDV) (Zhang et al., 2007[304]), Doppler Global Velocimetry (DGV), Laser Induced Fluorescence (LIF), Particle Image Displacement Velocimetry (PIDV) or, as it is now most often called, Particle Image Velocimetry (PIV) (Liu et al., 2009[177]), micro-PIV (Wei et al., 2012[290]) and Particle Tracking Velocimetry (PTV) are the most known methods applied in fluid dynamics.

The Taylor-Couette flow is obtained when the rotational speed is sufficiently low and the viscous forces are more important than the centrifugal forces. It corresponds to a stable and axisymmetric flow (Andereck et al., 1986[17]; Coufort, 2004[70]).

The first transition to the "vortex flow" or "Taylor vortex flow" ((a) in Figure II.5 and Figure A.1 is achived if the rotational speed increases to Ta = critical Taylor number $Ta_c = 1712$. It marks the appearance of flow instability. In 1923, Taylor highlighted the existence of this flow with colored markers. At the establishment of this second regime, characteristic toroidal vortices (Figure A.1) appear and succeed each other throughout the height of the reactor (Coufort, 2004[70]).

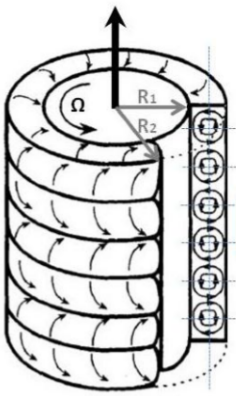

Figure A.1: Diagram of the structure of the Taylor vortex flow where the toroidal vortices are observed (based on Ohmura et al., 1997[217]).

If the rotational speed increases, this vortex flow also becomes unstable and other flows make their appearances. At Ta = 1.27 Ta_c, the vortices begin to undulate and a "wavy vortex flow (WVF)" appears (b in Figure II.5).

For even higher Ta (for $Ta = 40\ Ta_c$) (c in Figure II.5), waves present at the vortex levels disappear, but their vortex structures are preserved. Turbulent Vortex Flow (TVF) is established. For Ta = 700 Ta_c vortex structures disappear, axisymmetric flow begins to develop and the cells present at the ends of the reactor shrink. Beyond this phase, vortices are broken by turbulence and the flow is purely tangential and fully turbulent (Turbulent Taylor Flow (TTF)) (Coufort, 2004[70]).

A.6 Various Ta and Re data for regimes transitions

In Table A.2, three studies using Taylor-Couette reactor for biofilm development were compared concerning their geometric parameters (η and Γ), and their Ta and Re numbers for flow transitions. The geometric parameters in Coufort, 2004[70] TCR are very close to the TCR in this study (Table II.1). So for this study it is considered that a turbulent flow regime is established from $Ta > 40\ Ta_c$ (Table A.2).

Table A.2: Three different studies showing the critical values of the number of Taylor and that of Reynolds, who leads to transitions.

Transitions	Coufort 2004 ($\eta = 0.869$) ($\Gamma = 13.33$)	Nemri 2013 ($\eta = 0,85$) ($\Gamma = 480$)	Mehel 2006 ($\eta = 0,91$) ($\Gamma = 44.3$)
Couette	$Ta < 1712$	$Re < 125$	$Ta < 43.3$
Taylor Vortex Flow	$Ta = Ta_c = 1712$	$Re_c = 125$	$43.3 \leq Ta < 49.6$
Wavy Vortex Flow	$Ta = 1,27\ Ta_c$	$1.32Re_c < Re < 5.44Re_c$	$49.6 \leq Ta < 266$
Modulated Wavy Vortex Flow	-	$4,8Re_c < Re < 9,2Re_c$	$266 \leq Ta \leq 700$
Turbulent Vortex Flow	$Ta = 40\ Ta_c$	-	-
Turbulent Flow	$Ta = 700\ Ta_c$	$Re_c > 9,2Re_c$	$4500 \leq Ta$

A.7 Shear stress calculation inside the drippers

This dripper operates with a nominal flow rate of 36 ml/min (2.16 l/h). It produces a turbulent flow to regulate the dripper discharge and to prevent particles from settling and such causing dripper clogging. Micro-PIV was used by Al-Muhammad et al., 2016[10] as an experimental technique to characterize the labyrinth-channel flow and to analyze regions that can be sensitive to clogging. The experiments were conducted by varying flow rates from 24 ml/min (1.44 l/h) to 48 ml/min (2.88 l/h) which

corresponds to Reynolds numbers from 400 to 800, respectively (Eq.A.3), based on the mean velocity at the dripper inlet and hydraulic diameter; more information can be found in the work of Al-Muhammad et al., 2016[10] work. The Reynolds number in a dripper is given as:

$$Re = \frac{qD_h}{A_c\nu} \tag{A.3}$$

where q is the discharge of dripper (m^3/s); D_h is the hydraulic diameter of the tube (m); A_c is the cross-sectional area (m^2); and ν is the kinematic viscosity ($1.00E-06\ m^2/s$ for water).

With a Reynolds number from 400 to 800, the flow is quite turbulent in the labyrinth-channel according to Nishimura et al., 1984[212] and Pfahler et al., 1990[226]. There are several complex geometries of the labyrinth channel. It is composed of several baffles, and the turbulence varies accordingly. There is as yet no appropriate theory to calculate the critical Reynolds number in such geometries.

Numerical simulations have been performed on the labyrinth-channel geometry presented in Figure II.6 using the commercial computational fluid dynamics (CFD) software ANSYS/ Fluent V14.0. These simulations allow calculation of the strain rate (s^{-1}). The strain rate fields are plotted in the middle of the labyrinth-channel depth (at $z = 0.5\ mm$) and presented in Figure A.2 for two Reynolds numbers, 400 and 800, using standard k-epsilon model (see Al-Muhammad et al., 2016[10] for more details). Then, the average strain rate, S_m, was calculated over the area of the flow (Figure A.2) applying the following relationship:

$$S_m = \sum_{i=1}^{n} \frac{A_i S_i}{A_t} \tag{A.4}$$

where n is the cells number in the area; A_i is the i cell surface and A_t is the surface of the total area; and S_i is the i cell strain rate. The shear stress was calculated using this formula:

$$\tau = S_m \times \mu \tag{A.5}$$

where τ the shear stress (Pa); μ the dynamic viscosity of the fluid (1.00×10^{-3} Pa.s) and S_m the average strain rate (s^{-1}).

For Re = 400 (flow rate = 24 ml/min or 1.44 l/h), the average strain rate calculated was $S_m = 2210s^{-1}$ corresponding to a shear stress of $\tau = 2.2\ Pa$ (Eq.A.5). For Re = 800 (flow rate = 48 ml/min or 2.88 l/h) $S_m = 4422s^{-1}$ corresponding to a shear stress of $\tau = 4.4\ Pa$ (Eq.A.5).

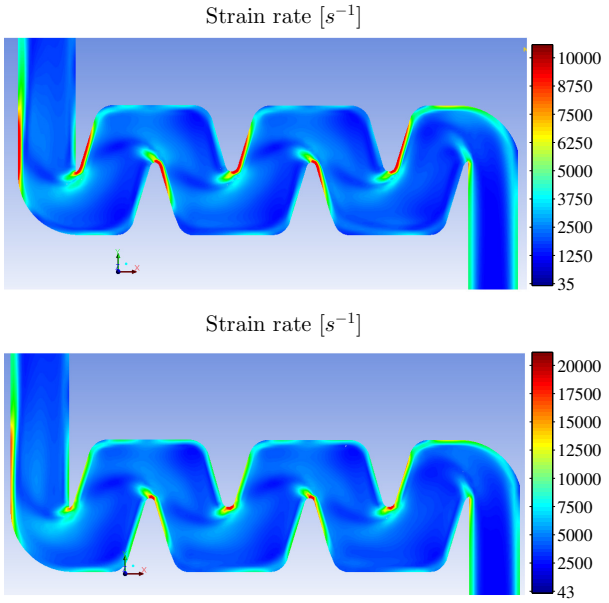

Figure A.2: The strain rate fields inside the labyrinth-channel middle at Re = 400 (top) and Re = 800 (bottom) using standard k-epsilon model (Al-Muhammad et al., 2016[10])

A.8 Plate preparation and sampling

Plates are prepared from low density polyethylene irrigation pipes (LDPE) (Φ $16mm$) having a rugosity of 50 μm. The rugosity of the plates was measured using a Leica Map Premium 7.3.7690 microscope generating height maps of surface topography. Pieces of pipes with a length of 64 cm are crosscut and then stuck between two circular iron plates. To have well flattened plate, the assembly is heated in an oven for 72h at 50°C to preclude deterioration of the surface conditions. Removed from the oven, the plates are cooled to room temperature and then fixed on polyvinyl chloride strips (PVC) which are then driven with the rotation of the inner cylinder. Every plate has a width of 3.8 cm, occupying a total area equal to 1216 cm^2, where biofilms were grown. Biofilm samples were collected on each plate surrounding the inner cylinder. The biofilm is scraped with a small soft plastic band and then collected in ceramic crucibles for analysis. The plate is then cleaned with a soft towel under running tap water then macerated for 10 min in a slightly acid solution (0.01 M $H_2PO_4^-$) to remove the remains of the fouling. Before a second use, a final rinse with distilled water is carried out.

A.9 Average and standard deviation of the water quality at the outlet of Mauguio WWTP

Date	BOD5 (mg O_2/L)	Tot Nitrogen (mg N/L)	Tot P (mg P/L)	pH	SS mg/L
8/26/2013	3	3	0.2	7.8	5.6
9/24/2013	3	3.3	0.3	8	3.2
10/15/2013	3	3.9	0.27	8	2
11/18/2013	3	3.7	0.2	7.9	3
12/17/2013	3	8.3	0.17	7.8	3
12/24/2013	3	7	0.16	7.6	3
1/17/2014	3	3.3	0.21	7.9	2
2/14/2014	3	4.4	0.6	7.6	4
3/11/2014	3	3.7	1.4	7.7	3
4/17/2014	3	6	1	7.9	2
5/16/2014	7	6.1	1.2	8.1	5
6/20/2014	3	3.9	1.5	7.9	3
7/17/2014	3	4.1	0.6	7.7	7
8/18/2014	3	4.6	0.75	8.1	4
9/12/2014	3	3.8	0.24	8.1	2
10/17/2014	3	6.5	2.5	7.9	2
12/11/2014	3	7.8	1	7.9	4
1/15/2015	3	5.5	0.9	7.9	2
2/18/2015	3	3.3	0.4	7.8	2
3/16/2015	5	3.4	0.77	6.9	8
4/14/2015	3	2	0.62	8.1	5
7/16/2015	3	2.4	0.65	8.1	6
9/17/2015	3	3.1	0.31	7.9	3
1/13/2016	3	2.7	0.42	7.9	3
2/17/2016	3	2.7	0.36	8.1	4
3/31/2016	3	2.4	0.23	7.9	6
Average	3.230769231	4.265384615	0.652307692	7.86538462	3.72307692
Standard Deviation	0.862910995	1.7195214	0.54196906	0.24648295	1.68767478

A.10 Yield rate calculation and values of consumed DCO

The development of the biofilm being homogeneous over the entire surface of the reactor, it is assumed that each week the same weight of biofilm will be developed. In the first week no scraping was done so the weight of the biofilm at week one was not taken into account. The amount of COD consumed was measured only during the week of scraping.

The value of consumed DCO is equal to: [DCO] mg/l x volume of the reactor (2L) x 7 (one week = 7 days).

Week	**1**	**2**	**3**	**4**	**5**	**6**	**7**	**8**
Biofilm age on each plate	1	2	1	2	3	4	5	6
	1	2	3	1	2	3	4	5
	1	2	3	4	1	2	3	4
	1	2	3	4	5	1	2	3
	1	2	3	4	5	6	1	2
Total biofilm mass (mg)	x	28.5	76	48.3	67.9	65	x	x
Consumed DCO (mg)	x	182	308	280	322	294	x	x
Y (mg/mg)	x	0.156	0.246	0.172	0.21	0.22	x	x

A.11 XRD pattern for the different shear stress

Diffraction peaks of organic and inorganic matter samples for TS and IM (after TS calcination) for a shear stress of 0.7 and 2.2 Pa.

TS - 0.7 Pa:

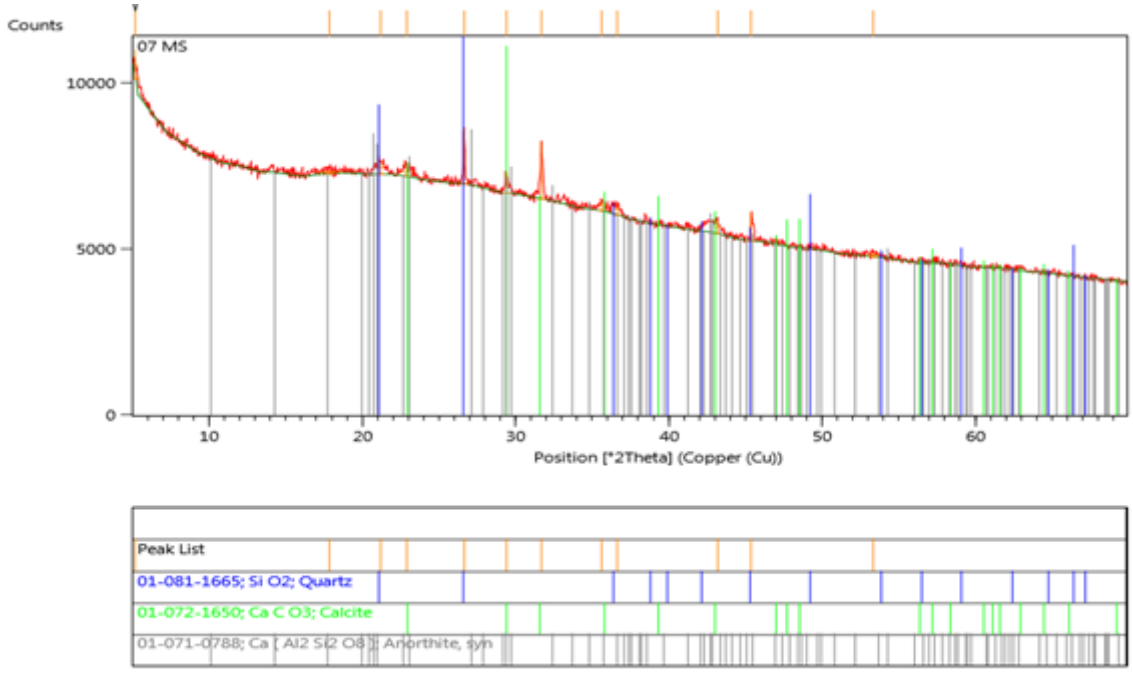

IM - 0.7 Pa:

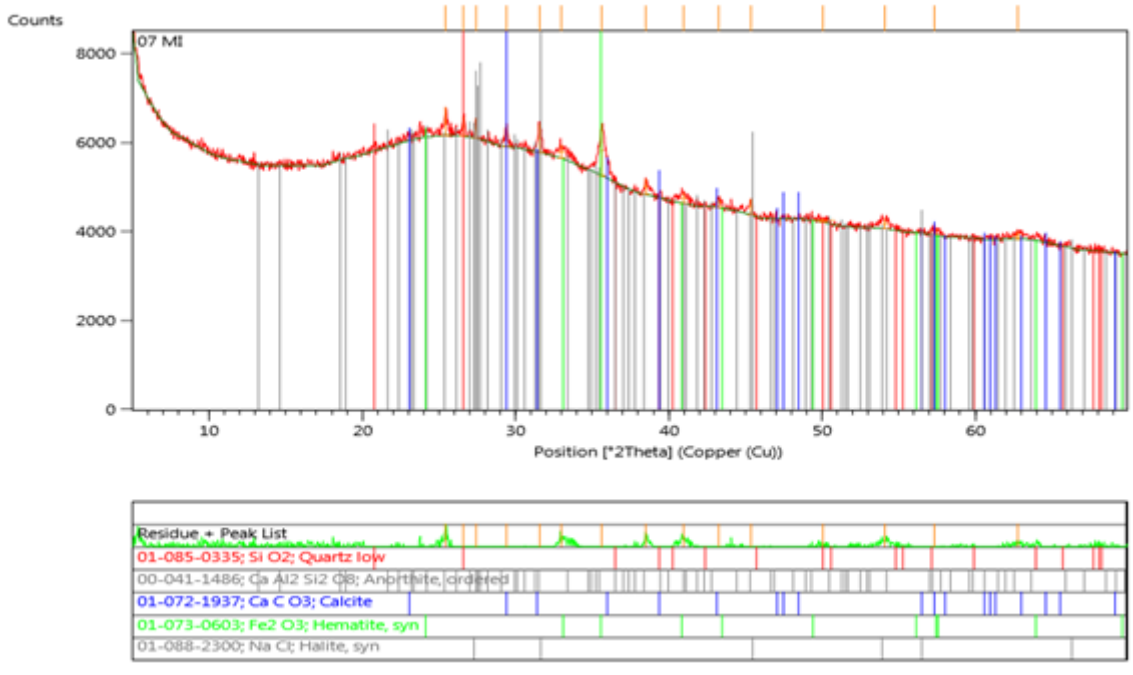

TS - 2.2 Pa:

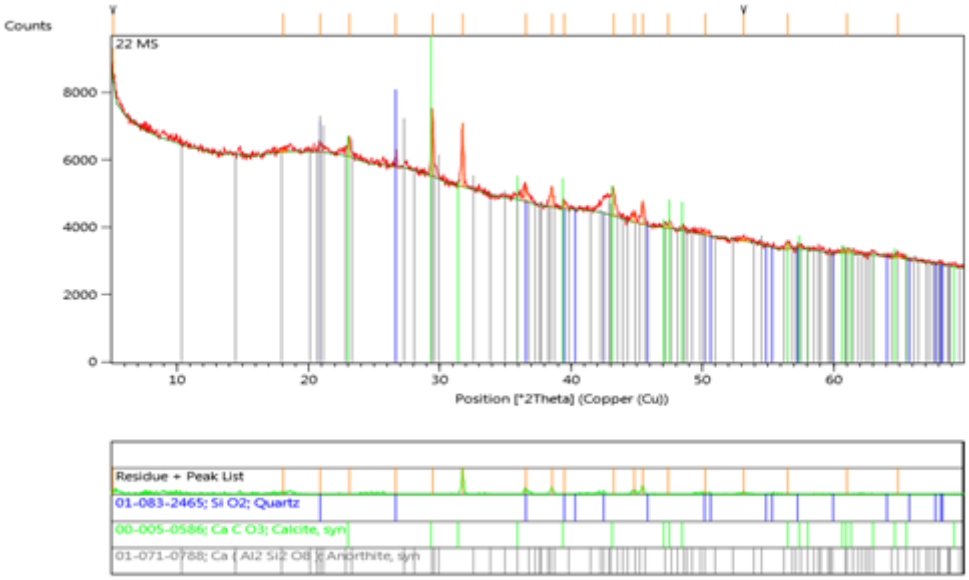

IM - 2.2 Pa:

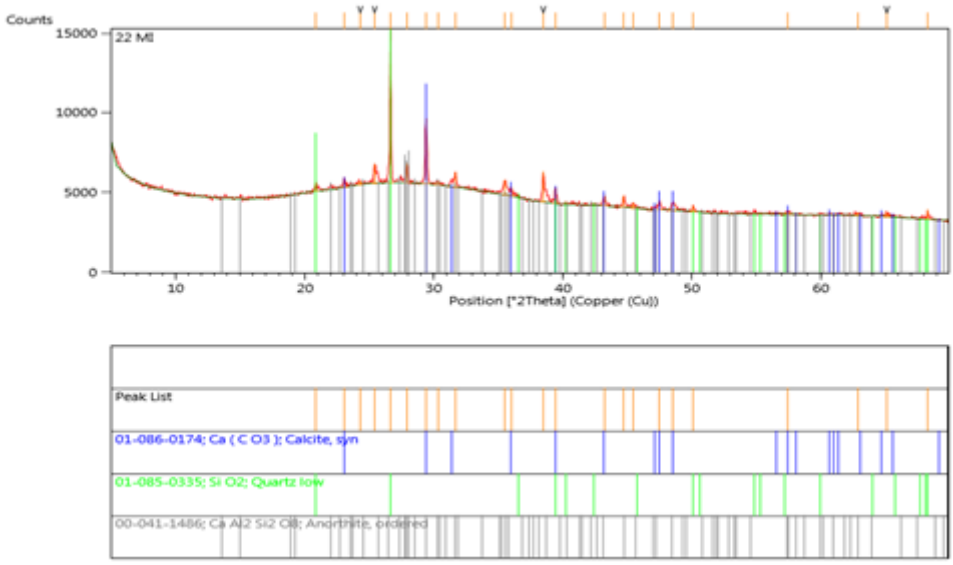

A.12 TGA pattern for the different shear stress

TGA thermal curve and chromatogram showing the characteristic peaks for the ions having a specific mass-to-charge ratio (m/z) or Thomson equal to 44. The objective is to detect the decomposition of calcium carbonate which induces a release of CO_2 in the temperature range 600-800°C. Depending on the apparatus used and the experimental protocol, the CO_2 peak may vary. In this study it is between 600 and 700°C. According to Basler Morill (1998) CO_2 is one of the most common elements that have an m/z = to 44. The other compounds being organic are not taken into account in this work. The blue arrow shows the corresponding peak.

TS - 0.7 Pa:

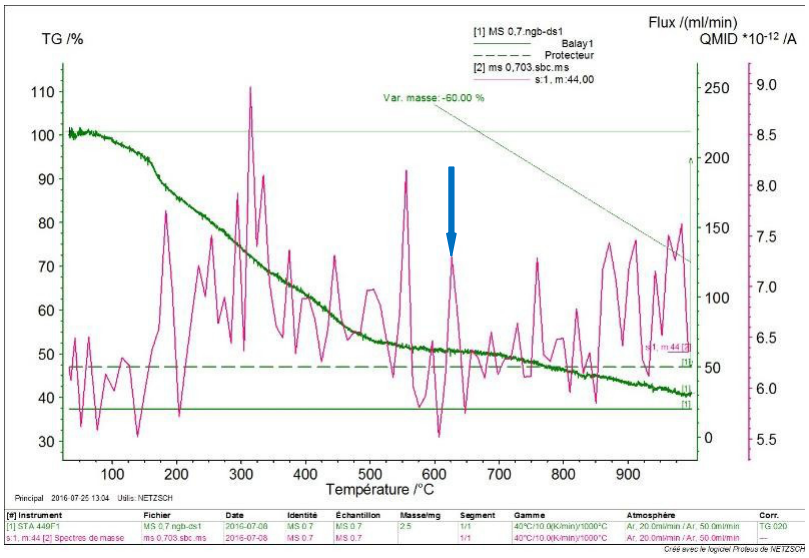

IM – 0.7 Pa:

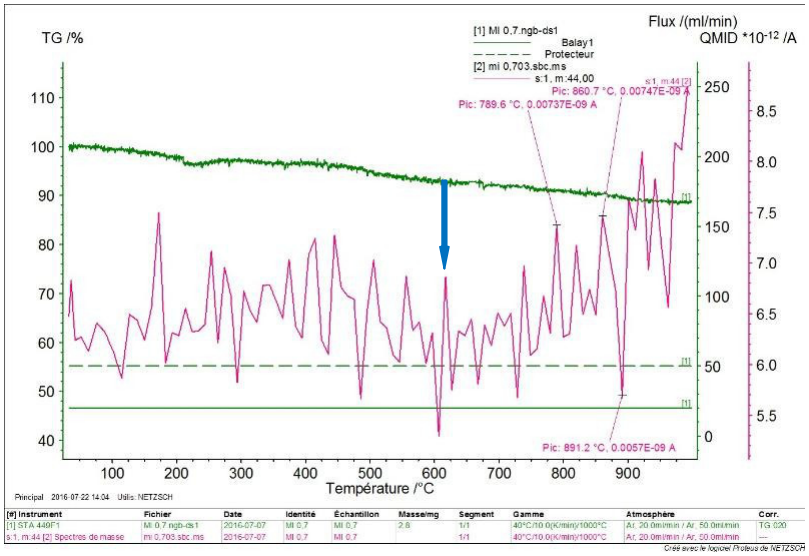

Here another representation of the chromatogram is shown in this case the peaks are smoothed. The peak of interest appears at a temperature of 666°C for TS and 596°C for IM. Here also the blue arrow shows the corresponding peak.

TS - 2.2 Pa:

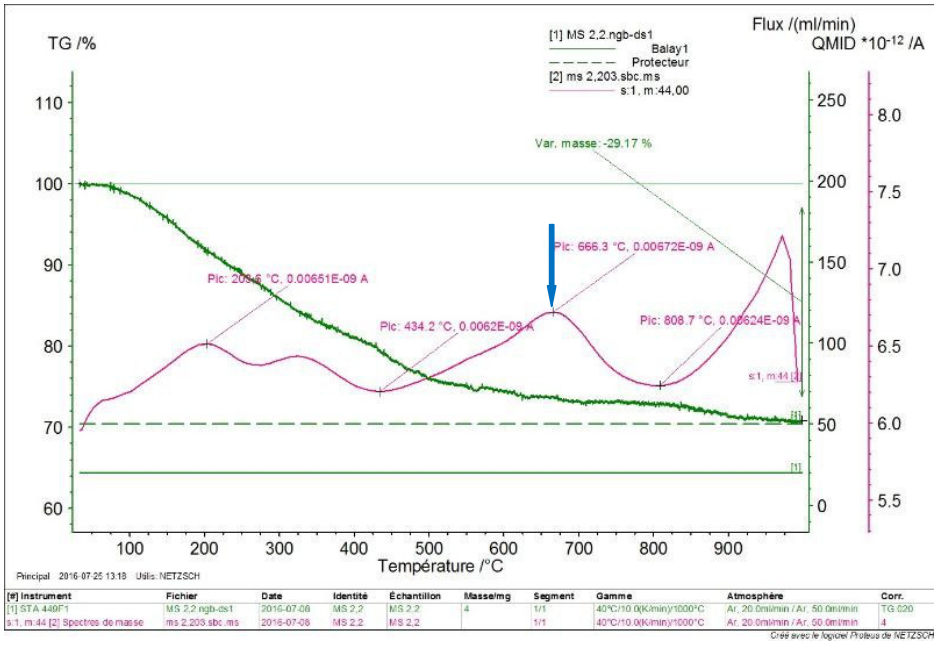

IM – 2.2 Pa:

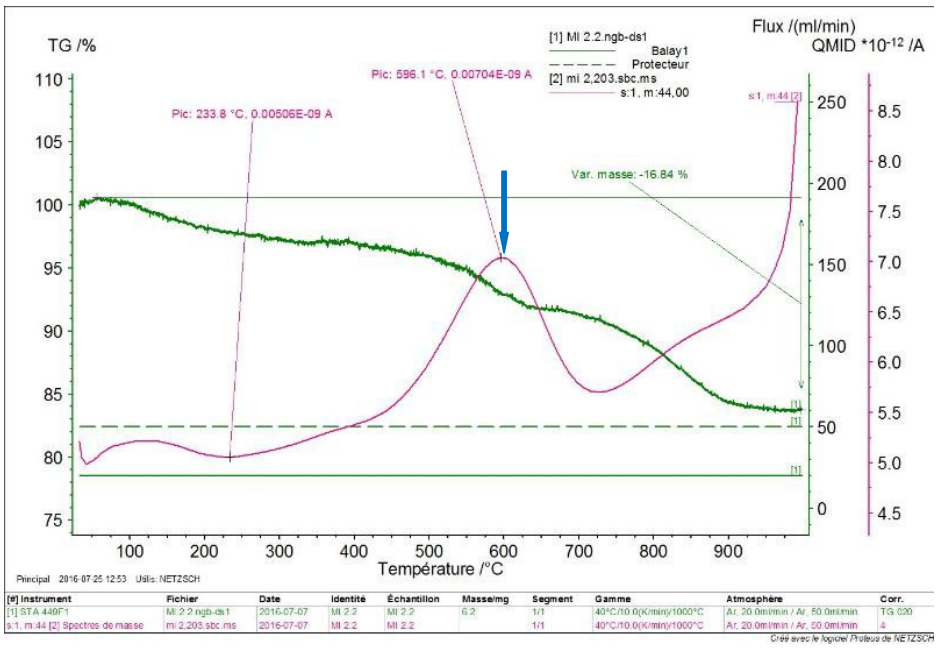

In this case the way to show the chromatogram was changed. It is not only for an m / z = 44 but rather for a full scan. Full scan records ions over a wide range of m / z ratios (Bouchonnet 2009). For “TS – 4.4

Pa" and "IM-4.4 Pa" the full scan was divided into 3 zones. The first zone was from 0 to 19 Thomson showing an interesting peak for m/z 18 (H_2O^+). The second zone from 21 to 35 Thomson showing two interesting peaks for m / z 28 (N_2^+ and CO^+) and m / z 32 (O_2^+). The third zone from 41 to 300 Thomson showing an interesting peak for m / z 44 (CO_2^+). This peak in showed by a blue arrow.

TS - 4.4 Pa (zone 1 and the corresponding mass spectrum):

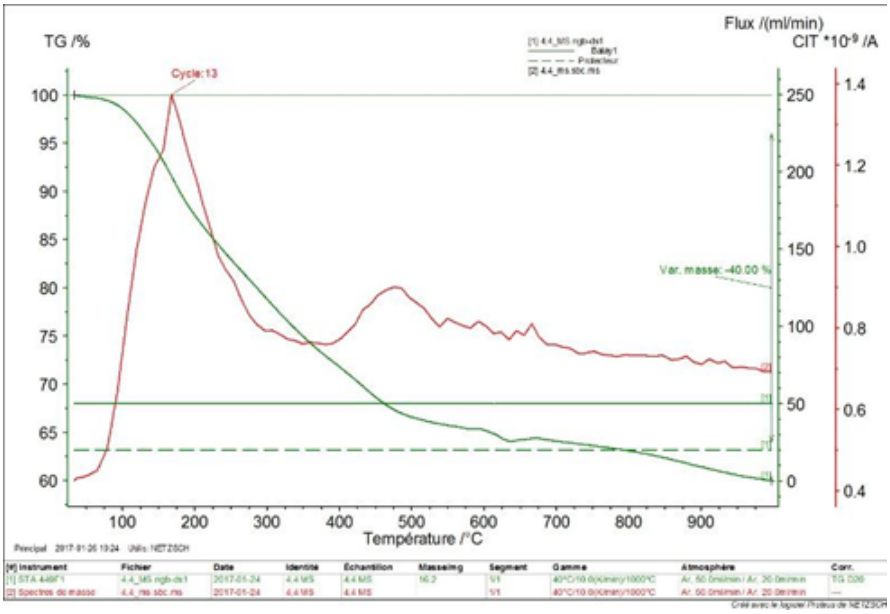

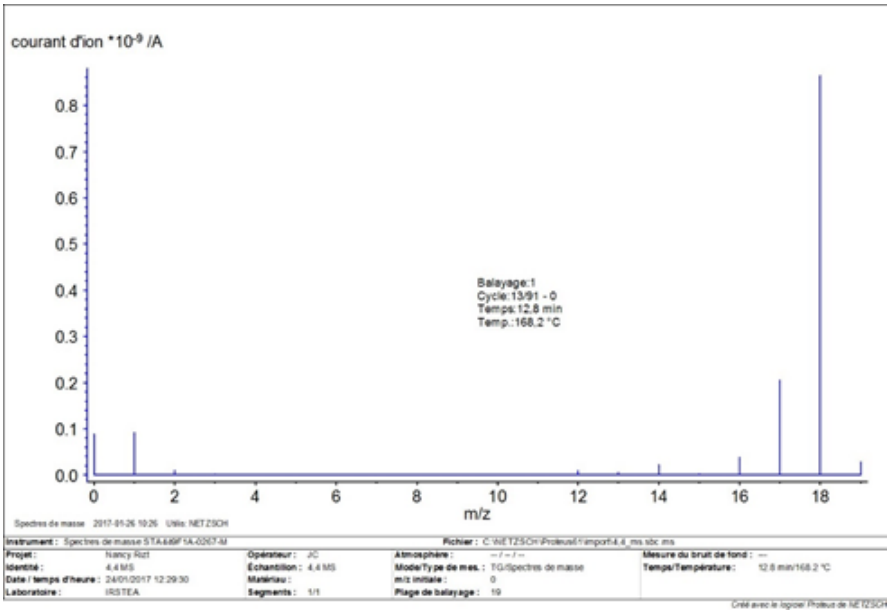

TS - 4.4 Pa (zone 2 and the corresponding mass spectrum):

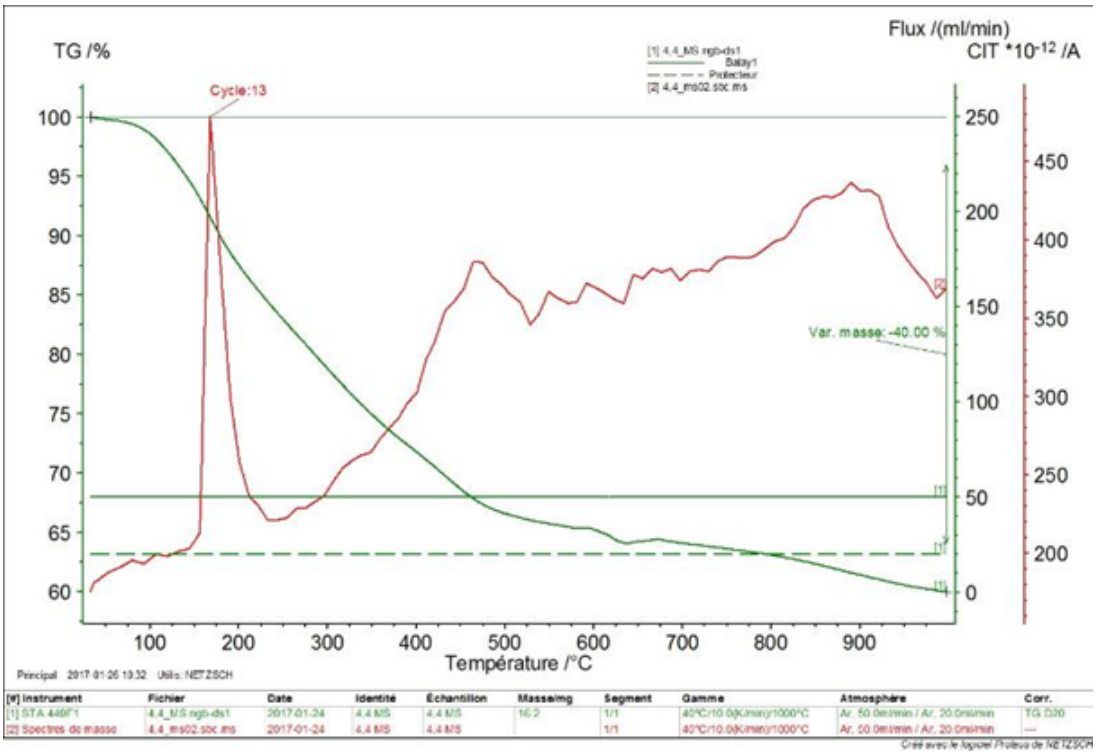

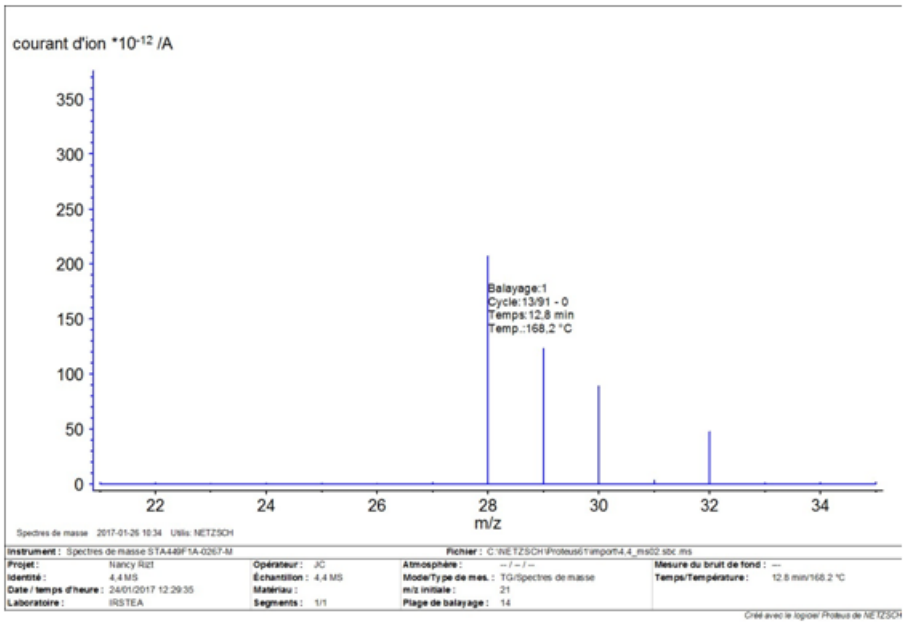

TS - 4.4 Pa (zone 3 and the corresponding mass spectrum):

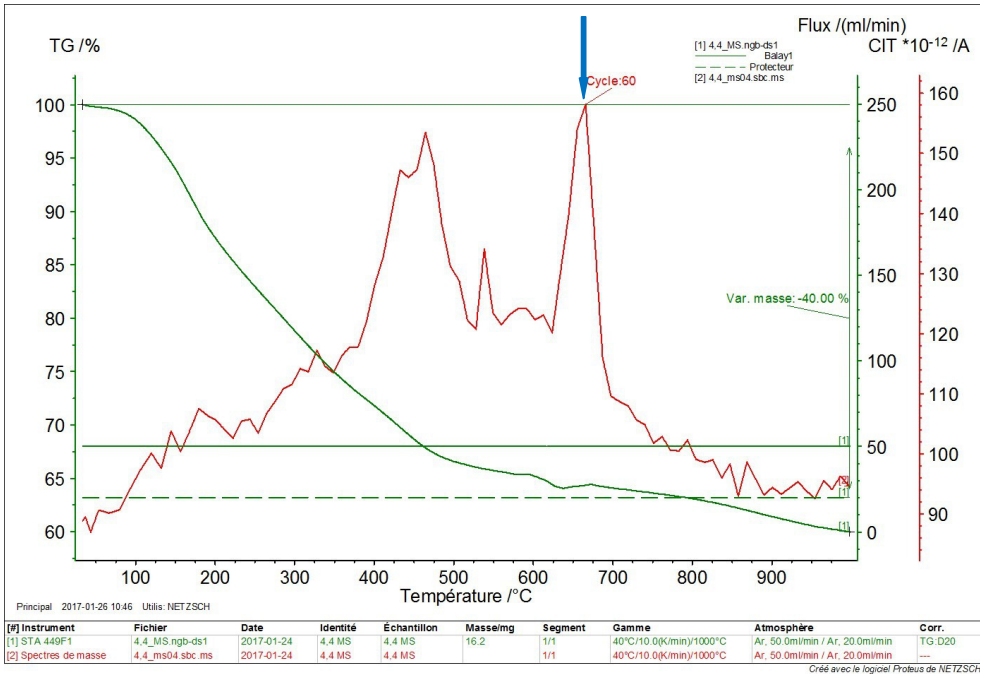

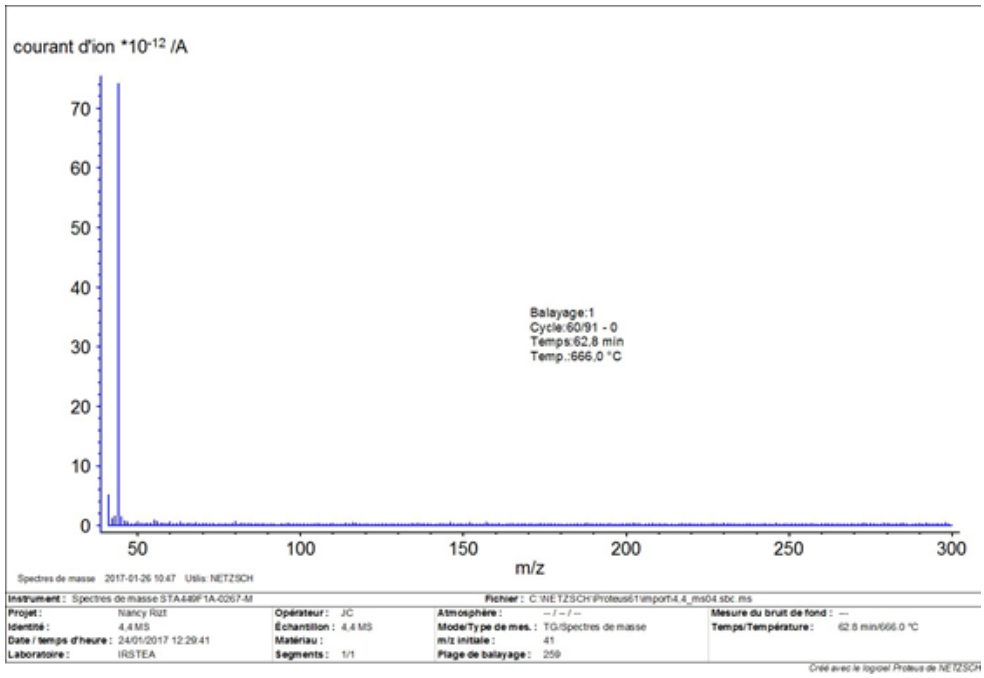

IM – 4.4 Pa (zone 1 and the corresponding mass spectrum):

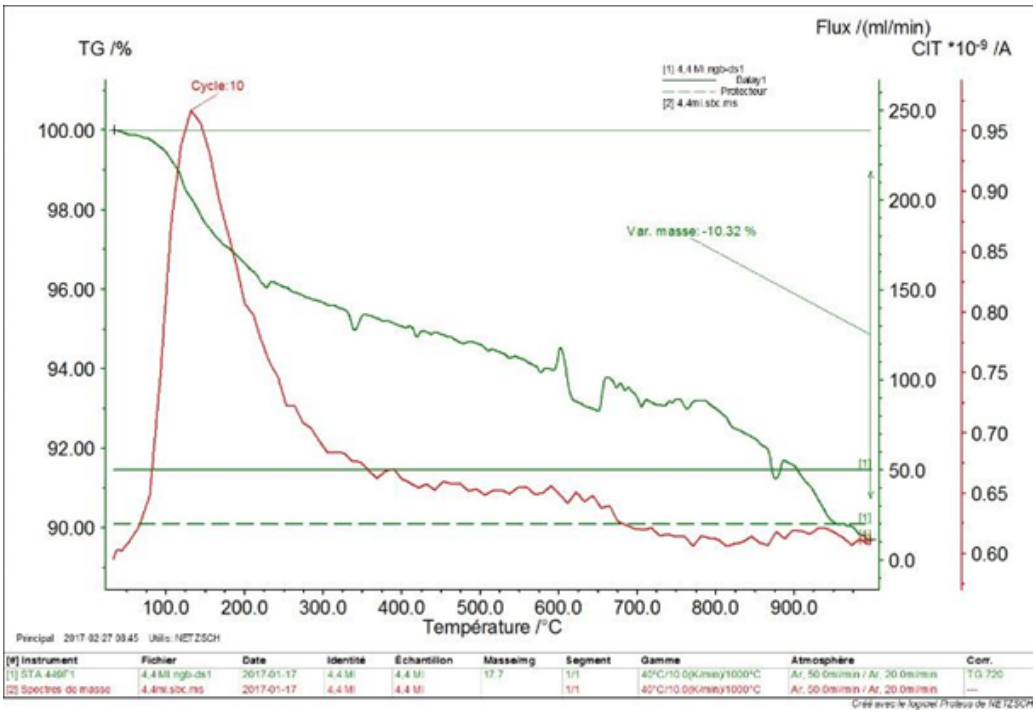

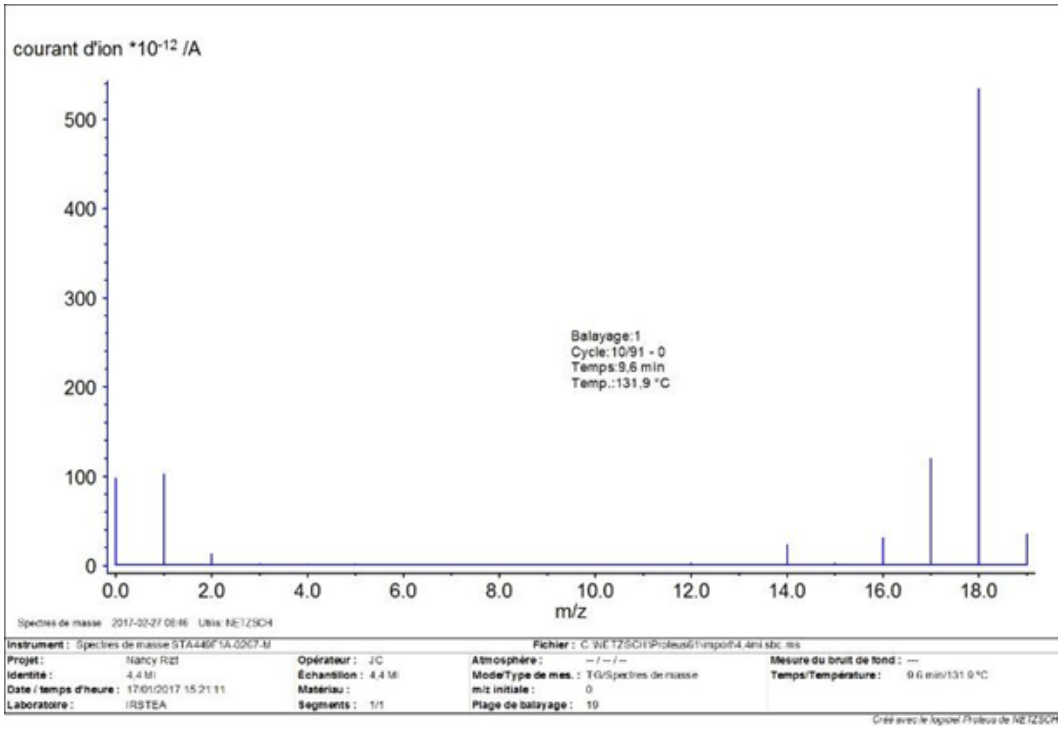

IM – 4.4 Pa (zone 2 and the corresponding mass spectrum):

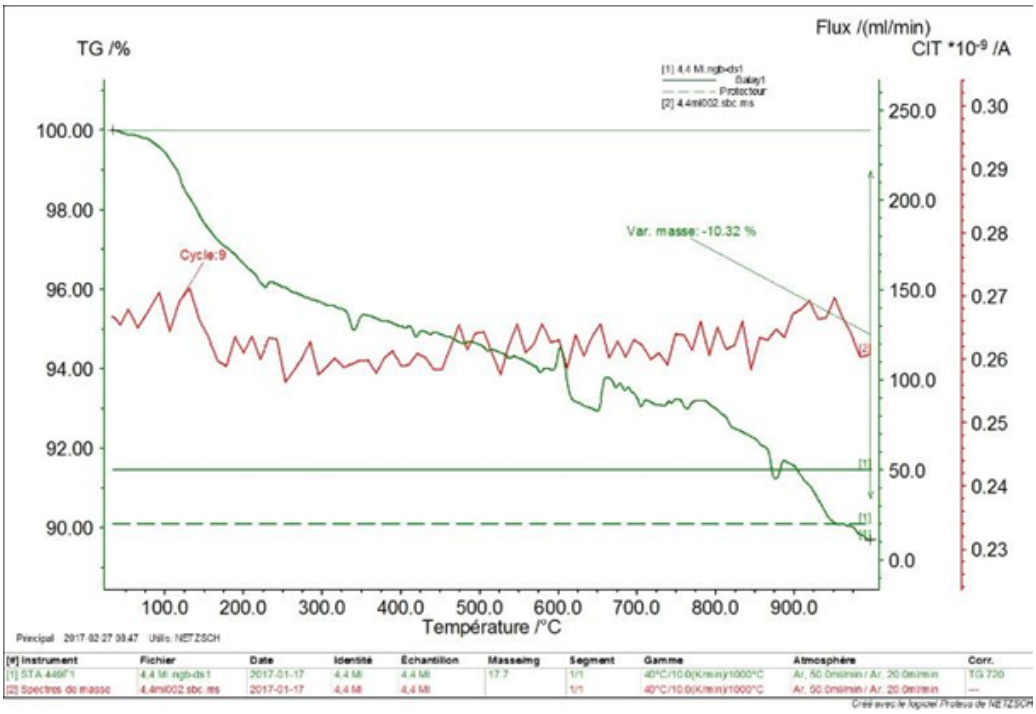

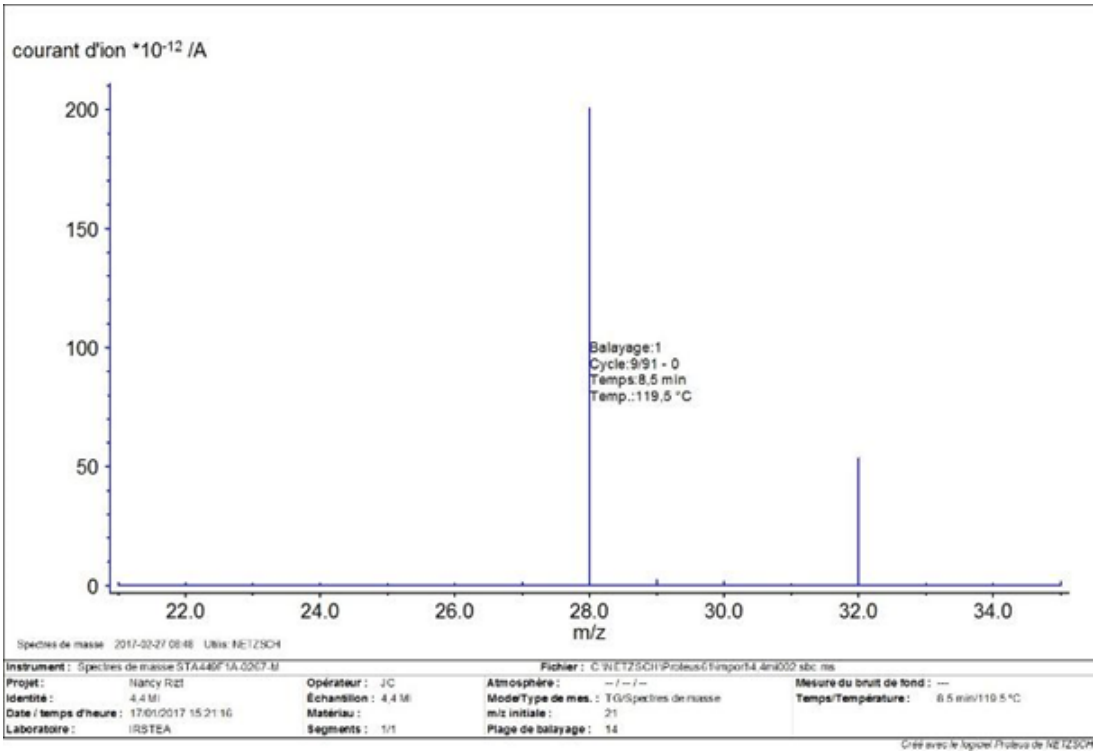

IM – 4.4 Pa (zone 3):

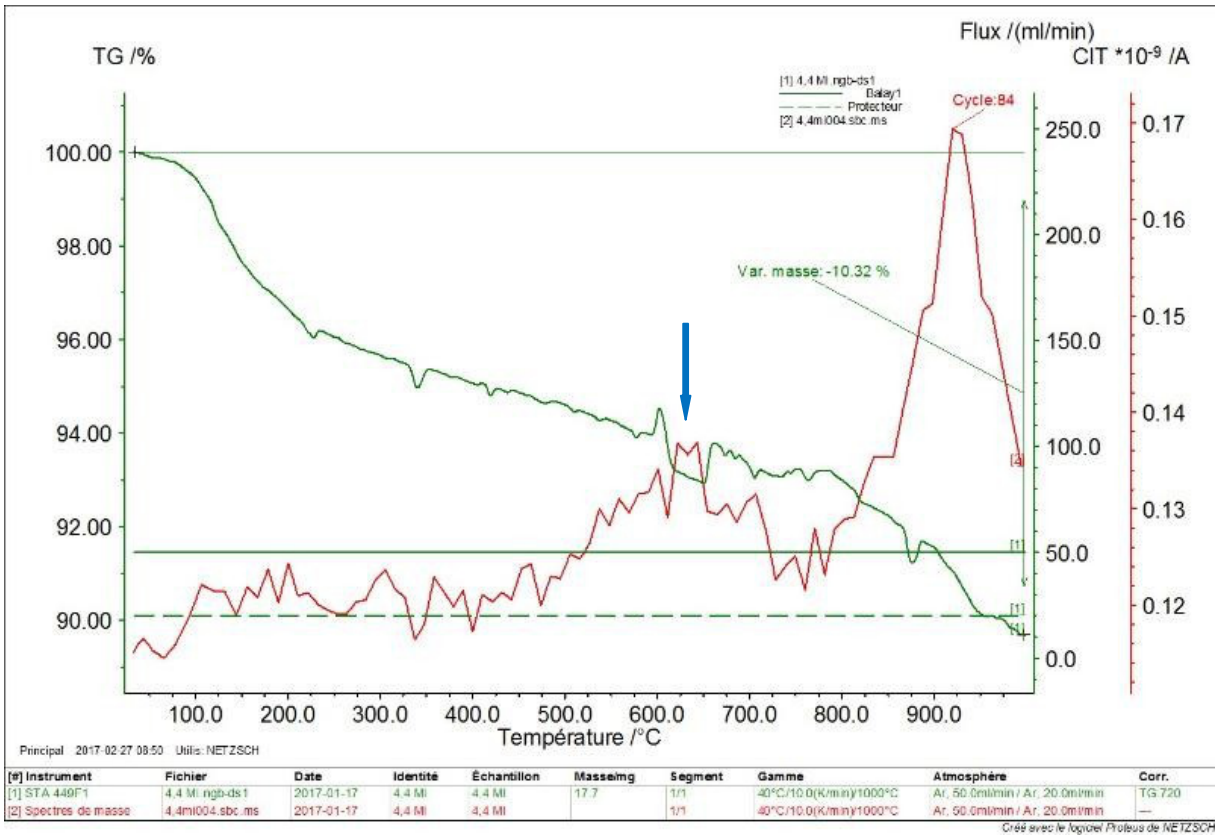

[#] Instrument	Fichier	Date	Identité	Échantillon	Masseimg	Segment	Gamme	Atmosphère	Corr.
[1] STA 449F1	4.4 MI.ngb-ds1	2017-01-17	4.4 MI	4.4 MI	17.7	1/1	40°C/10.0(K/min)/1000°C	Ar, 50.0ml/min / Ar, 20.0ml/min	TG 720
[2] Spectres de masse	4.4ml004.sbc.ms	2017-01-17	4.4 MI	4.4 MI		1/1	40°C/10.0(K/min)/1000°C	Ar, 50.0ml/min / Ar, 20.0ml/min	—

Créé avec le logiciel Proteus de NETZSCH

A.13 Measurement of COD inside T1 and T2

In both experiments, the initial concentration of COD was the same ($200 mg/l$) (section II.3.3) and during the experiments consumed COD was the same too ($23\ mg/l$/jour).

As described in the section II.3.3, synthetic effluent was renewed once a week for both experiments. In both cases, the COD decreases from 200 to $50\ mg/l$ in 7 days, which highlights the biofilm development. This constitutes proof that a more frequent renewal of synthetic effluent is essential to have constant concentration throughout the experiment. In the present case, this was impossible since 120 liters of demineralized water was used for each change.

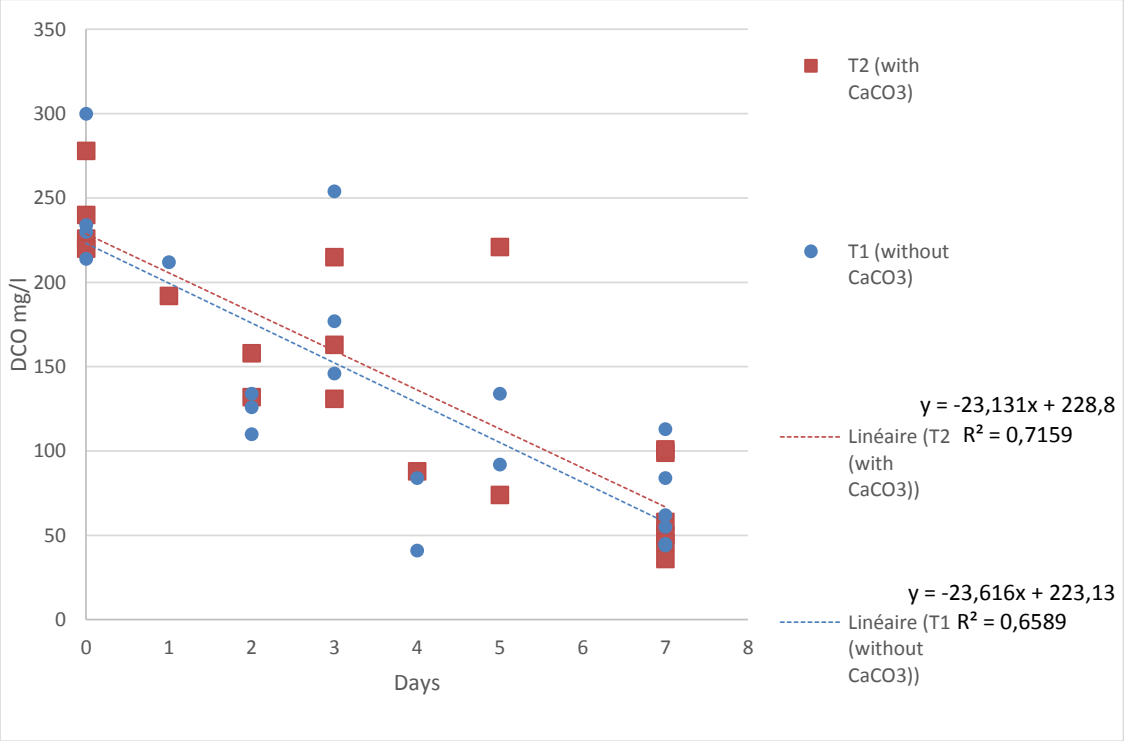

A.14 DRX graph for T1 and T2

Experiments runs without calcium carbonate:

IM at week 4 without calcium carbonate:

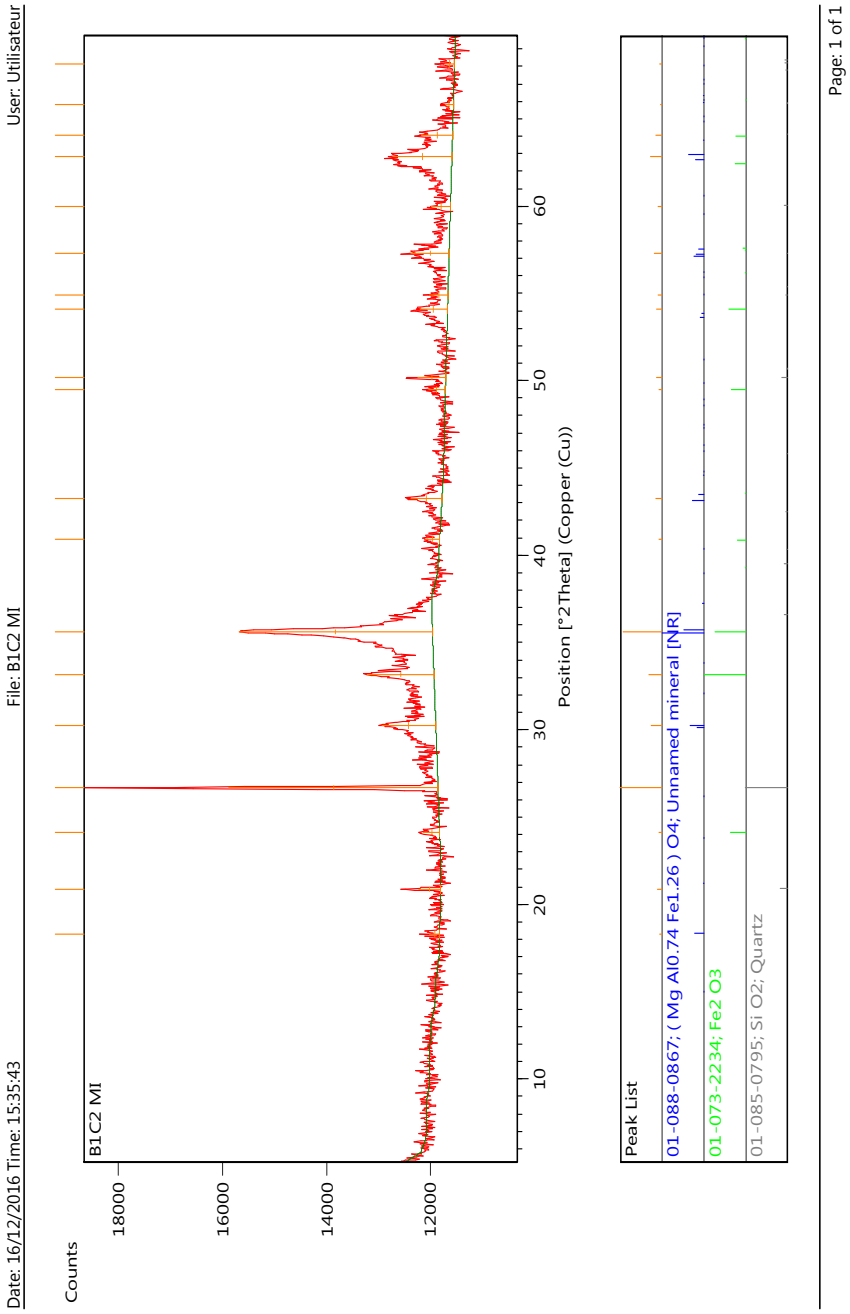

IM at week 6 without calcium carbonate:

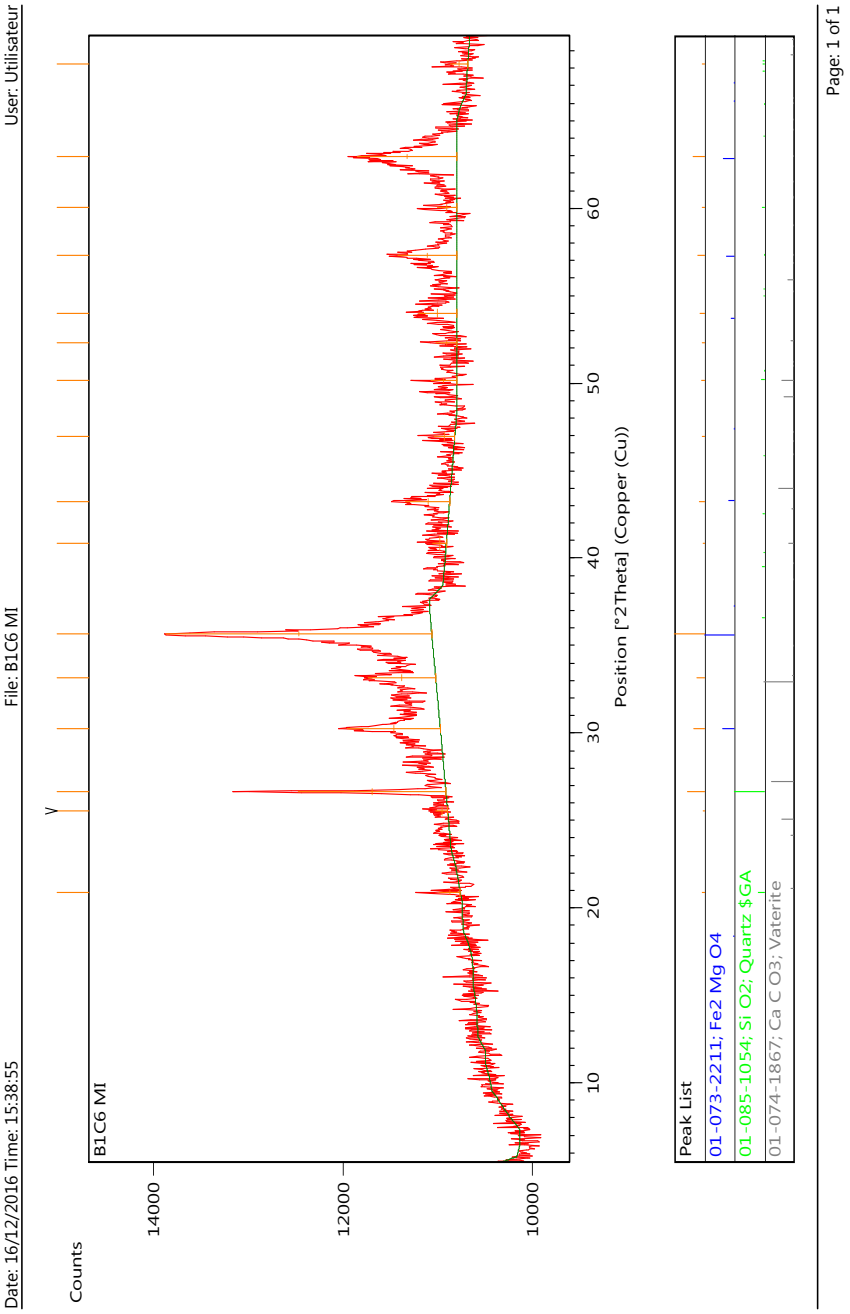

Experiments runs with calcium carbonate:

TS at week 1 with calcium carbonate:

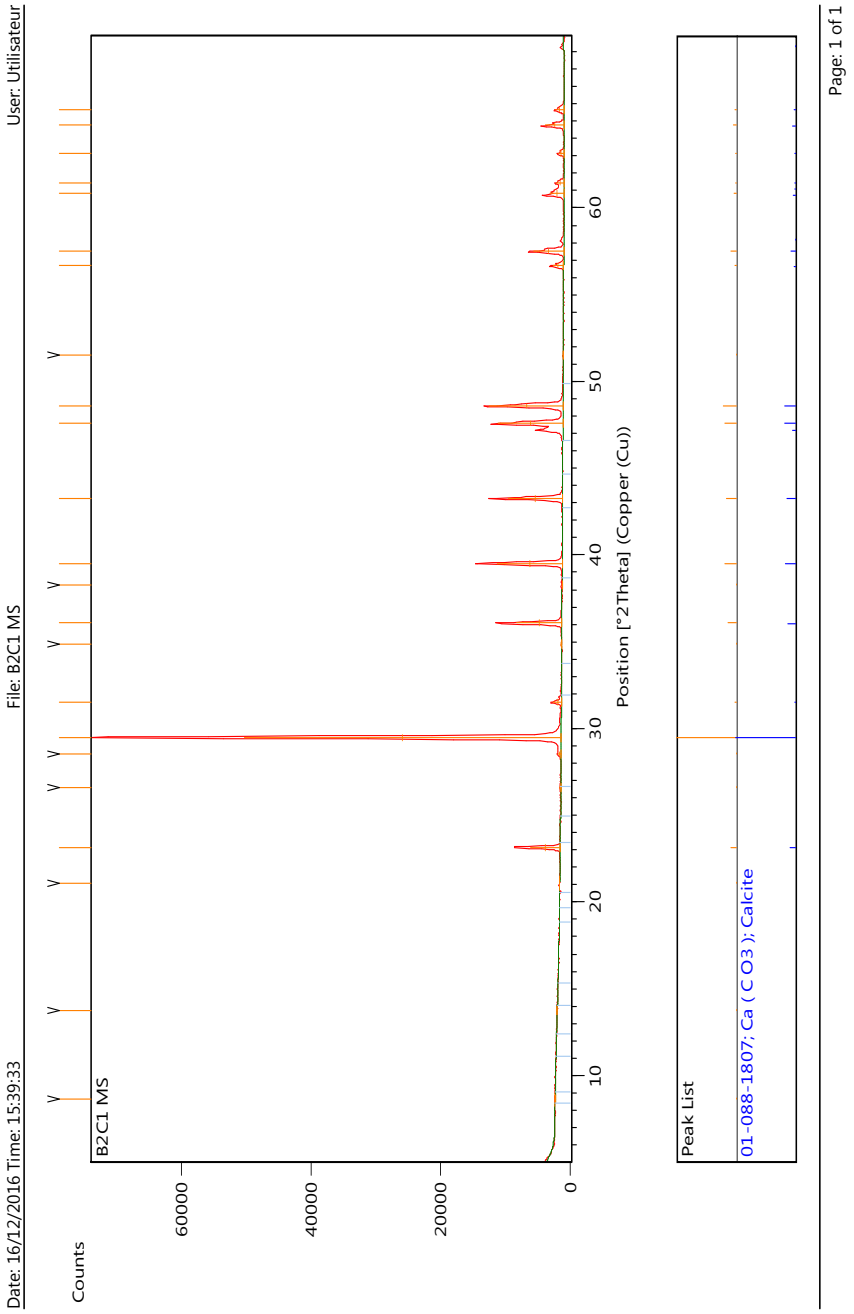

IM at week 2 with calcium carbonate:

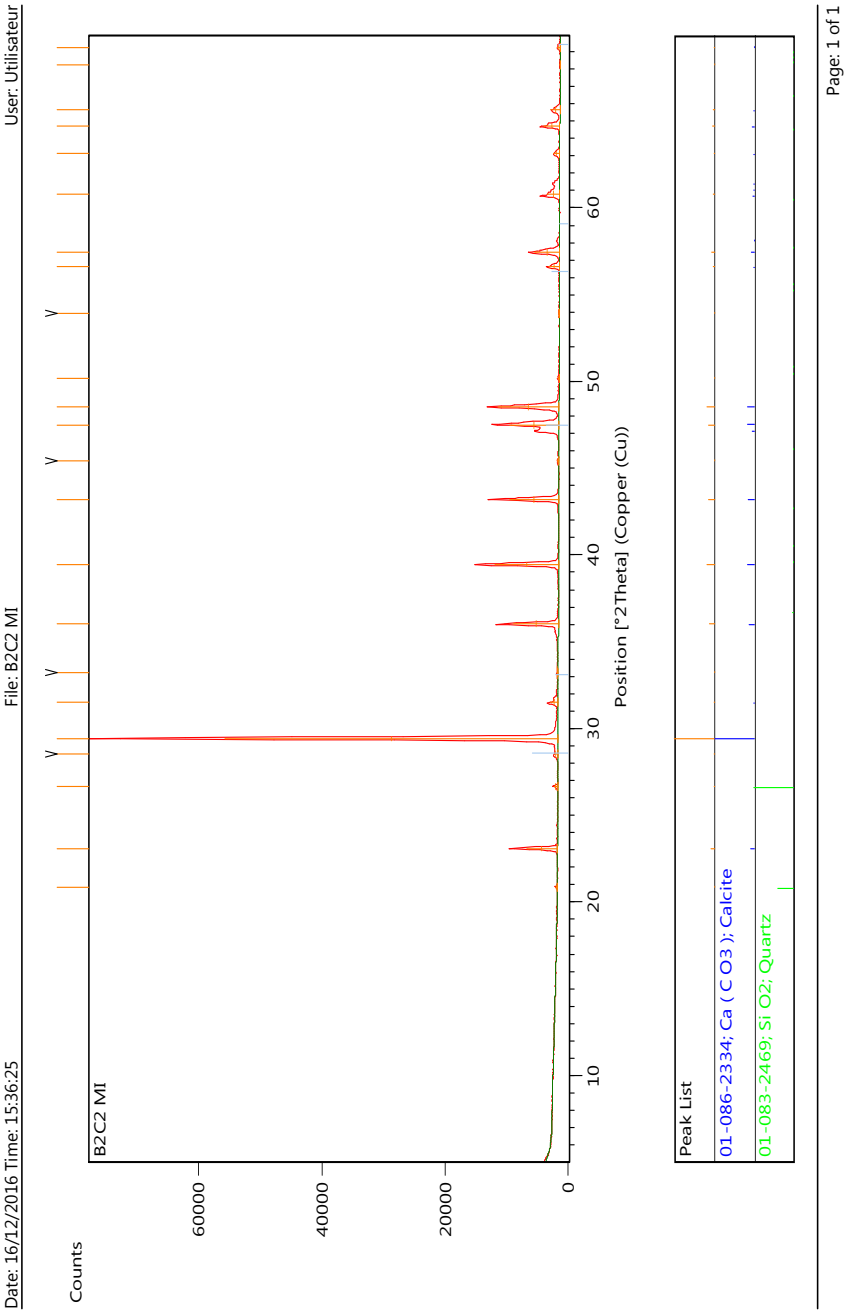

TS at week 4 with calcium carbonate:

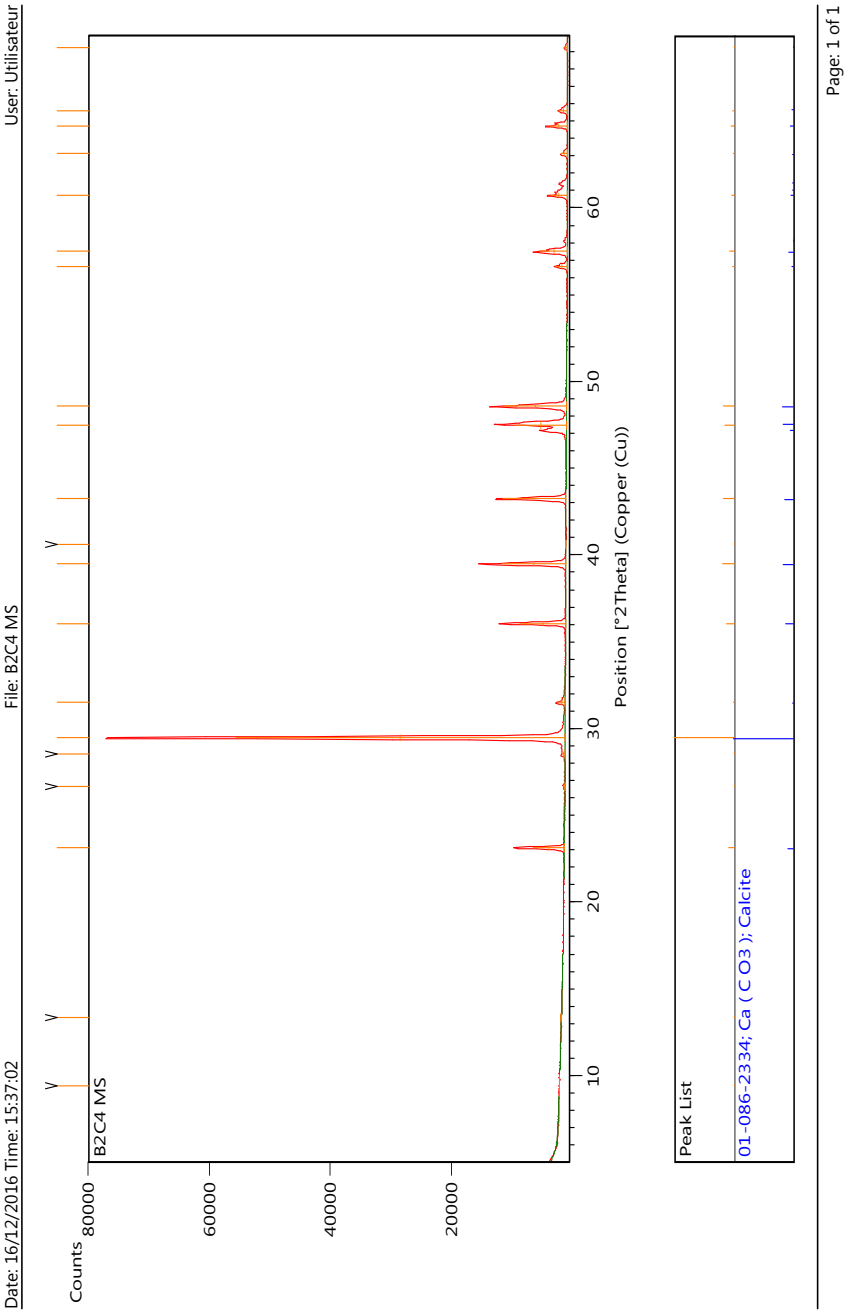

A.15 TGA/MS thermal curves for T1 and T2

TS at week 1 without calcium carbonate:

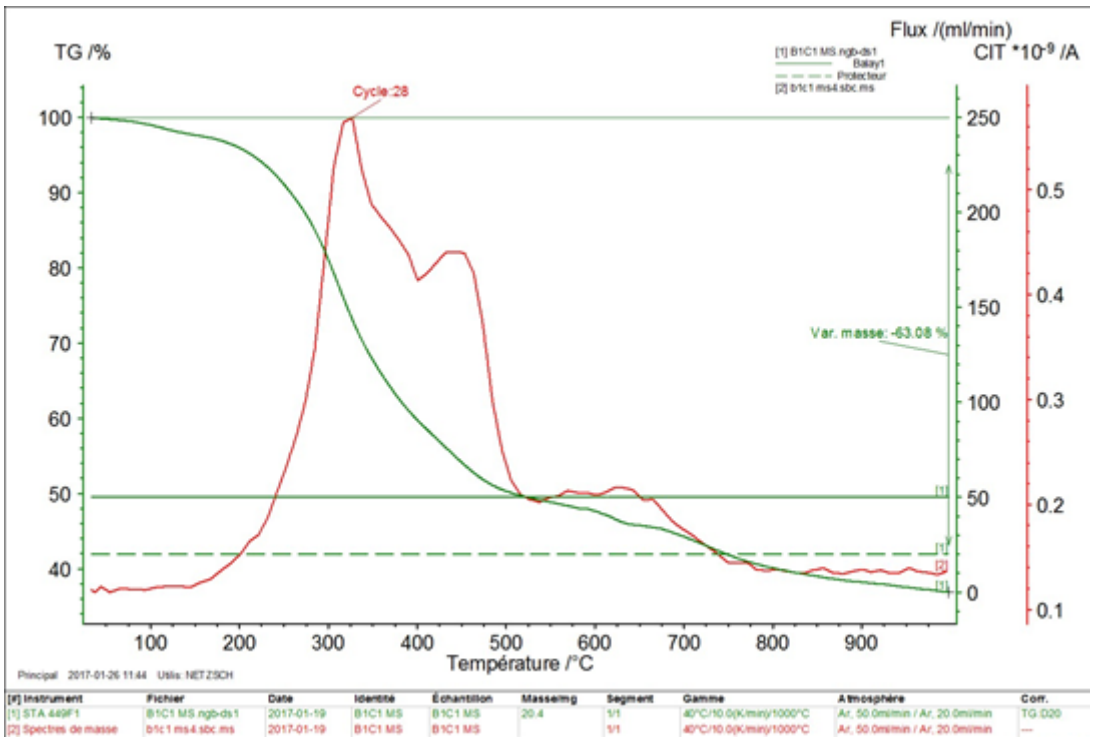

IM at week 1 without calcium carbonate:

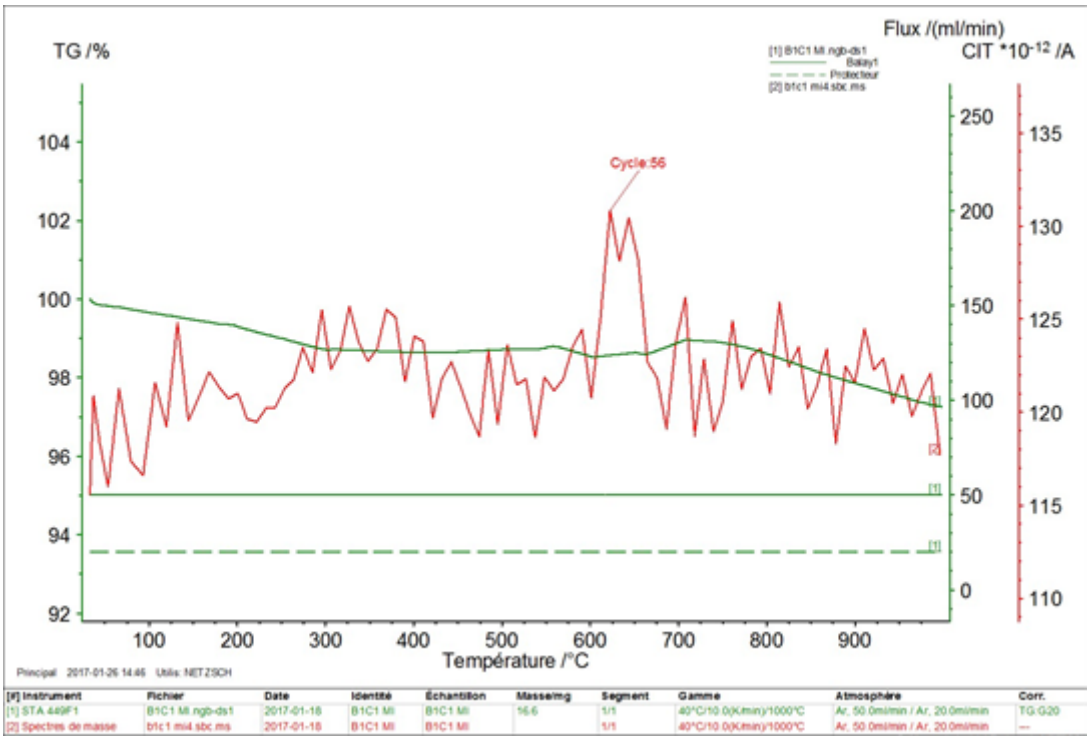

IM at week 6 without calcium carbonate:

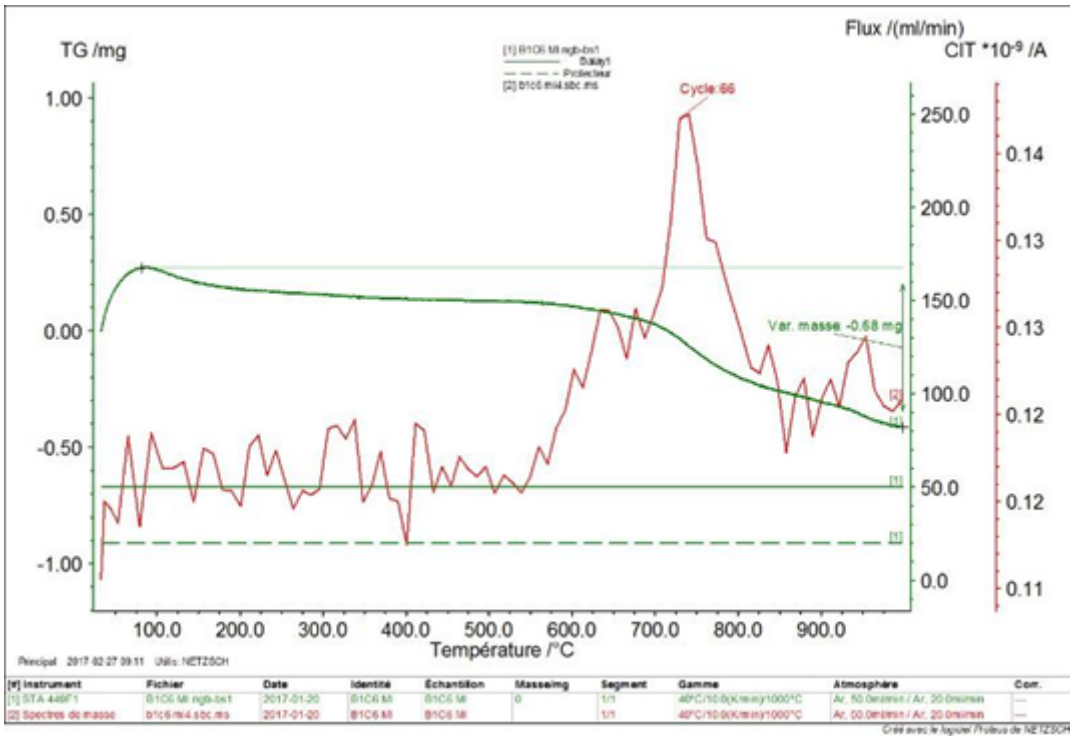

TS at week 1 with calcium carbonate:

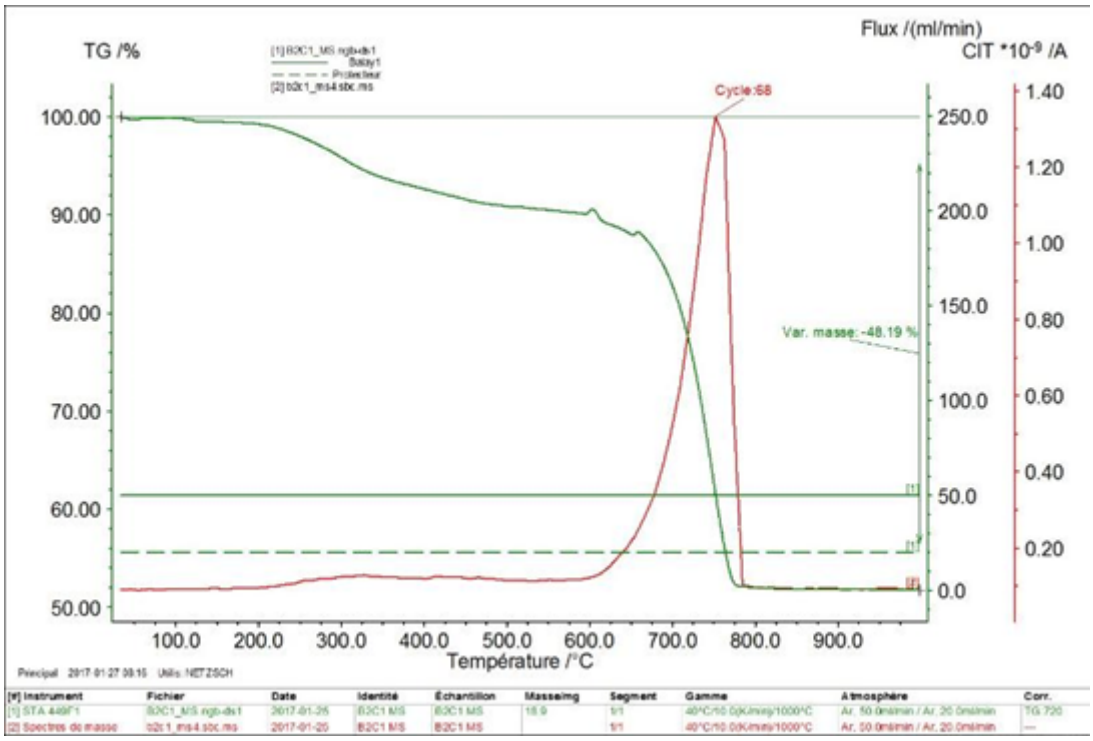

A.16 Drippers optical observation

Experiments run without calcium carbonate:

Flow rate = 1.674 l/h


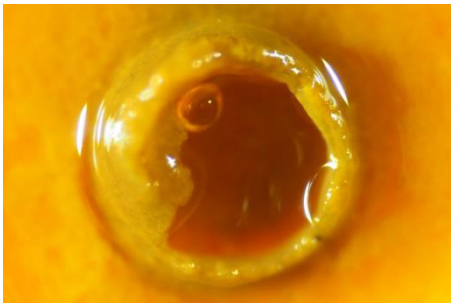

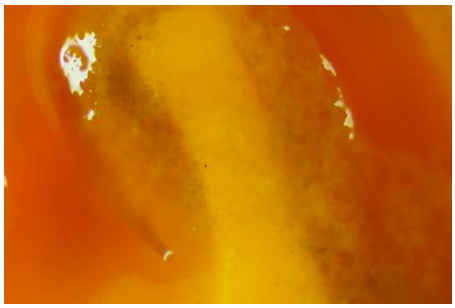

Flow rate: 1.77 l/h


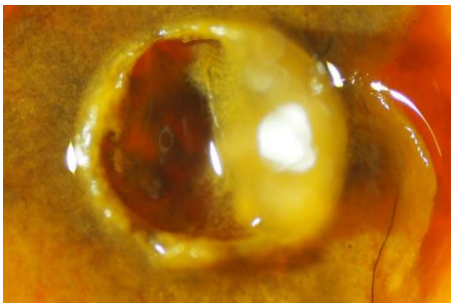
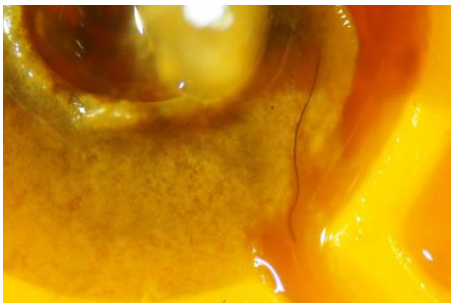

Flow rate: 1.428 l/h


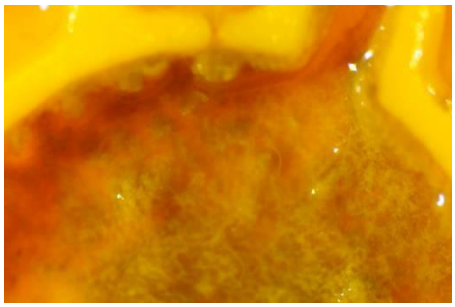
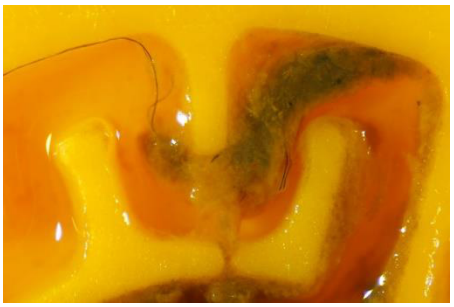

Flow rate: 1.524 l/h

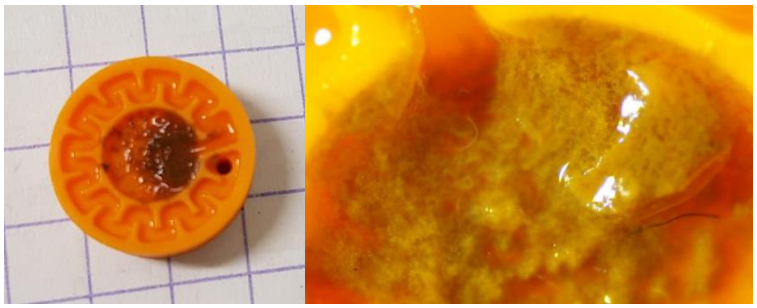

Flow rate: 1.992 l/h

Flow rate: 2.142 l/h

Flow rate: 1.968 l/h

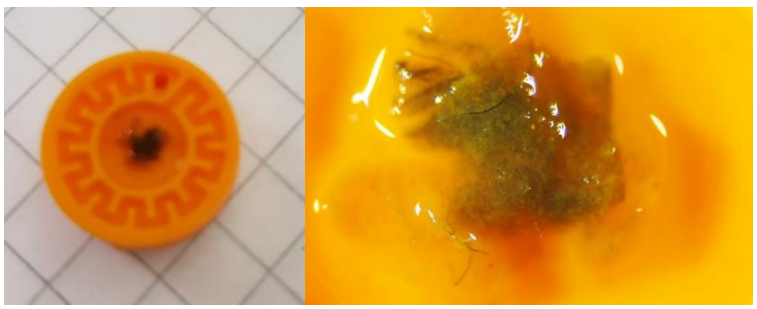

Experiments run with calcium carbonate:

Flow rate: 1.698 l/h

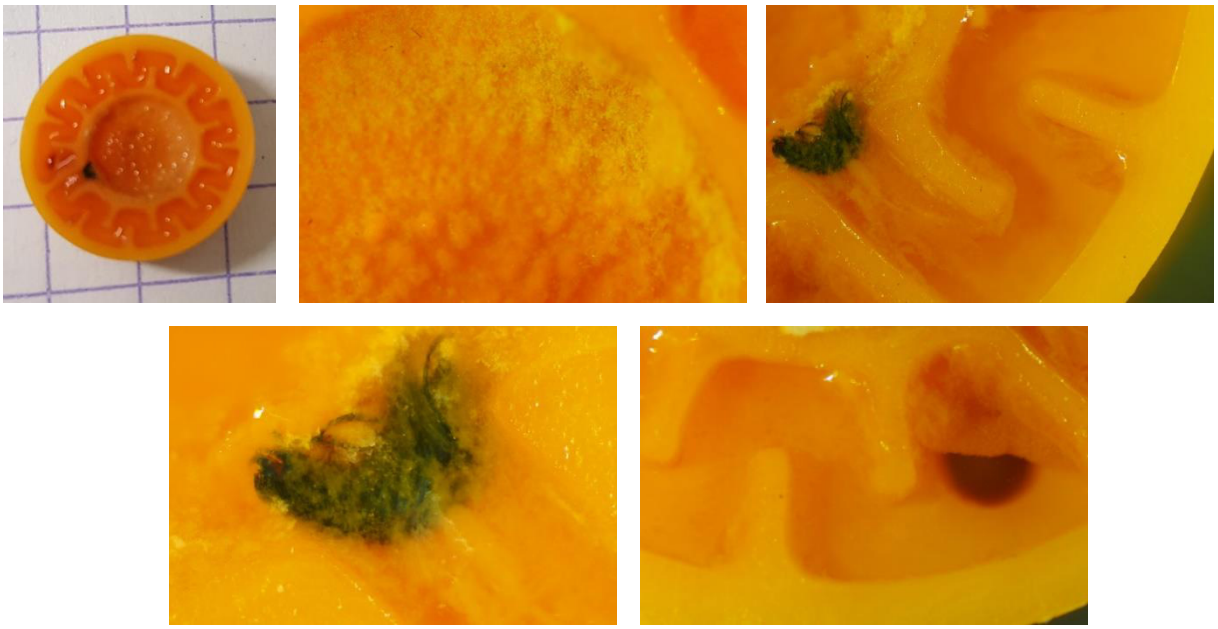

Flow rate: 1.944 l/h

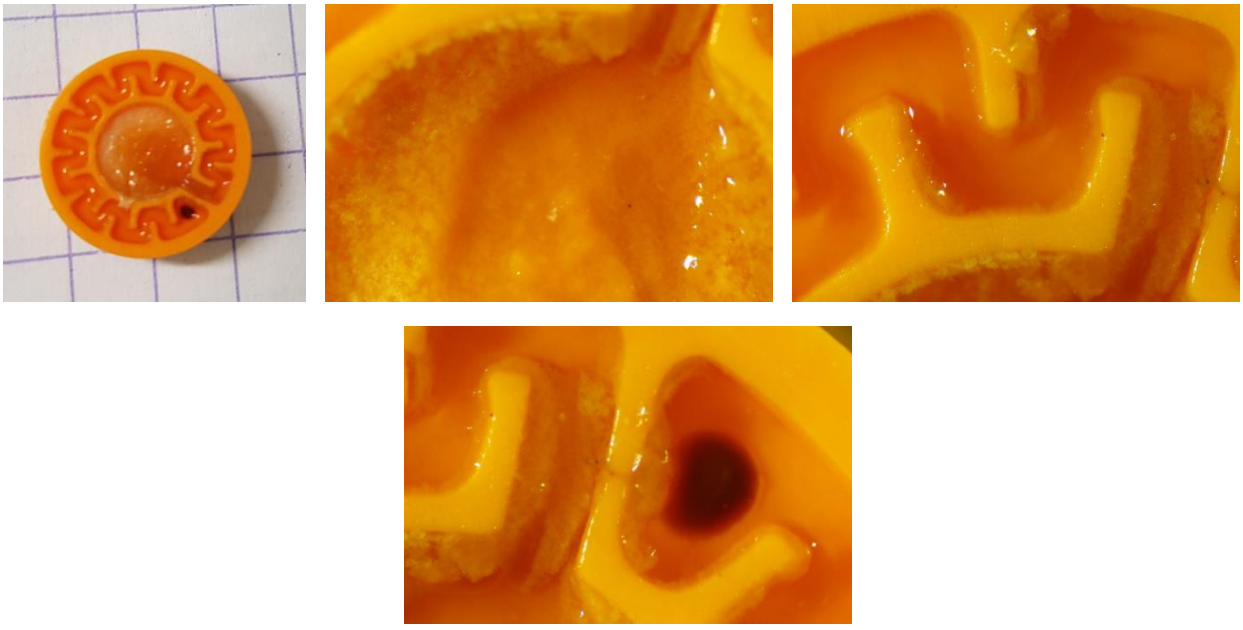

Flow rate: 1.626 l/h


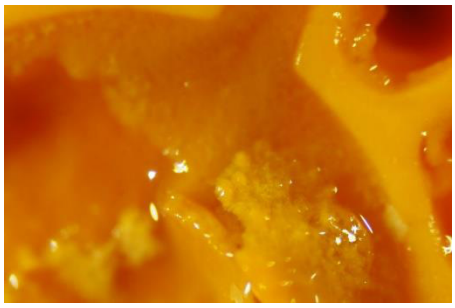

Résumé:

Dans le contexte d'un changement global atteignant les paramètres hydro-écologiques et biodémographiques généraux, la micro-irrigation utilisée en agriculture avec des eaux usées traitées constitue une approche prometteuse visant à réduire les dépenses en eau. Cependant, le colmatage des systèmes de micro-irrigation constitue une contrainte à l'utilisation de ces eaux contenant des micro-organismes, nutriments et sels dissous. Ces contaminants peuvent entrainer des précipitations chimiques avec développement de biofilms qui dégradent les performances des systems d'irrigation. Consécutivement on peut ainsi situer les objectifs de cette étude: i) Caractériser la précipitation des sels dissous due aux variations des conditions opératoires le long des systems de micro-irrigation, ii) étudier le développement des biofilms par l'utilisation d'une eau usée traitée sous différentes conditions hydrodynamiques, iii) analyser certaines interactions entre la précipitation chimique et le développement du biofilm.

En premier lieu une étude fut conduite sur l'impact des paramètres qui influent sur la précipitation chimique, comme la température le pH et la pression partielle du CO_2. Cette étude a permis de quantifier l'augmentation de la masse du précipité produit sous forme de calcite (carbonate de calcium) en fonction de l'augmentation du pH et de la température. Les résultats expérimentaux ont permis de valider et de calibrer la modélisation de la précipitation sous PHREEQC. Ce modèle numérique permet de prédire et de quantifier la précipitation chimique pour une qualité d'eau donnée dans des conditions opératoire variées de pH, de température et de pression partielle du CO_2. Des expérimentations ont ensuite été réalisées à l'aide d'un banc d'essai d'irrigation pour étudier l'influence du carbonate de calcium sur la croissance des biofilms au niveau des conduites de micro-irrigation et des goutteurs (organe de distribution). En parallèle un réacteur de Taylor-Couette (RTC) fut utilisé pour étudier l'influence de la contrainte de cisaillement sur le développement des biofilms. Selon la position dans le système d'irrigation, 3 contraintes de cisaillement ont été identifiées puis analysées. Dans la conduite une contrainte de 0.7 Pa a été retenue et 2.2 et 4.4 Pa dans les goutteurs. On constate que le biofilm a tendance à se développer selon la plus forte contrainte de cisaillement. Une précipitation du carbonate de calcium sous forme de calcite, à été observée en interaction avec la croissance du biofilm.

Mots-clés: Biofilm, carbonate de calcium, contrainte de cisaillement, précipitation chimique, PHREEQC.

Abstract:

In the context of global change reaching the general hydro-ecological and biodemographic parameters, micro-irrigation used in agriculture with treated wastewater is a promising approach to reduce water expenditure. However, the clogging of micro-irrigation systems constitutes a constraint on the use of these waters containing micro-organisms, nutrients and dissolved salts. These contaminants can lead to chemical precipitation with the development of biofilms that degrade the performance of irrigation systems. Consequently, the objectives of this study can be defined as follows: (i) to characterize the precipitation of dissolved salts due to variations in operating conditions along the micro-irrigation systems, (ii) to study the development of biofilms through the use of treated wastewater under different hydrodynamic conditions, and (iii) to analyze some interactions between chemical precipitation and the development of biofilm.

First, a study was implemented to identify the impact of the parameters that influence chemical precipitation. These parameters are temperature, pH and partial pressure of CO_2. This study permits the quantification of the increase in the mass of the precipitate produced in the form of calcite (calcium carbonate) as a function of the increase in pH and temperature. The experimental results allowed validation and calibration of the modeling of the precipitation under PHREEQC's software. This numerical model allows prediction and quantification of chemical precipitation for a given water quality under various operating conditions of pH, temperature and CO_2 partial pressure.

Experiments were then carried out using an irrigation set-up to study the influence of calcium carbonate on the growth of biofilms in micro-irrigation pipes and drippers (distribution drippers). In parallel, a Taylor-Couette reactor (TCR) was used to study the influence of shear stress on the development of biofilms. Depending on the position in the irrigation system, 3 shear stresses were identified and analyzed. In the pipe, a shear stress of 0.7 Pa was retained and in the drippers the shear stress was between 2.2 and 4.4 Pa. It is observed that the biofilm tends to develop under the highest shear stress. Precipitation of calcium carbonate in the form of calcite was observed in interaction with the growth of the biofilm.

Keywords: Biofilm, calcium carbonate, chemical precipitation, PHREEQC, shear stress.